Natural and synthetic lipid nanoparticles for therapeutic RNA delivery

Martijn J.W. Evers

COLOFON

Natural and synthetic lipid nanoparticles for therapeutic RNA delivery

Natuurlijke en synthetische lipide nanodeeltjes voor de afgifte van RNA-medicijnen

(met een samenvatting in het Nederlands)

Proefschrift

ter verkrijging van de graad van doctor aan de
Universiteit Utrecht
op gezag van de
rector magnificus, prof.dr. H.R.B.M. Kummeling,
ingevolge het besluit van het college voor promoties
in het openbaar te verdedigen op

donderdag 19 januari 2023 des middags te 2.15 uur

door

Martijn Johannes Wilhelmus Evers

geboren op 6 februari 1992
te 's-Hertogenbosch

Promotoren:
Prof. dr. R.M. Schiffelers
Prof. dr. W.W. van Solinge

Copromotoren:
Dr. P. Vader
Dr. S.A.A. Kooijmans

Beoordelingscommissie:
Prof. dr. R.A.H. Adan (voorzitter)
Prof. dr. G. Storm
Dr. S.A. Fuchs
Prof. dr. M. Barz
Prof. dr. R. Vandenbroucke

Aan Mirte
Aan mijn ouders

TABLE OF CONTENTS

Introduction

1

INTRODUCTION

RNA Therapeutics

The past decade has witnessed major breakthroughs in drug development such as the approval of multiple cell- and gene-therapies, new antibody therapies and first-in-class RNA based therapeutics.[1,2] The clinical introduction of RNA-based therapeutics, such as Nusinersen (Spinraza®), Patisiran (Onpattro®), and Givosiran (GIVLAARI®), has revolutionized the way in which we are able to treat disease: almost directly at their biological origin. Currently, mRNA-based vaccines, such as BNT162b2 (Pfizer/BioNTech;Comirnaty ®) and mRNA-1273 (Moderna) have a major, if not leading role in the world-wide vaccination campaign against severe acute respiratory syndrome coronavirus 2 (SARS-CoV-2).

RNA therapeutics directly influence gene expression levels. Using RNA therapeutics, we can influence pathological processes at their root cause.[3,4] The three most developed classes of RNA therapeutics are:

- Small inhibitory RNAs (siRNAs) / microRNAs (miRNAs)
- Messenger RNAs (mRNAs)
- Clustered regularly interspaced short palindromic repeats RNA (CRISPR-RNAs)

siRNA/miRNA

siRNAs and miRNAs both act via a mechanism called RNA interference (RNAi). RNAi was first discovered in *Caenorhabditis elegans* where the introduction of large dsRNA molecules resulted in the suppression of genes based on sequence homology.[5] The RNAi effect is mediated via small, 21-23 bp, dsRNA molecules. These small RNA molecules guide the RNA induced silencing complex (RISC), containing the protein Argonaute 2, to a complementary target mRNA where RISC binds and cleaves the mRNA in a sequence-dependent manner.[6,7] As a consequence, expression of the protein encoded by the target mRNA is reduced. Target cleavage of mRNA by siRNAs is highly dependent on complementary base-pairing between siRNA and target mRNA. Mismatches between siRNA and target mRNA reduce silencing activity, making RNAi-mediated gene silencing a highly specific process.[8,9] An intriguing feature of RNAi is that the RISC complex containing the siRNA molecule is not consumed during its action, enabling the breakdown of multiple mRNAs by a single siRNA molecule.[10]

The effect of miRNA molecules is also mediated via RNAi, though their mode of action can differ from that of siRNA. miRNA molecules are endogenously expressed small RNA molecules which are generally only partially complementary to their target mRNA. As a result, they can target a number of different mRNA transcripts with varying efficiency. Binding of a miRNA/RISC complex to a target mRNA is minimally orchestrated via the 'seed region' at nucleotides 2-8 of miRNAs 5'end. If the miRNA is not entirely complementary to the target mRNA, binding of miRNA/RISC does not always induce mRNA cleavage but instead results in repression of translation initiation, post-initiation inhibition, or activation of RNA decapping/deadenylating enzymes. This ultimately also results in mRNA degradation and/or silencing of gene expression. [11] Via RNAi, both siRNA and miRNA act as potent suppressors of gene expression thereby shaping the possibility to treat disease at the mRNA level.

mRNA

The use of mRNA as therapeutic modality is straightforward and versatile. Delivery of mRNA into the cytoplasm of cells can lead to its translation resulting in expression of the encoded protein. This concept can be used for example in protein replacement therapies, vaccination and immunotherapy.[12]

CRISPR-RNAs

The third category of RNA-based therapeutics is based on the clustered regularly interspaced palindromic repeats (CRISPR)-Cas9 system and related technologies such as base-editing and prime-editing. CRISPR-Cas9 technology is based on the ability of a protein-RNA gene editing complex, i.e. Cas9 combined with a guide RNA (gRNA), to sequence-specifically recognize and modify a target DNA sequence. Using this system, different gene editing strategies can be employed, dependent on the variant of Cas9 and type of gRNA used. In CRISPR/Cas9 genome editing, Cas9 induces a double-strand break in the cell's DNA. This break is subsequently repaired, either via non-homologous end joining (NHEJ) resulting in small insertions or deletions (indels) or via homology directed repair (HDR) where the sequence is restored based on sequence homology to a DNA template.[13] Functionally, NHEJ mostly leads to frameshift mutations causing premature stop-codons resulting in a truncated or dysfunctional protein. HDR results in repair of the damaged DNA based on sequence similarity to a DNA template. Via the latter way, it may be possible to correct disease causing mutations by co-delivery of a DNA template encoding the correct DNA sequence. However, HDR-mediated repair is inefficient, and as a result of the double-strand break, might cause concomitant indels or activate DNA-damage-repair processes which limit its efficiency. In addition, HDR is limited to dividing cell types, reducing its applicability.[14,15]

More recently, by making use of a nuclease deficient Cas9 enzyme (dCas9) or Cas9 nickase (nCas9), single base-pair editing systems have been developed. Here, a combination of nCas9 or dCas9 and a DNA modifying enzyme (deaminase) can be employed to specifically edit a single nucleotide with high precision without the need for a DNA template or DSB.[16] Base-pair editing was initially limited to adenine and cytosine base editors, facilitating only 4 nucleotide transitions.[16,17] More recently, it was shown that adenine base editors also have the ability to convert cytosine to guanine or thymine.[18] In addition, the repertoire of base editing has expanded to C-to-G base editors.[19,20] The newly developed prime-editing platform offers more widespread editing possibilities. The prime-editing system consists of nCas9 combined with a modified reverse transcriptase and prime-editing guide RNA (pegRNA). The pegRNA is critical for prime-editing as it directs the Cas9-reverse transcriptase protein to the designated place and provides the correct DNA template which is used to edit the genome. As a result, it is possible to perform al 12 transition and transversion mutations via prime-editing.[21]

The CRISPR/Cas9 system and related technologies can be delivered in several compositions and combinations. The Cas9 enzyme can be delivered as protein or encoded in mRNA/plasmid DNA whereas the sgRNA and or donor DNA template are delivered as nucleic acid. For therapeutic purposes, the Cas9 enzyme is preferentially delivered either as mRNA or as protein since plasmid DNA-based delivery might result in genomic integration at unwanted

locations in the genome and continuous expression may result in higher off-target effects.[13] These components need to be delivered to the cytoplasm or nucleus of the cell, depending on the form in which they are developed. Hence, they face similar challenges as RNAi- and mRNA-based therapeutics, as discussed below.

Limitations of RNA molecules as a therapeutic

It is clear that RNA therapeutics bear huge potential to alter the way in which we treat human disease. However, clinical translation of RNA therapeutics has been hampered by three important bottlenecks limiting widespread application:

1)   RNA stability 2) RNA immunogenicity 3) cytosolic RNA delivery.

For RNA therapy to succeed, RNA molecules should be resistant to nuclease degradation. Unmodified, naked RNA molecules are rapidly degraded in serum.[22] In addition, dsRNA molecules can be highly immunogenic: especially molecules >30bp of dsRNA induce a fierce type I interferon response.[23] Smaller RNA molecules are also able to activate pattern recognition receptors such as TLR3, 7 and 8 or cytoplasmic receptors as RIG-1.[24] Despite the risk of activating these RNA sensors, RNA needs to reach the cytoplasm to exert its function. To quote Steven Dowdy: *"to successfully deliver RNA-based therapeutics, we need to tackle a billion years' worth of evolutionary defenses."*[25] Since RNA molecules are large, highly charged molecules, they cannot passively cross cellular membranes. Even when RNA molecules are taken up by the cell, they are trapped in the endo-lysosomal pathway from which spontaneous escape to the cytosol is unlikely.[25]

These bottlenecks make development of effective RNA-based drugs highly challenging. It is therefore not surprising that it took more than a decade of both academic and corporate research to enable the bench-to-bedside transition of only a handful RNA therapeutics. Increased knowledge on RNA biology, RNA design and improvements in drug delivery technology led to the approval of the first RNA therapeutic in 2018: Onpattro®.[26,27]

Delivery technology as an enabler for RNA therapeutics

The main goal of drug delivery technology is to increase the therapeutic window of drugs either by decreasing side-effects or increasing therapeutic efficacy. Two major trends in RNA delivery technology can be identified. The first trend is the chemical modification of therapeutic RNA molecules: improvements in RNA chemistry have enhanced stability, reduced immunogenicity and increased specificity.[22,28–30] The second trend is the use of drug delivery vehicles such as lipid nanoparticles (LNPs), siRNA-conjugates and biologically derived nanoparticles such as extracellular vesicles or viruses to improve intracellular delivery of RNA therapeutics.[25,31–33]

Innovations in RNA chemistry to increase stability and reduce immunogenicity

By chemically modifying RNA molecules, it is possible to alleviate many drawbacks related to RNA stability and immunogenicity. In the past decades, the chemist's toolbox to modify RNA molecules has expanded considerably.

Chemical modification of RNA molecules was first pioneered for antisense oligonucleotides yielding backbone modifications such as phosphorothioate bonds and 2' ribose modifications such as 2'-O-methoxyethyl, which improved oligonucleotide stability and enhanced target affinity. Most interestingly, phosphorothioate-modified oligonucleotides are spontaneously taken up by cells.[34,35]

Quickly after the discovery of siRNA, the importance of RNA modifications for the development of RNAi-based therapeutics was also recognized.[36] Findings from the antisense oligonucleotide-field could rapidly be applied in siRNA development although this was complicated by the complex interaction of an siRNA molecule with the RNAi machinery.[37] Whether modification of an siRNA yields a functional, metabolically stable molecule depends on the modified strand and nucleotide position. This holds especially true for the antisense strand that needs to interact with a variety of proteins in order to function correctly.[38] Currently, clinical siRNAs designs can be fully modified with 2'-O-methyl and 2'-fluorine modifications on optimized positions.[29] In addition, it was found that incorporation of a destabilizing glycol nucleic acid at position 5 in the seed sequence increases specificity, thereby reducing off-target toxicity effects.[28] More recently, the importance of chemical engineering of short RNAs was confirmed in CRISPR/Cas9 therapy where chemical modification of the short, ± 120bp sgRNA molecule yielded an significant improvement in gene-editing efficiency as compared to unmodified sgRNAs.[39]

The structure of mRNA molecules is much more complex compared to siRNA/ molecules and contains various designated elements such as 5'Cap, 5' UTR, ORF, 3' UTR and a Poly (A) tail. Since therapeutic mRNA is produced via in vitro transcription (IVT) rather than chemical synthesis, which is the production method of siRNA molecules, it is difficult to specifically incorporate modified nucleobases at designated positions. Modification of mRNA is currently mainly based on incorporation of modified nucleobases, such as pseudo-uridine, 5 methylcytidine and N1-methyl-pseudouridine in defined ratios with their natural analogs. Modified nucleotides result in reduced immunogenicity and increased translational capacity of the molecule.[30,40–42]

For small oligonucleotides, chemical modification of the RNA has resulted in significant improvements in RNA stability and reduced immunogenicity. As a result, antisense oligonucleotides can be directly injected without the need of a carrier system. However, modified siRNA molecules still benefit from drug delivery technology since they are not taken up by cells in their native state. Given its large size and limited possibilities for chemical stabilization, mRNA also benefits from delivery vehicles which protect the molecule from nuclease activity, reduce immunogenicity and enhance its uptake.

Drug Delivery Technology for Intracellular Delivery of RNA therapeutics
To further capitalize on RNA therapeutics, systems need to be developed to successfully deliver RNA therapeutics to the cellular cytoplasm. RNA can be complexed either using synthetic or biological materials but can also be conjugated to a receptor ligand, all with the ultimate aim of improving its pharmacodynamic or kinetic properties. Three meaningful classes of RNA delivery technologies can be distinguished: synthetic nanoparticles, RNA-conjugates and biological

nanoparticles. Here, we will only discuss synthetic nanoparticles and biological nanoparticles, as those are the focus of this thesis.

Synthetic Nanoparticles

Synthetic nanoparticles can be based on a wide variety of materials such as polymers and lipids. Lipid-based nanoparticles are currently the most clinically advanced nanoparticles. Clinically used LNPs generally contain 4 types of lipid: an ionizable lipid (e.g. DLin-MC3-DMA), a helper lipid (e.g. DSPC/DOPE), a PEGylated lipid (e.g. PEG-DMG) and cholesterol **(Chapter 2)**. These particles are able to complex the RNA based on electrostatic interactions between the ionizable lipid and the RNA. Together with the 'helper lipid', cholesterol, and a PEG-lipid, RNA-loaded particles can be formed via different mixing methods such as T-junction mixing, ethanol injection or microfluidic mixing. These particles protect the RNA from nucleases in the serum and prevent renal excretion. Upon intravenous administration, the PEG-lipid rapidly dissociates from the particle leading to opsonization with serum proteins and uptake by target cells via endocytosis.[43] The current hypothesis is that upon acidification of the endosomes, the ionizable lipid becomes cationically charged and interacts with the anionic endosomal membrane forming non-bilayer structures leading to the release of encapsulated nucleic acids to the cytoplasm.[32]

Initial iterations of the LNP platform were hampered by low efficacy limiting their clinical viability. The discovery that the cationic lipid was the main determinant for hepatic siRNA delivery resulted in the development and screening of multiple lipid / lipid like molecule libraries which led to the discovery of lipid/lipid like polymers such as C12-200, CKK-E12, and DLin-MC3-DMA. [32,44–47] The latter lipid is currently being used in the clinical formulation Onpattro® (Patisiran) for the treatment of transthyretin amyloidosis.

Currently, the main focus of study of LNPs for RNA delivery seems to have shifted from siRNA delivery towards mRNA delivery or combined Cas9 mRNA/sgRNA delivery.[48] Given the differences in physicochemical structure between siRNA and mRNA, and the fact that lipids were initially screened and optimized for hepatic siRNA delivery, the efficacy of LNP-siRNA formulations cannot be extrapolated to other target organs and payloads such as mRNA.[49] The use of LNP-mRNA as therapeutic in for instance protein replacement therapy might require different LNP characteristics, such as the biodegradability of the lipids used in the LNP, to enable a repetitive dosing regime.[50] Current LNP development is therefore focused on identification of novel ionizable cationic lipids or LNP formulations tailored to extra-hepatic RNA delivery or the adaptation of current formulations to mRNA delivery.

Natural nanoparticles/extracellular vesicles

Extracellular vesicles (EVs) are lipid-enclosed vesicles and are considered to be intercellular communicators transporting a wide variety of bioactive molecules such as mRNA, miRNA, and proteins from cell to cell.[51] EVs, as nature's carrier of RNA, are hypothesized to be highly efficient in terms of RNA delivery efficiency, have specific, intrinsic cell targeting properties and reduced toxicity/immunogenicity compared to synthetic systems.[52–59] Therefore, the use of EVs for therapeutic RNA delivery is appealing.

The use of extracellular vesicles for RNA delivery is as a technology relative in its infancy compared to well established lipid nanoparticles and still faces many practical and methodological challenges. Evidence on horizontal RNA transfer provided by initial reports is still debated and might be insufficient to substantiate the cargo transfer hypothesis.[60–62] Moreover, landmark papers where functional transfer of RNA is shown use cargo loading techniques of which the appropriateness is still under discussion.[57,58,63]

However, recent developments on the use of EVs as carrier systems for RNA are encouraging. Via RNA transfer reporter systems, it is now possible to accurately study horizontal transfer of RNA molecules.[64] In addition, the ability to load siRNAs via endogenous loading mechanisms made it possible to study functional gene knockdown *in vivo*. When stoichiometrically compared to state-of-the-art LNPs, EVs were found to be 20-300 times more effective in delivering their RNA cargo.[53,54] These data highlight the future potential of extracellular vesicles in therapeutic RNA delivery.

Drug Delivery Technology beyond the liver?
It might be evident from clinical data that with the development of enhanced stability chemistry GalNac conjugates and LNPs, hepatic siRNA delivery has been 'tackled'.[65–67] However, for mRNA and extra-hepatic siRNA targets, this is definitely not the case. Achieving clinically relevant levels of therapeutic RNAs at extra-hepatic locations remains challenging using current delivery technology. Here further finetuning of LNPs or other carriers still can provide a clinical benefit.

OUTLINE OF THIS THESIS

In this thesis, we investigated the applicability of LNP systems for RNA delivery in cardiovascular disease. In addition, we validated a state-of-the-art high throughput methodology based on sequencing of DNA barcodes to screen the tissue distribution of multiple LNP formulations in a single animal. Finally, we took a biomimetic approach based on extracellular vesicles to improve the functional characteristics of LNP formulations.

In **Chapter 2** we reviewed how the lipid composition and structure of lipid nanoparticles affect pharmacokinetics and pharmacodynamics of LNP based RNA delivery systems. Moreover, we highlighted meaningful developments in LNP production technology and the use of LNPs for mRNA and CRISPR/Cas9 delivery.

In **Chapter 3** we showed that LNPs encapsulating multiple different siRNAs, so called siPools™, effectively silenced the expression of two enzymes belonging to the de novo ceramide synthesis pathway in mice and influenced plasma ceramide concentrations. This is highly relevant in several cardiometabolic diseases, such as non-alcoholic steatohepatitis and atherosclerosis, where increased levels of specific ceramides are thought to play a role in the pathophysiology.

In **Chapter 4** we investigated LNP-mRNA delivery to the hard-to-reach damaged myocardium after ischemia-reperfusion injury. To this end, we analyzed tissue distribution and functional delivery of mRNA in a murine model of ischemia-reperfusion injury.

In **Chapter 5** we aimed to set up and validate a high-throughput method to analyze tissue distribution of multiple different LNP formulations in a single animal. This technique makes use of short DNA barcodes which are encapsulated in LNPs. Each LNP formulation encapsulates a unique DNA barcode which can be traced and counted in organs by next generation sequencing. We aimed to validate this method in vitro and in vivo.

A relatively new 'kid on the block' in the drug delivery field are extracellular vesicles. These biological membrane vesicles are nature's carrier of RNA molecules and most likely are evolved to be more efficient at RNA delivery compared to current synthetic delivery systems. In **Chapter 6** we generated EV-liposome hybrid nanoparticles based on components of EVs and LNP. The aim was to evaluate the effect of incorporating EV components into synthetic delivery systems on cellular uptake and nucleic acid delivery. Moreover, we generated EV-liposome hybrid nanoparticles using EVs derived from cardiac progenitor cells and showed that some of the hallmark characteristics of these EVs, such as activation of endothelial cell migration, were retained in EV-liposome hybrid nanoparticles.

Finally, in **Chapter 7,** we summarized and critically reflected on the results obtained in the work described in this thesis. Moreover, we discussed current and future challenges for lipid based delivery systems.

REFERENCES

1   Morrison C. Fresh from the biotech pipeline—2017. Nat Biotechnol. 2018;36(2):131–6.

2.   Senior M. Fresh from the biotech pipeline: too much, too fast? Nat Biotechnol. 2022;40(2):155–62.

3.   de Fougerolles A, Vornlocher HP, Maraganore J, Lieberman J. Interfering with disease: A progress report on siRNA-based therapeutics. Nat Rev Drug Discov. 2007;6(6):443–53.

4.   Sahin U, Karikó K, Türeci Ö. MRNA-based therapeutics-developing a new class of drugs. Nat Rev Drug Discov. 2014;13(10):759–80.

5.   Fire A, Xu S, Montgomery MK, Kostas SA, Driver SE, Mello CC. Potent and specific genetic interference by double-stranded RNA in Caenorhabditis elegans. Nature. 1998;391(6669):806–11.

6.   Elbashir SM, Harborth J, Lendeckel W, Yalcin A, Weber K, Tuschl T. Duplexes of 21-nucleotide RNAs mediate RNA interference in cultured mammalian cells. Nature. 2001 May;411(6836):494–8.

7.   Rivas F V, Tolia NH, Song J-J, Aragon JP, Liu J, Hannon GJ, et al. Purified Argonaute2 and an siRNA form recombinant human RISC. Nat Struct Mol Biol. 2005;12(4):340–9.

8.   Elbashir SM. Functional anatomy of siRNAs for mediating efficient RNAi in Drosophila melanogaster embryo lysate. EMBO J. 2001;20(23):6877–88.

9.   Tomari Y, Zamore PD. Perspective: Machines for RNAi. Genes Dev. 2005;19(5):517–29.

10. Ameres SL, Martinez J, Schroeder R. Molecular Basis for Target RNA Recognition and Cleavage by Human RISC. Cell. 2007;130(1):101–12.

11. Bartel DP, Lee R, Feinbaum R. MicroRNAs: Genomics, Biogenesis, Mechanism, and Function. Cell. 2004;116:281–97.

12. Weissman D. mRNA transcript therapy. Expert Rev Vaccines. 2015;14(2):265–81.

13. Oude Blenke E, Evers MJW, Mastrobattista E, van der Oost J. CRISPR-Cas9 gene editing: Delivery aspects and therapeutic potential. J Control Release. 2016;244:139–48.

14. Nami F, Basiri M, Satarian L, Curtiss C, Baharvand H, Verfaillie C. Strategies for In Vivo Genome Editing in Nondividing Cells. Trends Biotechnol. Elsevier Ltd; 2018;36(8):770–86.

15. Komor AC, Badran AH, Liu DR. CRISPR-Based Technologies for the Manipulation of Eukaryotic Genomes. Cell. 2017;168(1–2):20–36.

16. Komor AC, Kim YB, Packer MS, Zuris JA, Liu DR. Programmable editing of a target base in genomic DNA without double-stranded DNA cleavage. Nature. 2016;533(7603):420–4.

17. Gaudelli NM, Komor AC, Rees HA, Packer MS, Badran AH, Bryson DI, et al. Programmable base editing of A•T to G•C in genomic DNA without DNA cleavage. Nature. 2017;551(7681):464–71.

18. Kim HS, Jeong YK, Hur JK, Kim J-S, Bae S. Adenine base editors catalyze cytosine conversions in human cells. Nat Biotechnol. 2019;37(10):1145–8.

19. Kurt IC, Zhou R, Iyer S, Garcia SP, Miller BR, Langner LM, et al. CRISPR C-to-G base editors for inducing targeted DNA transversions in human cells. Nat Biotechnol. 2020/07/20. 2021 Jan;39(1):41–6.

20. Zhao D, Li J, Li S, Xin X, Hu M, Price MA, et al. Glycosylase base editors enable C-to-A and C-to-G base changes. Nat Biotechnol. 2021;39(1):35–40.

21. Anzalone A V, Randolph PB, Davis JR, Sousa AA, Koblan LW, Levy JM, et al. Search-and-replace genome editing without double-strand breaks or donor DNA. Nature. 2019;576(7785):149–57.

22. Morrissey D V, Lockridge JA, Shaw L, Blanchard K, Jensen K, Breen W, et al. Potent and persistent in vivo anti-HBV activity of chemically modified siRNAs. Nat Biotechnol. 2005;23(8):1002–7.

23. Kleinschmidt WJ, Ellis LF, Van Fbank RM, Murphy EB. Interferon stimulation by a double stranded RNA of a mycophage in statolon preparations. Nature. 1968;220(5163):167–8.

24. Whitehead KA, Dahlman JE, Langer RS, Anderson DG. Silencing or Stimulation ? siRNA Delivery and the Immune System. Annu Rev Chem Biomol Eng. 2011;2:77–96.

25. Dowdy SF. Overcoming cellular barriers for RNA Therapeutics. Nat Biotechnol. 2017;35(3):222–9.

1

26. Alnylam Pharmaceuticals I. Alnylam Announces First-Ever FDA Approval of an RNAi Therapeutic, ONPATTRO™ (patisiran) for the Treatment of the Polyneuropathy of Hereditary Transthyretin-Mediated Amyloidosis in Adults [Internet]. 2019 [cited 2019 Jun 13]. Available from: http://investors.alnylam.com/news-releases/news-release-details/alnylam-announces-first-ever-fda-approval-rnai-therapeutic

27. Alnylam Pharmaceuticals I. Alnylam Receives Approval of ONPATTRO™ (patisiran) in Europe [Internet]. 2019 [cited 2019 Jun 13]. Available from: http://investors.alnylam.com/news-releases/news-release-details/alnylam-receives-approval-onpattrotm-patisiran-europe

28. Janas MM, Schlegel MK, Harbison CE, Yilmaz VO, Jiang Y, Parmar R, et al. Selection of GalNAc-conjugated siRNAs with limited off-target-driven rat hepatotoxicity. Nat Commun. 2018;9(723).

29. Foster DJ, Brown CR, Shaikh S, Trapp C, Schlegel MK, Qian K, et al. Advanced siRNA Designs Further Improve In Vivo Performance of GalNAc-siRNA Conjugates. Mol Ther. 2018;26(3):708–17.

30. Karikó K, Muramatsu H, Welsh FA, Ludwig J, Kato H, Akira S, et al. Incorporation of Pseudouridine Into mRNA Yields Superior Nonimmunogenic Vector With Increased Translational Capacity and Biological Stability. Mol Ther. 2008 Nov;16(11):1833–40.

31. Juliano RL. The delivery of therapeutic oligonucleotides. Nucleic Acids Res. 2016;44(14):6518–48.

32. Cullis PR, Hope MJ. Lipid Nanoparticle Systems for Enabling Gene Therapies. Mol Ther. 2017;25(7).

33. De Jong OG, Kooijmans SAA, Murphy DE, Jiang L, Evers MJW, Sluijter JPG, et al. Drug Delivery with Extracellular Vesicles: From Imagination to Innovation. Acc Chem Res. 2019;52(7).

34. Eckstein F. Phosphorothioates, essential components of therapeutic oligonucleotides. Nucleic Acid Ther. 2014;24(6):374–87.

35. Juliano RL, Ming X, Carver K, Laing B. Cellular uptake and intracellular trafficking of oligonucleotides: Implications for oligonucleotide pharmacology. Nucleic Acid Ther. 2014;24(2):101–13.

36. Manoharan M. RNA interference and chemically modified siRNAs. Nucleic Acids Symp Ser. 2003;3(1):115–6.

37. Khvorova A, Watts JK. The chemical evolution of oligonucleotide therapies of clinical utility. Nat Biotechnol. 2017;35:238–48.

38. Bramsen JB, Laursen MB, Nielsen AF, Hansen TB, Bus C, Langkjoør N, et al. A large-scale chemical modification screen identifies design rules to generate siRNAs with high activity, high stability and low toxicity. Nucleic Acids Res. 2009;37(9):2867–81.

39. Finn JD, Smith AR, Patel MC, Shaw L, Youniss MR, van Heteren J, et al. A Single Administration of CRISPR/Cas9 Lipid Nanoparticles Achieves Robust and Persistent In Vivo Genome Editing. Cell Rep. 2018;22(9):2227–35.

40. Andries O, Mc Cafferty S, De Smedt SC, Weiss R, Sanders NN, Kitada T. N1-methylpseudouridine-incorporated mRNA outperforms pseudouridine-incorporated mRNA by providing enhanced protein expression and reduced immunogenicity in mammalian cell lines and mice. J Control Release. 2015;217:337–44.

41. Karikó K, Buckstein M, Ni H, Weissman D. Suppression of RNA recognition by Toll-like receptors: the impact of nucleoside modification and the evolutionary origin of RNA. Immunity. 2005;23(2):165–75.

42. Mauger DM, Cabral BJ, Presnyak V, Su S V, Reid DW, Goodman B, et al. mRNA structure regulates protein expression through changes in functional half-life. Proc Natl Acad Sci. 2019;116(48):24075–83.

43. Akinc A, Querbes W, De S, Qin J, Frank-Kamenetsky M, Jayaprakash KN, et al. Targeted delivery of RNAi therapeutics with endogenous and exogenous ligand-based mechanisms. Mol Ther. 2010;18(7):1357–64.

44. Akinc A, Zumbuehl A, Goldberg M, Leshchiner ES, Busini V, Hossain N, et al. A combinatorial library of lipid-like materials for delivery of RNAi therapeutics. Nat Biotechnol. 2008;26(5):561–9.

45. Semple SC, Akinc A, Chen J, Sandhu AP, Mui BL, Cho CK, et al. Rational design of cationic lipids for siRNA delivery. Nat Biotechnol. 2010;28(2):172–6.

46. Jayaraman M, Ansell SM, Mui BL, Tam YK, Chen J, Du X, et al. Maximizing the potency of siRNA lipid nanoparticles for hepatic gene silencing in vivo. Angew Chem, Int Ed. 2012;51(34):8529–33.

47. Dong Y, Love KT, Dorkin JR, Sirirungruang S, Zhang Y, Chen D, et al. Lipopeptide nanoparticles for potent and selective siRNA delivery in rodents and nonhuman primates. Proc Natl Acad Sci U S A. 2014;111:3955–60.

48. Kowalski PS, Rudra A, Miao L, Anderson DG. Delivering the Messenger: Advances in Technologies for Therapeutic mRNA Delivery. Mol Ther. 2019;27(4):710–28.

49. Evers MJW, Kulkarni JA, van der Meel R, Cullis PR, Vader P, Schiffelers RM. State-of-the-Art Design and Rapid-Mixing Production Techniques of Lipid Nanoparticles for Nucleic Acid Delivery. Small Methods. 2018;2(9):1700375.

50. Sabnis S, Kumarasinghe ES, Salerno T, Mihai C, Ketova T, Senn JJ, et al. A Novel Amino Lipid Series for mRNA Delivery : Improved Endosomal Escape and Sustained Pharmacology and Safety in Non-human Primates. Mol Ther. 2018;26(6):1509–19.

51. Yáñez-Mó M, Siljander PRM, Andreu Z, Bedina Zavec A, Borràs FE, Buzas EI, et al. Biological properties of extracellular vesicles and their physiological functions. J Extracell Vesicles. 2015;4(1):27066.

52. Elsharkasy OM, Vader. Extracellular vesicles as drug delivery systems: why and how? Adv Drug Deliv Rev. 2020;159:332–43.

53. Reshke R, Taylor JA, Savard A, Guo H, Rhym LH, Kowalski PS, et al. Reduction of the therapeutic dose of silencing RNA by packaging it in extracellular vesicles via a pre-microRNA backbone. Nat Biomed Eng. 2020;4:52–68.

54. Murphy DE, de Jong OG, Evers MJW, Nurazizah M, Schiffelers RM, Vader P. Natural or Synthetic RNA Delivery: A Stoichiometric Comparison of Extracellular Vesicles and Synthetic Nanoparticles. Nano Lett. 2021 Feb 24;21(4):1888–95.

55. Hoshino A, Costa-Silva B, Shen TL, Rodrigues G, Hashimoto A, Tesic Mark M, et al. Tumour exosome integrins determine organotropic metastasis. Nature. 2015;527(7578):329–35.

56. Rana S, Yue S, Stadel D, Zöller M. Toward tailored exosomes: The exosomal tetraspanin web contributes to target cell selection. Int J Biochem Cell Biol. 2012;44(9):1574–84.

57. Alvarez-Erviti L, Seow Y, Yin H, Betts C, Lakhal S, Wood MJA. Delivery of siRNA to the mouse brain by systemic injection of targeted exosomes. Nat Biotechnol. 2011;29(4):341–5.

58. Kamerkar S, LeBlue VS, Kalluri R. Exosomes Facilitate Therapeutic Targeting of Oncogenic Kras in Pancreatic Cancer. Nature. 2017;546(7659):498–503.

59. Grapp M, Wrede A, Schweizer M, Hüwel S, Galla HJ, Snaidero N, et al. Choroid plexus transcytosis and exosome shuttling deliver folate into brain parenchyma. Nat Commun. 2013;4(2123).

60. Valadi H, Ekström K, Bossios A, Sjöstrand M, Lee JJ, Lötvall JO. Exosome-mediated transfer of mRNAs and microRNAs is a novel mechanism of genetic exchange between cells. Nat Cell Biol. 2007;9(6):654–9.

61. Pegtel DM, Cosmopoulos K, Thorley-Lawson DA, van Eijndhoven MAJ, Hopmans ES, Lindenberg JL, et al. Functional delivery of viral miRNAs via exosomes. Proc Natl Acad Sci. 2010;107(14):6328–33.

62. Somiya M. Where does the cargo go ?: Solutions to provide experimental support for the " extracellular vesicle cargo transfer hypothesis ." J cell comunnication Signal. 2020;14:135–46.

63. Kooijmans SAA, Stremersch S, Braeckmans K, de Smedt SC, Hendrix A, Wood MJA, et al. Electroporation-induced siRNA precipitation obscures the efficiency of siRNA loading into extracellular vesicles. J Control Release. 2013;172(1):229–38.

64. de Jong OG, Murphy DE, Mäger I, Willms E, Garcia-Guerra A, Gitz-Francois JJ, et al. A CRISPR-Cas9-based reporter system for single-cell detection of extracellular vesicle-mediated functional transfer of RNA. Nat Commun. 2020;11:1113.

65. Nair JK, Attarwala H, Sehgal A, Wang Q, Aluri K, Zhang X, et al. Impact of enhanced metabolic stability on pharmacokinetics and pharmacodynamics of GalNAc – siRNA conjugates. Nucleic Acids Res. 2017;45(19):10969–77.

66. Nair JK, Willoughby JLS, Chan A, Charisse K, Alam R, Wang Q, et al. Multivalent N - Acetylgalactosamine-Conjugated siRNA Localizes in Hepatocytes and Elicits Robust RNAi-Mediated Gene Silencing. J Am Chem Soc. 2014;136:16958–61.

67. Setten RL, Rossi JJ, Han S. The current state and future directions of RNAi-based therapeutics. Nat Rev Drug Discov. 2019;18:421–46.

1

State-of-the-art design and rapid-mixing production techniques of lipid nanoparticles for nucleic acid delivery

Martijn J.W. Evers[1], Jayesh A. Kulkarni[2], Roy van der Meel[1,2], Pieter R. Cullis[2], Pieter Vader [1,3], Raymond M. Schiffelers[1]*

[1] Department of Clinical Chemistry and Haematology, University Medical Center Utrecht, Utrecht, The Netherlands
[2] Department of Biochemistry and Molecular Biology, University of British Columbia, Vancouver, British Columbia, Canada
[3] Department of Experimental Cardiology, University Medical Center Utrecht, Utrecht, The Netherlands

2

ABSTRACT

Lipid nanoparticles (LNPs) are currently the most clinically advanced non-viral carriers for the delivery of short interfering RNA (siRNA). Free siRNA molecules suffer from unfavorable physicochemical characteristics and rapid clearance mechanisms, hampering the ability to reach the cytoplasm of target cells when administered intravenously. As a result, the therapeutic use of siRNA is crucially dependent on delivery strategies. LNPs can encapsulate siRNA to protect it from degradative endonucleases in the circulation, prevent kidney clearance, and provide a vehicle to deliver siRNA in the cell and induce its subsequent release into the cytoplasm. Here, the structure and composition of LNP-siRNA are described including how these affect their pharmacokinetic parameters and gene-silencing activity. In addition, the evolution of LNP-siRNA production methods is discussed, as the development of rapid-mixing platforms for the reproducible and scalable manufacturing has facilitated entry of LNP-siRNA into the clinic over the last decade. Finally, the potential of LNPs in delivering other nucleic acids, such as messenger RNA and CRISPR/Cas9 components, is highlighted alongside how a design-of-experiment approach may be used to improve the efficacy of LNP formulations.

INTRODUCTION

The efficient delivery of nucleic acids to target cells *in vivo* is challenging due to their rapid degradation in biological media and rapid clearance from the circulation. In order to exert their function, nucleic acids are required to reach their target tissue within the body without alterations to their relatively complex structure (and sequence), and subsequently, the cytosol and/or nucleus of target cells. As free nucleic acids are rapidly degraded by endonucleases and cleared by the kidney, reaching the target site as a functional molecule is unlikely.[1] Therefore, delivery systems are required to truly capitalize on the therapeutic potential of nucleic acid payloads. Lipid nanoparticles (LNPs) represent the most clinically advanced nonviral vectors for delivery of therapeutic small interfering RNA (siRNA).[2] Recently, an LNP-siRNA formulation for the treatment of transthyretin-induced amyloidosis (Patisiran) met all primary and secondary endpoints in a Phase-III clinical trial.[3] The sponsor (Alnylam Pharmaceuticals) applied for market access in late 2017 which will, if approved, mark the first LNP-siRNA therapeutic.[4] Additionally, LNPs encapsulating siRNA treating other liver diseases have entered the clinic and are in Phase-I/II trials **(Table 1).**[2] Alongside LNP-siRNA development, formulations for the delivery of messenger RNA (mRNA) have also reached clinical stages. The ongoing trials with various nanoparticle formulations are outlined in Table 1.

Table 1. Currently active clinical trials (November 2017) lipid nanoparticles/liposomes encapsulating nucleic acids

Drug name	Nucleic acid	Disease	Phase	ClinicalTrial.gov identifier
Liposomal Grb2	Antisense Oligonucleotide	Cancer	I	NCT02923986, NCT02781883, NCT01159028
MTL-CEBPA	siRNA	Cancer	I	NCT02716012
siRNA-EphA2-DOPC	siRNA	Cancer	I	NCT01591356
DCR-PH1	siRNA	Primary Hyperoxaluria 1	I	NCT02795325
ARB-1467	siRNA	Chronic Hepatitis B infection	II	NCT02631096
mRNA-1325	mRNA	Zika	I/II	NCT03014089
mRNA-1440 / VAL-506440	mRNA	Influenza A /H10N8	I	NCT03076385
mRNA-1851	mRNA	Influenza A /H9N7	Not disclosed	ND
mRNA-2416	mRNA	Cancer	I	NCT03323398
SGT-53	pDNA	Cancer		NCT02340156, NCT02354547, NCT02340117
JVRS-100	pDNA	Cancer	I	NCT00860522

Functionally, siRNAs enable specific silencing of virtually any gene in the human genome via a mechanism referred to as RNA interference.[5–7] After reaching the cytoplasm, siRNA interacts with the RNA-induced silencing complex (RISC). The siRNA molecule is loaded into the

argonaute 2 protein and unwound, after which the sense strand is discarded leaving the antisense strand loaded in the RISC.[8] mRNA with a complementary sequence to the antisense strand is degraded by the RISC complex resulting in decreased expression of the protein encoded by the target mRNA.[9] The broad therapeutic applicability of siRNA is evident by ×20 ongoing clinical trials for the treatment of different types of cancer, liver fibrosis and hypercholesterolemia.[10] In contrast to the effect of siRNA molecules, administration of mRNA or plasmid DNA (pDNA), encoding a specific protein, could potentially lead to the (transient) overexpression of that protein.[11] In addition, administration of the genome-editing system "clustered regularly interspaced palindromic repeats" (CRISPR)/Cas9 could either lead to specific gene knockdown or to insertion of a specific gene sequence at a locus determined by the short-guide RNA (sgRNA) sequence (see Section 4.3).[12]

Over the years, a number of vehicles have been developed to enable the therapeutic application of siRNA. Several classes of nanoscale drug delivery vehicles can be defined, such as LNPs, polymeric nanoparticles and different types of conjugates (e.g. dynamic polyconjugates and N-acetylgalactosamine conjugates). Excellent reviews have been written on these vehicles and conjugates.[13–16] Here, we focus on the LNP formulations composed of four different lipid types: an ionizable amino-lipid or cationic lipid, a helper lipid, cholesterol and a poly(ethylene glycol) (PEG)-lipid.[17] Of particular interest is the development of specialized ionizable amino-lipids that are tailored to the delivery needs of the siRNA molecule, such as intracellular trafficking to the cytoplasm, which has resulted in enhanced activity of LNP-siRNA.[18,19] At the same time, the development of rapid-mixing methods has facilitated the clinical translation and commercial success of LNPs.[2] Using rapid-mixing methods such as a staggered herringbone mixer (SHM), a uniform population of LNPs could be produced while achieving near 100% entrapment of the siRNA at small to large scale.[20,21]

A vast amount of work has been performed on the development of LNP-siRNA for therapeutic applications, and as such, here, we will focus on the design, composition and formulation of LNP-siRNA systems with frequent references to nanoparticles encapsulating other nucleic acids such as mRNA, pDNA and CRISPR/Cas9 components including sgRNA. We further highlight the advantages and disadvantages of various conventional and rapid-mixing production methods.

DESIGN PRINCIPLES FOR LIPID NANOPARTICLES FOR SIRNA DELIVERY

From Liposomes to Lipid Nanoparticles

Liposomes were initially developed in the 1960s by Alec Bangham.[22] Since then, a vast amount of work has been performed to develop liposomes as drug carriers. Liposomes can act as a carrier of a wide variety of therapeutic molecules, ranging from small-molecule drugs to large proteins and nucleic acids.[23–26] They can shield therapeutic agents from degradative enzymes, improve their pharmacokinetic profile, enhance drug targeting towards specific tissues and/ or avoid tissues that are prone to side effects.[27] In the context of nucleic acids, these systems

have to fulfil two roles, namely efficient entrapment of nucleic acids and intracellular delivery of the payload. We broadly define entrapment/encapsulation efficiency as the sequestration of the nucleic acids from the external environment sufficiently to protect its structure and function. Complexation efficiency only considers the ability of the vector to interact with the nucleic acid

Initial work on neutral liposomes for the delivery of oligonucleotides was hampered by low encapsulation efficiencies.[28] With the development of cationic lipids, the charge interaction between the anionic nucleic acid and the cationic lipid improved the encapsulation of nucleic acids. Liposomes were produced using a thin-lipid film evaporation method and an encapsulation efficiency ranging from ≈30% to 40% was observed.[28,29] Buyens *et al.* reasoned that if the cationic lipid is equally distributed among the bilayer, the encapsulation efficiency should maximally approach 50% since only half of the cationic lipid complexed with siRNA is located in the interior core of the liposome leaving the other half exposed at the surface of the liposome.[29] The presence of 40% ethanol when hydrating the lipid film with antisense oligonucleotides dissolved in citrate buffer at 65 °C resulted in an improved encapsulation efficiency of ≈70%.[28] A simplification of this method involved mixing lipids dissolved in ethanol with a solution of antisense oligonucleotides in citrate buffer (pH 4.0) at a ratio of 2:3 (v/v, ethanol/aqueous) at 65 °C. The resulting liposomes were large unilamellar vesicles or small multilamellar vesicles depending on the antisense oligonucleotide-to-lipid ratio used.[28] More recently, greater control was achieved over the mixing process when performed by T-junction mixing,[30–32] microfluidic mixing using a SHM,[21,33] or microfluidic hydrodynamic focusing (MHF) [34] (see section 4). Depending on the lipid formulation, nucleic acid payload, and production method, particles containing an electron-dense core were produced for T-junction mixing and SHM with reported encapsulation efficiencies > 90%.[33,35] These observations suggested that the particle morphology was not that of a traditional liposome characterized by a lipid bilayer surrounding an aqueous core, but rather a particle characterized by an electron-dense core, referred to as LNPs (**Figure 1).** For LNPs, it is assumed that almost all cationic/ionizable lipids are located at the interior core of the particle, yielding high encapsulation efficiencies.[33]
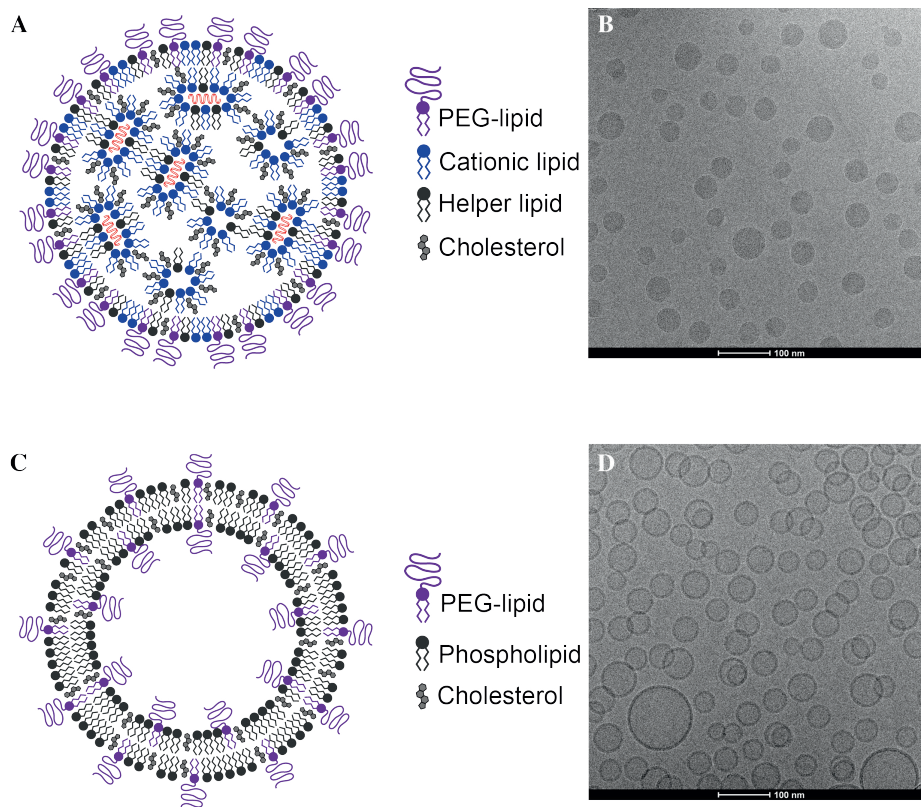
Figure 1: Structure of LNP-siRNA as compared to liposomes. A,B) The proposed structure of LNP-siRNA formulations containing ionizable amino-lipids within **A)** inverted micellar structures surrounding siRNA (in red) and **B)** the corresponding cryo-TEM image. The electron-dense core structure observed in the LNP-siRNA is likely the result of electron diffraction from lipid and nucleic acid within the particle. **C,D)** In contrast, liposomal formulations (depicted in (C)), contain an aqueous core with electron-densities consistent with the exterior of the liposome.

Here, we define particles with a unilamellar lipid bilayer and aqueous core as liposomes, whereas particles comprising other structures are referred to as LNPs, unless particles can obviously be qualified as other well-defined structures such as cubic-phase particles. The physicochemical properties of LNPs play a profound role when dealing with barriers they encounter in the body, such as renal filtration, degradation by endonucleases, opsonization, and removal by the mononuclear phagocytes, extravasation, cellular uptake, and endosomal escape[36,37]. It is therefore important to understand which physicochemical properties define the performance of LNPs and how these characteristics contribute to overcoming biological barriers for nucleic acids. In general, the following physicochemical properties of LNPs are considered to be important: lipid composition, surface properties, size, and size distribution.[14,36,37] These parameters are critical to the design and function of nanoparticles.

The Lipid Composition and Surface Properties of LNP-siRNA

The lipid composition of LNPs can influence particle size, particle morphology, encapsulation efficiency, and surface properties. The most efficient LNPs used for hepatic gene silencing in the clinic contain four types of lipids: an ionizable amino-lipid (e.g., dilinoleylmethyl-4-dimethylaminobutyrate, DLin-MC3-DMA), a helper lipid (e.g., 1,2-distearoyl-*sn*-glycero-3-phosphocholine, DSPC), a PEG lipid (e.g., 1,2-dimyristoyl-*sn*-glycerol, methoxypolyethylene glycol, PEG-DMG) and cholesterol[17] (**Figure 2**). The role of these individual lipids are discussed below.
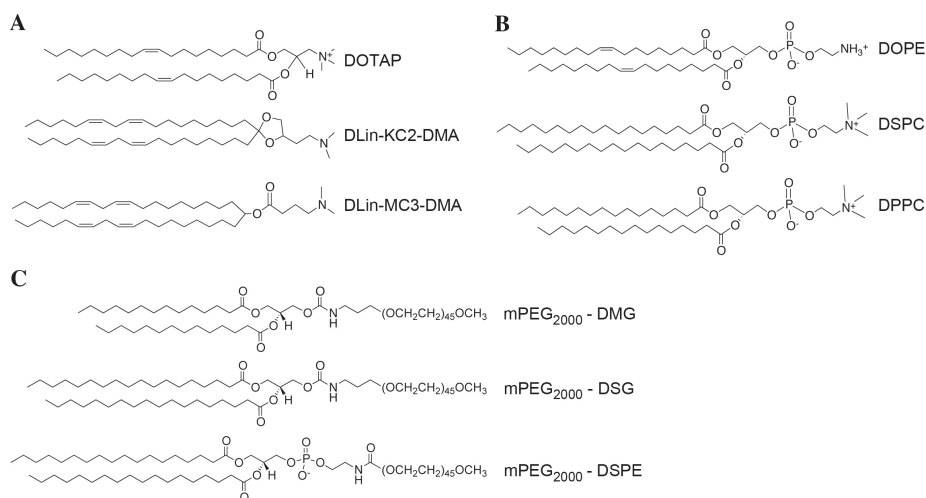

Figure 2: A-C) Structures of commonly reported A) cationic and ionizable amino-lipids, B) helper lipids, and C) PEGylated lipids

Development of Potent Ionizable Amino-Lipids

Ionizable amino-lipids are characterized by a functional group in the polar moiety of the lipid molecule with an acid-dissociation constant (pK_a) generally below 7.0.[6,18] At physiological pH (≈7.4) these lipids are largely neutral, and at acidic pH (< 6.0) they are positively charged. Ionizable amino-lipids are designed to serve two purposes: the first is the entrapment of nucleic acids at acidic pH allowing high encapsulation efficiencies, yet at physiological pH maintaining a neutral surface charge. For *in vivo* purposes, the neutral surface charge is preferred over the use of permanently charged cationic lipids such as 1,2-dioleoyl-3-trimethylammonium-propane (DOTAP) to prevent nonspecific adsorption of negatively charged biomolecules.[38] The second role is to facilitate endosomal escape. The cationic lipid interacts with the anionic endosomal membrane, which might result in the formation of a nonbilayer hexagonal (H$_{II}$) phase temporarily destabilizing the endosomal membrane leading to the release of the payload.[39,40] The most potent ionizable amino-lipids formulated in LNPs for *in vivo* applications have an apparent pK_a

around 6.2-6.5, as they display an optimal balance between the neutral charge in circulation and a strong positive charge at endosomal pH.[19]

In recent years, considerable effort has been made to elucidate the relationship between the molecular structure of ionizable amino-lipids and the *in vivo* gene-silencing activity of LNP-siRNA incorporating these lipids, especially in hepatocytes.[18,19] The lipid-tail saturation, the type of linker between the lipid tail and polar head group, and the pK_a of the lipid have been found to affect hepatic gene silencing.[18,19,41] In 2005, lipids containing 2 *cis* double bonds (1,2-dilinoleyloxy-*N,N*-dimethyl-3-aminopropane, (DLin-DMA)) showed improved gene silencing over lipids containing 0, 1 or 3 *cis* double bonds (1,2-distearyloxy-*N,N*-dimethyl-3-aminopropane, 1,2-dioleyloxy-*N,N*-dimethyl-3-aminopropane, and 1,2-dilinolenyloxy- N,N-dimethyl-3-aminopropane, respectively) in an *in vitro* model of luciferase expressing Neuro2A-G cells.[41] The underlying basis for the difference in activity was suggested to be the increased ability of the unsaturated lipid to form the inverted hexagonal (H$_{II}$) phase with the anionic endosomal membrane leading to destabilization of the membrane and release of the siRNA.[39,40]

Semple et al. determined preferences within the structure of the lipid head group and linker between the lipid head group and alkyl chain.[18] Several linkers, namely ester-, alkoxy-, and ketal-linkers, between the lipid head group and alkyl chain using 1,2-dilinoleoyl-3-dimethylaminopropane (DLin-DAP), DLin-DMA and 2,2-dilinoleyl-4-dimethylaminomethyl-[1,3]-dioxolane (DLin-K-DMA), respectively, were evaluated for *in vivo* silencing activity in a murine factor VII (FVII) model[42] by measuring the amount of residual FVII in serum 24 h after injection of LNP-siRNA.[18] The observed potency of the ionizable amino-lipids was DLin-K-DMA > DLin-DMA > DLin-DAP, suggesting that for these ionizable amino-lipids, incorporation of a ketal linker was superior over other linkers tested. By addition of methylene groups to the linker, it was seen that the contribution of a single methylene group (2,2-dilinoleyl-4-(2-dimethylaminoethyl)-[1,3]-dioxolane, (DLin-KC2-DMA)) showed a fourfold increase in activity over DLin-K-DMA.[18] The apparent pK_a of the lipid formulated in an LNP was shown to be a critical factor for determining the potency. Of all lipids screened, the most potent formulation was based on the ionizable amino-lipid DLin-MC3-DMA with an apparent pK_a of 6.44.[19] At the same time, it was observed that optimization of the lipid formulation itself, i.e., the molar ratio between the different lipids used in the LNP influenced the observed metric for LNP potency (the effective dose to achieve 50% gene silencing or ED$_{50}$). For a formulation composed of DLin-MC3-DMA/DSPC/cholesterol/PEG-lipid at 40/10/40/10 mol%, the observed ED$_{50}$ was 0.03 mg per kg bodyweight, whereas the same formulation at 50/10/38.5/1.5 mol% had an ED$_{50}$ of 0.005 mg per kg bodyweight.[19] The structure of several cationic and ionizable amino-lipids are shown in **Figure 2** and **Table 2,** respectively.

Table 2. Characteristics of several LNPs based on cationic/ionizable amino-lipids. Lipid composition is displayed as a molar ratio of "cationic/ionizable amino-lipid"/DSPC/cholesterol/PEG-C14

Lipid	Composition	Production method	Apparent pK_a	ED50 [mg kg^{-1}]	Year of development	Author[Ref.]
DLinDAP	40/10/40/10	Preformed vesicle method	6.2 ± 0.05	40-50	2010	Semple et al.[18]
DLinDMA	40/10/40/10	Preformed vesicle method	6.8 ± 0.1	1	2005	Heyes et al.[41]
DLin-KC2-DMA	40/10/40/10	Preformed vesicle method	6.7 ± 0.08	0.1	2010	Semple et al.[18]
DLin-MC3-DMA	40/10/40/10	Preformed vesicle method	6.44	0.3	2012	Jayaraman et al.[19]
DLin-MC3-DMA	50/10/38.5/1.5	Preformed vesicle method	6.44	0.005	2012	Jayaraman et al.[19]
C12-200	50/10/38.5/1.5	T-junction		0.01	2009	Love et al.[44]
cKK-E12	50/10/38.5/1.5	T-junction		0.002	2014	Dong et al.[43]

Concurrently, a combinatorial-chemistry approach led to the discovery of several other lipid-like molecules (LLM) such as C12-200 and cKK-A12.[42–45] The efficacy of particles formulated with the latter lipid for hepatic gene silencing seems to be in a similar range when compared to DLin-MC3-DMA. Similarly, Harashima and co-workers developed ionizable lipids such as YSK-05 and YSK13-C3.[46,47] The ED$_{50}$ of siRNA against FVII formulated in a particle containing YSK13-C3/cholesterol/PEG-DMG (68/29.1/2.9 mol%) was reported to be 0.015 mg kg^{-1} in mice.[46]

Helper Lipids and Cholesterol

1,2-Dioleoyl-*sn*-glycero-3-phosphoethanolamine (DOPE) was one of the first helper lipids used for the delivery of nucleic acids using cationic liposomes. DOPE has unsaturated acyl chains and a relatively small head group resulting in a conical shape.[14] DOPE is often referred to as a fusogenic lipid since it has the intrinsic ability to form the H$_{II}$ phase.[48,49] The presence of DOPE in cationic lipid formulations enhances their transfection efficacy by promoting membrane fusion.[39,50–52] On the other hand, Cheng and Lee suggested it decreases the colloidal stability of particles containing DOPE designed for the delivery of siRNAs.[53]

Currently, DSPC is often used as the helper lipid in LNP-siRNA, although the functional role is not well understood.[32] DSPC has saturated acyl chains and a large head group. This results in a cylindrical geometry and strongly supports bilayer formation.[54] Thus, it is thought that DSPC stabilizes the LNP.[33] When DSPC was substituted with DOPE in formulations containing 40% ionizable lipid, the *in vitro* gene-silencing efficiency decreased, indicating DSPC's importance for gene-silencing activity of these particles.[55] It is remarkable that addition of the fusogenic lipid DOPE led to a decrease in gene-silencing efficacy since, based on DOPE's fusogenic character and results obtained for other formulations containing DOPE, the opposite may have been expected. It was observed that the uptake of particles containing DOPE was decreased, although this only partly explained the difference in silencing efficacy.[55] The field would greatly benefit

from enhanced insight in such observations. Additionally, computer modelling revealed that DSPC might be involved in an interaction with siRNA.[33] Increasing the amount of DSPC in an LNP-siRNA formulation from 10 to 30 mol% at the expense of the ionizable amino-lipid resulted in the formation of lamellar structures at the outer membrane layer.[56] These data indicated that high mol% of DSPC can interfere with the inverted micellar structure observed in some LNP formulations.

Cholesterol is a major component of eukaryotic membranes[57]. Cholesterol can influence the lipid packing, membrane fluidity, and permeability of the bilayer. This has obvious implications for model membrane systems. For example, it was shown that a lipid bilayer of pure dimyristoylphosphatidylcholine in its fluid state became more condensed after incorporation of cholesterol. Incorporation of cholesterol decreased the surface area per lipid in what is known as the "condensation effect", and this depended on the lipid formulation and temperature. [58] Moreover, as a result of a tighter lipid packing, membrane permeability was reduced.[59,60] In vivo, it was shown that cholesterol influenced the pharmacokinetics of liposomes; pure DSPC liposomes had a circulation half-life of seconds in CD-1 mice. Incorporation of 30 mol% cholesterol increased the circulation half-life of DSPC liposomes to ≈5h. A further increase to 40 or 50 mol% cholesterol did not improve circulation half-life.[61]

Early research on the behavior of cholesterol in liposomes indicated cholesterol can exchange between lipid bilayers to equilibrate across a concentration gradient, if present.[62,63] It could therefore be reasoned that incorporation of equimolar concentrations of cholesterol, compared to endogenous membranes, would not lead to a net loss or gain of cholesterol, thereby helping to maintain particle integrity. In addition, it was also hypothesized that cholesterol restricts the diffusion of phospholipids to high-density lipoproteins in a concentration-dependent manner,[64] thereby improving particle stability in vivo. LNP-siRNAs have a hypothesized structure deviating from the typical bilayer structure. Therefore, it is questionable if the functional influences of cholesterol observed in liposomes equally apply for LNPs.

Data on the structural and functional role of cholesterol in LNP-siRNA formulations are limited. An interesting experiment by Leung et al. in 2015 showed that progressive replacement of cholesterol with DLin-KC2-DMA resulted in decreased entrapment and an increase in particle size. This observation suggested that an extremely large molar fraction of DLin-KC2-DMA inhibits the packing of lipids in a manner that supports entrapment.[56]

PEG-lipids

An important milestone for the clinical use of LNPs in the delivery of nucleic acids is the development of PEG-lipids. PEG-lipids shield the LNP surface thereby protecting them against opsonins and uptake by the mononuclear phagocyte system, as well as preventing their aggregation in the circulation.[65] Moreover, PEG-lipids prevent aggregation during production and storage, and their incorporation can dictate LNP size.[21,66] These two functions serve to increase the overall stability of the LNP, but in doing so, potentially decrease apolipoprotein E (ApoE) adsorption to LNPs, and particle fusogenicity, both of which are paramount to achieving LNP transfection of hepatocytes.[67–70] In order to find an optimal balance in this so-called "PEG-dilemma"[71,72] a variety of "diffusible" PEG -lipids were developed.[73,74] PEG-lipids

containing shorter acyl chains (e.g., C8-14) have been found to diffuse out of the LNP more rapidly compared to the longer counterparts (e.g ., C16-24) in the presence of a lipid sink (i.e., plasma lipoproteins).[69,73,74]

In 1998, a set of PEG-ceramide conjugates was developed by Webb et al.[73] It was shown that the circulation time of egg sphingomyelin/cholesterol liposomes could be tuned using different ceramide anchors attached to the PEG-moiety. PEG-ceramide C20 (PEG-C20) and PEG-ceramide C24, but not PEG-ceramide C8 (PEG-C8) or PEG-ceramide C14 (PEG-C14), were found to significantly extend the circulation time of the particles. In 2005, an analogous set of PEG-diacylglycerols was synthesized, and their effect on the pharmacokinetic profiles of LNP was found to be similar to PEG-ceramides.[74] PEG-diacylglycerols were considered superior over PEG-ceramides due to the straightforward synthesis.[74] Despite longer circulation of particles with PEG-C20 or poly(ethylene glycol)-1,2-distearoyl-*sn*-glycero-3-phosphoethanolamine (PEG-DSPE) after a single injection, repeated administration led to an immune response leading to decreased particle circulation levels, which was not observed for PEG-C14.[75] When mice were injected weekly with liposomes, it was revealed that an increased antisense-oligonucleotide-to-lipid ratio resulted in a more severe immune response as observed after the second injection. Above a ratio of 0.08 (w/w), a rapid decrease in carrier circulation levels 1 h post injection was observed. This immune-mediated phenomenon was not observed for PEG-C14 LNPs encapsulating antisense oligonucleotides and empty DPSC/Chol liposomes. This indicated that the presence of PEG-C20/PEG-DSPE in antisense oligonucleotide particles resulted in a rapid immune response after repeated administration.[75] Currently, PEG-diacylglycerols (PEG-DMG with C14 acyl chains) are still used as the PEG-lipid in clinical LNP-siRNA systems.

For LNP-siRNA, the dissociation of different PEG-lipids (C14, C16, and C18) from the particle was correlated to the pharmacokinetic profile and transfection efficacy of the particles.[69] The dissociation rate of the PEG-lipid from the LNP was, in particular, correlated to the length of the acyl chain. PEG-C14, -C16, and -C18 were found to desorb from the LNP *in vivo* at a rate of 45%, 1.3%, and 0.2% hour[-1], respectively.[69] Interestingly, when mice were administered with LNPs containing these PEG-lipids, the circulation half-life of the particles containing C16 and C18 acyl chain PEG –lipids was greater than particles with C14 acyl chain PEG-lipids. Within 4 hours, ≈55 % of the LNPs containing PEG-C14 accumulated in the liver. For LNPs containing PEG-C16 and C18, maximally 35% and 25%, respectively, accumulated in the liver and these maxima were reached at a later time point compared to PEG-C14. Not surprisingly, for extra hepatic targets such as tumors, longer circulating LNPs using PEG-C18 are used to improve tissue accumulation.[76]

When the LNPs containing different PEG-lipids were tested for hepatic gene silencing in the murine FVII model, no difference in gene silencing was observed between particles containing up to 1.5 mol% of PEG-lipid. Particles formulated with >1.5 mol% PEG-C14 retained their gene-silencing activity whereas the activity of particles containing >1.5 mol% PEG-C18 decreased. This effect was suggested to correspond with the PEG-coverage; at >1.5% of PEG, the surface of the LNP is fully covered with PEG, whereas at 1.5 mol% and lower, this is not the case.[69] When > 1.5% PEG is used, the more rapid dissociation of PEG-C14 ensures that the surface is exposed more readily than when C18 is used. When the surface of a particle containing ionizable amino-lipids

is gradually exposed, it is opsonized by ApoE. Subsequent uptake of the particle is mediated by ApoE-dependent uptake via the low-density lipoprotein receptor.[70] The importance of ApoE adsorption for the efficacy of LNPs containing an ionizable lipid was illustrated using ApoE knockout mice (ApoE -/-). When LNPs encapsulating an siRNA against FVII were administered to both wild type (WT) and ApoE -/- mice, the gene silencing was attenuated in the latter. When LNPs were pre incubated with various concentrations of ApoE, the gene-silencing activity was rescued in a ApoE dose-dependent manner.[70] The opposite was observed for particles designed for tumor accumulation. Increasing the amount of PEG-C18 from 2.5 to 5.0 mol% resulted in elongated circulation times and an increased accumulation in tumor tissue.[76] This highlights how, by altering the PEG anchor and density, LNP pharmacokinetics and tissue distribution may be tuned for specific applications.

Nitrogen-to-phosphate (N/P) Ratio

An important aspect of LNP-siRNA design is the ratio of elemental nitrogen and phosphate (N/P-ratio). This ratio describes the charge interaction between the cationic charge of the amino (N^+) group in the ionizable amino-lipid to anionic charge of the phosphate (PO_4^-) groups in the backbone of nucleic acids and is the basis of the complexation of siRNA with the ionizable amino-lipid. Patisiran is generated at N/P = 3 with 1.5 mol% PEG-lipid (resulting in a particle size of ≈50 nm). When 30 nm LNP-siRNA containing 50 mol% of the ionizable amino-lipid 3-(dimethylamino)propyl(12Z,15Z)-3-[(9Z,12Z)-octadeca-9,12-dien-1-yl]henicosa-12,15-dienoate and 5 mol% PEG-DMG were formulated at N/P ratios of 1-12, modest changes to the N/P (up to 6) improved the achieved ED_{50} from 1.15 mg kg^{-1} at N/P = 1 to 0.45. At higher N/P values, no further improvement in gene silencing was observed.[66] Chen et al. suggested that this was an indication that additional ionizable amino-lipids, which do not interact with the encapsulated siRNA, should be available to enhance endosomal escape.[66]

Size

Size is regarded as an important physicochemical parameter that affects the *in vivo* behavior of LNPs.[36,37] LNP diameter size, here, is displayed as a *Z*-average measured by dynamic light scattering (DLS), unless stated otherwise. Size influences the pharmacokinetic profile of LNPs, as smaller particles display longer circulation times and slower clearance from the bloodstream. [77] Previous reports in CD-1 mice have indicated that LNP size for hepatic gene silencing should be limited to sub-100 nm particles since these nanoparticles can readily pass the liver fenestrae, enter the space of Disse, and interact with hepatocytes.[66,78]

The development of rapid-mixing methods has improved the ability to produce homogeneous particles, thereby enabling the study of particle size on pharmacokinetic behavior as size distributions are more uniform.[20,21,33,79] Andar et al. were able to produce relatively monodisperse liposome populations of ≈40 nm, ≈72 nm, ≈98 nm, ≈162 nm and ≈277 nm without overlapping size distributions as measured by asymmetric flow field-flow fractionation (AF^4) in line with multiangle laser light scattering and quasi-electric light scattering (QELS).[79] It was shown that uptake of 1,2-dipalmitoyl-sn-glycero-3-phosphocholine(DPPC)/cholesterol/dipalmitoylphosphatidylethanolamine- PEG2000 (50/40/10 mol%) liposomes by

Caco-2 cells showed size-dependent trends, whereby the cells favored smaller (≈40 nm) over larger particles (>98 nm). Although these experiments were not performed using LNP-siRNA, these data illustrate that particle uptake can be influenced by size. Moreover, the endocytic processing differed based on particle size. Endocytosis of 40 nm LNPs was shown to be mainly dynamin dependent, whereas particles larger than 98 nm were influenced mainly by the clathrin-dependent pathway,[79] although it must be noted that clathrin-dependent endocytosis also critically depends on dynamin,[80] making it difficult to draw strong conclusions from these observations. The uptake mechanism is of importance as the intracellular processing of nanoparticles can be influenced by the uptake pathway.[81–83] For LNP-siRNA containing the ionizable lipid DLin-MC3-DMA, two uptake pathways were shown to be active: clathrin-mediated endocytosis and macropinocytosis. It was observed that the majority of the gene-silencing effect resulted from particles taken up via macropinocytosis.[83] This indicates that the route of uptake has consequences for the efficacy of LNPs. Moreover, as shown for LNP-siRNA, the escape of siRNA to the cytoplasm only occurred at a low rate and in a specific part of a cellular trafficking pathway.[83,84]

The hepatic gene silencing of FVII in mice using 27, 38, 43, 78, and 117 nm sized LNP-siRNAs (as measured by DLS, number-weighted) was investigated by Chen et al.[66] The gene silencing of FVII was strongly dependent on particle size. The hepatic gene silencing of 38-78 nm sized particles was far more efficient compared to particles of 117 or 27 nm with the 78 nm sized particles showing maximal gene silencing. It was suggested that the large 117 nm particles were unable to pass through the fenestrations (≈100 nm) in the liver vasculature, resulting in a less potent formulation. For the smaller 27 nm particles, the decrease in efficacy was shown to correlate to a decreased particle stability in serum. When the pharmacokinetic profiles of 27, 43, and 78 nm particles were evaluated, liver accumulation was substantially affected by size, favoring smaller 27 and 43 nm particles over 80 nm particles.[66] In addition, the size-dependent stability of nanoparticles influenced the *in vivo* efficacy of the nanoparticles. In smaller LNPs, the ionizable amino-lipid more rapidly dissociated from the particles, resulting in lower gene-silencing efficiency. When smaller particles (e.g., 27 nm) were formulated at a higher N/P-ratio of 6, improvements in transfection efficacy were seen compared to particles formulated at an N/P ratio of <3. The decrease in gene-silencing potency of smaller particles (27 nm) could not solely be ascribed to a decreased content of ionizable amino-lipid.[66] A major confounding factor in this study could be the amount of PEG-DMG lipid in the particle. The size of the particles was tuned by varying the amount of PEG-lipid within a particle. Particles of 30 nm contained ≈5 mol% PEG-DMG whereas particles of 80 nm contained ≈0.5 mol% PEG-DMG. It is known that these LNPs are taken up via ApoE-dependent endocytosis and that PEGylation prevents ApoE from binding to the particle, thereby possibly influencing the gene silencing. An additional explanation could be the decreased siRNA payload per particle for the 30 nm particle compared to the 80 nm particle.[66]

Taken together, these studies show the impact of various design parameters, such as lipid composition and size, on LNP-siRNA pharmacokinetics and (hepatic) gene-silencing efficacy. Future research could be aimed at reaching targets beyond the liver by exploiting the multitude of possibilities offered by the LNP platform.

PRODUCTION OF LIPOSOMES AND LIPID NANOPARTICLES

Liposomes and LNPs can be produced using several methods. First, we shortly discuss the characteristics of the most commonly reported conventional ones: lipid-film hydration followed by extrusion, sonication, or homogenization methods, and ethanol injection. For in-depth information on these, the reader is referred to the reviews and excellent book chapters written on (conventional) liposome production.[85–89] Second, we describe three more recent methods based on the principle of the ethanol-injection method: in-line T-tube mixing, MHF, and SHM.

Conventional Methods for the Production of Liposomes

Thin Film-Hydration and Size-Reduction Techniques

The thin-film hydration method is a common manufacturing method for the production of liposomes and is considered a top-down approach where large lipid vesicles are re-formed to small vesicles using high-energy size-reduction methods.[85] Lipids are dissolved in an organic solvent (e.g., chloroform) and transferred to a steel production vessel or round-bottom flask. The organic solvent is removed in vacuo resulting in a lipid film on the surface of the vessel or flask. Upon hydration with an aqueous solution, large multilamellar vesicles are formed. This population of vesicles is very heterogeneous and the size distribution is centered around several micrometers in size.[85,88] Size-reduction steps, such as extrusion or sonication, are generally used to generate small unilamellar vesicles. Extrusion is the process of repeatedly forcing a heterogeneous suspension of particles through a polycarbonate or inorganic filter of a designated pore size (e.g., 0.1 µm). This results in a population of unilamellar vesicles, with sizes in the range of the size of the pores.[85,90] Sonication is an alternative method to reduce particle size using a probe sonicator or bath sonicator**.** For probe sonication, the tip is placed in a dispersion of multilamellar vesicles.[88,91,92] The size of the particles after sonication depends on the lipid composition and the time of sonication, although sonication offers significantly less control over the resulting size than processes such as extrusion.[89] An additional method for size reduction, mostly used for larger batches, is high-pressure homogenization. Particles can be homogenized using different machines, such as high-pressure machines with a ring shaped gap valve (e.g., French pressure cell) or with an interaction chamber where two fluids collide (microfluidization).[88,93] In microfluidization, the liposomal suspension is pumped at high velocity through an inlet that is divided into two streams and progressively bifurcates. These streams eventually collide within an interaction chamber leading to the formation of smaller particles due to extreme conditions of turbulence and pressure.[91,93]

Liposomes containing siRNA have been prepared using the lipid-film method and subsequent postprocessing method such as extrusion and sonication. For example, cationic lipoplexes produced using thin-film hydration and subsequent bath sonication yielded particles with a size of 196 nm.[94] Additionally, liposomes were produced by hydrating a lipid film of DOTAP/DOPE/DSPE-PEG (47.5/47.5/5 mol%) with a solution of siRNA in N-(2-hydroxyethyl)-1-piperazineethanesulfonic acid (HEPES) resulting in particles ranging between ≈80 nm and ≈300 nm and an encapsulation efficiency of ≈43%.[29] For liposomes prepared using the thin-film method, encapsulation efficiencies generally approach ≈50%.[29,95] It was shown by Semple et

al. that the addition of 40% of ethanol during lipid-film hydration improved the encapsulation efficiency of pDNA to 70%.[28] This method could be simplified by mixing preheated solutions of lipids in ethanol and oligonucleotides in buffer and subsequent dialysis. This method is referred to as the preformed vesicle method.[28] As a result, a mixed population of small (80-140 nm, measured by freeze-fracture electron microscopy and QELS) uni- and multilamellar vesicles was formed.

Ethanol-Injection Method

The ethanol injection method was first described by Batzri and Korn and was developed as improved alternative to the thin film-hydration method combined with sonication, which has several drawbacks (see section 4.2.).[96] A solution of lipids in ethanol was injected via a syringe to a solution of KCl diluting the ethanol to a concentration of 7.5% (v/v). A relatively homogenous solution of particles was formed with an average size of ≈27 nm (measured by electron microscopy). This size approached the smallest size achievable for a liposome of composition phosphatidylcholine/stearylamine (91.25/8.75 mol%). When the ethanol was quickly diluted in the aqueous buffer, lipid vesicles self-assembled due to a rise in solvent polarity.[96]

The cross-flow injection method was developed as an alternative to the ethanol-injection method, since the latter method was confined to the batch production of low-lipid-concentration products, and reproducibility between batches was considered improvable.[97] This system contained a crossflow module where two stainless-steel tubes were welded perpendicular to one another, and a small injection hole was present at the intersection between the tubes. Through this injection hole, ethanol containing lipids could be injected into a stream of aqueous buffer resulting in the formation of liposomes. Liposome size could be influenced by several parameters; at higher flow rates of the aqueous buffer streams, smaller-sized particles were obtained. In addition, at higher injection pressures of the ethanol solution containing lipids, the resulting particles were found to be smaller.[97]

Drawbacks of Conventional Production Methods

Currently, these "conventional" methods of lipid-film hydration and ethanol injection are still widely used for the production of nanoparticles. However, the labor-intensive processes, the lack of scalability, and the reproducibility of certain steps have been cited as the major drawbacks of these techniques.[85]

The thin-film hydration method is a labor-intensive, multistaged manufacturing method that is costly and difficult to scale up.[85,98–100] The multiple steps of the thin-film hydration method, including evaporation of organic solvent, extrusion of large volumes of liposomes and possibly passive loading of liposomes, are time consuming at a large scale. For example, evaporation of organic solvent might take multiple hours at large volumes.[85] Additionally, most size-reduction methods are prone to scalability issues; extruding large volumes of lipid vesicles might result in clogging of the membrane leading to product losses,[98] although a simple solution is to determine the maximum achievable lipid per surface area of membrane, and set an operating threshold below this number. Sonication is also very difficult to scale up.[20,101] Microfluidization is a method to produce liposomes at a large scale, but the high pressure during this process

can cause shear stress and may be harmful to labile compounds. The potential for channel blocking may also exist.[87] Furthermore, the transition from a lab-scale production of liposomes to a clinical-scale production is reported to be challenging since physicochemical properties might vary when batches are produced at larger scale.[102,103]

Regarding reproducibility within a large production vessel, manufacturing conditions might vary within and between batches resulting in variability and heterogeneity.[104] Even when producing small batches, the relative size of the round-bottom flask compared to the size of the particles is several orders of magnitude. This discrepancy might lead to local hydration conditions, which are nonuniform at the scale of a liposome, and variability in the interliposomal composition, even when produced at the laboratory scale.[104,105] Specific methods have been established to deal with the heterogeneity in the case of lipid-film hydration. For example, extrusion is reported to give quite reproducible results although it introduces an additional manufacturing step.[106] For the ethanol-injection method, at a stirred batch scale, reproducibility is also difficult to achieve.[97] The improved crossflow injection method may provide a well-defined, controllable and reproducible alternative.[97]

Sample contamination and degradation have also been reported to be potential issues for some of the methods mentioned above. For example, sonication can lead to oxidation and degradation of lipids or the drug content, as well as to local overheating of the sample. Probe sonication has been shown to leach titanium particles into the product.[96,107]

Furthermore, it is important to mention that when nanoparticles are produced for *in vivo* applications (i.e., parenteral administration), sterile aseptic technique/maintenance of sterility is critical in commercial-scale processes. Sterile filtration after production using a 0.2 μm membrane is a very straightforward and convenient method for the sterilization of small (<200 nm) liposomes/LNPs but does not remove toxins. If this is not a possibility due to particle size, the entire manufacturing process would have to be sterile, which is more complex and expensive compared to sterile filtration.[88]

Entrapment of hydrophilic drugs into liposomes by passive-loading techniques generally yields a low encapsulation efficiency. This can be partly circumvented by active-loading techniques as reported for amphipathic molecules (remote loading) or for nucleic acids (complexation with ionizable amino or cationic lipids).[108] However, remote loading is certainly not applicable to all drugs and mostly suitable for amphipathic molecules.[109] Addition of ethanol during lipid-film hydration leads to improved encapsulation efficiencies for nucleic acids. However, this method depends on adequate mixing of ethanol and water, and methods such as ethanol injection or preformed vesicle method do not provide adequate control over the mixing process, resulting in suboptimal formulations.[85,97]

Nevertheless, despite the mentioned drawbacks, conventional methods for the production of liposomes/LNPs remain popular, as they are easy to implement[110] and execute at a laboratory scale and not necessarily hamper large-scale production, evidenced by approved liposomal products such as Doxil®. The necessary equipment is relatively inexpensive, making these methods widely accessible.[86,111] However, it should be emphasized that a lack of scalability is one of multiple causes for the lack of clinical translation of nanomedicine.[112] To address this issue, the European Union has funded several initiatives, including The European Pilot Line for

good manufacturing practice manufacturing of batches for clinical trials and the European Nanomedicine Characterization Laboratory, where promising nanomedicines can be developed while fully taking into account downstream considerations. Therefore, the development and implementation of new production methods that deal with the issue of scalability may be of utmost importance for the clinical success of nanomedicine. New production methods, based on rapid mixing of ethanol and water to encapsulate nucleic acids have the characteristics to deal with these issues of reproducibility, scalability of production, and encapsulation efficiency.

New Production Methods for Lipid Nanoparticles

Several improved strategies based on the ethanol-injection method have been developed more recently. In-line T-junction mixing has been used to mix an organic and aqueous phase in a controlled manner for the production of LNP-pDNA and LNP-siRNA.[30–32] Alternatively, two microfluidic methods have been redesigned for the production of LNPs: MHF[34] and SHM.[21,33] Microfluidic mixers can be differentiated based on an active or passive type of mixer. For example, the flow of liquids can be actively influenced by electro-hydrodynamic disturbances, whereas in passive mixers, the geometry of the microfluidic chip is used to increase the interface between two fluids to improve the mixing.[113] Both MHF and SHM are passive microfluidic mixers.

The three aforementioned rapid-mixing methods differ in the 3D structure of the devices, but they all possess the ability to induce rapid mixing of an organic and an aqueous phase in a controlled environment. The general principle of LNP production is therefore the same. LNPs are formed by a quick increase in polarity of the environment induced by rapid mixing of the two miscible phases. This rapid mixing induces supersaturation of lipid molecules which leads to the self-assembly of LNPs (**Figure 3**). In this regard, these production methods are considered bottom-up approaches since LNPs self-assemble into the desired structure without the need for size-reduction methods. The main benefits of rapid-mixing processes over conventional methods for LNP production are the enhanced control of physicochemical properties,[114] improved encapsulation efficiencies, and an improved ability to scale up.
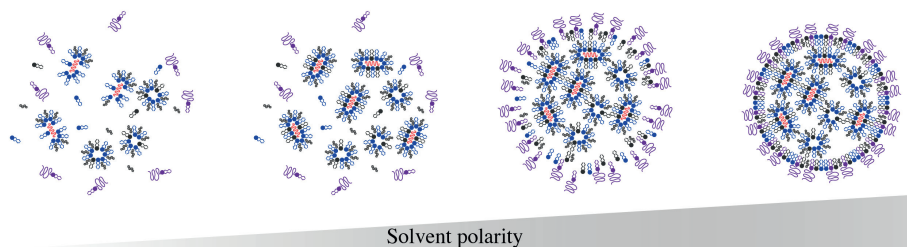
Solvent polarity

Figure 3: Increase in solvent polarity drives the self-assembly of LNP-siRNA formulations. LNP-siRNA are hypothesized to form an electron-dense core structure as a result of significant lipid and nucleic acid present in the internal compartment. The first interactions to occur, upon mixing of the ethanol and aqueous streams, are those between the cationic lipids and negatively charged nucleic acids. As the solvent polarity progressively increases, the hydrophobic inverted micellar structures coalesce, generating the core of the LNP. As mixing continues, the more polar lipids (such as PEG-lipid and DSPC) coat the surface of the nanoprecipitates. The resulting part has an electron-dense core structure surrounded by a lipid monolayer.

T-Junction Mixing

The use of T-junction mixing in lipid-based drug delivery was first described in 1999 by Hirota et al. as a method for the production of DNA-lipoplexes, providing an alternative to macroscopic mixing methods.[115] The T-junction mixer provided a controlled mixing environment compared to macroscopic mixing methods (e.g., vortexing or pipetting), leading to reproducible production of lipoplexes.[115,116] The rapid mixing occurred when the two input streams in the T-junction collided, resulting in a turbulent output flow **(Figure 4).**[117] This production method has also been applied to the production LNP-siRNA.[30,35,41,118] The mechanism of LNP formation was based on the precipitation of lipids as the solvent polarity increased upon dilution of the ethanolic phase into the aqueous phase.[119] Unfortunately, limited data are available on the influence of operating controls such as flow and flow-rate ratio (FRR) on the polydispersity index (PDI) and particle size of LNP-siRNA. However, the effect of these variables might be illustrated using data from the production of LNPs containing a hydrophobic core of triolein encapsulating iron oxide nanoparticles. For these systems, increasing flow rates resulted in smaller particle size. At a flow rate of 10 mL min^{-1}, particles sizes were found to be 75 ± 6 nm, whereas at a flow rate of 40 mL min^{-1} much smaller particles were formed (36 ± 2 nm) (cryo-transmission electron microscopy (TEM) and DLS, number weighted). At lower flow rates, the PDI was higher compared to higher flow rates indicating how particle characteristics could be tuned using the flow rate.[117]
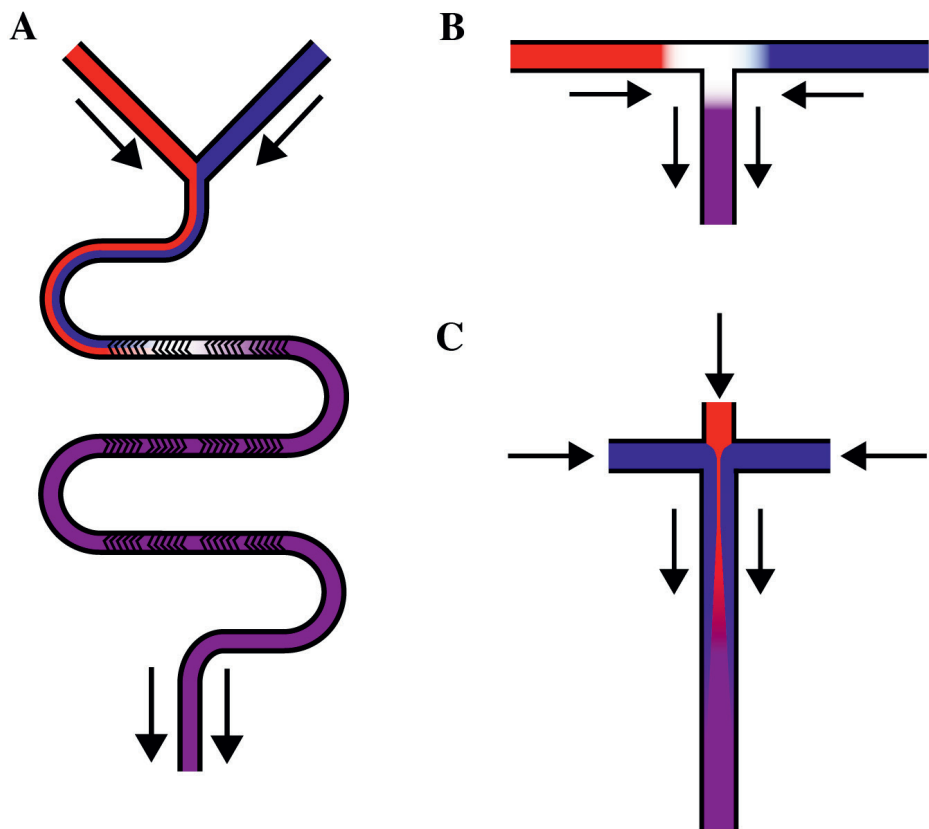
Figure 4: A-C) Schematic illustration of new mixing methods: microfluidic mixing using **A)** a staggered herringbone mixer, **B)** in-line T-junction mixing, and **C)** microfluidic hydrodynamic mixing. The aqueous phase is illustrated in blue, the organic phase in red, and the resulting mixture containing particles in purple

Relatively few siRNA- and DNA-loaded nanoparticles have been produced at a laboratory scale using T junction mixing, although some knowledge is obtained on particle size, morphology, and encapsulation efficiency. Jeffs *et al.* used a T-junction with a diameter of 1.6 mm to mix a solution of lipids in ethanol and pDNA dissolved in Tris-ethylenediaminetetraacetic acid-buffer at a flow rate of 1 ml s^{-1} in order to produce liposomes.[31] T-junction mixing was used to stepwise dilute the ethanol content. Two consecutive passages through the T-junction system were applied, diluting the ethanol content: first from 100% to 45 (v/v) then from 45% to 22.5 (v/v). The resulting particles were 116 ± 54 nm in size (QELS, volume-weighted) and the encapsulation efficiency was 74%. When a single ethanol-dilution step to 22.5% (v/v) was performed, the encapsulation efficiency dropped to 17%. A combination of uni- and multilamellar vesicles were observed.[31] A similar T-junction mixing setup was used for the production of LNP-siRNA (DLin-DMA/DSPC/Chol/ PEG-c-DMA; 30/20/48/2 mol%). The resulting particles were found to be 140 ± 6 nm in size (PDI of 0.11).[41] Similarly, an adaption to the protocol of Jeffs et al. was used by Abrams et al. who produced particles (CLinDMA/cholesterol/PEG-DMG, 50/44/6 mol%) using

a T-junction mixer at a flow rate of 40 mL min^{-1} diluting the ethanol in a single step.[30] The resulting particles were 140 nm and the encapsulation efficiency was 82%. Crawford et al. showed that LNP size and morphology are influenced by the lipid composition of the particles. [35] When the mol% of PEG-DMG was increased (while at the same time decreasing the mol% of cholesterol), a decrease in size was observed: particles containing 2 mol% PEG-DMG were 120 nm (PDI of 0.075), whereas particles containing 5.4 mol% PEG-DMG were 63 nm (PDI of 0.083). In addition, the morphology of the particles containing 2 mol% was considered to be more spherical compared to particles containing 5.4 mol% PEG-DMG.[35]

Together, these results suggest that LNP-siRNA can be produced using T-junction mixing. Encapsulation efficiencies are generally higher as compared to conventional methods. However, the use of this method at a laboratory scale is limited due to the high flow rates required to ensure rapid mixing, which can be difficult to reconcile with small laboratory-scale batches.[119] Nevertheless, in-line T-junction mixing is the preferred method of production on a large scale by companies engaged in the production of LNP-siRNA.[55]

An alternative to the setup of conventional T-junction mixers can be the use of microfluidic T-shaped designs. In these microfluidic designs, solutions experience laminar flow, and mixing is then characterized by diffusion, which is relatively slow.[120,121] In diffusional mixing, the degree of mixing is dependent on the length of the channel and the contact surface area of the two streams.[122] At higher Reynolds numbers, caused by higher flow rates, chaotic flows lead to improved mixing efficiencies.[120] Shorter mixing times lead to a decreased influence of mass-transport effects, which are known to cause lipid aggregation and heterogeneous particle populations.[20] Stroock et al. have shown that addition of herringbone-like structures improves the mixing of a Y-shaped channel at low Reynolds numbers, thereby making it possible to ensure rapid millisecond mixing at lower flow rates.[122] This offers the opportunity to prepare smaller-scale batches and may therefore be preferred over T-junction mixing designs.[119]

Microfluidic Hydrodynamic Focusing

MHF is a microfluidic-mixing technique[123] used to manufacture liposomes in a reproducible and scalable fashion.[104] MHF is a continuous-flow technique where, in the case of liposome production, lipids dissolved in an organic solvent are hydrodynamically focused using an aqueous phase (**Figure 4)**. This technique, applied for the production of liposomes, was extensively investigated between 2004 and 2010 by Jahn et al.[104,124]

The flow within the system is characterized as laminar. These laminar conditions result in a well-defined interface between the organic and aqueous phase where interfacial forces dominate. By influencing this interface using the operating parameters, the operator can gain control of the size and PDI.[104]

The operating parameters of this system were found to be the total flow rate of both phases (volume/time) and the ratio in flow rates between the aqueous and organic phases which influenced the degree of hydrodynamic focusing (i.e., width of the center stream).[104,124] Moreover, the influence of these two variables on particle size and polydispersity index varied with different microfluidic channel geometries. The basis of nanoparticle formation in MHF was a decrease in lipid solubility at the interface between the organic solvent and water. At a critical level, it was

energetically favorable for the lipid to first form disc-like shapes and then close into a confined spherical form.[104,124,125] The size and size distribution of the nanoparticle were dependent on the characteristics of the diffusion, which in turn were influenced by the degree of hydrodynamic focusing.[124,126] A higher FRR (aqueous-to-organic flow rate) resulted in smaller particles with a narrower size distribution. Increasing the total flow rate resulted in larger particles at low FRRs. At high FRRs, this effect was negligible. Additionally, the microfluidic chip geometry had an influence on the operating variables FRR and flow rate. When the diameter of the channel was reduced from 65 μm to 10 μm, equally sized particles were obtained at a twofold lower FRR.[124]

Flow Rate and Ratio Determine Particle Size by Influencing Mixing
The influence of flow rate and FRR on particle size might be explained by their effect on the process of particle formation during MHF. Mixing in the MHF-setup was found to be either diffusive mixing or convective-diffusive mixing, wherein the latter induced faster mixing.[124] Convective-diffusive mixing occurred in the focusing region, whereas diffusive mixing was present in the downstream mixing channel. Rapid convective-diffusive mixing of ethanol and buffer led to formation of small particles with a narrow size distribution, whereas slow diffusive mixing led to larger particles with broader size distributions.[124] The total flow rate and the degree of hydrodynamic focusing influenced the ratio between particle formation in the convective-diffusive versus the diffusive regions, thereby affecting particle sizes and size distributions. High focusing occurred at a high FRR, shifting particle formation toward the convective-diffusive region and reducing particle size, whereas low focusing resulted in a broader center stream enhancing diffusive particle formation, thereby increasing particle size and size distribution.[124]

Krzysztoń et al. used a similarly shaped device as Jahn et al. to produce siRNA-loaded "monomolecular nucleic acid/lipid particles".[34] Using this method, small liposomes (≈20 nm, measured using fluorescence correlation spectroscopy) consisting of DOTAP/DOPE/1,2-dioleoyl-*sn*-glycero-3-phosphocholine (DOPC)/DSPE-PEG2000 (8.2/41/41/8.2/1.6 mol %) could be produced encapsulating ≈70% of 21bp dsDNA at an N/P of 6.[34] Hood and DeVoe noted that the low flow rates of MHF limit the scale-up opportunities, and developed a vertical flow-focusing device (VFF) producing 100 mg h^{-1} liposomes at a flow rate of 4.5 mL min^{-1}.[99,127] Nevertheless, the use of MHF for the production of LNP-siRNA has therefore been limited.

Staggered Herringbone Mixing
Microfluidic mixing by chaotic advection using an SHM for the production of LNPs was pioneered by the group of Pieter Cullis and subsequently commercialized by Precision Nanosystems. [20] This method was developed in order to improve the control over the mixing process and shorten the mixing time.[2,21] Similar to other microfluidic techniques, the main characteristic is controlled millisecond mixing of two miscible phases, usually ethanol and an aqueous buffer. The structure of the staggered herringbone mixer allows efficient wrapping of the two fluids around each other resulting in an exponential enlargement of the interface between the fluids ensuring rapid mixing[122] **(Figure 4)**. The sudden, rapid increase in polarity of the environment of lipid molecules leads to supersaturation, and is thought to result in the formation of LNPs. [21,105] The particle size and size distribution have been found to be controlled by the total flow

rate and the FRR.[20,21,128] For commercial instruments, such as the NanoAssemblr, the geometry of the microfluidic method is predetermined. Therefore, size and size distribution cannot be influenced by microfluidic chip design. It was found that parameters that could be varied, such as lipid composition and payload, influenced the size and morphology of LNPs.[20,21,32,56] LNP production using the SHM can be readily scaled up by parallelization of microfluidic chips.[21,100]

Operating Parameters Influence Particle Characteristics

Zhigaltsev et al. postulated that the increase in polarity is determined by two factors: "the rate of mixing and the ratio of aqueous to ethanol volumes that are being mixed."[20] The rate of mixing was observed to be determined by the total flow rate. The same rationale applied to the ratio between the volumes. A larger difference in volumes between the two fluids resulted in faster mixing and an increased dilution effect.[20] For electron-dense LNP-siRNAs consisting of DLin-KC2-DMA/DSPC/cholesterol/PEG-c-DMA (40.0/11.5/47.5/1.0 mol%), it was seen that at flow rates > 0.2 mL min^{-1} particle size remained constant at ≈55 nm with a low (< 0.1) PDI (DLS, number weighted).[21] The encapsulation efficiency was >95%. Flow rates below 0.2 mL min^{-1} resulted in larger, more polydisperse sized samples (PDI > 0.1) indicating suboptimal mixing. Therefore, it seemed that above a certain threshold flow rate, particles remained equally sized, whereas below this threshold, particle size and polydispersity index increased.[21] This may have resulted from increased mixing times at low velocities. Increased mixing times might have caused pockets of ethanol which led to the growth of larger intermediate structures and subsequently larger LNPs.[129]

The FRR generally shows an inverse relationship with particle size, i.e. an increase in FRR leads to a smaller particle size with a low (<0.2) PDI as a result of decreased mixing time.[21,130] For DOTAP/DOPE (50:50 mol%) liposomes, it was observed that an increase in FRR resulted in smaller particles as expected, although the PDI increased. At a flow rate ratio of 5:1 (aqueous/ethanol) and a flow rate of 2.0 mL min^{-1}, the resulting particle population showed a PDI of 0.4.[131] However, compared to the LNP-siRNA produced by Belliveau et al., which were 55 nm with a PDI < 0.1 at flow rates > 0.2 ml min^{-1}, these particles were much more polydisperse.[21,130] In general, an increasing FRR or flow rate is suggested to lead to rapid-mixing rates so that particles will adopt a minimal size based on the lipid constituents.[131] The high PDI (0.4) of these DOTAP/DOPE liposomes may indicate that a combination of DOTAP/DOPE might not result in a stable liposomal system.

Limit-Size Concept

The limit-size concept, as set out by Zhighaltsev et al., suggests that when particles are produced using SHM under rapid-mixing conditions, they adapt the smallest thermodynamically stable size based on the physical properties of lipids and the specific lipid composition of the particle.[20] The basis of the limit-size calculations is the packing properties of the combination of lipids based on their physical properties. Belliveau *et al.* reasoned that if sub-limit particles are formed during the manufacturing process, these particles ultimately coalesce to form particles determined by the physical constraints of the lipid components.[21] Given this reasoning, changes in lipid composition would result in different particle sizes. This has been shown for

particles containing different amounts of PEGylated lipid, 1-palmitoyl-2-oleoyl-*sn*-glycero-3-phosphocholine (POPC)/cholesterol and POPC/triolein.[20,21,131]

Morphological Differences among LNPs Produced by SHM
The lipid constituents do not only determine LNP size but also morphology. When LNP-siRNA were produced using SHM, two different morphologies could be distinguished based on cryo-TEM images:[56] particles containing an electron-dense core and (multi)-lamellar nanoparticles. Differences in morphology were attributed to differences in lipid composition and the interplay with the nucleic acid payload.[56]

 LNP-siRNA were also observed as having an electron-dense core structure by Leung et al.[33] Using cryo-TEM and *in silico* simulations, it was shown that in the presence and absence of siRNA, LNPs containing DLin-KC2-DMA/DSPC/cholesterol/PEG-c-DMA (40/11.5/47.5/1 mol%) had an electron-dense core. This core was hypothesized to consist of inverted micelles of ionizable amino-lipid complexed with or without siRNA[33] (**Figure 1A**). Upon mixing in an SHM, the relatively hydrophobic complexes of siRNA and ionizable amino-lipid precipitate out of solution and act as nucleation point.[21,33] Subsequently, these inverted micelles are coated with a layer of polar lipids such as DSPC and PEG-lipid.

 It is important to realize that not all LNPs containing siRNA form these electron-dense particles per se. The formation of these electron-dense LNPs was shown to be dependent on the lipid formulation.[56] It was observed that an increase in DSPC content in a LNP formulation from 10 to 30 mol% resulted in lamellar structures on the outer layer of the LNP. This might not be surprising, as DSPC has a high propensity to form bilayers.[54] In addition, when the saturation of the acyl chains of ionizable amino-lipids was increased (using the dioleoyl analogue of DLin-KC2-DMA), more bilayer-structures arose around the electron-dense core[56]. Interestingly, an increase of ionizable amino-lipid above 70 mol% in a formulation containing 1 mol% PEG-lipid led to a decrease of siRNA encapsulation efficiency from ≈90% to ≈60%. At high concentrations of PEG-lipid (i.e., 5 mol%), a concentration of 50 mol% ionizable amino-lipid already led to a decrease in encapsulation efficiency from ≈90% to ≈80%. The influence of PEG-lipid on encapsulation efficiency was partly explained by the fact that higher concentrations of PEG-lipid led to smaller particles accompanying higher surface-to-volume ratios whereby the ionizable amino-lipid would be exposed at the particles surface leaving the siRNA un-encapsulated. In addition, Leung et al. reasoned that the formation of the inverted micellar structure was not only caused by interaction of ionizable amino-lipid with siRNA molecules but was aided by cholesterol and DSPC.[56] At high concentrations of cationic lipid, the amount of cholesterol in the particles was significantly lowered. The packing constraints of this combination of ionizable amino-lipid, cholesterol, DSPC, and PEG-lipid interfered with proper siRNA encapsulation. This effect could be counteracted by substitution of the DSPC lipid by DOPE. Compared to DSPC, DOPE has a more conical shape resulting in improved packing of the lipids at a high concentration of ionizable amino-lipid.[56]

 Together, these findings indicate that the interplay between formulation and packing properties of lipid and nucleic acids largely determines the morphology of LNPs formed by SHM and that that the electron-dense morphology of these LNPs deviates from the traditional

lamellar structure of liposomes.[56] In addition, encapsulation efficiencies are influenced by the packing properties of specific lipid combinations.

Comparison of New Rapid-Mixing Techniques

It is challenging to directly compare the rapid-mixing methods since particle formulations tested between different methods vary. However, some general differences can be pointed out (**Table 3).**

Table 3. Comparison of different production methods for LNP-siRNA

Production Method	Advantages	Disadvantages
Lipid film hydration + Extrusion	Easy to perform Accessible	Low encapsulation efficiency Large-scale production might be challenging Multistep production process, time consuming Relies on the use of chloroform/methanol-tolerable residual solvent limits are much lower than ethanol (cannot perform with ethanol)
Preformed vesicle method	Moderate encapsulation efficiency (70%) Particle size	Mixing is relatively uncontrolled Requires high concentration of PEG-lipid which could decrease transfection efficiency
Crossflow injection	Controlled mixing Already in use for large-scale production	Less suited for labscale production No data present on LNP-siRNA
SHM	Controlled mixing High encapsulation efficiency (>95%) Uniform particles (PDI <0.1) Easily scalable between small and large batches based on parallelization Easy to implement and handle	Limited use of solvents due to cyclic olefin copolymer Clogging of micro channels might occur Requires parallelization for scale-up
MHF	Controlled mixing environment High encapsulation efficiency (≈70%)	Mixing is slower at low FRRs High FRR leads to low particle concentrations Requires parallelization for scale-up
T-junction	Controlled rapid mixing High encapsulation efficiency Uniform particles Broad solvent compatibility	Less suited for lab-scale production Requires parallelization for scale-up

The speed and type of mixing vary between methods. Mixing in SHM is based on chaotic advection, while mixing in MHF is based on convective-diffusive mixing, and mixing in a

T-junction is characterized as turbulent. The FRR differs between these methods. Particles in SHM and T-junction mixing are produced at lower FRRs compared to MHF, leading to higher concentrations of LNPs in SHM and T-junction mixing, since the percentage of the organic phase is higher. Furthermore, total flow rates, and thus arguably productivity, also differ between methods.[21,30,104]

An important issue in the clinical translation is the ability to scale up production. For MHF, the VFF allows scaling up by vertically expanding the microfluidic setup, thereby increasing the output of the system. Scale-up of LNPs using SHM can be achieved relatively easily by parallelization of microfluidic chips or transition to larger-scale systems. T-junction mixing and cross-flow injection systems operate at a larger scale and are based on the similar principle of ethanol dilution.

<u>Drawbacks of Rapid-Mixing Techniques</u>
A drawback of all abovementioned rapid-mixing techniques is that they incorporate a large amount of organic solvent in the manufacturing process, which can be present in the final product and bear an explosion risk at manufacturing scales. Additionally, strict guidelines exist for the amount of residual solvent present in parenteral therapeutics. Ethanol is the preferred solvent, as it can easily be removed using dialysis, and concentrations up to 0.5% (v/v) are accepted under the current guidelines in Europe and America (Ph.Eur. and USP, respectively). Another disadvantage of rapid-mixing systems is the limited solubility of some lipids in ethanol resulting in lower concentrations of LNPs in the mixed solutions. Ultrafiltration (e.g., by tangential flow filtration) can be used to concentrate the LNP suspension. Furthermore, mixing using SHM may create solvent incompatibilities as the mixers are produced with Poly(dimethylsiloxane) or cyclic olefin copolymer.[132] It is reported that this is not the case for T-junction mixing.[117]

When it comes to ease of implementation and use of each of these techniques, SHM is available "off-the-shelf", similar to microfluidic hydrodynamic focusing devices. Systems for T-junction mixing are not readily available, and a production platform has to be set up on a case-by-case basis.

STATE-OF-THE-ART PRODUCTION OF LIPID NANOPARTI-CLES ENCAPSULATING MRNA, PDNA AND CRISPR/CAS9 COMPONENTS

LNPs have also been used for the encapsulation of other nucleic acids besides siRNAs, such as mRNA, pDNA, and CRISPR/Cas9 components.[17,133–144] The use of similar lipid materials for encapsulating nucleic acids other than siRNA may be challenging, as mRNA, pDNA, and sgRNA are larger molecules and contain more negative charges and will not per se result in nanoparticles with an electron-dense LNP morphology. Here, the development of nanoparticles encapsulating mRNA, pDNA, and sgRNA is discussed.

Design of Experiment Approaches to Develop LNP-mRNA

It is evident that mRNA and siRNA structurally differ based on size and charge. These differences might result in variations of lipid packing and LNP structure.[133] Several approaches have been used to adapt LNPs for the delivery of mRNA: changing the ratios of different lipids in the formulation[17] as well as the development of new, proprietary lipids[133,137–139] and a combination of both.[141]

Formulation optimization for the delivery of such payloads has been largely based on one-factor at a time (OFAT) studies.[17] In OFAT studies, only one factor (or variable) is changed, while the other variables remain constant. A general drawback of such studies is that a possible optimal formulation might be overlooked due to the fact that higher order (second and third) interactions between variables (e.g., lipids in the formulation) are ignored.[145] The implication for formulation design is that changing only one lipid in the formulation at a time ignores possible interactions between the lipid constituents of an LNP/liposome, which might lead to suboptimal formulations. Alternatively, more optimal formulations are potentially overlooked due to limited sampling or changes in variables that are too small. In contrast, a design of experiment (DoE) approach, which aims to maximize gain of information using a minimal amount of experiments, leads to a more efficient use of resources.[17,145] A DoE approach for the formulation of microfluidic-manufactured LNPs containing EPO-mRNA and the lipid C12-200 resulted in an approximately sevenfold increase in efficacy over the formulation initially optimized for siRNA (C12-200/DSPC/cholesterol/C14-PEG; 50/10/38.5/1.5 mol%).[44] Compared to LNP optimized for hepatic delivery of siRNA, the total amount of cationic lipid was decreased from 50% to 35%; the helper lipid DSPC was substituted with DOPE; the amount of helper lipid was increased from 10% to 16% and the C14-PEG from 1.5 to 2.5%, resulting in an approximately sevenfold increase in serum erythropoietin (EPO) concentration *in vivo*. Analysis of the results obtained by this DoE experiment revealed that the choice of phospholipid (i.e., DOPE or DSPC) was the most important parameter for *in vivo* production of EPO. LNPs containing the phospholipid DOPE were superior in the ability to induce EPO production compared to LNPs containing DSPC. A second important parameter of efficacy was the weight ratio C12-200 to mRNA. Additionally, several significant second-order interactions were found, such as an interaction between the mol% of C12-200 and the weight ratio C12-200 to mRNA. The particle characteristics also changed: size decreased from 152 to 102 nm (DLS, intensity weighted), the polydispersity index increased from 0.102 to 0.158, and the zeta potential increased from -25.4 to -5.0 mV.[17]

When tailoring these particles for cancer immunotherapy, a new DoE was used based on various cationic lipids, which were synthesized by combinatorial chemistry.[43–45] Ovalbumin mRNA was formulated in a wide variety of LNPs and these particles were tested for their ability to induce a CD8 T-cell response. Parameters that were found to influence the percentage of antigen-specific CD8 T cells included the type of cationic lipid and mol% of cationic lipid favoring cKK-E12 and 10 mol%, respectively. The DoE approach resulted in an optimal formulation, B-11, containing cKK-E12/DOPE/cholesterol/PEG-C14/sodium lauryl sulfate (10/15/40.5/2.5/16 mol%). This formulation showed the best ability to generate an antigen-specific CD8 T-cell response 7 days after administration. The particle had an average size of 152 nm (DLS, intensity weighted; PDI: 0.217) with a multilamellar morphology. Cell types, other than hepatocytes, such

as neutrophils and dendritic cells, were also successfully transfected. A single immunization with particles containing mRNA encoding tumor-associated antigens gp100 and TLR2 led to a strong CD8+ T-cell response leading to tumor shrinkage in mice.[140] These data illustrate the value of DoE over an OFAT design in developing more potent LNPs. Based on the therapeutic strategy for which the LNPs are employed, e.g., protein expression versus cancer immunology, distinct optimal formulations were found. The formulation of ovalbumin mRNA differed in physicochemical properties from the siRNA optimized formulation in terms of particle morphology and size/charge.

Various new proprietary ionizable lipids with novel functionalities have been developed to improve the efficacy of LNP-mRNA formulations. Vaccines containing a newly developed proprietary lipid from Acuitas Therapeutics were used in an LNP formulation containing an ionizable lipid/helper lipid/cholesterol/PEG lipid in a molar ratio of 50/10/38.5/1.5 mol% lipid as a vaccine against the Zika virus. Mice and non-human primates were protected against challenges with Zika virus 5 months or 5 weeks after administration of these LNPs, respectively. [142] Currently, an mRNA vaccine against H10N8 is being tested in a Phase-I clinical trial, for which the interim results indicate a sound prophylactic response accompanied by mild-to-moderate adverse effects.[138] Weissman and co-workers also showed that a formulation similar to the LNP used for siRNA delivery was used to passively immunize mice against a challenge with HIV-1. [146] LNPs encapsulating mRNA encoding an anti-HIV-1 antibody were successfully delivered to the liver resulting in the production of a monoclonal antibody protecting mice from an HIV-1 challenge.[146] The ionizable lipid that was used in this formulation has not been reported in the public domain. Ramaswamy et al. used a proprietary ionizable amino-lipid from Arcturus Therapeutics (ATX) containing an ionizable amino head group and a biodegradable lipid tail containing a cleavable ester bonds for the hepatic delivery of human factor IX mRNA.[133] By incorporating ester bonds in the acyl chains, the lipid was made biodegradable. Incorporation of this feature could be beneficial in terms of biocompatibility. For such LNPs, some constituents were enzymatically degraded and eliminated upon delivery of their content.[147] When the proprietary lipid was compared to DLin-MC3-DMA for both the delivery of siRNA and mRNA using payload-optimized formulations in mice, it was found to lead to five times more efficient gene silencing and two times higher protein expression, respectively.[133] In a quest to develop new LLMs for improved *in vivo* delivery of mRNA, Li et al. evaluated lipid-like nanoparticles as alternative to LNPs containing ionizable amino-lipids. Particles containing the lipid-like molecule O-TT3 were able to deliver mRNA encoding human Factor IX to mice resulting in the expression of Factor IX at therapeutic levels.[139]

Fenton et al. recently claimed to have developed the most potent lipid known for mRNA delivery, referred to as OF-02, outperforming both cKK-E12 and C12-200.[141] The development of these optimized lipids, ATX and OF-02, for the delivery of mRNA is likely a preface for more potent LNPs carrying nucleic acids in the future. It is interesting to note that LNPs containing the biodegradable variant of OF-02 resulted in an increased protein expression in the spleen compared to the liver. However, particle tracking showed that most particles accumulated in the liver while only 15% of the expressed protein originated there. When the nondegradable OF-02 lipid was used, protein expression was not observed in the spleen, rather only in the liver. These

observations are still not fully explained, however they indicate that, based on lipid composition, particles might be directed to either liver protein expression or spleen protein expression.[143]

LNPs for the Delivery of pDNA

LNPs can be utilized as a transfection reagent to introduce pDNA to eukaryotic cells in order to induce sustained protein expression. Only a limited amount of data is available on the adaption of LNPs for the formulation of pDNA. It has to be mentioned that the use of LNP-pDNA is limited to dividing cells, since these particles do not facilitate nuclear entry and therefore pDNA access to the nucleus is restricted to conditions wherein the nuclear membrane is temporarily compromised (as in cell division).[148–150] Several ionizable amino-lipids, namely DLin-MC3-DMA, DLin-KC2-DMA and DLin-DMA, have been evaluated for their use for the delivery of pDNA. Superior results were obtained using the lipid DLin-KC2-DMA over DLin-MC3-DMA.[32] Moreover, the influence of the helper lipid within the formulation containing DLin-KC2-DMA was tested. When the helper lipid DSPC was substituted with unsaturated phosphatidylcholines (1-stearoyl-2-oleoyl-*sn*-glycero-3-phosphocholine (SOPC) or DOPC) additional improvement of the particles' transfection efficacy was obtained.[32] In these formulations, the helper lipid had no influence on the particle electron-dense core morphology. Interestingly, when HeLa cultures were treated with LNPs in a medium containing fetal bovine serum (FBS), DOPC, and SOPC showed significant improvements over DSPC-LNPs. When the FBS was replaced with murine serum, DOPE formulations showed significant improvements. This suggests a clear role of serum components in modulating the efficacy of LNP formulations. Furthermore, PEG-lipids were observed to influence the transfection efficacy of lipoplexes encapsulating pDNA. Transfection efficacy was shown to be dependent on the acyl chain length of the PEG-lipid favoring shorter acyl chains since they diffuse more rapidly from the liposomal membrane exposing the cationic surface needed for efficient DNA transfections.[51]

LNPs for the Functional Delivery of Components of the CRISPR-Cas9 Genome-Editing System

CRISPR is a prokaryotic adaptive immune system[151] that has been successfully modified for human gene editing purposes.[152,153] One of the CRISPR systems used for mammalian genome editing is composed of the Cas9 enzyme (e.g., *Streptococcus pyogenes* Cas9) accompanied by an sgRNA.[152] The sgRNA molecules mediate sequence-specific cleavage of DNA by the Cas9 enzyme, resulting in a double-strand break (DSB) of the targeted DNA.[152] The subsequent activation of the endogenous repair mechanism of nonhomologous end joining may lead to permanent suppression of a target gene. In contrast, by activation of homology-directed repair, a specific gene sequence can be inserted, if a DNA template with sequence homology to the flanking nucleotides of the DSB site is present.[154]

The components of the CRISPR-Cas9 system can be delivered in various forms, such as mRNA, pDNA, or as an sgRNA-protein complex.[10] The delivery of sgRNA/mRNA/pDNA is hampered by similar issues as siRNA.[155] Therefore, delivery systems are a prerequisite for *in vivo* applications of CRISPR/Cas9 and LNPs might provide a valuable option for this purpose.

[156] LNP-mediated Cas9 mRNA delivery is especially challenging considering the Cas9 mRNA length of ≈4500nt.[144]

Both existing and novel lipids/LLMs have been proposed for delivery of CRISPR/Cas9 elements *in vivo*. For example, C12-200 was used to formulate Cas9-mRNA in LNPs. Co-administration of LNP-Cas9 mRNA with an adeno-associated viral particle encoding a sgRNA and a DNA donor template led to correction of mice hepatocytes containing a mutated gene coding for fumarylacetate hydrolase. Systemic administration led to correction of 6.2 ± 1.0% of the hepatocytes as observed by immune-histochemistry.[134] In addition, several novel lipids/LLMs have been developed concurrently with the specific aim of delivering sgRNA and Cas9 (as protein or mRNA). Examples include 3-014B, MPA-A&AB, and ZA3-EP10.[135,136,144] Nanoparticles containing the biodegradable lipid 3-014B were able to form nanoparticles with Cas9/sgRNA-complexes.[135] The resulting structures were relatively large (≈292 ± 15.3 nm) and slightly negatively charged. When HEK293T cells expressing enhanced green fluorescent protein (eGFP) were incubated with these LNPs at concentrations of 25 nM of Cas9:sgRNA with 6 µg mL^{-1} lipid , a 70% reduction in eGFP expression was observed.[135] However, the feasibility of these particles for systemic administration (e.g., intravenous injection) can be questioned due to their unfavorable physicochemical properties.

In an attempt to improve the delivery of Cas9 mRNA, Zhang et al. developed several new biodegradable LLMs.[136] These LLMs were formulated in particles containing LLM/DOPE/cholesterol/DMG-PEG (≈22/33.1/44.1/0.8 mol %). Both *in vitro* and *in vivo* data showed delivery of Cas9 mRNA to target cells. After incubation of cells stably expressing eGFP and eGFP sgRNA with nanoparticles at dose of 50ng Cas9 mRNA per well in a 24-well plate, a decrease in fluorescence intensity was observed. Furthermore, when these particles were administered intratumorally to mice carrying xenograft tumors of the earlier-mentioned eGFP-HEK293T cells, a decrease of 41% in eGFP fluorescence intensity was observed, indicating *in vivo* delivery of Cas9 mRNA to HEK293T tumors.[136] However, this murine model does not fully represent the challenge of delivering a complete CRISPR/Cas9 system *in vivo* as the model HEK293T cells already expressed eGFP sgRNA, which, in a drug product for commercial applications, needs to be co-delivered to the same cell.

Miller et al. developed zwitterionic amino lipids (ZALs) especially for the delivery of Cas9 mRNAs and sgRNAs.[144] These lipids incorporated, according to the authors, multiple characteristics derived from successful cationic and ionizable amino-lipids, as well as from zwitterionic lipids into a single lipid, which might improve the delivery of larger RNAs. ZAL ZA3-EP10 was efficient in delivering an sgRNA and mRNA *in vitro*. Furthermore, these nanoparticles of unknown morphology containing ZA3-EP10, formulated with cholesterol and a PEG-lipid (ZAL/cholesterol/PEG-lipid; 56.18/43.26/0.56 mol%), produced using SHM, were able to deliver mRNA sequences for mCherry and luciferase. It was reasoned that co-delivery of sgRNA and mRNA encapsulated within a single nanoparticle is beneficial since both are needed for efficient genome editing.[144] Therefore, they co-formulated mRNA and sgRNA in a ratio of 3:1 (w/w) and reported successful co-delivery of Cas9 mRNA and an sgRNA *in vivo*. Mice expressing the Rosa26 promoter Lox-Stop-Lox tdTomato (tdTO) cassette were injected with a particle containing an sgRNA targeting the LoxP sequence. In this reporter setup, successful delivery

2

of mRNA and sgRNA would lead to deletion of the stop-sequence enabling expression of the tdTO resulting in a fluorescence signal. Intravenous administration of the particles resulted in a fluorescence signal within the lungs, kidney and liver.[144] Interestingly, several companies involved in CRISPR/Cas9 gene editing are exploring the possibilities of LNP-mediated gene delivery, indicating that LNPs are considered as a suitable option for the delivery of the CRISPR/Cas9 system.[157,158]

As discussed above, different approaches have been used to optimize LNPs for the delivery of mRNA/pDNA/sgRNA using microfluidic manufacturing. Both optimization of the lipid formulation and the development of new proprietary lipids have resulted in significant improvements and impressive preclinical results for *in vivo* models. Data of LNPs containing different nucleic acid payloads indicate that initial optimized formulations for siRNA delivery cannot be extrapolated to mRNA, pDNA, or sgRNA carrying nanoparticles, but need to be adapted to their specific nucleic acid cargo. The use of a DoE approach has resulted in significant improvements of several formulations, illustrating its added value in optimizing lipid formulations for *in vivo* efficacy. In the future, DoE approaches may be of substantial importance when tailoring nucleic-acid-loaded particles to other cells than cell types described here.

FUTURE PERSPECTIVES/CONCLUSIONS

The use of LNPs for RNA delivery has made tremendous progress over the past decade. In this light, the recent successful outcome of the Phase-III study on Patisiran may, for the time being, be considered a highpoint for the field.

A key development has been the design of ionizable amino-lipids that are neutral at physiological pH as a replacement of the permanently charged cationic lipids. This avoids nonspecific interactions with blood components and nontarget cells. In addition, small structural variations in these ionizable amino-lipids have been shown to result in large improvements in functional delivery. These improvements are not always well understood. The continuing emergence of novel lipids with high efficiency may help in identifying and rationally optimizing the ionizable amino-lipid component of LNPs even further.

The development of sheddable PEG-coatings represents a balancing act between particle stability during production in the circulation on the one hand, and subsequent regulated opsonization with desired proteins, such as ApoE, and triggered exposure of an interactive surface, on the other. The gradual loss of PEG from the LNP through the use of short-chain ceramides helps to make these seemingly incompatible demands meet.

Up to now, opsonization by ApoE *in vivo* has enabled hepatocyte delivery, but delivery to other tissues remains challenging. Modulation of the particle surface to attract other opsonins may help to reach other tissues beyond the liver.

The initial observational studies on LNP performance have yielded a broad set of design characteristics for LNP-siRNA. However, it has to be kept in mind that some of these physicochemical properties are only general guidelines.[159] Further insight into the relationship between a nanoparticle's physicochemical properties and its efficacy might lead to further

improvements of LNPs potency. An important step to establish the best characteristics may be increased use of DoE-based optimization. Using DoE analysis, higher-order relationships between LNP composition, characteristics, and performance may be uncovered. A prerequisite for clinical development is the reproducible and scalable manufacturing of tunable LNPs. The development of rapid-mixing methods, described here, provides a platform for the production of such systems. The use of rapid-mixing methods is currently being applied to other nucleic acids, such as mRNA and sgRNA. The development of LNPs encapsulating these RNA types has made clear that formulations need to be optimized for each type of nucleic acid payload and are certainly not interchangeable. Early success has been shown for LNPs encapsulating mRNA with applications in single-dose vaccines for Zika virus, Influenza virus H10N8 and H7N9, as well as protein replacement therapy for FIX and EPO.[17,133,137,138,142] These developments further highlight that LNPs are a versatile platform for unlocking the therapeutic potential of several types of nucleic acid-based therapeutics.

ACKNOWLEDGEMENTS

REFERENCES

1.   Wittrup A, Lieberman J. Knocking down disease: a progress report on siRNA therapeutics. Nat Rev Genet. 2015;16(9):543–52.
2.   Cullis PR, Hope MJ. Lipid Nanoparticle Systems for Enabling Gene Therapies. Mol Ther. 2017;25(7).
3.   Alnylam Pharmaceuticals Inc. Alnylam and Sanofi Report Positive Topline Results from APOLLO Phase 3 Study of Patisiran in Hereditary ATTR (hATTR) Amyloidosis Patients with Polyneuropathy [Internet]. 2017 [cited 2017 Sep 25]. Available from: http://investors.alnylam.com/releasedetail.cfm?ReleaseID=1041081
4.   Alnylam Pharmaceuticals Inc. Alnylam Completes Submission of New Drug Application to U.S. Food and Drug Administration (FDA) for Patisiran for the Treatment of Hereditary ATTR (hATTR) Amyloidosis [Internet]. 2017 [cited 2018 Jan 15]. Available from: http://investors.alnylam.com/news-releases/news-release-details/alnylam-completes-submission-new-drug-application-us-food-and
5.   Whitehead KA, Langer R, Anderson DG. Knocking down barriers: advances in siRNA delivery. Nat Rev Drug Discov. 2009 Feb;8(2):129–38.
6.   Tam Y, Chen S, Cullis P. Advances in Lipid Nanoparticles for siRNA Delivery. Pharmaceutics. 2013;5(4):498–507.
7.   Fire A, Xu S, Montgomery MK, Kostas SA, Driver SE, Mello CC. Potent and specific genetic interference by double-stranded RNA in Caenorhabditis elegans. Nature. 1998;391(6669):806–11.
8.   Matranga C, Tomari Y, Shin C, Bartel DP, Zamore PD. Passenger-strand cleavage facilitates assembly of siRNA into Ago2-containing RNAi enzyme complexes. Cell. 2005;123(4):607–20.
9.   Ameres SL, Martinez J, Schroeder R. Molecular Basis for Target RNA Recognition and Cleavage by Human RISC. Cell. 2007;130(1):101–12.
10. Kaczmarek JC, Kowalski PS, Anderson DG. Advances in the delivery of RNA therapeutics: from concept to clinical reality. Genome Med. Genome Medicine; 2017;9(1):60.
11. Wolff JA, Malone RW, Williams P, Chong W, Acsadi G, Jani A, et al. Direct Gene Transfer into Mouse Muscle in Vivo. Science (80-). 1990;247(4949):1465–8.
12. Doudna JA, Charpentier E. The new frontier of genome engineering with CRISPR-Cas9. Science (80-). 2014;346(6213).
13. Yin H, Kanasty RL, Eltoukhy AA, Vegas AJ, Dorkin JR, Anderson DG. Non-viral vectors for gene-based therapy. Nat Rev Genet. 2014;15(8):541–55.
14. Kanasty R, Dorkin JR, Vegas A, Anderson D. Delivery materials for siRNA therapeutics. Nat Mater. 2013;12(11):967–77.
15. Juliano RL. The delivery of therapeutic oligonucleotides. Nucleic Acids Res. 2016;44(14):6518–48.
16. Shen X, Corey DR. Chemistry, mechanism and clinical status of antisense oligonucleotides and duplex RNAs. Nucleic Acids Res. 2018;46(4):1584–600.
17. Kauffman KJ, Dorkin JR, Yang JH, Heartlein MW, Derosa F, Mir FF, et al. Optimization of Lipid Nanoparticle Formulations for mRNA Delivery in Vivo with Fractional Factorial and Definitive Screening Designs. Nano Lett. 2015;15(11).
18. Semple SC, Akinc A, Chen J, Sandhu AP, Mui BL, Cho CK, et al. Rational design of cationic lipids for siRNA delivery. Nat Biotechnol. 2010;28(2):172–6.
19. Jayaraman M, Ansell SM, Mui BL, Tam YK, Chen J, Du X, et al. Maximizing the potency of siRNA lipid nanoparticles for hepatic gene silencing in vivo. Angew Chem, Int Ed. 2012;51(34):8529–33.
20. Zhigaltsev I V, Belliveau N, Hafez I, Leung AKK, Huft J, Hansen C, et al. Bottom-Up Design and Synthesis of Limit Size Lipid Nanoparticle Systems with Aqueous and Triglyceride Cores Using Millisecond Microfluidic Mixing. Langmuir. 2012;28(7):3633–40.
21. Belliveau NM, Huft J, Lin PJ, Chen S, Leung AK, Leaver TJ, et al. Microfluidic Synthesis of Highly Potent Limit-size Lipid Nanoparticles for In Vivo Delivery of siRNA. Mol Ther - Nucleic Acids. 2012;1(May):e37.
22. Deamer DW. From "banghasomes" to liposomes: a memoir of Alec Bangham, 1921-2010. FASEB J. 2010;24(5):1308–10.

23.   Gregoriadis G. Drug entrapment in liposomes. FEBS Lett. 1973;36(3):292–6.

24.   Dimitriadis GJ. Entrapment of ribonucleic acids in liposomes. FEBS Lett. 1978;86(2):289–93.

25.   Gregoriadis G, Leathwood PD, Ryman BE. Enzyme entrapment in liposomes. FEBS Lett. 1971;14(2):95–9.

26.   Gregoriadis G. Liposomes in drug delivery: How it all happened. Pharmaceutics. 2016;8(2):1–5.

27.   Torchilin VP. Recent advances with liposomes as pharmaceutical carriers. Nat Rev Drug Discov. 2005;4(2):145–60.

28.   Semple SC, Klimuk SK, Harasym TO, Dos Santos N, Ansell SM, Wong KF, et al. Efficient encapsulation of antisense oligonucleotides in lipid vesicles using ionizable aminolipids: formation of novel small multilamellar vesicle structures. Biochim Biophys Acta. 2001;1510(1–2):152–66.

29.   Buyens K, Demeester J, De Smedt SS, Sanders NN. Elucidating the encapsulation of short interfering RNA in PEGylated cationic liposomes. Langmuir. 2009;25(9):4886–91.

30.   Abrams MT, Koser ML, Seitzer J, Williams SC, DiPietro MA, Wang W, et al. Evaluation of Efficacy, Biodistribution, and Inflammation for a Potent siRNA Nanoparticle: Effect of Dexamethasone Co-treatment. Mol Ther. 2010;18(1):171–80.

31.   Jeffs LB, Palmer LR, Ambegia EG, Giesbrecht C, Ewanick S, MacLachlan I. A scalable, extrusion-free method for efficient liposomal encapsulation of plasmid DNA. Pharm Res. 2005;22(3):362–72.

32.   Kulkarni JA, Myhre JL, Chen S, Tam YYC, Danescu A, Richman JM, et al. Design of lipid nanoparticles for in vitro and in vivo delivery of plasmid DNA. Nanomedicine Nanotechnology, Biol Med. 2017;13(4):1377–87.

33.   Leung AKK, Hafez IM, Baoukina S, Belliveau NM, Zhigaltsev I V, Afshinmanesh E, et al. Lipid Nanoparticles Containing siRNA Synthesized by Microfluidic Mixing Exhibit an Electron-Dense Nanostructured Core. J Phys Chem C. 2012;116(34):18440–50.

34.   Krzysztoń R, Salem B, Lee DJ, Schwake G, Wagner E, Rädler JO. Microfluidic self-assembly of folate-targeted monomolecular siRNA-lipid nanoparticles. Nanoscale. 2017;9(22):7442–53.

35.   Crawford R, Dogdas B, Keough E, Haas RM, Wepukhulu W, Krotzer S, et al. Analysis of lipid nanoparticles by Cryo-EM for characterizing siRNA delivery vehicles. Int J Pharm. 2011;403(1–2):237–44.

36.   Petros RA, DeSimone JM. Strategies in the design of nanoparticles for therapeutic applications. Nat Rev Drug Discov. 2010;9(8):615–27.

37.   Blanco E, Shen H, Ferrari M. Principles of nanoparticle design for overcoming biological barriers to drug delivery. Nat Biotechnol. 2015;33(9):941–51.

38.   Chonn A, Semple SC, Cullis PR. Association of blood proteins with large unilamellar liposomes in vivo. Relation to circulation lifetimes. J Biol Chem. 1992;267(26):18759–65.

39.   Hafez IM, Maurer N, Cullis PR. On the mechanism whereby cationic lipids promote intracellular delivery of polynucleic acids. Gene Ther. 2001;8(15):1188–96.

40.   Xu Y, Szoka FC. Mechanism of DNA Release from Cationic Liposome/DNA Complexes Used in Cell Transfection,. Biochemistry. 1996;35(18):5616–23.

41.   Heyes JA, Palmer L, Bremner K, MacLachlan I. Cationic lipid saturation influences intracellular delivery of encapsulated nucleic acids. J Control Release. 2005;107(2):276–87.

42.   Akinc A, Zumbuehl A, Goldberg M, Leshchiner ES, Busini V, Hossain N, et al. A combinatorial library of lipid-like materials for delivery of RNAi therapeutics. Nat Biotechnol. 2008;26(5):561–9.

43.   Dong Y, Love KT, Dorkin JR, Sirirungruang S, Zhang Y, Chen D, et al. Lipopeptide nanoparticles for potent and selective siRNA delivery in rodents and nonhuman primates. Proc Natl Acad Sci U S A. 2014;111:3955–60.

44.   Love KT, Mahon KP, Levins CG, Whitehead KA, Querbes W, Dorkin JR, et al. Lipid-like materials for low-dose, in vivo gene silencing. Proc Natl Acad Sci U S A. 2010;107(5):1864–9.

45.   Whitehead KA, Dorkin JR, Vegas AJ, Chang PH, Veiseh O, Matthews J, et al. Degradable lipid nanoparticles with predictable in vivo siRNA delivery activity. Nat Commun. 2014;5(1):4277.

46.   Yamamoto N, Sato Y, Munakata T, Kakuni M, Tateno C, Sanada T, et al. Novel pH-sensitive multifunctional envelope-type nanodevice for siRNA-based treatments for chronic HBV infection. J Hepatol. 2016;64(3):547–55.

47. Sato Y, Hatakeyama H, Sakurai Y, Hyodo M, Akita H, Harashima H. A pH-sensitive cationic lipid facilitates the delivery of liposomal siRNA and gene silencing activity in vitro and in vivo. J Control Release. 2012;163(3):267–76.

48. Hafez IM, Cullis PR. Roles of lipid polymorphism in intracellular delivery. Adv Drug Deliv Rev. 2001;47(2):139–48.

49. Cullis PR, De Kruijff B. The polymorphic phase behaviour of phosphatidylethanolamines of natural and synthetic origin. A 31P NMR study. Biochim Biophys Acta, Biomembr. 1978;513(1):31–42.

50. Farhood H, Serbina N, Huang L. The role of dioleoyl phosphatidylethanolamine in cationic liposome mediated gene transfer. Biochim Biophys Acta, Biomembr. 1995;1235(2):289–95.

51. Mok KWC, Lam AMI, Cullis PR. Stabilized plasmid-lipid particles: Factors influencing plasmid entrapment and transfection properties. Biochim Biophys Acta, Biomembr. 1999;1419(2):137–50.

52. Hope MJ, Mui B, Ansell S, Ahkong QF. Cationic lipids, phosphatidylethanolamine and the intracellular delivery of polymeric, nucleic acid-based drugs (Review). Mol Membr Biol. 1998;15(1):1–14.

53. Cheng X, Lee RJ. The role of helper lipids in lipid nanoparticles (LNPs) designed for oligonucleotide delivery. Adv Drug Deliv Rev. 2016;99:129–37.

54. Thewalt JL, Bloom M. Phosphatidylcholine: cholesterol phase diagrams. Biophys J. 1992;63(4):1176–81.

55. Leung AKK. Biophysical Characterization of Lipid Nanoparticles Containing Nucleic Acid Polymers As Produced By Microfluidic Mixing. PhD Proposal. The University of British Columbia; 2015.

56. Leung AKK, Tam YYC, Chen S, Hafez IM, Cullis PR. Microfluidic Mixing: A General Method for Encapsulating Macromolecules in Lipid Nanoparticle Systems. J Phys Chem B. 2015;119(28):8698–706.

57. Demel RA, De Kruyff B. The function of sterols in membranes. Biochim Biophys Acta - Rev Biomembr. 1976;457(2):109–32.

58. Hung W-C, Lee M-T, Chen F-Y, Huang HW. The Condensing Effect of Cholesterol in Lipid Bilayers. Biophys J. 2007;92(11):3960–7.

59. Demel RA, Bruckdorfer KR, Van Deenen LLM. The effect of sterol structure on the permeability of lipomes to glucose, glycerol and Rb+. Biochim Biophys Acta - Biomembr. 1972;255(1):321–30.

60. Papahadjopoulos D, Nir S, Ohki S. Permeability properties of phospholipid membranes: effect of cholesterol and temperature. Biochim Biophys Acta,. 1971;266:561–83.

61. Semple SC, Chonn A, Cullis PR. Influence of cholesterol on the association of plasma proteins with liposomes. Biochemistry. 1996;35(8):2521–5.

62. Rodrigueza W V., Haydn Pritchard P, Hope MJ. The influence of size and composition on the cholesterol mobilizing properties of liposomes in vivo. Biochim Biophys Acta, Biomembr. 1993;1153(1):9–19.

63. Rodrigueza W V., Klimuk SK, Kitson CN, Wheeler JJ, Hope MJ. Transbilayer Movement and Net Flux of Cholesterol and Cholesterol Sulfate between Liposomal Membranes. Biochemistry. 1995;34(18):6208–17.

64. Kirby C, Clarke J, Gregoriadis G. Cholesterol content of small unilamellar liposomes controls phospholipid loss to high density lipoproteins in the presence of serum. FEBS Lett. 1980;111(2):324–8.

65. Allen TM. The use of glycolipids and hydrophilic polymers in avoiding rapid uptake of liposomes by the mononuclear phagocyte system. Adv Drug Deliv Rev. 1994;13(3):285–309.

66. Chen S, Tam YYC, Lin PJC, Sung MMH, Tam YK, Cullis PR. Influence of particle size on the in vivo potency of lipid nanoparticle formulations of siRNA. J Control Release. 2016;235:236–44.

67. Bao Y, Jin Y, Chivukula P, Zhang J, Liu Y, Liu J, et al. Effect of PEGylation on biodistribution and gene silencing of siRNA/lipid nanoparticle complexes. Pharm Res. 2013;30(2):342–51.

68. Chen S, Tam YYC, Lin PJC, Leung AKK, Tam YK, Cullis PR. Development of lipid nanoparticle formulations of siRNA for hepatocyte gene silencing following subcutaneous administration. J Control Release. 2014;196:106–12.

69. Mui BL, Tam YK, Jayaraman M, Ansell SM, Du X, Tam YYC, et al. Influence of Polyethylene Glycol Lipid Desorption Rates on Pharmacokinetics and Pharmacodynamics of siRNA Lipid Nanoparticles. Mol Ther - Nucleic Acids. 2013;2(12):e139.

70. Akinc A, Querbes W, De S, Qin J, Frank-Kamenetsky M, Jayaprakash KN, et al. Targeted delivery of RNAi therapeutics with endogenous and exogenous ligand-based mechanisms. Mol Ther. 2010;18(7):1357–64.

71. Mishra S, Webster P, Davis ME. PEGylation significantly affects cellular uptake and intracellular trafficking of non-viral gene delivery particles. Eur J Cell Biol. 2004;83(3):97–111.

72. Hatakeyama H, Akita H, Kogure K, Oishi M, Nagasaki Y, Kihira Y, et al. Development of a novel systemic gene delivery system for cancer therapy with a tumor-specific cleavable PEG-lipid. Gene Ther. 2007;14(1):68–77.

73. Webb MS, Saxon D, Wong FMP, Lim HJ, Wang Z, Bally MB, et al. Comparison of different hydrophobic anchors conjugated to poly(ethylene glycol): Effects on the pharmacokinetics of liposomal vincristine. Biochim Biophys Acta, Biomembr. 1998;1372(2):272–82.

74. Ambegia E, Ansell S, Cullis P, Heyes J, Palmer L, MacLachlan I. Stabilized plasmid-lipid particles containing PEG-diacylglycerols exhibit extended circulation lifetimes and tumor selective gene expression. Biochim Biophys Acta. 2005;1669(2):155–63.

75. Semple SC, Harasym TO, Clow K a, Ansell SM, Klimuk SK, Hope MJ. Immunogenicity and rapid blood clearance of liposomes containing polyethylene glycol-lipid conjugates and nucleic Acid. J Pharmacol Exp Ther. 2005;312(3):1020–6.

76. Lee JB, Zhang K, Tam YYC, Quick J, Tam YK, Lin PJ, et al. A Glu-urea-Lys Ligand-conjugated Lipid Nanoparticle/siRNA System Inhibits Androgen Receptor Expression In Vivo. Mol Ther - Nucleic Acids. 2016;5(May):e348.

77. Harashima H, Kiwada H. Liposomal targeting and drug delivery: Kinetic consideration. Advanced Drug Delivery Reviews. 1996. p. 425–44.

78. Wisse E, Jacobs F, Topal B, Frederik P, De Geest B. The size of endothelial fenestrae in human liver sinusoids: implications for hepatocyte-directed gene transfer. Gene Ther. 2008;15(17):1193–9.

79. Andar AU, Hood RR, Vreeland WN, Devoe DL, Swaan PW. Microfluidic preparation of liposomes to determine particle size influence on cellular uptake mechanisms. Pharm Res. 2014;31(2):401–13.

80. Kirchhausen T. Imaging endocytic clathrin structures in living cells. Trends Cell Biol. 2009;19(11):596–605.

81. Yameen B, Choi W Il, Vilos C, Swami A, Shi J, Farokhzad OC. Insight into nanoparticle cellular uptake and intracellular targeting. J Control Release. 2014;190:485–99.

82. Sahay G, Querbes W, Alabi C, Eltoukhy A, Sarkar S, Zurenko C, et al. Efficiency of siRNA delivery by lipid nanoparticles is limited by endocytic recycling. Nat Biotechnol. 2013;31(7):653–8.

83. Gilleron J, Querbes W, Zeigerer A, Borodovsky A, Marsico G, Schubert U, et al. Image-based analysis of lipid nanoparticle-mediated siRNA delivery, intracellular trafficking and endosomal escape. Nat Biotechnol. 2013;31(7):638–46.

84. Wittrup A, Ai A, Liu X, Hamar P, Trifonova R, Charisse K, et al. Visualizing lipid-formulated siRNA release from endosomes and target gene knockdown. Nat Biotechnol. 2015;33(8):870–6.

85. Meure LA, Foster NR, Dehghani F. Conventional and Dense Gas Techniques for the Production of Liposomes: A Review. AAPS PharmSciTech. 2008;9(3):798.

86. Grimaldi N, Andrade F, Segovia N, Ferrer-Tasies L, Sala S, Veciana J, et al. Lipid-based nanovesicles for nanomedicine. Chem Soc Rev. 2016;45(23):6520–45.

87. Elizondo E, Moreno E, Cabrera I, Córdoba A, Sala S, Veciana J, et al. Liposomes and other vesicular systems: Structural characteristics, methods of preparation, and use in nanomedicine. Prog Mol Biol Transl Sci. 2011;104:1–52.

88. Lasch J, Weissig V, Brandl M. Preparation of Liposomes. In: Torchilin V, Weissig V, editors. Liposomes: A practical approach. 2nd ed. Oxford University Press; 2003. p. 3–29.

89. Szoka F, Papahadjopoulos D. Comparative Properties and Methods of Preparation of Lipid Vesicles (Liposomes). Annu Rev Biophys Bioeng. 1980;9(1):467–508.

90. Mayer LD, Hope MJ, Cullis PR. Vesicles of variable sizes produced by a rapid extrusion procedure. Biochim Biophys Acta. 1986;858(1):161–8.

91. Mozafari MR. Nanoliposomes: Preparation and Analysis. In: Liposomes, Method in Molecular Biology (Methods and Protocols). Humana Press; 2010.

92. Szoka F, Papahadjopoulos D. Procedure for preparation of liposomes with large internal aqueous space and high capture by reverse-phase evaporation. Proc Natl Acad Sci. 1978;75(9):4194–8.

93. Mayhew E, Lazo R, Vail WJ, King J, Green AM. Characterization of liposomes prepared using a microemulsifier. Biochim Biophys Acta - Biomembr. 1984;775(2):169–74.

94. Kim SI, Shin D, Choi TH, Lee JC, Cheon G-J, Kim K-Y, et al. Systemic and Specific Delivery of Small Interfering RNAs to the Liver Mediated by Apolipoprotein A-I. Mol Ther. 2007;15(6):1145–52.

95. Buyens K, De Smedt SC, Braeckmans K, Demeester J, Peeters L, van Grunsven LA, et al. Liposome based systems for systemic siRNA delivery: Stability in blood sets the requirements for optimal carrier design. J Control Release. 2012;158(3):362–70.

96. Batzri S, Korn ED. Single bilayer liposomes prepared without sonication. Biochim Biophys Acta - Biomembr. 1973 Apr;298(4):1015–9.

97. Wagner A, Vorauer-Uhl K, Kreismayr G, Katinger H. the Crossflow Injection Technique: an Improvement of the Ethanol Injection Method. J Liposome Res. 2002;12(3):259–70.

98. Wagner A, Vorauer-Uhl K. Liposome Technology for Industrial Purposes. J Drug Deliv. 2011;2011:1–9.

99. Hood RR, DeVoe DL. High-Throughput Continuous Flow Production of Nanoscale Liposomes by Microfluidic Vertical Flow Focusing. Small. 2015;11(43):5790–9.

100. Garg S, Heuck G, Ip S, Ramsay E. Microfluidics: a transformational tool for nanomedicine development and production. J Drug Target. 2016;24(9):821–35.

101. Wan C, Allen TM, Cullis PR. Lipid nanoparticle delivery systems for siRNA-based therapeutics. Drug Deliv Transl Res. 2014;4(1):74–83.

102. Paliwal R, Babu RJ, Palakurthi S. Nanomedicine Scale-up Technologies: Feasibilities and Challenges. AAPS PharmSciTech. 2014;15(6):1527–34.

103. Desai N. Challenges in Development of Nanoparticle-Based Therapeutics. AAPS J. 2012;14(2):282–95.

104. Jahn A, Vreeland WN, Gaitan M, Locascio LE. Controlled Vesicle Self-Assembly in Microfluidic Channels with Hydrodynamic Focusing. J Am Chem Soc. 2004;126(9):2674–5.

105. Walsh C, Ou K, Belliveau NM, Leaver TJ, Wild AW, Huft J, et al. Microfluidic-Based Manufacture of siRNA-Lipid Nanoparticles for Therapeutic Applications. In: Jain KK, editor. Drug Delivery System. New York, NY: Springer New York; 2014. p. 109–20.

106. Hope M, Nayar R, Mayer L. Reduction of liposome size and preparation of unilamellar vesicles by extrusion techniques. In: Liposome technology. CRC Press, Inc.; 1993. p. 123–39.

107. Hauser HO. The effect of ultrasonic irradiation on the chemical structure of egg lecithin. Biochem Biophys Res Commun. 1971;45(4):1049–55.

108. Pattni BS, Chupin V V, Torchilin VP. New Developments in Liposomal Drug Delivery. Chem Rev. 2015;115(19):10938–66.

109. Cern A, Marcus D, Tropsha A, Barenholz Y, Goldblum A. New drug candidates for liposomal delivery identified by computer modeling of liposomes' remote loading and leakage. J Control Release. 2017;252:18–27.

110. Koynova R, Tenchov B. Recent Progress in Liposome Production, Relevance to Drug Delivery and Nanomedicine. Recent Pat Nanotechnol. 2015;9(2):86–93.

111. Patil YP, Jadhav S. Novel methods for liposome preparation. Chemistry and Physics of Lipids. 2014. p. 8–18.

112. Valencia PM, Farokhzad OC, Karnik R, Langer R. Microfluidic technologies for accelerating the clinical translation of nanoparticles. Nat Nanotechnol. 2012;7(10):623–9.

113. Lee CY, Chang CL, Wang YN, Fu LM. Microfluidic mixing: A review. Int J Mol Sci. 2011;12(5):3263–87.

114. Carugo D, Bottaro E, Owen J, Stride E, Nastruzzi C. Liposome production by microfluidics: potential and limiting factors. Sci Rep. 2016;6(1):25876.

115. Hirota S, De Ilarduya CT, Barron LG, Szoka FC. Simple mixing device to reproducibly prepare cationic lipid-DNA complexes (lipoplexes). Biotechniques. 1999;27(2):286–90.

116. Davies LA, Nunez-Alonso GA, Hebel HL, Scheule RK, Cheng SH, Hyde SC, et al. A novel mixing device for the reproducible generation of nonviral gene therapy formulations. Biotechniques. 2010;49(3):666–8.

117. Kulkarni JA, Tam YYC, Chen S, Tam YK, Zaifman J, Cullis PR, et al. Rapid synthesis of lipid nanoparticles containing hydrophobic inorganic nanoparticles. Nanoscale. 2017;9(36):13600–9.

118. Zimmermann TS, Lee ACH, Akinc A, Bramlage B, Bumcrot D, Fedoruk MN, et al. RNAi-mediated gene silencing in non-human primates. Nature. 2006;441(7089):111–4.

119. Leung AKK, Tam YYC, Cullis PR. Chapter Four – Lipid Nanoparticles for Short Interfering RNA Delivery. In: Advances in Genetics. 2014. p. 71–110.

120. Andreussi T, Galletti C, Mauri R, Camarri S, Salvetti MV. Flow regimes in T-shaped micro-mixers. Comput Chem Eng. 2015;76:150–9.

121. Williams MS, Longmuir KJ, Yager P. A practical guide to the staggered herringbone mixer. Lab Chip. 2008;8(7):1121.

122. Stroock AD, Dertinger SKW, Ajdari A, Mezić I, Stone HA, Whitesides GM. Chaotic Mixer for Microchannels. Science (80-). 2002;295(5555):647–51.

123. Knight JB, Vishwanath A, Brody JP, Austin RH. Hydrodynamic focusing on a silicon chip: Mixing nanoliters in microseconds. Phys Rev Lett. 1998;80(17):3863–6.

124. Jahn A, Stavis SM, Hong JS, Vreeland WN, Devoe DL, Gaitan M. Microfluidic mixing and the formation of nanoscale lipid vesicles. ACS Nano. 2010;4(4):2077–87.

125. Jahn A, Lucas F, Wepf RA, Dittrich PS. Freezing continuous-flow self-Assembly in a microfluidic device: Toward imaging of liposome formation. Langmuir. 2013;29(5):1717–23.

126. Jahn A, Vreeland WN, Devoe DL, Locascio LE, Gaitan M. Microfluidic directed formation of liposomes of controlled size. Langmuir. 2007;23(11):6289–93.

127. Michelon M, Oliveira DRB, de Figueiredo Furtado G, Gaziola de la Torre L, Cunha RL. High-throughput continuous production of liposomes using hydrodynamic flow-focusing microfluidic devices. Colloids Surfaces B Biointerfaces. 2017;156:349–57.

128. Guimarães Sá Correia M, Briuglia ML, Niosi F, Lamprou DA. Microfluidic manufacturing of phospholipid nanoparticles: Stability, encapsulation efficacy, and drug release. Int J Pharm. 2017;516(1–2):91–9.

129. Chen D, Love KT, Chen Y, Eltoukhy AA, Kastrup C, Sahay G, et al. Rapid Discovery of Potent siRNA-Containing Lipid Nanoparticles Enabled by Controlled Microfluidic Formulation. J Am Chem Soc. 2012;134(16):6948–51.

130. Kastner E, Verma V, Lowry D, Perrie Y. Microfluidic-controlled manufacture of liposomes for the solubilisation of a poorly water soluble drug. Int J Pharm. 2015;485(1–2):122–30.

131. Zhigaltsev I V., Tam YK, Leung AKK, Cullis PR. Production of limit size nanoliposomal systems with potential utility as ultra-small drug delivery agents. J Liposome Res. 2015;26(2):96–102.

132. Lee JN, Park C, Whitesides GM. Solvent Compatibility of Poly(dimethylsiloxane)-Based Microfluidic Devices. Anal Chem. 2003;75(23):6544–54.

133. Ramaswamy S, Tonnu N, Tachikawa K, Limphong P, Vega JB, Karmali PP, et al. Systemic delivery of factor IX messenger RNA for protein replacement therapy. Proc Natl Acad Sci. 2017;114(10):E1941–50.

134. Yin H, Song C, Dorkin JR, Zhu LJ, Li Y, Wu Q, et al. Therapeutic genome editing by combined viral and non-viral delivery of CRISPR system components in vivo. Nat Biotechnol. 2016;34(3):328–33.

135. Wang M, Zuris JA, Meng F, Rees H, Sun S, Deng P, et al. Efficient delivery of genome-editing proteins using bioreducible lipid nanoparticles. Proc Natl Acad Sci. 2016;113(11):2868–73.

136. Zhang X, Li B, Luo X, Zhao W, Jiang J, Zhang C, et al. Biodegradable Amino-Ester Nanomaterials for Cas9 mRNA Delivery in Vitro and in Vivo. ACS Appl Mater Interfaces. 2017;9(30):25481–7.

137. Richner JM, Himansu S, Dowd KA, Butler SL, Salazar V, Fox JM, et al. Modified mRNA Vaccines Protect against Zika Virus Infection. Cell. 2017;168(6):1114-1125.e10.

138. Bahl K, Senn JJ, Yuzhakov O, Bulychev A, Brito LA, Hassett KJ, et al. Preclinical and Clinical Demonstration of Immunogenicity by mRNA Vaccines against H10N8 and H7N9 Influenza Viruses. Mol Ther. 2017;25(6):1316–27.

139. Li B, Luo X, Deng B, Wang J, McComb DW, Shi Y, et al. An Orthogonal Array Optimization of Lipid-like Nanoparticles for mRNA Delivery in Vivo. Nano Lett. 2015;15(12):8099–107.

140. Oberli MA, Reichmuth AM, Dorkin JR, Mitchell MJ, Fenton OS, Jaklenec A, et al. Lipid Nanoparticle Assisted mRNA Delivery for Potent Cancer Immunotherapy. Nano Lett. 2017;17(3):1326–35.

2

141. Fenton OS, Kauffman KJ, McClellan RL, Appel E a., Dorkin JR, Tibbitt MW, et al. Bioinspired Alkenyl Amino Alcohol Ionizable Lipid Materials for Highly Potent In Vivo mRNA Delivery. Adv Mater. 2016;28(15):2939–43.

142. Pardi N, Hogan MJ, Pelc RS, Muramatsu H, Andersen H, DeMaso CR, et al. Zika virus protection by a single low-dose nucleoside-modified mRNA vaccination. Nature. 2017;543(7644):248–51.

143. Fenton OS, Kauffman KJ, Kaczmarek JC, McClellan RL, Jhunjhunwala S, Tibbitt MW, et al. Synthesis and Biological Evaluation of Ionizable Lipid Materials for the In Vivo Delivery of Messenger RNA to B Lymphocytes. Adv Mater. 2017;29(33):1606944.

144. Miller JB, Zhang S, Kos P, Xiong H, Zhou K, Perelman SS, et al. Non-Viral CRISPR/Cas Gene Editing In Vitro and In Vivo Enabled by Synthetic Nanoparticle Co-Delivery of Cas9 mRNA and sgRNA. Angew Chemie Int Ed. 2017;56(4):1059–63.

145. Montgomery DC. Design and Analysis of Experiments. 8th ed. Design. John Wiley & Sons, Inc.; 2012.

146. Pardi N, Secreto AJ, Shan X, Debonera F, Glover J, Yi Y, et al. Administration of nucleoside-modified mRNA encoding broadly neutralizing antibody protects humanized mice from HIV-1 challenge. Nat Commun. 2017;8:14630.

147. Maier MA, Jayaraman M, Matsuda S, Liu J, Barros S, Querbes W, et al. Biodegradable Lipids Enabling Rapidly Eliminated Lipid Nanoparticles for Systemic Delivery of RNAi Therapeutics. Mol Ther. 2013;21(8):1570–8.

148. Tseng WC, Haselton FR, Giorgio TD. Transfection by cationic liposomes using simultaneous single cell measurements of plasmid delivery and transgene expression. J Biol Chem. 1997;272(41):25641–7.

149. Tseng WC, Haselton FR, Giorgio TD. Mitosis enhances transgene expression of plasmid delivered by cationic liposomes. Biochim Biophys Acta, Gene Struct Expr. 1999;1445(1):53–64.

150. MacLachlan I, Cullis P, Graham RW. Progress towards a synthetic virus for systemic gene therapy. Curr Opin Mol Ther. 1999;1(2):252–9.

151. van der Oost J, Jore MM, Westra ER, Lundgren M, Brouns SJJ. CRISPR-based adaptive and heritable immunity in prokaryotes. Trends Biochem Sci. 2009;34(8):401–7.

152. Jinek M, East A, Cheng A, Lin S, Ma E, Doudna J. RNA-programmed genome editing in human cells. Elife. 2013;2:e00471.

153. Ran FA, Hsu PD, Wright J, Agarwala V, Scott DA, Zhang F. Genome engineering using the CRISPR-Cas9 system. Nat Protoc. 2013;8(11):2281–308.

154. Yin H, Xue W, Chen S, Bogorad RL, Benedetti E, Grompe M, et al. Genome editing with Cas9 in adult mice corrects a disease mutation and phenotype. Nat Biotechnol. 2014;32(6):551–3.

155. Haussecker D. Stacking up CRISPR against RNAi for therapeutic gene inhibition. FEBS J. 2016;283:3249–60.

156. Oude Blenke E, Evers MJW, Mastrobattista E, van der Oost J. CRISPR-Cas9 gene editing: Delivery aspects and therapeutic potential. J Control Release. 2016;244:139–48.

157. Silence Therapeutics. CRISPR/Cas9 gene editing data [Internet]. 2016 [cited 2017 Sep 28]. Available from: http://silence-therapeutics.com/media/1162/st-crispr-15nov16.pdf

158. Intellia Therapeutics. Strategy [Internet]. [cited 2017 Sep 28]. Available from: http://www.intelliatx.com/strategy/

159. Time to deliver. Nat Biotechnol. 2014 Oct 9;32(10):961–961.

2

Lipid nanoparticles containing siRNAs targeting the ceramide synthesis pathway reduce circulating ceramide levels *in vivo*

Martijn J.W. Evers[1], Xiaodong Yu[2], Chenyuan Huang[2,3], Xiaoyuan Wang[2], Suet Yen Chong[2], Michael Hannus[4], Reijo Laaksonen[5,6], Roy van der Meel[7], Sander Kooijmans[1], Sven Even Borgos[8], Terkel Hansen[8], Gert Storm[2,9,11,12], Raymond Schiffelers[1], Jiong-Wei Wang[2,3,9,10]

[1] CDL Research, University Medical Center Utrecht, 3584 CX Utrecht, the Netherlands
[2] Cardiovascular Research Institute (CVRI), National University Heart Centre Singapore (NUHCS), 117599 Singapore, Singapore
[3] Department of Surgery, Yong Loo Lin School of Medicine, National University of Singapore, 119228 Singapore, Singapore
[4] siTOOLs Biotech, D-82152 Planegg/Martinsried, Germany
[5] Finnish Cardiovascular Research Center Tampere, Tampere University, FI-33014 Tampere, Finland.
[6] Zora Biosciences,02150, Espoo, Finland.
[7] Laboratory of Chemical Biology, Department of Biomedical Engineering and Institute for Complex Molecular Systems, Eindhoven University of Technology, 5600 MB Eindhoven, The Netherlands.
[8] Department of Biotechnology and Nanomedicine, SINTEF Industry, Trondheim, Norway
[9] Nanomedicine Translational Research Programme, Centre for NanoMedicine, Yong Loo Lin School of Medicine, National University of Singapore, 117609 Singapore, Singapore
[10] Department of Physiology, Yong Loo Lin School of Medicine, National University of Singapore, Singapore 117593, Singapore
[11] Department of Pharmaceutics, Faculty of Science, Utrecht University, 3584 CG Utrecht, the Netherlands
[12] Department of Biomaterials, Science and Technology, Faculty of Science and Technology, University of Twente, 7522 NB Enschede, the Netherlands

3

ABSTRACT

Ceramides have been associated with the development and negative clinical outcomes in several cardiometabolic diseases such as type 2 diabetes, non-alcoholic steatohepatitis and atherosclerosis. Although the exact pathophysiology of increased levels of plasma ceramides in these diseases still needs to be defined, some preliminary studies in rodent models indicated that suppression of ceramide *de novo* synthesis with small molecule inhibitors could alleviate hallmark symptoms such as insulin insensitivity, vascular dysfunction and cardiac injury.

Enzymes of the *de novo* ceramide synthesis pathway, such as ceramide synthase 2 (CerS2) and dihydroceramide desaturase 1 (DegS1) can post-transcriptionally be silenced by administration of a short-interfering RNA (siRNA) molecule which targets the mRNA transcript for degradation in a sequence specific manner. For more than a decade, the therapeutic potential of siRNA molecules remained untapped as adequate delivery to the cytosol of target cells was limited. The development of lipid nanoparticles (LNPs) has enabled therapeutic delivery of siRNA to the liver. Since the liver is the major organ for ceramide production, we hypothesized that LNP mediated delivery of siRNA targeting key enzymes of the *de novo* ceramide synthesis pathway, being CerS2 and DegS1, could reduce plasma levels of ceramides. To test our hypothesis, we prepared LNPs encapsulating siPools™, a mixture of 30 different targeting siRNAs (LNP-siCerS2 or LNP-siDegS1). We determined the knockdown efficiency of CerS2 and DegS1 and the impact on plasma levels of ceramides. Both *in vitro* and *in vivo*, potent knockdown of CerS2 and DegS1 was achieved by administration of LNP-siRNA targeting CerS2 and DegS1, respectively. As demonstrated by lipidomics, knockdown of DegS1 resulted in decreased conversion of dihydroceramides to ceramides in liver and plasma samples. In contrast, knockdown of CerS2 in the murine liver had no effect on liver levels of ceramides, likely due to insufficient gene silencing.

In summary, this proof-of-concept study show that LNP-siRNA platform could be used for inhibiting ceramide *de novo* synthesis by targeting specific enzymes in the liver. Our findings may help to understand the pathophysiology of ceramides in cardiometabolic disease.

INTRODUCTION

Ceramides are a class of sphingolipids that can be found as a structural element in the plasma membrane, albeit at a lower concentration than glycerol phospholipids.[1,2]

Besides their structural function in cellular membranes, ceramides can act as signaling molecules and are most likely involved in cellular stress response and apoptosis.[3,4] Increased levels of specific plasma ceramides have been associated with major adverse events in cardiovascular disease, the development of nonalcoholic steatohepatitis, and type 2 diabetes in obese patients.[5–12]

The exact mechanism and pathophysiology of ceramide-related disorders remain yet to be unraveled, however increased lipid deposition and resulting toxic lipid metabolites in non-adipose tissue likely play a role.[7,11,13–20] Increased plasma ceramide concentrations can be the result of upregulated synthesis in the liver via the *de novo* ceramide synthesis pathway. This could be a consequence of saturation of common storage pathways of free fatty acids. Alternatively, it might also be a consequence of increased activity of sphingomyelin hydrolysis by SMase.[5,15,19,21–23]

The strong association of elevated levels of ceramides with various diseases has fueled the idea that inhibition of ceramide synthesis, in analogy to other lipid-lowering therapeutic strategies, might improve clinical outcomes of patients affected by cardiometabolic disorders.

Several enzymes of the *de novo* ceramide synthesis pathway, such as serine palmitoyltransferase (SPT), ceramide synthase (CerS) and dihydroceramide desaturase (DegS) can be attractive therapeutic targets. **(Figure 1)**

Several studies in rodent models found that inhibition of ceramide synthesis by suppressing SPT, could prevent insulin resistance, vascular dysfunction and reduce heart ischemia-reperfusion injury.[24–28] Ceramide synthases also received attention as potential therapeutic targets.[29–33] Inhibition of DegS1, either via the small molecular compound fenretinide or via (tissue-specific) deletion of *Degs1*, can prevent insulin resistance.[29,31] However, inhibition of DegS1 using fenretinide failed to reduce the development of atherosclerosis despite its lipid-lowering effect. The effect was attributed to drug-related side effects highlighting the importance of the need for specific inhibitors of the *de novo* ceramide pathway.[15,29,34]

Altogether, these studies illustrate the potential of *de novo* ceramide synthesis inhibition as a possible therapeutic strategy. However, there is still an unmet need for specific inhibitors of enzymes belonging to the ceramide synthesis pathway to improve understanding of the relationship between ceramides and cardiometabolic diseases and to develop future therapies.[15,32]

A promising approach could be the silencing of such enzymes via RNA interference (RNAi). RNAi is an endogenous pathway where mRNA is degraded in a sequence-specific manner by the RNA-induced silencing complex (RISC) composed of, amongst others, a small inhibitory RNA (siRNA) and the RNase Argonaute 2. The 21 base-pair siRNA sequence interacts with the complementary mRNA resulting in its degradation by RISC. The sequence specificity enables targeting of virtually any mRNA transcript for degradation.[35,36] Unfortunately, successful clinical translation of RNAi therapeutics has been limited for a long period mainly because of

3

the presence of off-target effects and lack of appropriate delivery methods.[37–41] Nowadays, for hepatic delivery of siRNA multiple delivery strategies are at hand. One of them is the lipid nanoparticle (LNP) platform. Here, siRNA molecules are encapsulated in a nanosized lipid particle which protects the siRNA cargo from endonucleases. Furthermore, ionizable lipids enable cytosolic delivery of the siRNA where it can exert its function.[42] Moreover, multiple strategies have been developed to mitigate the off-target effects of siRNAs such as chemical modifications of nucleotides and pooling of multiple specific siRNAs e.g. siPOOLs siRNA which combines 30 targeting siRNAs.[43–47] The LNP platform therefore provides a clinically relevant and translatable system to study silencing of specific enzymes of the ceramide synthesis pathway in the liver.

We hypothesize that gene-silencing of enzymes of the *de novo* ceramide synthesis pathway via LNP mediated delivery of siRNA could potentially reduce liver and plasma concentrations of specific ceramides. In this study, we aimed to silence 2 enzymes of the *de novo* synthesis pathway: CerS2 and DegS1. Inhibition of CerS2 potentially leads to a reduction of Cer (d18:0/24:0) which has been associated with CAD, however it's applicability as therapeutic target is not undisputed.[48,49] Silencing of DegS1 is expected to result in a decrease in overall ceramide concentration. To achieve this, LNPs encapsulating an siRNA targeting CerS2 or DegS1 were administered to mice and mRNA transcript levels, protein expression and liver/plasma ceramide concentrations were analyzed at 2 and 7 days after administration.

CerS Isoform	Specificity
1	C18
2	C22-C26
3	>C22
4	C18-C20
5	C14-C16
6	C14-C16
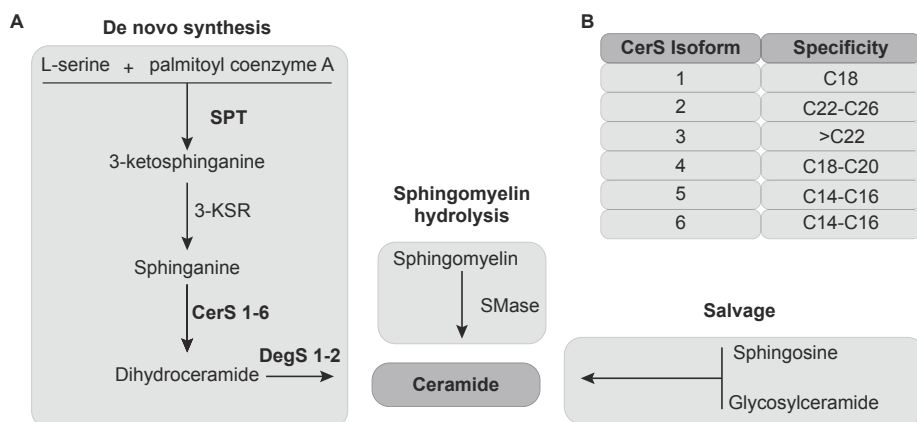
Figure 1: Ceramide synthesis. **A)** Three main pathways of ceramide synthesis: *de novo* synthesis, sphingomyelin hydrolysis, and the salvage pathway. The two targets, ceramide synthase 2 (CerS2), and dihydroceramide desaturase 1 (DegS1), both belong to the *de novo* synthesis pathway (left side). Here, ceramide synthesis is initiated by the conversion of L-serine and palmitoyl coenzyme A to 3-ketosphinganine, a reaction that is catalyzed by SPT. 3-ketosphinganine is then reduced to sphinganine by 3-ketosphinganine reductase (3-KSR), which subsequently reacts with a fatty acid chain, catalyzed by CerS, to form a dihydroceramide. Finally, dihydroceramides are reduced to ceramide, a reaction catalyzed by DegS. **B)** The structural diversity of ceramides is the result of N-acylation of the spingoid long chain base with different lengths of the N-acyl chain guided by different isoforms of the CerS enzyme.

MATERIALS & METHODS

Materials

DLin-MC3-DMA (VKB, India), Cholesterol (Sigma Aldrich, Saint Louis, MO, USA), 1,2-distearoyl-sn-glycero-3-phosphocholine (DSPC) (Avanti Polar Lipids, Alabaster, AL, USA), and 1,2-dimyristoyl-rac-glycero-3-methoxypolyethylene glycol-2000 (DMG-PEG) (NOF corporation, JP) stock solutions were prepared in 100% ethanol (Merck, Darmstadt, Germany). siRNA pools (siPools™) targeting CerS2, DegS1, and a non-specific control (NS) were provided by siTOOLs as lyophilized powder containing each a mixture of 30 different siRNAs and reconstituted in ultrapure water. For LC-MS/MS analysis, lipid standards for Ceramide Cer (16:0), Cer (18:0), Cer (20:0), Cer (22:0), Cer (24:0), Cer (18:1), Cer (24:1) Dihydrocer (16:0), Dihydrocer (18:0), Dihydrocer (24:0) and Dihydrocer (24:1) were all purchased from Avanti Polar Lipids (Alabaster, AL, USA) while Dihydrocer (C20:0) and Dihydrocer (C22:0) were purchased from Santa Cruz Biotechnology Inc. (Dallas, TX, USA). All other chemicals were purchased from Sigma Aldrich.

LNP production

Lipid nanoparticles were prepared by rapid mixing through a T-junction mixer as previously described.[50–53] Flow was provided by two PhD ultra-syringe pumps (Harvard Apparatus, Holliston, MA, USA). A lipid solution in 100% ethanol was mixed with a siRNA solution in sodium acetate (pH 4.0) at a flow rate ratio (aqueous:ethanol) of 3:1 at a total flow rate of 12 mL/min. LNPs were composed of DLin-MC3-DMA/Cholesterol/DSPC/DMG-PEG at a molar ratio of 0.5/0.385/0.1/0.015 at a concentration ranging from 5-20 mM. siRNA was encapsulated at a N/P of 6. After production, samples were dialyzed against an excess of PBS. After dialysis, LNPs were sterilized using 0.22μm PVDF membrane filters and concentrated to an appropriate volume using Amicon® Ultra-15 centrifugation filter units with a molecular weight cutoff of 10 kDa.

Particle Analysis

LNP size was measured using dynamic light scattering on a Zetasizer Ultra (Malvern Panalytical, Malvern, UK). Samples were diluted using PBS to an appropriate concentration and measured in triplicate.

The total RNA concentration was determined using the Quant-It™ Ribogreen RNA assay kit (Thermo Scientific, Waltham, MA, USA) in the presence of 0.5% (v/v) Triton X-100 (RNA_{TX-100}) whereas free/unencapsulated siRNA ($RNA_{PBS/TE}$) was determined in TE or PBS. The encapsulation efficiency was then calculated using the following formula $((RNA_{TX-100} - RNA_{TE/PBS})/RNA_{TX-100})*100$.

The cholesterol concentration was determined using LabAssay Cholesterol (DAKO, JP). Sample concentration was determined using a reference calibration curve. Absorbance was measured at 600 nm on a EnSpire multilabel reader 2300 (Perkin Elmer, MA, USA)

In-vitro analysis of LNP-siRNA gene-silencing efficacy

Hepa 1-6 cells were cultured in Dulbecco's modified eagle medium supplemented with 10% (v/v) fetal calf plasma (Thermo Fisher, Paisley, UK) and 1% (v/v) penicillin-streptomycin (Thermo

Fisher, NY, USA). 10.000 cells / well were seeded in a 96-well plate 24 hours before transfection. Samples were added at concentrations ranging from 0 to 100 n**M** siRNA. As a positive control, cells were transfected using Lipofectamine RNAiMAX (Thermo Scientific, Waltham, MA, USA) according to the manufacturer's instructions and cultured for another 24 hours. Then, mRNA was extracted and gene-silencing was evaluated by RT-qPCR.

Animal Experiments
Ethical statement on animal experiments
All animal experiments involving animal handling were performed with prior approval and following the protocols and guidelines of the National University of Singapore's Institutional Animal Care and Use Committee (IACUC) (R18-0664).

mRNA knockdown kinetics after a single injection of LNP-siRNA targeting CerS2 and DegS1
LNPs were produced encapsulating siPools™ targeting CerS2 and DegS1. LNPs were administered i.v. to C57BL/6J animals at a dose of 0.3 mg/kg siRNA/animal (N=8; N=4 / formulation). Animals were sacrificed after 2 (N=2; N=1 / formulation), 4 (N=2; N=1 / formulation) , 7 (N=2; N=1 / formulation) or 14 days (N=2; N=1 / formulation). Animals were perfused with via the left ventricle with saline, organs were harvested, and immediately snap-frozen in liquid nitrogen.

Influence of CerS2 and DegS1 knockdown on liver and plasma ceramide concentrations
LNPs encapsulating siPools™ siRNA targeting CerS2, DegS1, and a non-specific control were administered intravenously to C57BL/6J animals at a dose of 0.3 mg siRNA / kg (N=18, N=6 / formulation). Animals were sacrificed after 2 (N=9; N=3 / formulation) and 7 days (N=9; N=3 / formulation). Before sacrifice, blood was collected in MiniCollect® K3E K3EDTA tubes (Greiner Bio-one, Kremsmünster, Austria). Animals were perfused via the left ventricle with saline, organs were harvested and immediately snap-frozen in liquid nitrogen. mRNA levels and protein expression were analyzed via RT-qPCR and western blot analysis, respectively. Liver and blood plasma dihydroceramide and ceramide concentrations were analyzed by LC-MS/MS.

RT-qPCR analysis of CerS2 and DegS1 mRNA expression
mRNA was extracted from cells or murine tissue using RNeasy mini kit (Qiagen, Hilden, Germany) and quantified by spectrophotometry on a Nanodrop 2000 spectrophotometer (Thermo Fisher, Deleware, USA). RNA was reverse transcribed to cDNA using a QuantiTect-Reverse-Transcription Kit (QIAGEN Mainz, Germany). qPCR was performed in triplicates using PowerUp™ SYBR™ Green Master Mix (Thermo in a real-time thermal cycler, QuantStudio 7 (ThermoFisher, California, USA). Cylcing conditions were 98°C for 1 second followed by 60°C for 30 seconds, repeated 40 cycles. GADPH was used as the housekeeping gene and mRNA expression levels were normalized to control. Primer sequences were as follows: CerS2: Forward '5- TCCATATCTTCTGGGCCTACT-'3. Reverse: '5-CCCTCTGAACTCTCTGTTTCTTC-'3. DegS1: Forward: '5-GCTTATCGACTAGAGCCGGG-'3. Reverse: '5-AAATGAAGCCAGCTGGACGA-'3.

GAPDH: Forward: '5- CATCACTGCCACCCAGAAGACTG-'3. Reverse: '5- ATGCCAGTGAGCTTC-CCGTTCAG-'3.

Western Blot Analysis of CerS2 and DegS1 protein expression

Animal tissues were weighed, transferred to a 2 mL tube containing a 5 mm bead and 10 µL of RIPA buffer was added for every milligram of tissue. Samples were homogenized on a Tissuelyser LT (Qiagen, Hilden, Germany), for 3 cycles of 25 seconds at an oscillation of 1/25. Samples were then centrifuged at 13.300 x *g* for 10 minutes at 4°C and supernatant was transferred to a new tube. Sample protein concentration was determined using BioRad Protein Assay (Biorad, Hercules, CA, USA) or Pierce™ BCA protein assay (Thermo Scientific, Waltham, MA, USA) according to the manufacturer's instructions. Samples were normalized for protein content and 4x Laemmli loading buffer (BioRad, Hercules, CA, USA) containing beta-mercaptoethanol or DTT was added. Samples were heated for at least 10 minutes at temperatures >70 °C, centrifuged for 2 min at 13.000 rpm and 15 µg was loaded on a NuPAGE™ 4-12% Bis-Tris Protein Gel (Thermo Scientific, Waltham, MA, USA). Samples were separated by gel electrophoresis and blotted on a PVDF membrane using an iBlot 2 Gel Transfer Device (Invitrogen, California, US). The membrane was blocked for 1 hour using a blocking buffer consisting of 5% (w/v**)** Blotting Grade Blocker (Bio-Rad, Hercules, CA, USA) in TBS-Tween (0.1 v/v% Tween 20). Primary antibodies were used overnight at 4 °C and included Rabbit pAb anti-CerS2 (ab85567; 1:10.000), Rabbit pAb anti-DegS1 (PA5-42741; 1:1.000), rabbit mAb anti-GAPDH (ab9485;1:10.000). Secondary goat anti-rabbit antibody (ab 6721;1:10.000) was incubated for 1 hour at room temperature in blocking buffer. The blot was imaged using Bio-Rad ChemDoc Touch (Bio-rad, Hercules, CA, USA). To this end, membranes were incubated with Immobilon Western Chemiluminescent HRP Substrate (Merck, Darmstadt, Germany). For Western Blots targeting DegS1 and CerS2, first DegS1/CerS2 were imaged. The blot was then stripped in Western Blot Stripping buffer (Expedeon, Heidelberg, Germany) for 20 minutes. The blot was then incubated again with secondary antibody and imaged to confirm proper removal of primary antibody. Then the blot was incubated with antibody against GAPDH and subsequently imaged.

Lipidomic analysis by LC-MS/MS of ceramides in blood plasma and liver tissue

LC-MS/MS sample preparation

The targeted quantification of ceramides and dihydroceramides is based on a modified protocol by Jiang et al.[54] In short: 20 µl plasma, liver lysate or standard was mixed with 150 µl extraction buffer (isopropyl alcohol: chloroform 9:1 (v/v)) containing internal standards. Concentrations for internal standards were as follows: Ceramide C_{16}-D7: 2.3 ng/ml, Ceramide C_{24}-D7: 136 ng/ml, and C13-dihydroceramide-d7(d18:0-d7/13:0): 18 ng/ml. The samples were vigorously vortexed for 15 minutes, followed by 10 minutes of centrifugation at 14.000 g at 4 °C. Ninety microliters of the supernatant was transferred to Total recovery vials and quantified by HPLC-MS/MS. Calibration curves were prepared by diluting pure ceramides and dihydroceramides in an extraction buffer. A calibration curve was run for all compounds investigated and ranged from 0.1778 ng/ml to 10 µg/ml.

<u>HPLC-MS/MS</u>

LC-MS/MS analysis was conducted on an Agilent 1290 Infinity UPLC system (Santa Clara, California, USA) coupled to an Agilent 6490 Triple Quad LC/MS mass spectrometer using multiple-reaction monitoring (MRM). Separation of ceramides and dihydroceramides was performed at 60 °C on a Waters Aquity UPLC BEH C18, 2.1 x 100 mm analytical column connected to an Acquity UPLC BEH C18 2.1 x 5 mm VanGuard Precolumn at a flow rate of 0.4 ml/min (Massachusetts, USA). The mobile phase consisted of 10 mM ammonium formate, 0.1 % formic acid in water (solvent A), and 10 mM ammonium formate, 0.1 % formic acid in isopropanol (solvent B). The stepwise gradient was as follows: 0 – 1 min: 65% solvent B, 1 – 5 min: 65 to 90% solvent B, 5 – 5.1 min: 90 to 100 % solvent B, 5.1 – 5.4 min: 100% solvent B; 5.4 - 5.5 min: 100 to 65 % solvent B, 5.5 – 7.0 min: 65 % solvent B. The HPLC eluate was directed into the mass spectrometer for data acquisition from 1 minute until the end of the run. The injection volume was 5 µL and the total runtime was 7 min. The ESI source gas temperature was 180 °C with 13 l/min flow. The nebulizer was set to 15 psi and sheet gas temperature was set to 400 °C with a flow of 12 l/min. The capillary voltage was 5 kV while nozzle voltage was set to 0. High-pressure RF was 140 V while low-pressure RF was 120 V. Transitions and optimized collision energies can be found in supporting information. Dwell time was set to 30 ms for all transitions.

All quantification was done with Agilent Technologies MassHunter Workstation Software, Quantitative Analysis, version B.09.00 for QQQ utilizing area under the peak for quantification.

Statistical Analysis

Statistical analysis was performed using GraphPad Prism v8.3 (Graphpad Software, San Diego, CA, USA).

RESULTS & DISCUSSION

LNPs encapsulating siPools™ siRNA effectively silence gene-expression *in-vitro* of enzymes of the *de novo* ceramide synthesis pathway

In order to successfully deliver siRNAs targeting CerS2 and DegS1 to hepatocytes, we encapsulated siRNA in an LNP formulation comparable to the clinically approved Onpattro™ that has shown to be able to functionally delivery siRNA molecules to hepatocytes in humans.[42] For each target, a siPools™ siRNA mixture was used which combined 30 siRNAs with different sequences targeting the same mRNA construct for degradation.

LNPs were produced via microfluidic mixing using a T-junction, which resulted in particles of 70 nm with a PDI of approximately 0.1 as measured by dynamic light scattering (DLS) **(Figure 2AB).** The siRNA encapsulation efficiency was found to be ± 90% **(Figure 2C).** The gene-silencing efficacy of the LNPs-siRNA was first assessed *in vitro* for siPOOLs™ siRNA targeting CerS2 and DegS1 and included an LNP encapsulating a non-specific control siPool™ siRNA that does not have a target mRNA sequence. Hepa 1-6 cells were incubated with LNPs-siRNA at concentrations ranging from 0 to 100 nM siRNA. Twenty-four hours after administration of LNP-siRNA, a dose-dependent decrease in mRNA expression of both targets was observed. The

non-specific siRNA did not show any dose-dependent effect on mRNA expression, confirming the sequence-specific knockdown of mRNA by LNP-siRNA **(Figure 2DE)**.
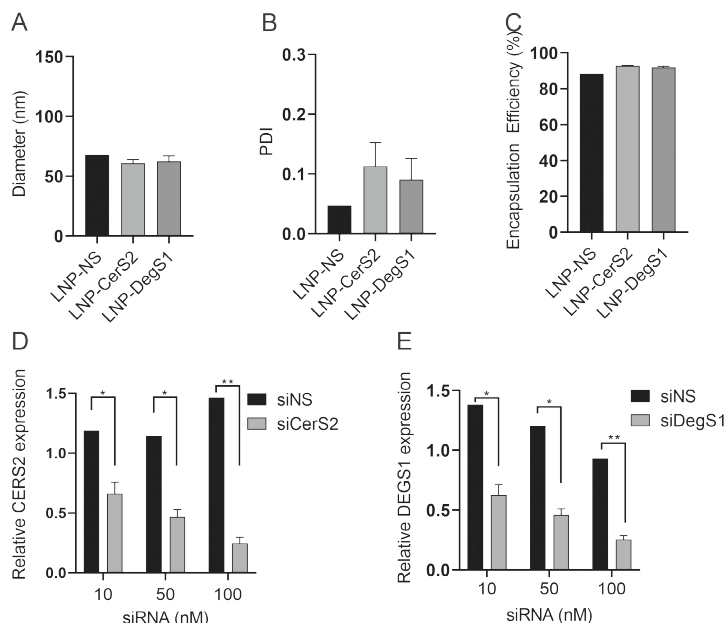
Figure 2: Characterization and in vitro efficacy of LNPs encapsulating siPool™ siRNA targeting different enzymes, CerS2 and DegS1 of the ceramide synthesis pathway. **A)** Nanoparticle size as determined by DLS **B)** Polydispersity index of nanoparticles as determined by DLS **C)** Encapsulating efficiency of different LNP formulations as determined by an RNA quantification assay **D)** RT-qPCR analysis of DegS1 mRNA expression in Hepa1-6 cells 24 h after administration of LNPs containing siPools™ siRNA targeting DegS1 and non-targeting siPools™ siRNA at concentrations ranging from 0-100 nM siRNA. mRNA transcript levels are expressed relative to untreated cells. **E)** RT-qPCR analysis of CerS2 mRNA expression in Hepa 1-6 cells 24 h after administration of LNPs containing siPools™ siRNA targeting CerS2 and non-targeting siPools™ siRNA at concentrations ranging from 0-100 nM siRNA. mRNA transcript levels are expressed relative to untreated cells. For size, PDI and encapsulation efficiency mean ± SD are displayed (n = 1-2). For qPCR mean ± SD are displayed (n = 1-3, biological replicates). Statistical significance was tested using a multiple T-test corrected for multiple testing using the Holm-Sidak method * = p < 0.05, ** = p<0.01.

CerS2 and DegS1 hepatic gene expression is reduced for two weeks after a single administration of LNP-siRNA targeting CerS2 and DegS1.

Next, we administered LNP-siRNA to mice to evaluate the effects *in vivo*. In an initial pilot study, mRNA expression levels in liver tissue were measured over time after a single dose of LNP-siRNA. To this end, we injected C57BL/6J mice with LNPs encapsulating siPools™ siRNA that target CerS2 or DegS1 at a dose of 0.3 mg siRNA / kg and measured mRNA and protein expression at day 2, 4, 7, and 14 after injection. **(Figure 3A)** mRNA expression of CerS2 decreased by approximately 95% at two days after injection, which persisted until day seven.

Two weeks after injection, mRNA expression recovered to 50% of its original level. For DegS1, approximately 60% reduction in gene expression was observed two days after injection, after which it gradually returned to pre-treatment levels at day 14. **(Figure 3B).** Hence, the siPool targeting DegS1 appeared to have a lower efficacy as compared to the siPool targeting CerS2. The difference in gene-silencing was unexpected as the in vitro gene-silencing efficacy in Hepa 1-6 cells was comparable between siRNA targeting CerS2 and DegS1. This observed difference might be explained by differences in mRNA turnover rates *in vivo*.

In addition to evaluating mRNA expression levels, we determined corresponding protein expression in the liver. The levels of CerS2 and DegS1 were analyzed via densitometric analysis of CerS2 and DegS1 western blots. For CerS2, we observed a maximal reduction in protein expression of 50% after seven days which was followed by an increase in protein expression levels at day 14. For DegS1, we observed a 50% reduction in protein expression on day 4 which restored to normal protein levels on day 7 **(Figure 3C-F)**. Overall, no correlation was found between CerS2/DegS1 mRNA expression levels and cognate protein expression. The most likely explanation for this phenomenon is the long protein half-life of both enzymes. Indeed, data obtained in literature from primary hepatocytes showed that *in-vitro* CerS2 protein half-life is approximately 55 hours. For DegS1, a half-life of 60 hours was reported though the quality of the data was marked as weak.[55] This could explain why there is no clear correlation between mRNA levels and protein expression at these time points.

Plasma and liver ceramide levels after administration of LNP-siRNA at 7 days after injection of LNP-siRNA targeting either CerS2 or DegS1.

Next, we evaluated the effect of gene knockdown of DegS1 or CerS2 on the ceramide concentrations liver and plasma. We injected animals with LNPs encapsulating siRNA targeting CerS2 or DegS1 or a non-specific siRNA (siNS) and, in addition to mRNA transcript levels and protein concentration, we measured the concentration of dihydroceramides - a ceramide precursor molecule – and ceramides at 2 and 7 days after injection. **(Figure 4A)**

At 2 and 7 days after injection, a significant decrease in mRNA expression of CerS2 and DegS1 was observed in the liver when treated with LNP-siRNA targeting CerS2 or DegS1, respectively. Administration of the non-specific siRNA did not affect mRNA transcript levels. **(Figure 4BC).** Unexpectedly, the gene-silencing effect of siCerS2 was reduced as compared to the pilot results obtained in Figure 3B, which could be a result of the low number of replicates

The protein concentration of CerS2 and DegS1 was analyzed by western blot. **(Figure 4DE)** Unfortunately, the previously used anti-DegS1 antibody was not available anymore and all other tested antibodies did not result in adequate detection of DegS1 so data on protein expression is lacking. We observed protein knockdown of CerS2 at day 7. The observed reduction, approximately 50%, was comparable to that observed in Figure 3CE.
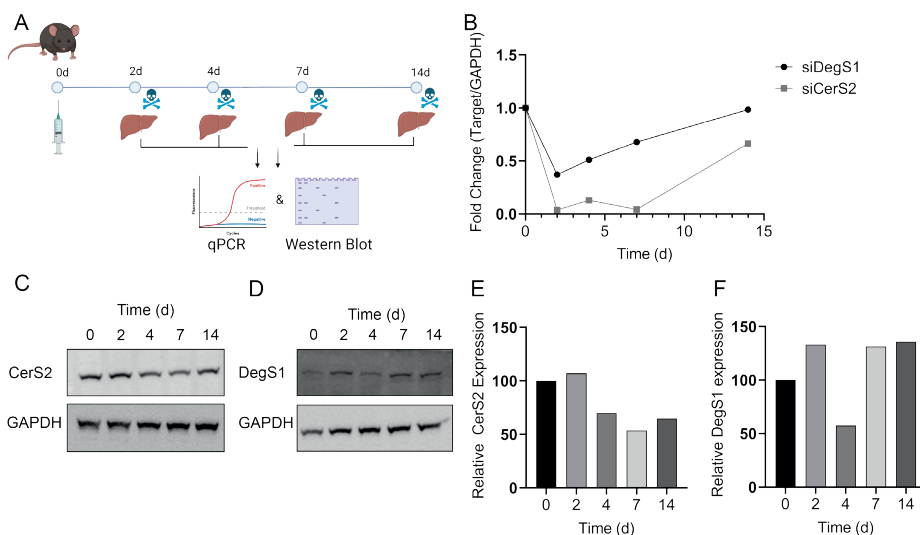
Figure 3: Gene-silencing of mRNA measured at 2, 4, 7 and 14 days after injection. The gene-silencing kinetics of LNP-siPools™ siRNA targeting DegS1 and CerS2 were analyzed by RT-qPCR and western blot analysis. **A)** LNPs encapsulating siPools™ siRNA targeting CerS2 or DegS1 were administered to C57Bl/6 mice at a dose of 0.3 mg siRNA / kg. mRNA and protein expression of CerS2 and DegS1 were analyzed at 2,4, 7, and 14 days after injection.(n=1) **B)** RT-qPCR analysis of CerS2 and DegS1 mRNA expression in C57Bl/6 mice 2,4,7, and 14 days after LNP injection. **C)** Western blot analysis of CerS2 and GAPDH protein levels in C57Bl/6 mouse livers 2,4,7, and 14 days after LNP injection. **D)** Western blot analysis of DegS1 and GAPDH protein levels in C57Bl/6 mouse livers 2,4,7, and 14 days after LNP injection. **E)** relative protein expression of CerS2 as measured by densitometry of the western blot **F)** relative protein expression of DegS1 as measured by densitometry of western blot. Figure 3A was created with BioRender.com

As we established reduced mRNA expression for both targets and confirmed reduced protein expression for CerS2, the concentrations of dihydroceramides and ceramides in liver tissue and blood plasma were measured via mass spectrometry. **(Supplementary Figure 1 & 2)**

For CerS2, a 50% reduction in expression did not translate to an effect on liver dihydroceramide or ceramide concentrations. We only observed a decrease in total plasma ceramides and of ceramide(d18:1/C24:1) at 7 days after injection. **(Figure 5)** This might indicate an effect of CerS2 reduction on ceramide synthesis, however this effect is not convincing as it is not observed for other ceramides. It is known that CerS2 is mainly involved in synthesis of very long chain (VLC) ceramides Cer(d18:1/C20:0), Cer(d18:1/C22:0), Cer(d18:1/C24:0) and, Cer(d18:1/C24:1) and is highly expressed in the liver.[56] We therefore anticipated that hepatic CerS2 knockdown would result in the reduced synthesis of all very long-chain dihydroceramides and subsequent ceramides in the liver. Moreover, hepatic CerS2 knockdown could also result in a corresponding decrease in plasma ceramides, as the liver is most likely a major source of plasma ceramides via the excretion of very-low-density lipoproteins (VLDL).[5,57,58]
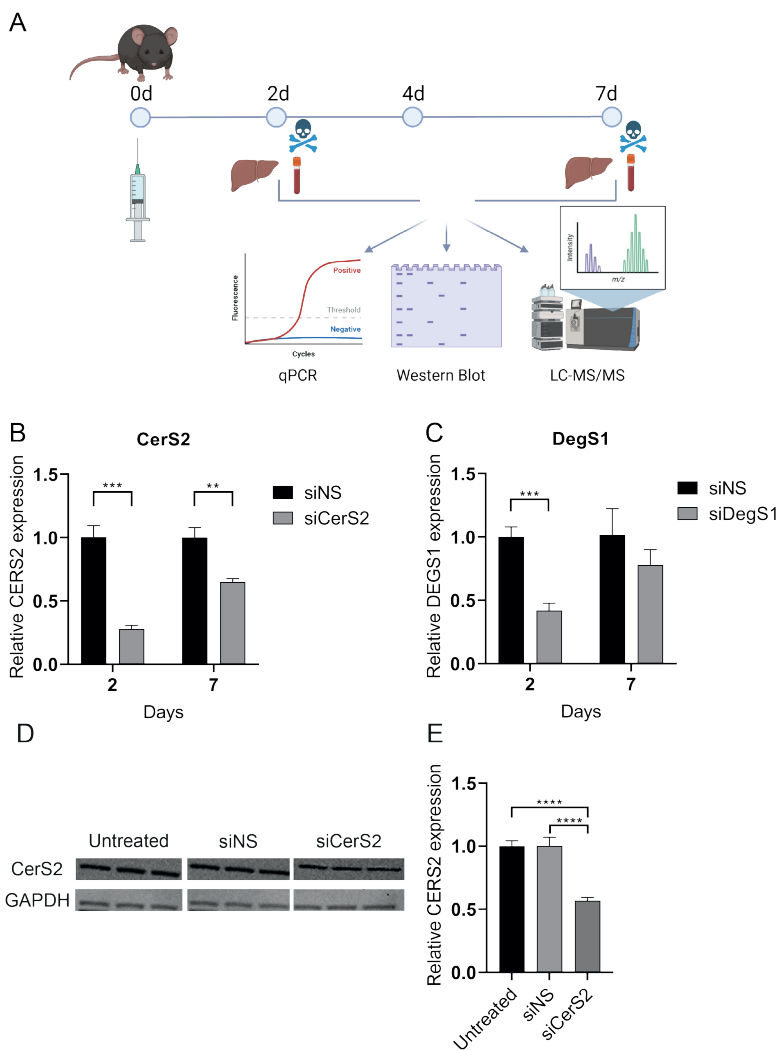
Figure 4: Specific knockdown of CerS2 and DegS1 by LNP-siCerS2 and LNP-siDegS1 A) C57BL/6 mice were injected with LNPs carrying siPools siRNA targeting CerS2, DegS1 or a non-specific control at a dose of 0.3 mg siRNA / kg and mRNA/protein expression was analyzed after 2 and 7 days. In addition, liver and plasma ceramide levels were analyzed by HPLC-MS/MS. **B)** CerS2 mRNA expression as measured by RT-qPCR 2 and 7 days after administration of LNP-siCerS2 and LNP-siNS. **C)** DegS1 mRNA expression as measured by RT-qPCR, 2 and 7 days after administration of LNP-siDegS1 and LNP-siNS. **D)** Western blot analysis of CerS2 and GAPDH in C57Bl/6 mice 7 days after administration of LNPs encapsulating siCerS1 or NS. In addition, CerS2 expression in untreated animals is shown. **E)** Relative protein expression of CerS2 as measured by densitometry of the western blot. All values are expressed as mean ±SD. Statistical differences in mRNA expression were tested using a multiple T-test corrected for multiple testing using the Holm-Sidak method. Statistical differences in protein expression were analyzed using a one-way ANOVA corrected for multiple testing using Tukey's method. ** = p<0.01, *** = p < 0.001, **** = p < 0.0001. siNS, non-specific siRNA; siCerS2, siRNA targeting ceramide synthase 2. Figure 4A was created with BioRender.com

Indeed, previous studies have shown the feasibility of this approach. In a study by Schmidt et al. 75% knockdown of CerS2 mRNA expression in the liver, following administration of an antisense oligonucleotide, resulted in a concomitant decrease of very long chain liver ceramides (C22-C24) at 7 days after injection. Moreover, after 5 weekly doses of the used Antisense Oligonucleotide, both liver and plasma ceramides were decreased providing evidence that reduced CerS2 expression in hepatocytes can result in decreased concentration of plasma VLC ceramides.[48] Therefore, the absence of liver ceramide inhibition after administration of LNP-siRNA in our study (despite mRNA knockdown) was unexpected.
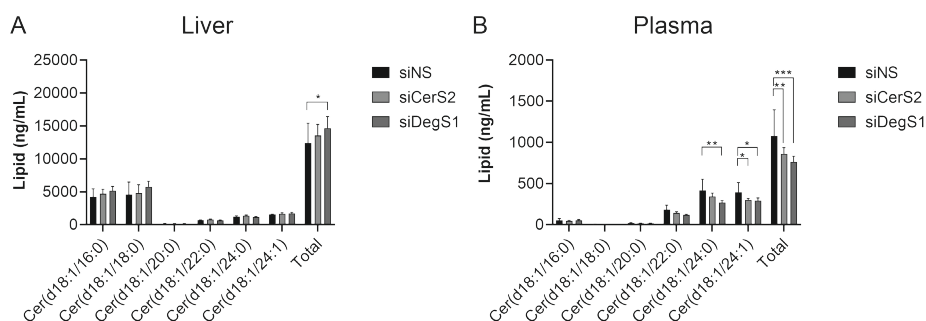
Figure 5: Liver and plasma ceramide concentrations at 7 days after injection of LNP-siCerS2 and LNP-siDegS1. A) Liver ceramide concentrations **B)** Plasma ceramide concentrations. Ceramide concentrations are displayed as mean ± SD. Two-way ANOVA with Tukey post-hoc test was used for statistical analysis. * = p < 0.05, ** = p < 0.01, *** = p < 0.001. Cer, ceramides; siNS, non-specific siRNA; siCerS2, siRNA targeting ceramide synthase 2; siDegS1, siRNA targeting dihydroceramide desaturase 1.

Inhibition of DegS1 can lead to accumulation of dihydroceramides as the conversion of dihydroceramides to ceramides is reduced. As a result, the ceramide to dihydroceramide ratio decreases.[31] We observed an increased accumulation of dihydroceramides at day 2 and 7 in both liver and blood plasma after treatment with LNP-siRNA targeting DegS1. This decrease was not at every time point accompanied by a simultaneous reduction in ceramide concentrations. **(Supplementary Figures 1 & 2)** Only at 7 days after administration of an LNP-siRNA targeting DegS1, plasma levels of ceramides were significantly decreased compared to animals treated with a non-specific siRNA. This effect was not observed in the liver, in which an increase of total ceramide concentration was observed **(Figure 5B)** We also observed a significant decrease in the ceramide to dihydroceramide ratio at day 7 in liver and plasma for all ceramides. When the ceramides species were stratified based on the chain length of the N-acyl chain, the ceramide to dihydroceramide ratio of several ceramides, C18:0 C22:0 C24:0 and C24:1 in the liver and C22:0 and C24:0 in plasma, was significantly decreased **(Figure 6)** Altogether, these results indicate that inhibition of DegS1, albeit only partially, inhibits the conversion of dihydroceramides to ceramides.
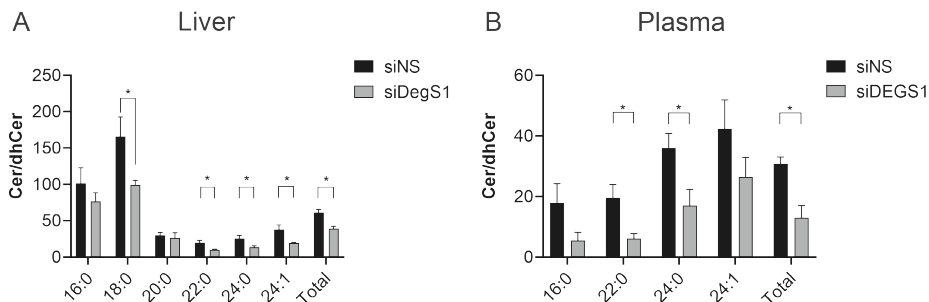
Figure 6: Ceramide to dihydroceramide ratio in liver and plasma at 7 days after injection of LNP-siDegS1 and LNP-siNS A) Liver ceramide to dihydroceramide ratio **B)** Plasma ceramide to dihydroceramide ratio. Ceramide to dihydroceramide ratios are displayed as mean ± SD. Differences were analyzed using a multiple T-test corrected for multiple comparisons using the Holm-Sidak method. Cer, ceramides; dhCer, dihydroceramides; siNS, non-specific siRNA; siDegS1, siRNA targeting dihydroceramide desaturase 1.

Taken together, we observed that a ~50% reduction in CerS2 expression only had a minor effect on plasma ceramide levels, whereas reduced DegS1 expression inhibited the conversion of dihydroceramides to ceramides. The absence of an widespread effect of CerS2 inhibition on liver and plasma ceramides can be attributed to the dose, dose regimen or potency of the siRNA molecule. Previously, It has been shown that reduced hepatic CerS2 expression has a pronounced effect on liver and plasma ceramides.[48] The potency of LNPs encapsulating siRNA targeting CerS2 and DegS1 can be increased via several ways. First, the stability and potency of the siRNA pool or siRNA molecule can be increased.[59] Second, the dose of LNP-siRNA could be increased. Third, we could repeatedly administer LNPs targeting DegS1 or CerS2 and analyze whether a sustained reduction of mRNA expression results in alterations in the liver or plasma ceramide profile. Such improvement could enable functional inhibition of ceramide synthesis, potentially alleviating cardiometabolic disease.

CONCLUSIONS

In this study, LNPs were loaded with siRNAs targeting different enzymes of the *de novo* ceramide synthesis pathway, namely CerS2 and DegS1. LNPs were produced via T-tube mixing and yielded sub 100 nm particles, which very efficiently encapsulated the siRNA. *In vitro*, delivery of siRNA resulted in potent knockdown of the targeted mRNA sequences as compared to non-specific siRNA controls. *In vivo*, we observed potent knockdown of targeted mRNA sequences over 7 days after which mRNA levels gradually returned to physiological levels. The degree of gene silencing varied per targeted mRNA sequence. A 50% decrease in mRNA expression of CerS2 did not result in an altered ceramide and dihydroceramide profile in liver and plasma measured 7 days after treatment. When LNPs targeting DegS1 were administered, we did observe a decreased conversion of dihydroceramides to ceramides given increased levels of dihydroceramides and reduced ceramide/dihydroceramide ratios over a broad range of lipid species.

Altogether these results demonstrate that LNP platform can be used to inhibit specific enzymes of the *de novo* ceramide synthesis pathway. These findings are of major importance for a range of potential applications. By targeting specific enzymes, we can dissect the impact of each of these enzymes for the lipid profiles *in vivo* and consequently for their roles in the pathophysiology of cardiometabolic disease. In addition, the LNP platform is relatively easy to scale-up, facilitating the translation of our findings to larger animal models and humans. We anticipate that this technology will thereby yield an improved understanding of the underlying relationship between ceramides and cardiometabolic disease.

3

REFERENCES

1. Maceyka M, Spiegel S. Sphingolipid metabolites in inflammatory disease. Nature. 2014;510(7503):58–67.
2. Meikle PJ, Summers SA. Sphingolipids and phospholipids in insulin resistance and related metabolic disorders. Nat Rev Endocrinol. 2017;13(2):79–91.
3. Pruett ST, Bushnev A, Hagedorn K, Adiga M, Haynes CA, Sullards MC, et al. Biodiversity of sphingoid bases ("sphingosines") and related amino alcohols. J Lipid Res. 2008;49(8):1621–39.
4. Nikolova-Karakashian MN, Rozenova KA. Ceramide in stress response. In: Chalfant C, Poeta M Del, editors. Sphingolipids as Signaling and Regulatory Molecules. 1st ed. Springer New York; 2010. p. 86–108.
5. Zelnik ID, Kim JL, Futerman AH. The Complex Tail of Circulating Sphingolipids in Atherosclerosis and Cardiovascular Disease. J Lipid Atheroscler. 2021;10(3):268.
6. Hilvo M, Wallentin L, Lakic TG, Held C, Kauhanen D, Jylhä A, et al. Prediction of residual risk by ceramide-phospholipid score in patients with stable coronary heart disease on optimal medical therapy. J Am Heart Assoc. 2020;9(10).
7. Laaksonen R, Ekroos K, Sysi-aho M, Hilvo M, Vihervaara T, Kauhanen D, et al. Plasma ceramides predict cardiovascular death in patients with stable coronary artery disease and acute coronary syndromes beyond. Eur Heart J. 2016;37:1967–76.
8. Hilvo M, Meikle PJ, Pedersen ER, Tell GS, Dhar I, Brenner H, et al. Development and validation of a ceramide- And phospholipid-based cardiovascular risk estimation score for coronary artery disease patients. Eur Heart J. 2020;41(3):371–80.
9. Nicholls M. Plasma ceramides and cardiac risk. Eur Heart J. 2017;38(18):1359–60.
10. Boon J, Hoy AJ, Stark R, Brown RD, Meex RC, Henstridge DC, et al. Ceramides contained in LDL are elevated in type 2 diabetes and promote inflammation and skeletal muscle insulin resistance. Diabetes. 2013;62(2):401–10.
11. Haus JM, Kashyap SR, Kasumov T, Zhang R, Kelly KR, Defronzo RA, et al. Plasma ceramides are elevated in obese subjects with type 2 diabetes and correlate with the severity of insulin resistance. Diabetes. 2009;58(2):337–43.
12. Adams JM, Pratipanawatr T, Berria R, Wang E, DeFronzo RA, Sullards MC, et al. Ceramide Content Is Increased in Skeletal Muscle from Obese Insulin-Resistant Humans. Diabetes. 2004;53(1):25–31.
13. Mantovani A, Lunardi G, Bonapace S, Dugo C, Altomari A, Molon G, et al. Association between increased plasma ceramides and chronic kidney disease in patients with and without ischemic heart disease. Diabetes Metab. 2021;47(1):101152.
14. Ji R, Akashi H, Drosatos K, Liao X, Jiang H, Kennel PJ, et al. Increased de novo ceramide synthesis and accumulation in failing myocardium. JCI insight. 2017;2(14):1–19.
15. Choi RH, Tatum SM, Symons JD, Summers SA, Holland WL. Ceramides and other sphingolipids as drivers of cardiovascular disease. Nat Rev Cardiol. 2021;18(10):701–11.
16. Chaurasia B, Summers SA. Ceramides - Lipotoxic Inducers of Metabolic Disorders. Trends Endocrinol Metab. 2015;26(10):538–50.
17. Chaurasia B, Summers SA. Ceramides in Metabolism: Key Lipotoxic Players. Annu Rev Physiol. 2021;83:303–30.
18. Summers SA, Chaurasia B, Holland WL. Metabolic Messengers: ceramides. Nat Metab. 2019;1(11):1051–8.
19. Pagadala M, Kasumov T, McCullough AJ, Zein NN, Kirwan JP. Role of ceramides in nonalcoholic fatty liver disease. Trends Endocrinol Metab. 2012;23(8):365–71.
20. Cantalupo A, Sasset L, Gargiulo A, Rubinelli L, Del Gaudio I, Benvenuto D, et al. Endothelial sphingolipid de novo synthesis controls blood pressure by regulating signal transduction and nO via ceramide. Hypertension. 2020;1279–88.
21. Kitatani K, Idkowiak-Baldys J, Hannun YA. The sphingolipid salvage pathway in ceramide metabolism and signaling. Cell Signal. 2008;20(6):1010–8.

22. Mullen TD, Hannun YA, Obeid LM. Ceramide synthases at the centre of sphingolipid metabolism and biology. Biochem J. 2012;441(3):789–802.

23. Pan W, Yu J, Shi R, Yan L, Yang T, Li Y, et al. Elevation of ceramide and activation of secretory acid sphingomyelinase in patients with acute coronary syndromes. Coron Artery Dis. 2014;25(3):230–5.

24. Hojjati MR, Li Z, Zhou H, Tang S, Huan C, Ooi E, et al. Effect of myriocin on plasma sphingolipid metabolism and atherosclerosis in apoE-deficient mice. J Biol Chem. 2005;280(11):10284–9.

25. Holland WL, Brozinick JT, Wang LP, Hawkins ED, Sargent KM, Liu Y, et al. Inhibition of Ceramide Synthesis Ameliorates Glucocorticoid-, Saturated-Fat-, and Obesity-Induced Insulin Resistance. Cell Metab. 2007;5(3):167–79.

26. Zhang QJ, Holland WL, Wilson L, Tanner JM, Kearns D, Cahoon JM, et al. Ceramide mediates vascular dysfunction in diet-induced obesity by PP2A-mediated dephosphorylation of the eNOS-Akt complex. Diabetes. 2012;61(7):1848–59.

27. Ji R, Goldberg IJ, Schulze PC, Ji R, Akashi H, Drosatos K, et al. Increased de novo ceramide synthesis and accumulation in failing myocardium. JCI insight. 2017;2(9):e82922.

28. Jiang M, Li C, Liu Q, Wang A, Lei M. Inhibiting ceramide synthesis attenuates hepatic steatosis and fibrosis in rats with non-alcoholic fatty liver disease. Front Endocrinol (Lausanne). 2019 Sep 26;10:665.

29. Bikman BT, Guan Y, Shui G, Siddique MM, Holland WL, Kim JY, et al. Fenretinide prevents lipid-induced insulin resistance by blocking ceramide biosynthesis. J Biol Chem. 2012;287(21):17426–37.

30. Blitzer JT, Wang L, Summers SA. DES1: A Key Driver of Lipotoxicity in Metabolic Disease. DNA Cell Biol. 2020;39(5):733–7.

31. Chaurasia B, Tippetts TS, Monibas RM, Liu J, Li Y, Wang L, et al. Targeting a ceramide double bond improves insulin resistance and hepatic steatosis. Science (80-). 2019;365(6451):386–92.

32. Turner N, Lim XY, Toop HD, Osborne B, Brandon AE, Taylor EN, et al. A selective inhibitor of ceramide synthase 1 reveals a novel role in fat metabolism. Nat Commun. 2018;9(1).

33. Hammerschmidt P, Ostkotte D, Nolte H, Gerl MJ, Jais A, Brunner HL, et al. CerS6-Derived Sphingolipids Interact with Mff and Promote Mitochondrial Fragmentation in Obesity. Cell. 2019 May;177(6):1536–52.

34. Busnelli M, Manzini S, Bonacina F, Soldati S, Barbieri SS, Amadio P, et al. Fenretinide treatment accelerates atherosclerosis development in apoE-deficient mice in spite of beneficial metabolic effects. Br J Pharmacol. 2020;177(2):328–45.

35. Elbashir SM, Harborth J, Lendeckel W, Yalcin A, Weber K, Tuschl T. Duplexes of 21-nucleotide RNAs mediate RNA interference in cultured mammalian cells. Nature. 2001;411(6836):494–8.

36. Fire A, Xu S, Montgomery MK, Kostas SA, Driver SE, Mello CC. Potent and specific genetic interference by double-stranded RNA in Caenorhabditis elegans. Nature. 1998;391(6669):806–11.

37. Setten RL, Rossi JJ, Han S. The current state and future directions of RNAi-based therapeutics. Nat Rev Drug Discov. 2019;18:421–46.

38. Jackson AL, Burchard J, Schelter J, Chau BN, Cleary M, Lim L, et al. Widespread siRNA "off-target" transcript silencing mediated by seed region sequence complementarity. RNA. 2006;12(7):1179–87.

39. Janas MM, Schlegel MK, Harbison CE, Yilmaz VO, Jiang Y, Parmar R, et al. Selection of GalNAc-conjugated siRNAs with limited off-target-driven rat hepatotoxicity. Nat Commun. 2018;9(723).

40. Juliano RL. The delivery of therapeutic oligonucleotides. Nucleic Acids Res. 2016;44(14):6518–48.

41. Nogrady B. Strand and deliver. Nature. 2019;574:S8–9.

42. Adams D, Gonzalez-Duarte A, O'Riordan WD, Yang C-C, Ueda M, Kristen A V., et al. Patisiran, an RNAi Therapeutic, for Hereditary Transthyretin Amyloidosis. N Engl J Med. 2018;379(1):11–21.

43. Schlegel MK, Foster DJ, Kel'in A V., Zlatev I, Bisbe A, Jayaraman M, et al. Chirality Dependent Potency Enhancement and Structural Impact of Glycol Nucleic Acid Modification on siRNA. J Am Chem Soc. 2017 Jun 28;139(25):8537–46.

44. Hannus M, Beitzinger M, Engelmann JC, Weickert MT, Spang R, Hannus S, et al. SiPools: Highly complex but accurately defined siRNA pools eliminate off-target effects. Nucleic Acids Res. 2014;42(12):8049–61.

3

45. Kittler R, Surendranath V, Heninger AK, Slabicki M, Theis M, Putz G, et al. Genome-wide resources of endoribonuclease-prepared short interfering RNAs for specific loss-of-function studies. Nat Methods. 2007;4(4):337–44.

46. Suter SR, Sheu-Gruttadauria J, Schirle NT, Valenzuela R, Ball-Jones AA, Onizuka K, et al. Structure-Guided Control of siRNA Off-Target Effects. J Am Chem Soc. 2016;138(28):8667–9.

47. Lee H-S, Seok H, Lee DH, Ham J, Lee W, Youm EM, et al. Abasic pivot substitution harnesses target specificity of RNA interference. Nat Commun. 2015 Dec 18;6(1):10154.

48. Schmidt S, Gallego SF, Zelnik ID, Kovalchuk S, Albæk N, Sprenger RR, et al. Silencing of ceramide synthase 2 in hepatocytes modulates plasma ceramide biomarkers predictive of cardiovascular death. Mol Ther. 2021;30(1):1–14.

49. Raichur S, Wang ST, Chan PW, Li Y, Ching J, Chaurasia B, et al. CerS2 Haploinsufficiency Inhibits β-Oxidation and Confers Susceptibility to Diet-Induced Steatohepatitis and Insulin Resistance. Cell Metab. 2014;20(4):687–95.

50. Chen S, Zaifman J, Kulkarni JA, Zhigaltsev I V, Tam YK, Ciufolini MA, et al. Dexamethasone prodrugs as potent suppressors of the immunostimulatory effects of lipid nanoparticle formulations of nucleic acids. J Control Release. 2018;286:46–54.

51. Jeffs LB, Palmer LR, Ambegia EG, Giesbrecht C, Ewanick S, MacLachlan I. A scalable, extrusion-free method for efficient liposomal encapsulation of plasmid DNA. Pharm Res. 2005;22(3):362–72.

52. Hirota S, De Ilarduya CT, Barron LG, Szoka FC. Simple mixing device to reproducibly prepare cationic lipid-DNA complexes (lipoplexes). Biotechniques. 1999;27(2):286–90.

53. Kulkarni JA, Darjuan MM, Mercer JE, Chen S, van der Meel R, Thewalt JL, et al. On the Formation and Morphology of Lipid Nanoparticles Containing Ionizable Cationic Lipids and siRNA. ACS Nano. 2018 May;12(5):4787–95.

54. Jiang H, Hsu FF, Farmer MS, Peterson LR, Schaffer JE, Ory DS, et al. Development and validation of LC-MS/MS method for determination of very long acyl chain (C22:0 and C24:0) ceramides in human plasma. Anal Bioanal Chem. 2013;405(23):7357–65.

55. Mathieson T, Franken H, Kosinski J, Kurzawa N, Zinn N, Sweetman G, et al. Systematic analysis of protein turnover in primary cells. Nat Commun. 2018;9(1):689.

56. Laviad EL, Albee L, Pankova-Kholmyansky I, Epstein S, Park H, Merrill AH, et al. Characterization of ceramide synthase 2: Tissue distribution, substrate specificity, and inhibition by sphingosine 1-phosphate. J Biol Chem. 2008;283(9):5677–84.

57. Mah M, Febbraio M, Turpin-Nolan S. Circulating Ceramides- Are Origins Important for Sphingolipid Biomarkers and Treatments? Frontiers in Endocrinology. 2021. p. 1–12.

58. Merrill AH, Lingrell S, Wang E, Nikolova-Karakashian M, Vales TR, Vance DE. Sphingolipid Biosynthesis de Novo by Rat Hepatocytes in Culture. J Biol Chem. 1995 Jun;270(23):13834–41.

59. Manoharan M. RNA interference and chemically modified small interfering RNAs Muthiah Manoharan. Curr Opin Chem Biol. 2004;8:570–9.

SUPPLEMENTARY INFORMATION
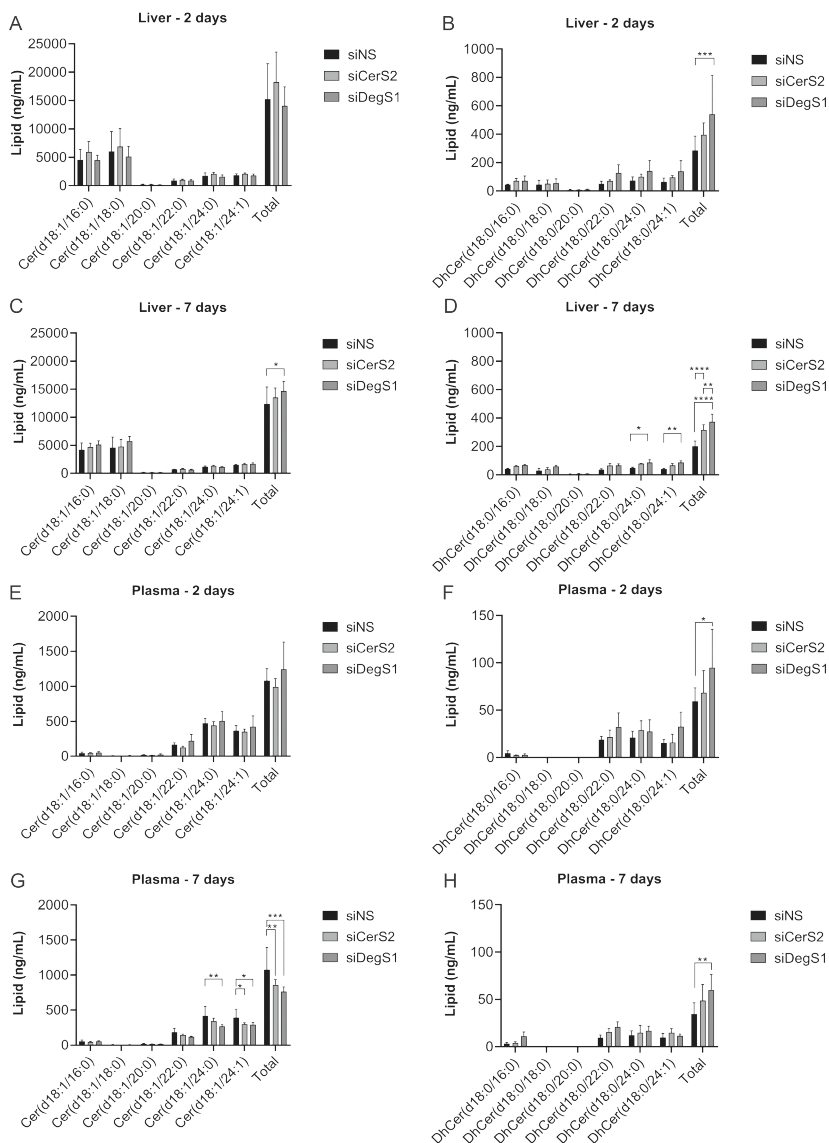
Supplementary Figure 1: Liver and plasma ceramides and dihydroceramides after administration of LNPs targeting CerS2 or DegS1 measured at 2 or 7 days after injection A) Liver ceramides, 2 days **B)** Liver dihydroceramides, 2 days **C)** Liver ceramides, 7 days **D**) Liver dihydroceramides, 7 days **E)** Plasma ceramides, 2 days **F)** Plasma dihydroceramides, 2 days **G)** Plasma ceramides, 7 days **H)** Plasma dihydroceramides, 7 days. Ceramide concentrations are displayed as mean ± SD. Two-way ANOVA with Tukey post-hoc test was used for statistical analysis. *** =** p < 0.05, ** = p < 0.01, *** = p < 0.001, **** = p < 0.0001. Cer, ceramides; dhCer, dihydroceramide; siNS, non-specific siRNA ; siCerS2, siRNA targeting ceramide synthase 2 ; siDegS1, siRNA targeting dihydroceramide desaturase 1.
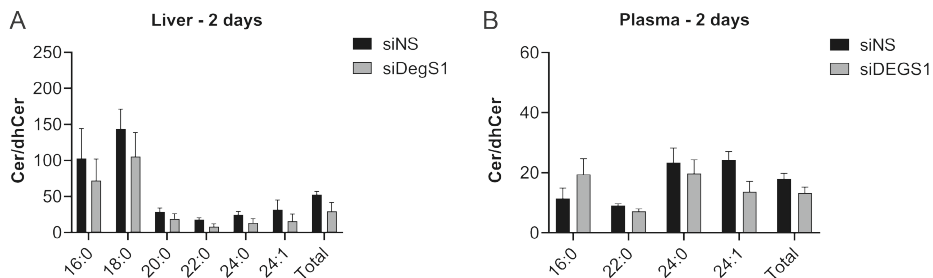
Supplementary Figure 2: Ceramide to dihydroceramide ratio in liver and plasma at 2 days after injection of LNP-siDegS1 and LNP-siNS A) Liver, 2 days **B)** Plasma, 2 days. Ceramide to dihydroceramide ratios are displayed as mean ± SD. Differences were analyzed using a multiple T-test corrected for multiple comparisons using the Holm-Sidak method. Cer, ceramides; dhCer, dihydroceramides; siNS, non-specific siRNA; siDegS1, siRNA targeting dihydroceramide desaturase 1.

LNPs containing siRNAs targeting the ceramide synthesis pathway reduce circulating ceramide levels *in vivo*

3

Delivery of modified mRNA to damaged myocardium by systemic administration of lipid nanoparticles

Martijn J.W. Evers[1]#, Wenjuan Du[2,6]#, Qiangbing Yang[1], Sander A.A. Kooijmans[1], Arjan Vink[4],Mies van Steenbergen[7],Pieter Vader[1,2], Saskia C.A. de Jager[2],Sabine A. Fuchs[5],Enrico Mastrobattista[7],Joost P.G. Sluijter[2,3]*, Zhiyong Lei[1,2]*,Raymond Schiffelers[1]*

1.CDL Research, UMC Utrecht, Utrecht, The Netherlands
2.Department of Experimental Cardiology, Circulatory Health Laboratory, UMC Utrecht, Utrecht, The Netherlands
3.Regenerative medicine Centre, UMC Utrecht, University Utrecht, Utrecht, The Netherlands
4. Department of Pathology, UMC Utrecht, Utrecht, The Netherlands
5. Division of Pediatric Gastroenterology, Wilhelmina Children's Hospital, UMC Utrecht, Utrecht, the Netherlands
6. Department of Cardiology, The Second Affiliated Hospital of Harbin Medical University Harbin, Heilongjiang Province, P.R. China
7. Department of Pharmaceutics, Utrecht Institute for Pharmaceutical Sciences (UIPS), Faculty of Science, Utrecht University, P.O. Box 80082, 3508 TB Utrecht, The Netherlands.
#, these authors contributed equally to this work

4

ABSTRACT

Lipid Nanoparticles (LNPs) are a promising drug delivery vehicle for clinical siRNA delivery. Modified mRNA (modRNA) has recently gained great attention as a therapeutic molecule in cardiac regeneration. However, for mRNA to be functional, it must first reach the diseased myocardium, enter the target cell, escape from the endosomal compartment into the cytosol and be translated into a functional protein. However, it is unknown if LNPs can effectively deliver mRNA, which is much larger than siRNA, to the ischemic myocardium. Here, we evaluated the ability of LNPs to deliver mRNA to the myocardium upon ischemia-reperfusion injury functionally. By exploring the bio-distribution of fluorescently labeled LNPs, we observed that, upon reperfusion, LNPs accumulated in the infarct area of the heart. Subsequently, the functional delivery of modRNA was evaluated by the administration of firefly luciferase encoding modRNA. Concomitantly, a significant increase in firefly luciferase expression was observed in the heart upon myocardial reperfusion when compared to sham-operated animals. To characterize the targeted cells within the myocardium, we injected LNPs loaded with Cre modRNA into Cre-reporter mice. Upon LNP infusion, Tdtomato+ cells, derived from Cre mediated recombination, were observed in the infarct region as well as the epicardial layer upon LNP infusion. Within the infarct area, most targeted cells were cardiac fibroblasts but also some cardiomyocytes and macrophages were found. Although the expression levels were low compared to LNP-modRNA delivery into the liver, our data show the ability of LNPs to functionally deliver modRNA therapeutics to the damaged myocardium, which holds great promise for modRNA-based cardiac therapies.

INTRODUCTION

Despite the advances in healthcare, heart failure is still one of the leading causes of death worldwide.[1] One of the most prevalent causes of heart failure is myocardial infarction. Part of the myocardium is starved of blood supply due to the occlusion of a coronary artery resulting in the loss of billions of cardiomyocytes.[2] Due to the limited regenerative capacity of the heart[3] and the lack of appropriate therapeutic interventions[4], the damaged heart has to compensate for the loss of cardiomyocytes via compensatory outward remodeling of the myocardium. This leads to the expansion of the infarction area and eventually results in heart failure.[1]

Stimulating cardiac repair and regeneration could be a potential therapeutic intervention to stop remodeling of the injured heart.[4] In the past years, researchers have identified several processes involved in cardiac development and regeneration.[3] Examples are the Hippo-Yap pathway[5-7], growth factors like NRG1[8, 9], VEGFA[10] and FGF2[11, 12], and the ability to reprogram fibroblast into cardiomyocytes[13, 14], which can be exploited to stimulate cardiac repair and regeneration in order to prevent pathological development of heart failure after myocardial infarction. However, these studies used transgenic animals[6-9, 11], direct injection of recombinant protein[10-12] or a viral approach[5, 13, 14] to increase the expression of specific proteins. Though these methods are very useful for proof of concept studies, they have limited clinical translatability due to either the potential immunogenicity and carcinogenicity of viral vectors[15] or the extremely short half-life of the delivered therapeutic proteins.[16]

Recent developments in the design and production of modified mRNA (modRNA) have significantly enhanced mRNA stability and reduced its immunogenicity.[17-19] These improvements helped modRNA emerge as an alternative to the genetic or viral approaches for the delivery of genetic material. The administration of naked VEGF[20] and FSTL1[21] modRNA into the myocardium has shown promising effects on vascular regeneration, cardiomyocytes proliferation after myocardial infarction.[20, 21]

However, administration of naked modRNA delivery is challenging since modRNA's physicochemical properties, including their large size and negative charge, make the spontaneous crossing of the cellular membrane virtually impossible.[19] Besides, direct administration of naked modRNAs to the myocardium requires direct intramyocardial injection via catheter-based intramyocardial delivery or invasive open chest surgery. Moreover, these methods come with the inavoidable quick removal pitfall via venous drainage observed for cell injection.[22] Therefore, modRNA's therapeutic delivery would benefit from a drug delivery system that could provide sufficient protection to the modRNA therapeutics, allow systemic administration with significant enrichment in the targeted disease domain. Lipid nanoparticles (LNPs) are one such delivery system.

The occlusion of the coronary artery results in vascular endothelium leakage, which enables nanoparticles to extravasate from the circulation in the ischemic area.[23] In line with these findings, we have shown that a lipid-based nanoparticle can access the myocardium after myocardial infarction, probably due to damage-induced vascular permeability: a phenomenon that is not observed in the healthy myocardium.[24] However, it is unknown whether such an approach also allows the delivery of functional modRNA to the damaged myocardium. This

study exploits the feasibility of using LNPs for functional delivery of modRNAs to the injured myocardium upon reperfusion.

MATERIALS & METHODS

Synthesis of DLin-MC3-DMA

Synthesis of DLin-MeOH

DLin-MeOH was synthesized according to the protocol reported before, with minor adaptions. [25] In short: Mg Turnings(2.2 g, 100 mmol) were added to a dry 500mL three-neck round-bottom (RB) flask equipped with a magnetic stirring bar, fluid cooled condenser and addition funnel. The setup was flushed with nitrogen and then 10 mL of anhydrous ether was added to the RB flask. Lineoleyl Bromide (24.04 g, 73 mmol) was dissolved in 45 mL anhydrous ether and loaded in the addition funnel. ~2 mL of this solution was added to the MG turnings and an exothermic reaction was observed. Iodine flakes (5 mg) were added to the reaction mixture to confirm formation of the Grignard reagent and the ether started refluxing. 43 mL of the Lineolyl bromide was subsequently added dropwise. After the addition of Lineolyl bromide, the reaction was kept under reflux at 35 degrees for 1 hr and then cooled in an ice bath. Ethyl Formate (2.46 g, 33.18 mmol) was dissolved in 35 mL anhydrous ether, transferred to the addition funnel and then added to the reaction mixture. The reaction was stirred for 1 hr at room temperature. The reaction was then quenched by dropwise addition of 4mL acetone and 24 mL of ice-cold water. The reaction mixture was then purified as described.[25] The crude product (17.32 g) was purified by flash column chromatography. Fractions were analyzed using Thin-layer Chromatography (TLC) and the product was pooled. The solvent was evaporated, yielding DLin-MeOH (9.7 g, 55%). DLin-MeOH was characterized via [1]H-Spectroscopy using a 400 MR-NMR spectrometer (Agilent Technologies, Santa Clara, CA, USA) as shown in Supplementary Figure S1

Synthesis of DLin-MC3-DMA

DLin-MC3-DMA was synthesized according to a previously described protocol, with minor modifications.[25] DLin-MeOH (1.32 g, 2.5 mmol) was dissolved in 8 mL of dichloromethane in a 50 mL RB flask. 1-ethyl-3-(3-dimethylaminopropyl) carbodiimide (EDC)*HCL (718 mg, 3.74 mmol), diisopropylamine (0.65 mL) and and 4-dimethylaminopyridine (DMAP) (30 mg, 0.25 mmol) were added. The reaction mixture was stirred for 5 min at room temperature. Dimethylaminobutyric acid (575 mg, 3,43 mmol) was added and stirred overnight at room temperature. Subsequently, the reaction was diluted in dichloromethane (30 mL) and washed with 50% saturated $NaHCO_3$ (20 mL), water (20 mL), and brine (30 mL). The combined organic layers were dried over anhydrous Na_2SO_4 and the solvent was removed *in vacuo*. The crude product (1.45 g) was then purified using flash column chromatography by a gradient elution form 99.5/0.5 dichloromethane/triethylamine to 97.5/2/0.5 (dichloromethane/methanol/triethylamine) to 96.5/3/0.5 (dichloromethane/methanol/triethylamine). Fractions were analyzed by TLC and pure fractions were pooled and solvent was vacuum evaporated yielding pure Dlin-MC3-DMA (700mg, 44%) as light-yellow oil. DLin-MC3-DMA was characterized via [1]H-Spectroscopy

using a 400 MR-NMR spectrometer (Agilent Technologies, Santa Clara, CA, USA) as shown in Supplementary Figure S2.

Preparation of modified Cre modRNA

The preparation method of modified Cre modRNA was similar to a previously described protocol.[26] In brief, Cre coding region was amplified by PCR from Cre-IRES-PuroR plasmid (addgene #30205). The backbone of pcDNA3.3-NDG (addgene #26820) without NDG gene was PCR amplified and subsequently assembled with Cre fragment to form pcDNA3.3-Cre using NEBuilder® HiFi DNA Assembly Cloning Kit (New England Biolabs (NEB), Ipswich, MA, USA). After sequencing validation, high purity pcDNA3.3-Cre plasmid was prepared using NucleoBondXtra Maxi kit for transfection-grade plasmid DNA (MACHEREY-NAGEL, Düren, Germany). The pcDNA3.3-Cre plasmid was linearized using Spe I to prevent from reading through of the Taq Polymerase. After purification, poly-(A) tail was added by PCR using High-Fidelity hot-start DNA Polymerase (Leishi Bio) according to the manufacture's instruction and the following primers: Primer 1: 5'-TTGGACCCTCGTACAGAAGCTAATACG-3'. Primer 2:T(120) CTTCCTACTCAGGCTTTATT CAAAGACCA. This PCR product was purified and checked by gel electrophoresis. *In vitro* transcription was carried out by mixing the following items: 3'-O-me-m7G cap analog (6.0 mM, Leishi Bio), GTP (1,5 mM, Leishi Bio), ATP (7,5 mM, Leishi Bio), Me-CTP(7.5 mM, Trilink Biotechnologies, San Diego, CA, USA), Pseudo-UTP(7.5 mM, Trilink Biotechnologies), Tailed PCR template (40 ng/ul) and T7 enzyme and buffer (Veni T7 RNA Synthesis kit, Leishi Bio) and incubated for 4 hours in a Thermocycler (Bio-Rad, Hercules, CA, USA). DNA templates were then removed by adding Turbo™ DNase (Thermo Scientific). After cleaning up, modRNA was treated with Antarctic phosphatase (NEB) to remove 5'-triphosphates from the uncapped RNA. After clearing up, the modRNA is aliquoted and stored at -80 ºC freezer before use.

Preparation of LNPs

LNPs were prepared by microfluidic mixing using the NanoAssemblr Benchtop (Precision Nanosystems, Vancouver, Canada). An ethanolic phase containing lipids was mixed with an acidic aqueous phase (25 mM sodium acetate, pH 4.0) containing modRNA leading to the formation of LNPs. LNPs were produced at a flow rate ratio (aquaous:organic) of 3:1 and a total flow rate of 4.0 mL/min. Cre modRNA was prepared in-house according to the previously decribed procedure. CD70 and firefly luciferase were a gift of eTheRNA Immunotherapies (Niel, Belgium). CD70 mRNA and firefly luciferase mRNA were unmodified, ARCA capped and purified by NaCl precipitation followed by LiCl precipitation. Lipids were dissolved in 100% Ethanol (Merck, Darmstadt, Germany) at a total lipid concentration of 20 mM. The LNPs were composed of DLin-MC3-DMA, Cholesterol (Sigma Aldrich, Saint Louis, MO, USA), DSPC (Lipoid, Ludwigshafen am Rhein, Germany) and PEG-DMG (NOF Corporation, Tokyo, JP) at a molar percentage of 50/38.5/10/1.5, respectively. mRNA/modRNA was encapsulated at a wt/wt ratio (ionizable lipid/RNA) of 10:1. Immediately after production, LNPs were dialyzed against an excess of phosphate buffered saline using Slide-a-Lyzer™ dialysis cassettes G2 with a membrane cutoff of 20kDa for 16-24 hours. After dialysis, LNPs were sterilized using 0.22 μm PVDF membrane filters and concentrated to an appropriate volume using Amicon® Ultra-15 centrifugational filter units with

a membrane cutoff of 10 kDa at 2000-4000 rpm at 4 ºC. Purified LNP was kept at 4 ºC and used within 7 days after production.

Nanoparticle Characterization

Size using Dynamic Light Scattering

The hydrodynamic diameter of LNPs was measured by Dynamic Light Scattering (DLS) using a Zetasizer Nano S (Malvern Panalytical, Malvern, UK) equipped with a 4 mW HeNe laser of 633nm. Samples were diluted appropriately in Dulbecco's PBS (DPBS) and scattering was measured at an angle of 173º at 37ºC for 10 seconds and repeated at least 10 times. This procedure was repeated three times for each sample.

Zeta Potential

The zeta potential of LNPs was measured using the Zetasizer Nano Z(Malvern Panalytical, Malvern, UK). Prior to analysis LNPs were diluted in 10mM HEPES (pH 7.4) or 0.1X DPBS (pH 7.4). Each sample was measured at least three times.

RNA determination and determination of encapsulation efficiency

The total RNA concentration was determined using the Quant-It™ Ribogreen RNA Assay kit (Thermo Scientific, Waltham, MA, USA) in the presence of 0.5% (v/v) Triton X-100 (RNA_{tx-100}), whereas free/unencapsulated mRNA($RNA_{TE/DPBS}$) was determined in TE or DPBS. The total mRNA/modRNA concentration (mg/mL) or free mRNA/modRNA concentration (mg/mL) was calculated using a reference calibration curve in 0.5% (v/v) Triton-X100 or TE/DPBS buffer. The encapsulation efficiency was then calculated using the following formula ((RNA_{tx-100}- $RNA_{TE/PBS}$)/RNA_{tx-100})*100.

Animal Experiments

Ethical statement on animal experiments

All animal experiments were performed with the Animal Welfare Body Utrecht's permission and complied with the Dutch Experiments on Animals Act (WOD) under license AVD115002015257. The research was carried out in accordance with the Guide for the Care and Use of Laboratory Animals.

Myocardial infarction and reperfusion

The left anterior descending coronary artery (LAD) was ligated for 60min before reperfusion was induced to induce myocardial ischemia and reperfusion injury. Briefly, mice were anesthetized with fentanyl (0.05mg/kg), midazolam (5mg/kg) and medetomidine (0.5mg/kg) by intraperitoneal injection. Surgical procedures were performed minimally invasive and under sterile conditions. Hearts were exposed by creating an opening between 3rd and 4th ribs and the LAD was ligated below the left atrial appendage with an 8-0 Ethilon monifil suture. After 60 minutes, the ligature was carefully removed to start reperfusion. After the chest was closed, anesthesia was antagonized (with atipamezole (2.5 mg/kg) and flumazenil (0.5 mg/kg)) and supplemented with Temgesic (0.1 mg/kg) for quick recovery and pain relief. Analgesia was given every 12 hours

after surgery for two days. At the end of each experiment, mice were terminated with overdose anesthesia with i.p. sodium pentobarbital 60 g/kg.

<u>In-vivo circulation time and bio-distribution of LNP-modRNA after Myocardial Infarction</u>
The biodistribution of LNPs encapsulating modRNA was assessed in 22 female C57Bl/6 mice (N= 22, weight between 22-25 gram, 12 week old, Charles River, Leiden, the Netherlands) with the use of fluorescently labeled LNPs (0.2 mol% DSPE – Cy5.5). Two mice died consequential to the MI surgery and as such they were excluded from the study. Animals were divided in 3 experimental groups: Animals in group 1 (N=8) underwent myocardial ischemia-reperfusion, animals in group 2 (N=8) were sham-operated animals and animals in group 3 (N=4) were control animals for background analysis of fluorescence. Sixty minutes after reperfusion, a dose of 50 mg LNP encapsulated modRNA was administered intravenously (i.v.) via the tail vein. Per animal, blood was collected at 3 pre-defined time points. Blood was collected either at t=1min, 30min and 240min (N=4) or at t=1 min, 2 h and 24 h (N=4). For control animals, the group size N=2. Blood was withdrawn via tail vein (T=1 min, 30 min, 2 h) or heart puncture (t=240 min or 24 h) and collected in EDTA anti-coagulated tubes. Blood samples were stored on ice and then centrifuged for 10min at 2000 xg and 4 ºC. Platelet-poor plasma was collected and stored at -80 ºC until further analysis.

At the end of each experiment, mice were terminated with overdose anesthesia with i.p. sodium pentobarbital 60 g/kg after 240 min (N=4) or 24 h (N=4)**(Figure 2A)**. Then, the mice were perfused with PBS via the left ventricle cavity. Organs were collected and tissue distribution of the LNPs was immediately analyzed by measurement of fluorescence signal using a Pearl Impulse Imager (Li-cor Biosciences, Lincoln, NE, USA). After imaging, organs were snap-frozen in liquid nitrogen and stored at -80 ºC until further analysis. Fluorescence in plasma and tissue lysates was analyzed by fluorescent spectroscopy on a Spectramax ID3 (Molecular Devices, San Jose, California, USA) at excitation/emission wavelengths of 675/720 nm , respectively. Plasma samples were first diluted 3x in Dulbecco's PBS; then 25µL of diluted platelet free plasma was transferred to a black 384 well plate and measured. Data is expressed as % of the value obtained at t=1 min. Tissue lysates were obtained from liver, spleen, lungs, a single femur, a single kidney, and the whole heart. Organs were weighed, transferred to a 2 mL tube containing ceramic beads (1.4 mm) and 3 µL of RIPA-buffer was added for every milligram of tissue. Tissues were homogenized using a Mini bead-beater 8 (Biospec, Bartlesville, OK, USA) for 60 s. Samples were centrifuged for 10min at 10.000 g and 4°C. 25µL of supernatant was transferred to a black 384 well plate and fluorescence was measured.

<u>Functional Delivery of firefly luciferase mRNA after myocardial infarction</u>
The efficacy of LNPs delivering luciferase mRNA was assessed after myocardial infarction by measurement of the luciferase activity 4h after administration. For this experiment, Ai9 mice (the Jackson laboratory,No: 007909) were used and received standard chow and water ad libitum. LNPs were administered at a single dose of 50 mg mRNA/animal 1 hr after the start of the reperfusion (N=4). As a control group, we used sham-operated mice(N=4). C57Bl/6 mice were used as blanks (N=2). Mice were sacrificed 4 hr post-injection and were perfused using 7 mL of

PBS **(Figure 3A).** Tissues were directly snap-frozen and stored at -80 °C until further processing. Luciferase activity was measured in tissue lysates. Tissues were weighed, transferred to a 2mL tube containing ceramic beads(1.4 mm) and 5 µL of Cell Culture Lysis Reagent was added for every milligram of tissue (Promega, Leiden, NL). Tissues were homogenized using a Mini bead-beater for 60 s. Samples were centrifuged for 10 min at 10000 g and 4°C. The supernatant was transferred to a fresh tube. Samples were stored at -80 °C until further analysis. Luciferase activity was measured using the Spectramax ID3 with the injector (Molecular Devices, San Jose, California, USA). 10 µL of supernatant was added to a white 96 well plate (Greiner,). 50 µL of Luciferase Assay Reagent (Promega, Leiden, Netherlands) was dispensed using the injector under shaking, incubated for 2 seconds and luminescence was measured at an integration time of 10 ms.

Functional delivery of Cre recombinase modRNA after myocardial infarction
The dose-dependent cell-type-specific uptake of LNP modRNA after myocardial infarction was investigated by microscopic study of tdTomato+ cells seven days after i.v. administration of LNP/ Cre modRNA. Eighteen 12-week old Ai9 mice (Jackson Laboratory, Bar Harbor, ME, USA, No: 007909) were operated on to induce myocardial infarction as described above. After the mice are recovered from anesthesia, mice were divided into six groups, three per group and injected with a single dose of LNPs containing 0 mg, 5 mg, 10 mg, 25 mg, 50 mg and 100 mg of Cre modRNA, respectively. The mice returned to standard housing with a warming pad and were terminated seven days post-injection.

Histology
Tissues (heart, lungs, kidney, spleen and liver) were collected, fixed and embedded in paraffin blocks. 3µm Paraffin sections were prepared with a microtome (Leica, RM2235). Antigen retrieval was performed with a pressure cooker method with citrate buffer (pH 6.0). Immunofluorescent staining was performed with the following primary and secondary antibodies: Anti-RFP (Rockland Immunochemicals, cat. # 600-401-379, 1:500), Mac3 (BD Bioscience, cat. # BDB553322, 1:100), anti-CD45(eBioscience, cat. # 30-F11, 1:100), FITC-labeled MF20 (Developmental Studies Hybridoma Bank, 1:500,), αSMA (Sigma-Aldrich, Cat.# A2547, 1:200), Donkey anti-Rabbit IgG (H+L) Highly Cross-Adsorbed Secondary Antibody Alexa Fluor 555 secondary antibody (Thermo-Fisher Scientific, Cat. # A-31572, Dilution) was used to visualize the primary anti-RFP antibody. Donkey anti-Rat IgG (H+L) Highly Cross-Adsorbed Secondary Antibody Alexa Fluor 488 (Thermo Fisher Scientific, Cat # A-21208, Dilution) was used to visualize Rat primary antibody. The whole tissue section was scanned with NanoZoomer S360 Digital slide scanner (Hamamatsu Photonics K.K, Hamamatsu Japan) and analyzed with NDP.view2 Viewing software: U12388-01 (Hamamatsu Photonics K.K, Hamamatsu Japan), to gain the overall distribution of the targeted cells in the whole tissue section. The liver toxicity was evaluated using H.E. staining and examined by an experienced pathologist.

Statistical Analysis

Statistical analysis was performed using GraphPad Prism v8.3 (Graphpad Software, San Diego, CA, USA). Tissue distribution of fluorescent LNPs and luciferase mRNA expression were analyzed per organ using an unpaired students t-test. Differences in plasma concentration of LNPs was analyzed per time point using an unpaired students t-test. A result was statistically significant if $P<0.05$.

RESULTS

Particle Characterization

Three different LNPs were produced by microfluidic mixing using the NanoAssemblr Benchtop device: LNPs encapsulating firefly luciferase mRNA, and LNPs containing Cre recombinase modRNA (Figure 1A and B). The size of all particles was below 100nm at a PDI <0.2. Incorporation of a fluorescent lipid, 0.2% DSPE-Cy5.5, in LNPs did not affect particle characteristics (Figure 1C). The batch-to-batch variability in terms of size and encapsulation efficiency between various LNP batches are shown in Figures 1D and E. The observed formulation characteristics of LNPs correspond well with particles of similar composition, reported previously.[27, 28]

Formulation	Components	Particle size(nm)	PDI	Zeta Potential (mV)	mRNA Encapsulation(%)	Batches
fLNP-mRNA	DLin-MC3-DMA/Cholesterol/DSPC/DMG-PEG2000/DSPE-PEG-Cy5.5 = 50/38,3/10/1,5/0,2	74	0,13	-4,2	98,6	1
LNP-mRNA fLuc	DLin-MC3-DMA/Cholesterol/DSPC/DMG-PEG2000 = 50/38,5/10/1,5	69	0,07	-4,8	98,0	1
LNP-mRNA Cre	DLin-MC3-DMA/Cholesterol/DSPC/DMG-PEG2000 = 50/38,5/10/1,5	87	0,10	-7,9	95,4	3
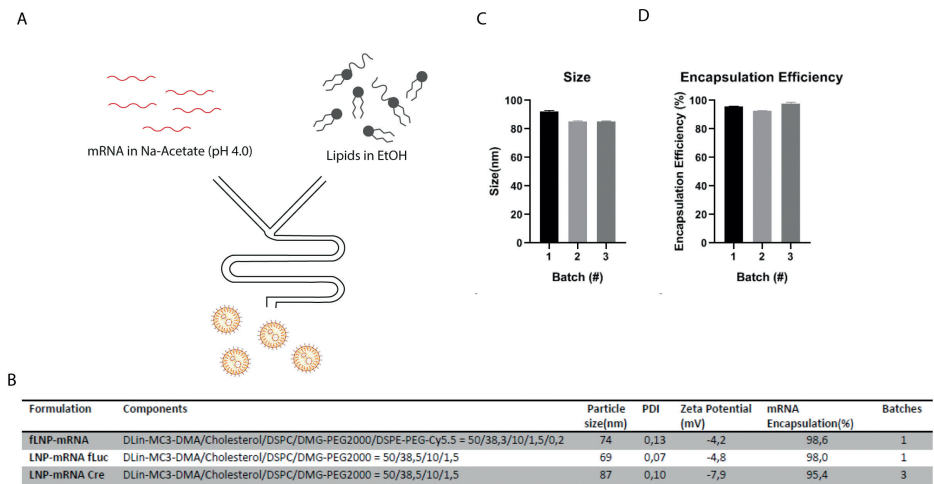
Figure 1: Production and Characterization of LNPs

A) Schematic Illustration of LNP production using microfluidic mixing. **B)** Tabular overview of LNP formulations and particle characteristics. Mean values of particle size (z-average), polydispersity index, z-potential, and encapsulation efficiency are reported**.** n=3 **C)** Batch to batch size variability. Three separate batches of LNP-modRNA Cre were produced over a period of 1 year. Z-average is reported as size; Mean ± SD. **D)** Batch-to-batch variability of encapsulation efficiency. n=3.

In-vivo biodistribution after ischemia reperfusion injury shows increased accumulation in the infarcted area of the heart

LNPs were fluorescently labeled using 0.2 mol% DSPE-Cy5.5 to allow the analysis of tissue distribution using fluorescent imaging and fluorescence quantification. Fluorescently labeled LNPs (fLNPs) were administered 1 hour after the start of reperfusion in a murine ischemia-reperfusion model and blood samples were taken at t = 1 min, 30 min, 60 min, 240 min and 24 h post-injection. Fluorescence in plasma samples was determined and expressed as a percentage of the fluorescence measured directly after injection (t = 1 min). Figure 2 shows that the majority of fLNPs were removed from circulation within 4 hours upon injection (Figure 2E). The ischemia-reperfusion injury did not influence fLNP plasma concentrations at any of the measured time points and no differences in blood plasma concentrations as measured by the fluorescence in blood plasma were observed between sham-operated and ischemia-reperfusion mice.

Directly after euthanasia, animals were perfused using PBS, whole organs were resected, and fluorescent tissue distribution imaged on a Pearl® Small Animal Imaging System. Imaging of indicated organs showed the accumulation of fLNPs in the heart upon ischemia-reperfusion 4 h after administration (Figure 2B). fLNPs mainly accumulated in the infarcted area just below the region where the left anterior descending artery was occluded. We did not observe any accumulation of LNPs in the heart of sham-operated or control animals. Differences in tissue distribution were still seen after 24 h but overall myocardial and tissue fluorescence decreased (Figure 2B). Taken together, upon ischemia-reperfusion injury, fLNP accumulated in the infarcted area of the heart.

Additionally, fluorescence levels were measured in tissue homogenates to quantify the amount of fluorescence in the organs. As indicated in Figures 2C and D, total fluorescence in the heart was increased in the ischemia-reperfusion injury group compared to the sham-operated group both at 4 and 24 h. No differences were found in other organs. Both fluorescent imaging of whole organs and quantification of fluorescence in tissue lysates indicated an increased accumulation of LNPs in cardiac tissue after ischemia-reperfusion injury. However, the intensity of the fluorescent signal was relatively low compared to organs such as the liver and spleen.

Administration of LNPs-mRNA after ischemia-reperfusion injury results in increased cardiac mRNA expression

To explore whether the increased accumulation of LNPs also affected the functional expression patterns of mRNAs, we intravenously injected LNP containing 50 mg of firefly luciferase mRNA 1h after the start of reperfusion and compared luciferase activity to the group of sham-operated mice. Figure 3 shows that myocardial luciferase activity in the ischemia-reperfusion injury group was significantly increased compared to the sham-operated control group. As expected from previous observations, cardiac luciferase activity was relatively low compared to organs in which LNPs typically accumulate, such as the liver and the spleen.
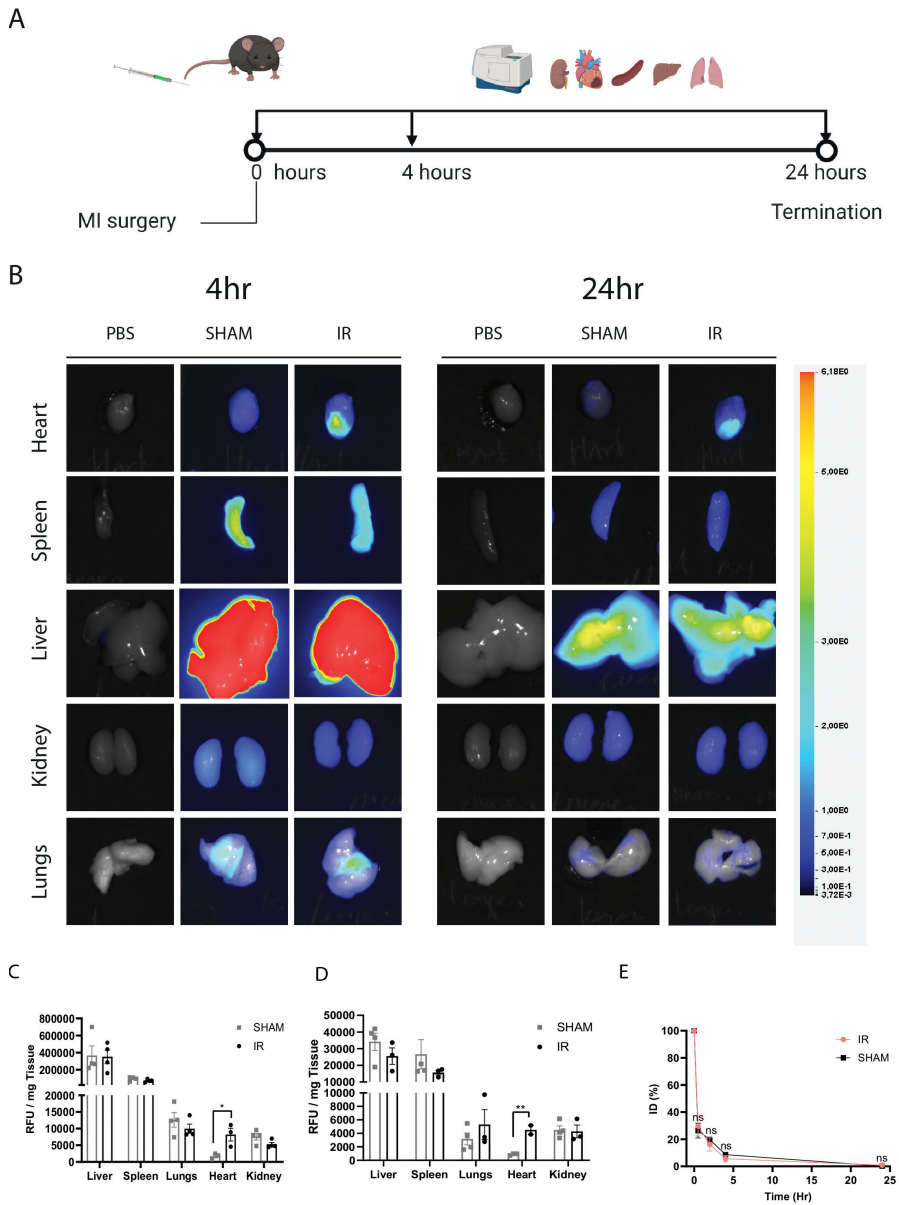
Figure 2: Biodistribution of fLNP-mRNA after sham-operation or ischemia-reperfusion injury
LNP-mRNA was administered at a dose of 50 μg mRNA to either sham-operated or ischemia-reperfusion injury animals. Mice were sacrificed after 4 or 24 h. **A)** Experimental design of the biodistribution study. **B)** Biodistribution of fluorescently labeled LNPs was measured by whole-organ fluorescence spectroscopy. Representative fluorescence/brightfield overlay images of murine organs harvested 4 and 24h after injection with 50 μg LNP-mRNA. Tissue distribution of fLNP after 4 hrs (C) or 24 hours (D) as determined by ex vivo luminescence of tissue lysates . Bars show mean RFU ± SD, n=4. **E)** Plasma concentration of fLNPs over time. Plasma concentration is expressed as a percentage of the plasma fluorescence directly measured after injection (t=1min). n = 4-8; mean ± SD. * represents P <0,05. ** represents P<0,01.
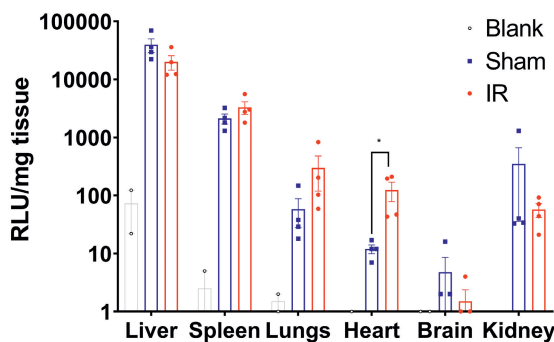
Figure 3: Luciferase activity in different organs lysates 4 hours after LNP-mRNA fLuc administration
Luciferase activity in homogenates of different organs 4 hours after intravenous administration of 50 μg firefly luciferase mRNA encapsulated in LNPs. LNPs were administrated 1hr after reperfusion of mice. Luciferase activity per mg tissue is plotted on a logarithmic scale. The untreated animals are C57/Bl6 mice without any treatment providing a background signal in different organs. N =2-4. * represents P <0,05.

LNPs-modRNA deliver modRNA to cells in the infarcted area of the heart, mainly αSMA+ cardiac fibroblasts

Different cell types play distinct roles in the pathological development of heart failure and therapeutic intervention can only achieve a maximum effect if the therapy reaches the desired organ region and cell type.[29-31]. To assess functional delivery of LNPs and identify the cells targeted, Cre/loxP reporter Ai9 mice were systemically injected with different doses of LNPs encapsulating Cre modRNA. In these mice, functional delivery of Cre recombinase modRNA results in Cre-mediated recombination, excising the STOP cassette, leading to the expression of tdTomato. Upon injection of a single dose of LNP-modRNA, we observed a dose-dependent increase of tdTomato+ cells in the heart as well as in the other organs, as shown in Figure 4 and Supplementary Figure 3**.** In the heart, we noticed that most of the tdTomoto+ cells were located in the infarcted area, but at higher doses (above 50 mg/mice), cells in the pericardial layer also became positive (Figure 4). We performed immunofluorescence staining with different cell-specific markers to identify these tdTomato+ cell types in the infarct area. Most of the tdTomato+ cells were identified as fibroblasts (αSMA+), whereas some tdTomato+ cardiomyocytes and macrophages could also be observed (Figure 5). In an independent experiment, we compared naked Cre modRNA with LNP encapsulated Cre modRNA in sham and MI operated animals. Here, we observed that naked Cre RNA injection resulted in only a low number of tdTomato+ cells (Supplementary Figure 4). To exclude liver toxicity by the use of the high doses of LNP-modRNA we performed H&E staining on the animals that were treated with high doses of LNP-modRNA (above 50 mg modRNA). Pathological examination revealed no difference compared with PBS controls, even at the highest dose (100 mg) used(Supplementary Figure 5).
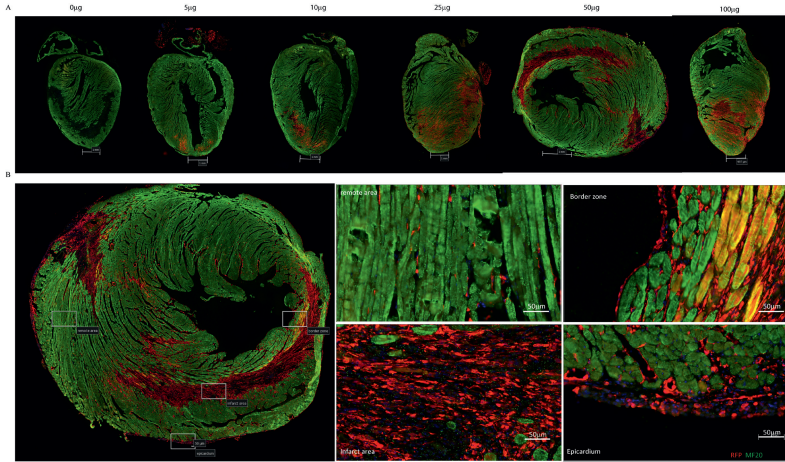
Figure 4: Dose-dependent delivery of LNP-encapsulated Cre modRNA to the infarcted myocardium.
A) A bird's-eye view of tdTomato+ cells at the different doses. tdTomato was stained with anti-RFP antibody in red, cardiomyocytes were stained using the MF20 antibody in green and Hoechst in blue. Note, the absence of green signal within myocardium indicated the infarcted areas. The scalebar represents 1mm. **B.** Identification of different locations within the heart. Infarct Area; Border Zone; Remote Area and epicardium. On the right, a zoom-in of tdTomato+ cells at different locations within the heart is shown. Orange cells in D indicate tdTomato+ cardiomyocytes which are stained positive in both red and green. Images were taken with NanoZoomer S360 Digital slide scanner and digitally magnified 20 times. The scalebar represents 50 µm
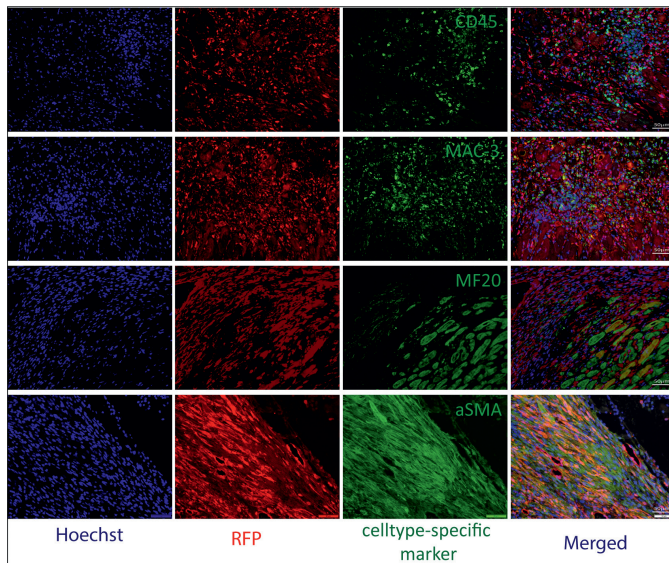
Figure 5: Characterization of Tdtomato+ cells after Cre modRNA delivery to the infarcted area of the myocardium. tdTomato was stained with anti-RFP in red, and co-stained with cell-type-specific markers CD45 (Leukocytes), MAC-3 (macrophages), MF20 (cardiomyocytes), and αSMA(fibroblasts) in green. Note, only small number of Mac-3+ and MF20+ cells were also tdTomato+, most of the tdTomato+ cells were fibroblasts. Nuclei were visualized with Hoechst 33342 in blue. The scalebar represents 50 µm.

DISCUSSION

This study explored the feasibility of functional mRNA/modRNA delivery to the myocardium after myocardial infarction using LPNs. modRNA therapy holds great promise in cardiac regeneration therapy. However, its functional delivery is challenged by the physicochemical properties of the RNA molecule including its size and charge limiting it's cellular uptake and release into the cytosol. Here, we explored the feasibility of lipid nanoparticles as a carrier for both modified and unmodified RNA to enable functional delivery to the myocardium via an intravenous route. After *i.v.* administration, LNPs accumulated in the ischemic region of the heart after ischemia-reperfusion injury. More importantly, increased tissue accumulation of LNP-modRNA led to increased functional protein production in the heart compared to sham-operated animals.

Tissue distribution of LNPs encapsulating modRNA to the ischemic area of the myocardium was not unexpected given the literature available on the administration of lipid nanoparticles after myocardial infarction.[23, 24] Ischemia-reperfusion injury leads to increased vascular permeability enabling extravasation of nanoparticles. This resulted in a clear increase in accumulation of LNPs in the heart after ischemia-reperfusion injury as observed by whole-organ fluorescent imaging and the measurement of fluorescence in tissue lysates. However, the measurement of LNP tissue biodistribution by fluorescent labeling of LNPs is not without its drawbacks. Firstly, labeling of the nanoparticle with a fluorescent lipid provides no data on the distribution of the actual therapeutic component: modRNA. Besides, previous reports have shown that fluorescent lipid probes can dissociate from PEGylated liposomes in a biological environment over a time course of 24 h.[32] Secondly, the quantitative data obtained via in vivo imaging of fluorescent nanoparticles may be influenced by quenching by blood components as well as differences in light scattering between organs.[33, 34] This study took all of these considerations into accounts. Diffusion of the PEG-lipid is expected to have limited influence since circulation half-time of the LNPs is expected to be ± 30 min. Organs were perfused with PBS prior to measurement to reduce possible interference of blood components. Apart from whole-organ imaging, fluorescence in tissue lysates was also analyzed to account for the eventual influence of light scattering on the results. Moreover, the functional bio-distribution of modRNA was evaluated by measurement of luciferase activity after administration of LNPs encapsulating firefly luciferase modRNA.

The increased delivery of LNP-mRNA to the infarcted heart also led to an increase in functional protein production of luciferase mRNA in IR-animals compared to a control group. In all other organs, no significant difference in luciferase activity was observed between sham and ischemia-reperfusion operated animals, typically observed for nanoparticles when administered intravenously.[35] Although LNP distribution and protein expression is increased in the heart after IR-injury by taking advantage of damage-induced vascular permeability phenomena, luciferase activity is still relatively low compared to the liver and spleen. Therefore, it would be interesting to study the timeframe of vascular leakage after myocardial infarction and determine at what time point within that timeframe is the most optimal time point for the injection of LNPs to improve the balance between on- and off-target delivery. For stable, chronic heart failure patients without myocardial infarction, the access of LNPs through vascular leakage will not occur.

Here, pretreatment with ultrasound-induced microbubble-destruction to induce local vascular permeability might be helpful.[36] Liver and splenic mRNA expression can also be attenuated by the incorporation of microRNA binding domains in the 3'-UTR of mRNA. Jain et al. showed that the incorporation of miR-122 binding sites in the 3'UTR led to diminished expression of mRNA in liver hepatocytes.[28] When miR-142 binding sites were incorporated, splenic mRNA expression was reduced.[28] Such an approach can be used to reduce the systemic translation of a protein, thereby reducing the risk of side effects in non-targeted organs. The biodistribution of LNP/mRNA can be affected by through optimization of the LNPs' lipid composition. For instance, Dahlman et al. have shown that variations in the structure of the PEG-lipid influences tissue distribution and that incorporation of different PEG-lipids can lead to increased accumulation in the heart.[37] Another potential approach to alter the expression pattern of the mRNAs using LNP is via the targeting approach. Recently, Peer's group has developed a self-assembly platform with an Fc domain anchored to the surfaced of LNP which can be easily combined with mAbs to target any cell type of interest.[38] In addition, an increasing number of infarct specific genes have been identified, the development of binders such as mAb and nanobodies will be very helpful to develop myocardial infarction enhanced delivery of LNP in the future.

Therapeutic use of modRNA in cardiac disease was already explored by others, albeit via other administration routes and/or mRNA drug delivery systems.[20, 21, 39-45] Most reported alternative administration routes are either direct intramyocardial injection or intraventricular injection with temporary aortic cross clamping. Compared to I.V. administration, these administration routes are more invasive. However, certainly for direct intramyocardial injection, the expression profile of the modRNA may be more localized in the heart with lower expression levels observed in spleen and liver which might be considered as an advantage.[46] Most interestingly, modRNA can also be functionally delivered to the heart via direct intracardiac injection in saline, citrate-saline buffer or a sucrose-citrate buffer with varying efficacy.[45] Functional delivery of naked modRNA, without an additional drug delivery vehicle, is only feasible in the heart, skin and skeletal muscle with no expression observed in liver, kidney and pancreas. [39] It is hypothesized that the modRNA is located along the cardiac sarcolemma providing a modRNA reservoir protecting the modRNA from RNAses. However, the exact mechanism of modRNA uptake and more interestingly the release of modRNA from the endo-lysosomal system to the cytosol is yet to be revealed. Currently, the high doses (100-150 mg modRNA per injection) used in functional studies might limit clinical translation due to the high dose associated costs and might warrant further investigation into lipid based drug delivery vehicles to enhance modRNA delivery to the heart.

Different cell types play distinct roles during the development of heart failure after myocardial infarction and therapeutic intervention can only achieve maximum effect if the desired therapy reaches the targeted cell type.[4, 29-31, 47] Therefore, it was of interest to evaluate which cell types in the myocardium were transfected by LNP-modRNA. Cre reporter mice gave us a possibility to precisely measure which cell types have taken up the LNP encapsulated Cre modRNAs using FACS or single cell sequencing technology. However, it turned out to be technically very challenging in the infarcted heart. The infarct scar is composed of fibrotic tissue which is very difficult to digest enzymatically. As a consequence, the cell types which are prone to

be single cells such as T cells, B cells will be over-represented in the final results cardiomyocytes and fibroblasts, which are sensitive to cell isolation procedures, will be underrepresented. Therefore, we decided to use the fluorescent microscopy approach which provides the spatial location of the cells that have taken up the LNP within the infarct myocardium even though it compromised in terms of quantification of the number of cells that have taken up the LNPs. Upon administering LNPs encapsulating Cre Recombinase modRNA to Cre-LoxP reporter mice, we observed that LNPs transfected cells both in the infarct region as well as the pericardial layer. Within the infarction area, the most efficiently targeted cell type was the cardiac fibroblast, which plays an important role in the development of cardiac fibrosis and during the remodeling phase in the heart.[48] The targeted delivery of therapeutic modRNA to these fibroblasts might be beneficial in two different potential therapeutic strategies. Firstly, it may be exploited to reduce the development of cardiac fibrosis directly.[29] Secondly, given the recent development in the aforementioned cardiac reprogramming technology, it can also be used to convert cardiac fibroblasts into cardiomyocytes directly.[49, 50] It must also be taken into account that the Cre-LoxP model is a very sensitive approach and given its binary "on/off'" nature, no data is obtained about the expression levels of the delivered modRNA in cardiac fibroblasts and whether or not this is sufficient to reach therapeutic concentrations.

These data suggest that LNPs encapsulating modRNA might be an alternative to various delivery methods currently used for reprogramming cardiac fibroblast to cardiomyocytes or for the expression of therapeutic proteins via plasmid DNA. Moreover, the delivery of LNPs encapsulating modRNA is also an alternative for recombinant protein administration.[51]

CONCLUSION

The results presented here demonstrate the feasibility of functional modRNA delivery by LNPs to the infarct region after myocardial infarction. Given the rapid progress in the cardiac regeneration field, an approach using LNPs to deliver modRNA might accelerate the translation of newly identified pro-cardiac regeneration genes into the clinic.

ACKNOWLEDGMENTS

4

SUPPLEMENTARY INFORMATION

Supplementary Figure S1: NMR Dlin-MeOH

^{1}H NMR (400 MHz, CDCL$_3$): **δ** (ppm) 5.65 − 5.06 (8H), 3.71 − 3.34 (1H), 2.87- 2.60 (4H), 2.23 − 1.73 (9H), 1.6 − 1.06 (51H), 0.96 − 0.72 (7H)
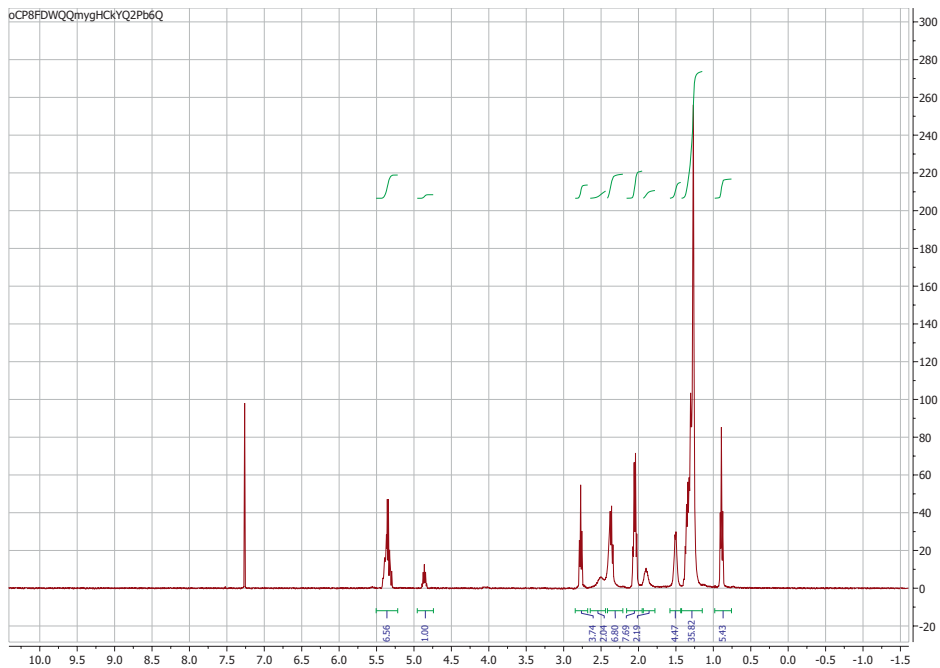
Supplementary Figure S2: NMR Dlin-MC3-DMA

^{1}H NMR (400 MHz, CDCL$_3$): **δ** (ppm) 5.51 − 5.22 (7H), 4.96- 4.74 (1H), 2.85 − 2.68 (4H), 2.64 − 2.44 (2H), 2.27-2.20 (7H), 2.16-1.95 (8H), 1.92 − 1.78 (2H), 1.58 − 1.44 (4H), 1.42 − 1.15 (36H), 0.98 − 0.76 (5H)
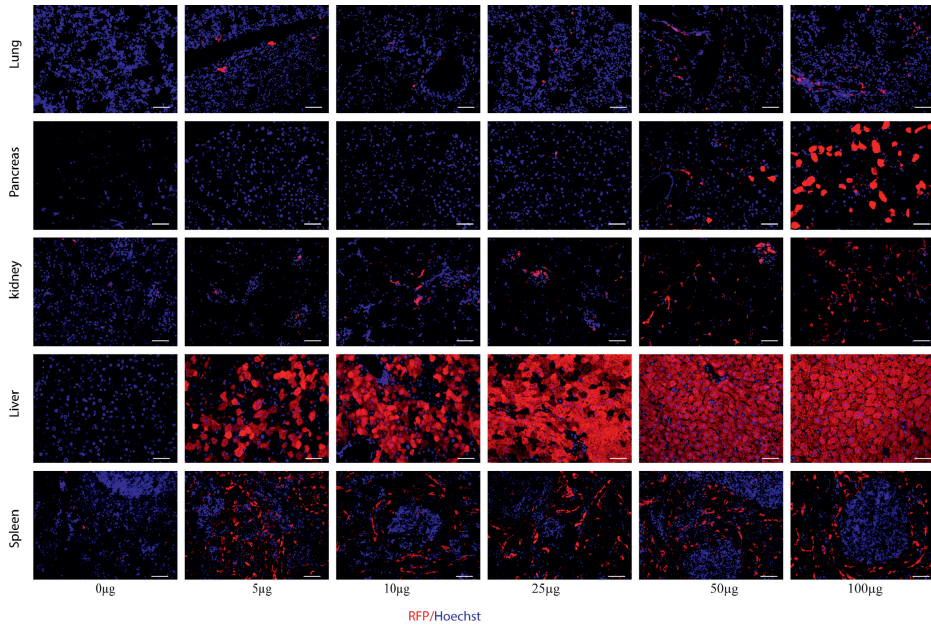
Supplementary Figure 3. Dose-dependent delivery of Cre modRNA to different organs besides the heart. tdTomato was stained with anti-RFP antibody in red, Nuclei were stained with Hoechst 33342 in blue. Scale bar represents 50 μm.
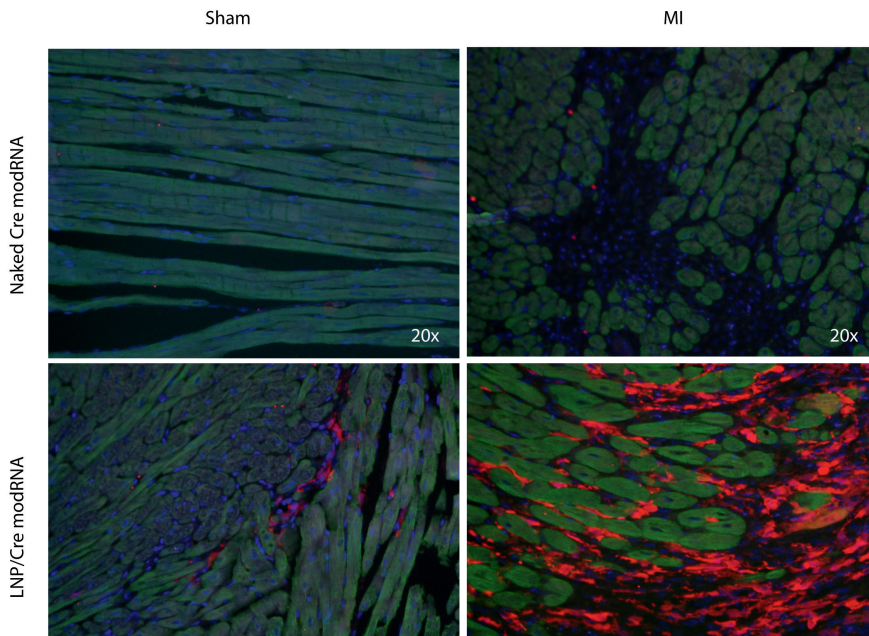
Supplementary Figure 4. Myocardial infarction enhanced LNP/Cre modRNA delivery in the heart. tdTomato was stained with anti-RFP antibody in red, Nuclei were stained with Hoechst 33342 in blue. Scale bar represents 50 μm.

| 0µg | 5µg | 10µg | 25µg | 50µg | 100µg |
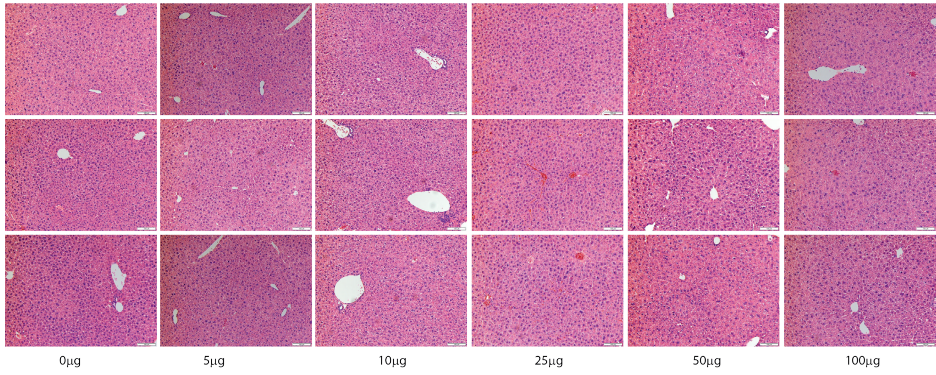
Supplementary Figure 5. Assessment of liver toxicity of the LNP/modRNA administration using H.E. staining. 3 mice treated with indicated dose of modRNAs are shown.

4

REFERENCES

1. Yancy CW, Jessup M, Bozkurt B, Butler J, Casey DE, Colvin MM, et al. 2017 ACC/AHA/HFSA focused update of the 2013 ACCF/AHA guideline for the management of heart failure: a report of the American College of Cardiology/American Heart Association Task Force on Clinical Practice Guidelines and the Heart Failure Society of America. J Am Coll Cardiol. 2017 Aug 8;70(6):776-803.
2. Laflamme MA, Murry CE. Heart regeneration. Nature. 2011;473(7347):326-35.
3. de Wit L, Fang J, Neef K, Xiao J, P AD, Schiffelers RM, et al. Cellular and Molecular Mechanism of Cardiac Regeneration: A Comparison of Newts, Zebrafish, and Mammals. Biomolecules. 2020;10(9):1204
4. Yang Q, Fang J, Lei Z, Sluijter JPG, Schiffelers R. Repairing the heart: State-of the art delivery strategies for biological therapeutics. Adv Drug Deliv Rev. 2020;160:1-18.
5. Lin Z, von Gise A, Zhou P, Gu F, Ma Q, Jiang J, et al. Cardiac-specific YAP activation improves cardiac function and survival in an experimental murine MI model. Circ Res. 2014;115(3):354-63.
6. von Gise A, Lin Z, Schlegelmilch K, Honor LB, Pan GM, Buck JN, et al. YAP1, the nuclear target of Hippo signaling, stimulates heart growth through cardiomyocyte proliferation but not hypertrophy. Proc Natl Acad Sci USA. 2012 Feb 14;109(7):2394-9.
7. Xin M, Olson EN, Bassel-Duby R. Mending broken hearts: cardiac development as a basis for adult heart regeneration and repair. Nat Rev Mol Cell Biol. 2013;14(8):529-41.
8. Bersell K, Arab S, Haring B, Kühn B. Neuregulin1/ErbB4 signaling induces cardiomyocyte proliferation and repair of heart injury. Cell. 2009;138(2):257-70.
9. D'Uva G, Aharonov A, Lauriola M, Kain D, Yahalom-Ronen Y, Carvalho S, et al. ERBB2 triggers mammalian heart regeneration by promoting cardiomyocyte dedifferentiation and proliferation. Nat Cell Biol. 2015;17(5):627-38.
10. Harada K, Friedman M, Lopez J, Wang S, Li J, Prasad P, et al. Vascular endothelial growth factor administration in chronic myocardial ischemia. Am J Physiol Heart Circ Phys. 1996;270(5):H1791-802.
11. House SL, Bolte C, Zhou M, Doetschman T, Klevitsky R, Newman G, et al. Cardiac-specific overexpression of fibroblast growth factor-2 protects against myocardial dysfunction and infarction in a murine model of low-flow ischemia. Circulation. 2003;108(25):3140-8.
12. Simons M, Annex BH, Laham RJ, Kleiman N, Henry T, Dauerman H, et al. Pharmacological treatment of coronary artery disease with recombinant fibroblast growth factor-2: double-blind, randomized, controlled clinical trial. Circulation. 2002;105(7):788-93.
13. Miyamoto K, Akiyama M, Tamura F, Isomi M, Yamakawa H, Sadahiro T, et al. Direct in vivo reprogramming with Sendai virus vectors improves cardiac function after myocardial infarction. Cell Stem Cell. 2018;22(1):91-103. e5.
14. Qian L, Huang Y, Spencer CI, Foley A, Vedantham V, Liu L, et al. In vivo reprogramming of murine cardiac fibroblasts into induced cardiomyocytes. Nature. 2012;485(7400):593-8.
15. Thomas CE, Ehrhardt A, Kay MA. Progress and problems with the use of viral vectors for gene therapy. Nature Rev Genet. 2003;4(5):346-58.
16. Meibohm B. Chapter 2: Pharmacokinetics and half-life of protein therapeutics. In: Kontermann R, editor. Therapeutic proteins: strategies to modulate their plasma half-lives. Wiley-Blackwell;2012;48.
17. Kariko K, Muramatsu H, Ludwig J, Weissman D. Generating the optimal mRNA for therapy: HPLC purification eliminates immune activation and improves translation of nucleoside-modified, protein-encoding mRNA. Nucleic Acids Res. 2011;39(21):e142.
18. Karikó K, Muramatsu H, Welsh FA, Ludwig J, Kato H, Akira S, et al. Incorporation of pseudouridine into mRNA yields superior nonimmunogenic vector with increased translational capacity and biological stability. Mol Ther. 2008;16(11):1833-40.
19. Stanton MG, Murphy-Benenato KE. Messenger RNA as a novel therapeutic approach. In: Garner A, editor. RNA Therapeutics. Topics in medicinal chemistry. Vol 27. Springer, Cham; 2017. p. 237-53.

20. Zangi L, Lui KO, Von Gise A, Ma Q, Ebina W, Ptaszek LM, et al. Modified mRNA directs the fate of heart progenitor cells and induces vascular regeneration after myocardial infarction. Nature Biotechnol. 2013;31(10):898-907.

21. Magadum A, Singh N, Kurian AA, Sharkar MTK, Chepurko E, Zangi L. Ablation of a Single N-Glycosylation Site in Human FSTL 1 Induces Cardiomyocyte Proliferation and Cardiac Regeneration. Mol Ther Nucleic Acids. 2018;13:133-43.

22. van den Akker F, Feyen DA, van den Hoogen P, van Laake LW, van Eeuwijk EC, Hoefer I, et al. Intramyocardial stem cell injection: go(ne) with the flow. Eur Heart J. 2017;38(3):184-6.

23. Caride VJ, Zaret BL. Liposome accumulation in regions of experimental myocardial infarction. Science. 1977;198(4318):735-8.

24. Allijn IE, Czarny BM, Wang X, Chong SY, Weiler M, Da Silva AE, et al. Liposome encapsulated berberine treatment attenuates cardiac dysfunction after myocardial infarction. J Control Release. 2017;247:127-33.

25. Jayaraman M, Ansell SM, Mui BL, Tam YK, Chen J, Du X, et al. Maximizing the potency of siRNA lipid nanoparticles for hepatic gene silencing in vivo. Angew Chem Int Ed Engl. 2012;51(34):8529-33

26. Warren L, Manos PD, Ahfeldt T, Loh Y-H, Li H, Lau F, et al. Highly efficient reprogramming to pluripotency and directed differentiation of human cells with synthetic modified mRNA. Cell Stem Cell. 2010;7(5):618-30.

27. Arteta MY, Kjellman T, Bartesaghi S, Wallin S, Wu X, Kvist AJ, et al. Successful reprogramming of cellular protein production through mRNA delivered by functionalized lipid nanoparticles. Proc Natl Acad Sci USA. 2018;115(15):E3351-E60.

28. Jain R, Frederick JP, Huang EY, Burke KE, Mauger DM, Andrianova EA, et al. MicroRNAs enable mRNA therapeutics to selectively program cancer cells to self-destruct. Nucleic Acid Ther. 2018;28(5):285-96.

29. Brown RD, Ambler SK, Mitchell MD, Long CS. The cardiac fibroblast: therapeutic target in myocardial remodeling and failure. Annu Rev Pharmacol Toxicol. 2005;45:657-87.

30. Shantsila E, Wrigley BJ, Blann AD, Gill PS, Lip GY. A contemporary view on endothelial function in heart failure. Eur J Heart Fail. 2012;14(8):873-81.

31. Yndestad A, Damås JK, Øie E, Ueland T, Gullestad L, Aukrust P. Role of inflammation in the progression of heart failure. Curr Cardiol Rep. 2007;9(3):236-41.

32. Münter R, Kristensen K, Pedersbæk D, Larsen JB, Simonsen JB, Andresen TL. Dissociation of fluorescently labeled lipids from liposomes in biological environments challenges the interpretation of uptake studies. Nanoscale. 2018;10(48):22720-4.

33. Liu Y, Tseng Y-C, Huang L. Biodistribution studies of nanoparticles using fluorescence imaging: a qualitative or quantitative method? Pharm Res. 2012;29(12):3273-7.

34. Meng F, Wang J, Ping Q, Yeo Y. Quantitative assessment of nanoparticle biodistribution by fluorescence imaging, revisited. ACS Nano. 2018;12(7):6458-68.

35. Pardi N, Tuyishime S, Muramatsu H, Kariko K, Mui BL, Tam YK, et al. Expression kinetics of nucleoside-modified mRNA delivered in lipid nanoparticles to mice by various routes. J Control Release. 2015;217:345-51.

36. Kwekkeboom RF, Sluijter JP, van Middelaar BJ, Metz CH, Brans MA, Kamp O, et al. Increased local delivery of antagomir therapeutics to the rodent myocardium using ultrasound and microbubbles. J Control Release. 2016;222:18-31.

37. Dahlman JE, Kauffman KJ, Xing Y, Shaw TE, Mir FF, Dlott CC, et al. Barcoded nanoparticles for high throughput in vivo discovery of targeted therapeutics. Proc Natl Acad Sci USA. 2017;114(8):2060-5.

38. Kedmi R, Veiga N, Ramishetti S, Goldschmit M, Rosenblum D, Dammes N, et al. A modular platform for targeted RNAi therapeutics. Nature Nanotech. 2018 ;13:214–219 (2018).

39. Carlsson L, Clarke JC, Yen C, Gregoire F, Albery T, Billger M, et al. Biocompatible, purified VEGF-A mRNA improves cardiac function after intracardiac injection 1 week post-myocardial infarction in swine. Mol Ther Methods Clin Dev. 2018;9:330-46.

40. Chen J, Ma Q, King JS, Sun Y, Xu B, Zhang X, et al. aYAP modRNA reduces cardiac inflammation and hypertrophy in a murine ischemia-reperfusion model. Life Sci Alliance. 2019;3(1): e201900424.

4

41.   Hadas Y, Vincek AS, Youssef E, Żak MM, Chepurko E, Sultana N, et al. Altering Sphingolipid Metabolism Attenuates Cell Death and Inflammatory Response after Myocardial Infarction. Circulation. 2020;141(11):916-30.

42.   Huang C-L, Leblond A-L, Turner EC, Kumar AH, Martin K, Whelan D, et al. Synthetic chemically modified mrna-based delivery of cytoprotective factor promotes early cardiomyocyte survival post-acute myocardial infarction. Mol Pharm. 2015;12(3):991-6.

43.   Magadum A, Singh N, Kurian AA, Munir I, Mehmood T, Brown K, et al. Pkm2 Regulates Cardiomyocyte Cell Cycle and Promotes Cardiac Regeneration. Circulation. 2020;141(15):1249-65.

44.   Sultana N, Hadas Y, Sharkar MTK, Kaur K, Magadum A, Kurian AA, et al. Optimization of 5' untranslated region of modified mRNA for use in cardiac or hepatic ischemic injury. Mol Ther Methods Clin Dev. 2020;17:622-633

45.   Sultana N, Magadum A, Hadas Y, Kondrat J, Singh N, Youssef E, et al. Optimizing cardiac delivery of modified mRNA. Mol Ther. 2017;25(6):1306-15.

46.   Turnbull IC, Eltoukhy AA, Fish KM, Nonnenmacher M, Ishikawa K, Chen J, et al. Myocardial delivery of lipidoid nanoparticle carrying modRNA induces rapid and transient expression. Mol Ther. 2016;24(1):66-75.

47.   Lei Z, Fang J, Deddens JC, Metz CHG, van Eeuwijk ECM, El Azzouzi H, et al. Loss of miR-132/212 Has No Long-Term Beneficial Effect on Cardiac Function After Permanent Coronary Occlusion in Mice. Front Physiol. 2020;11:590.

48.   de Boer RA, De Keulenaer G, Bauersachs J, Brutsaert D, Cleland JG, Diez J, et al. Towards better definition, quantification and treatment of fibrosis in heart failure. A scientific roadmap by the Committee of Translational Research of the Heart Failure Association (HFA) of the European Society of Cardiology. Eur J Heart Fail. 2019;21(3):272-85.

49.   Ma H, Wang L, Yin C, Liu J, Qian L. In vivo cardiac reprogramming using an optimal single polycistronic construct. Cardiovasc Res. 2015;108(2):217-9.

50.   Qian L, Huang Y, Spencer CI, Foley A, Vedantham V, Liu L, et al. In vivo reprogramming of murine cardiac fibroblasts into induced cardiomyocytes. Nature. 2012;485(7400):593-8.

51.   Magadum A, Kaur K, Zangi L. mRNA-based protein replacement therapy for the heart. Mol Ther. 2019;27(4):785-93.

4

Development and validation of a high throughput *in vivo* screening method for lipid nanoparticle tissue distribution based on next-generation DNA sequencing

Martijn J.W. Evers[1], N.A.M. van den Dungen[1], J.J.J.M. Gitz-Francois[1], M. Brans[2], Z.Lei[1,2], O.G. de Jong[1,3], R.M. Schiffelers[1], S.A.A. Kooijmans[1], M. Mokry[1], P. Vader[1,2]

[1]CDL Research, University Medical Center Utecht, Utrecht, the Netherlands
[2]Experimental Cardiology Laboratory, Department of Cardiology, University Medical Center Utrecht, Utrecht, the Netherlands
[3]Department of Pharmaceutics, Utrecht Institute for Pharmaceutical Sciences (UIPS), Faculty of Science, Utrecht University, Utrecht, The Netherlands

5

ABSTRACT

Lipid nanoparticles (LNPs) are currently the state-of-the-art delivery vehicles for RNA molecules. LNPs are generally composed of 4 different types of lipids which are mixed together at a specified ratio. The ratio between the lipids can be optimized to maximize desired properties such as *in vivo* tissue accumulation. However, the wide range of lipid species and possibility to vary the ratio between the different lipids results in near infinite number of LNPs to be analyzed *in vivo,* which is laborious, capital intensive and requires the use of many animals. A possible way to increase productivity and decrease the use of animals could be the use of DNA barcodes as payload surrogates for the simultaneous screening of multiple formulations in a single animal. Here, we set out to evaluate and validate DNA barcoding technology using LNPs with known *in vitro* and *in vivo* properties. We show *in vitro* that cellular uptake of LNPs loaded with fluorescently labelled siRNA is comparable to that of LNPs loaded with barcode DNA. Moreover, cellular uptake of a pool of three different barcoded formulations, could be analyzed with similar results as compared to individual formulations analyzed separately. *In vivo*, however, different pharmacokinetic profiles and liver accumulation for these formulations was found when comparing fluorescently labelled siRNA as compared to qPCR or next-generation sequencing of barcode DNA. Therefore, validation of the use of DNA barcodes as siRNA surrogate for the simultaneous in *vivo* screening of multiple LNP formulations requires additional work.

INTRODUCTION

Lipid nanoparticles (LNPs) have emerged as state-of-the-art delivery vehicles for RNA given the approval of 3 different LNP formulations over the past 3 years. First, an LNP-siRNA was approved for the treatment of transthyretin amyloidosis, an orphan disease.[1,2] During the SARS-CoV-2 pandemic, LNPs (e.g. mRNA-1273 (Moderna) and Comirnaty® (Biontech/Pfizer) have been used in vaccination programs all over the world. Moreover, multiple clinical trials are ongoing in which LNPs are being used as delivery vehicle for mRNA in cancer immunotherapy.[3] This emphasizes the huge value of LNPs as nucleic acid delivery systems with possible applications in immuno-oncology, vaccination and protein replacement therapy.[4–7] However, to date, this potential of lipid based carriers has remained largely untapped.

LNPs generally consist of 4 different lipid classes: an ionizable lipid, a 'helper-lipid', a PEG-lipid and cholesterol.[8] Over the past decade, the ionizable lipid has been recognized as the key driver of LNP efficacy in siRNA delivery.[9–12] However, more recently, increasing attention is also given to finetuning the composition of helper lipids, cholesterol and PEG-lipids in the LNP formulation.[13–15]

It is possible to optimize LNPs by changing the lipid formulation of the particle – i.e. the molar ratios and types of the lipids being used– in order to maximize efficacy or to achieve a desired tissue or cell type distribution. However, a one-factor-at-a-time optimization approach of individual lipid formulations may result in a high number of nanoparticle formulations to be screened *in vivo* which is obviously laborious and capital-intensive.[14] Pre-screening of LNPs *in vitro* can be considered as an alternative to *in vivo* analysis , however, *in vitro* behavior often does not predict which formulation behaves best *in vivo* as a result of poor *in vitro-in vivo* correlations. [16,17] As a result, pre-clinical development of an optimal LNP formulation for a specific application requires the use of large numbers of animals.

One possible way to reduce animal use could be by utilizing lipid nanoparticles with DNA barcodes to study the tissue distribution of hundreds of different LNP formulations in a single animal at the same time.[18] In this approach, each individual LNP formulation is equipped with a DNA oligo with a unique sequence, i.e. a DNA barcode, and multiple LNP formulations are mixed before administration. By analysis of barcode occurrence via next-generation DNA sequencing, the relative tissue distribution of all different formulations can be measured simultaneously. [14] Altogether, the use of barcoded LNPs appears to be a powerful state-of-the-art technique in pre-clinical LNP development which reduces the use of resources and animals while at the same time enables the screening of hundreds of formulations at the same time. Here, we set out to evaluate and validate barcoding technology using LNP siRNA formulations with known *in vivo* tissue distribution properties.

To this end, we prepared 3 different LNP formulations, each incorporating a different PEG2000-lipid, namely PEG-dimyristoyl glycerol (PEG-C14), PEG-dipalmitoyl glycerol (PEG-C16) or PEG-distearoyl glycerol (PEG-C18). It has previously been shown that the alkyl length of the PEG-lipid affects LNP circulation time and tissue distribution. **(Figure 1)**[19–21] We aimed to validate the use of DNA barcodes as siRNA surrogate at three levels. We first analyzed the physicochemical properties of LNP-siRNA and compared these properties to that of LNP-

barcode DNA. Second, we evaluated and compared cellular uptake *in vitro* of individual and mixed LNP formulations to investigate the possibility of pooled LNP analysis. We compared cellular uptake of three formulations in recipient cells *in vitro* based on analysis of either intracellular levels of fluorescently labeled siRNA or those of DNA barcodes. In these experiments, we administered barcoded LNPs both individually and pooled. Third, we analyzed the tissue distribution of different LNPs carrying a fluorescent siRNA *in vivo* and compared these results to the tissue distribution as measured by qPCR and NGS analysis of barcoded LNPs.
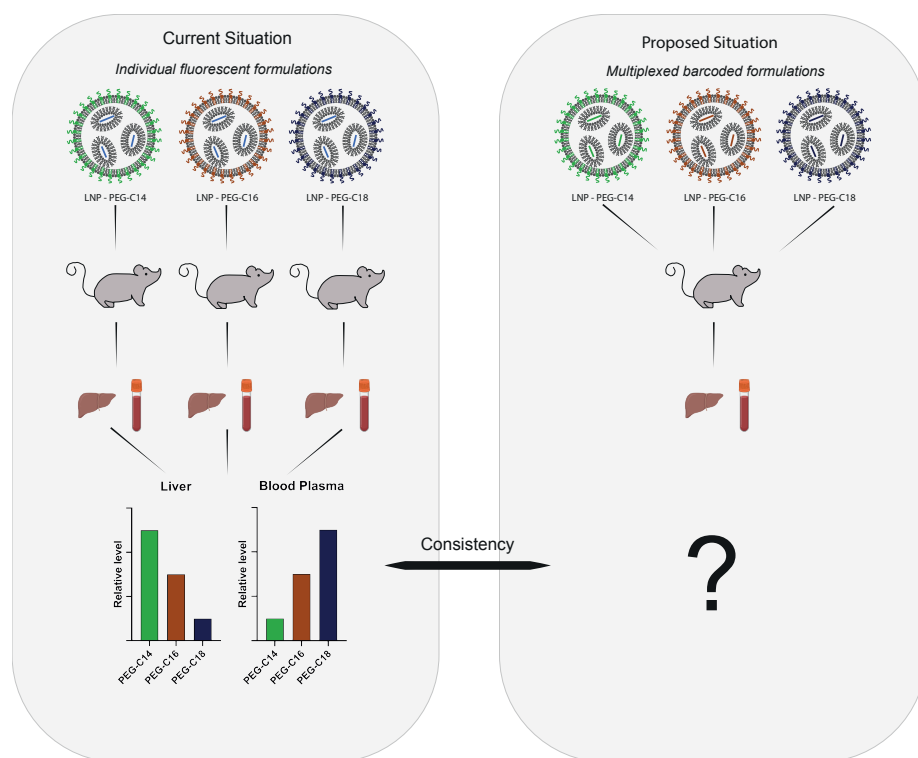
Figure 1: Multiplexed analysis of LNP tissue distribution via DNA barcoded LNPs. Currently, tissue distribution of nucleic acid encapsulating LNPs is routinely measured via fluorescent labelling of either the lipid components or the nucleic acids. Tissue distribution is subsequently measured via fluorescence based methods such as whole organ spectroscopy or fluorescence spectroscopy of tissue lysates. Tissue distribution and blood plasma concentrations of LNPs containing either PEG-C14, PEG-C16 or PEG-C18 is critically dependent on alkyl length of the PEG-lipid, resulting in distinct tissue distribution and blood plasma concentration profiles. Here, based on these previously described LNP pharmacokinetic characteristics, we validated the use of DNA barcodes for multiplexed tissue distribution analysis. Each LNP formulation encapsulated a specific barcode. These LNPs were subsequently mixed and administered. Tissue distribution was analyzed by relative barcode occurrence as measured via quantitative PCR (qPCR) or next-generation sequencing and compared to the data obtained via fluorescence-based methods.

MATERIALS & METHODS

Chemicals

DLin-MC3-DMA was produced by VKB (India), cholesterol was obtained from Sigma Aldrich (Saint Louis, MO, USA) and Distearoylphophatidylcholine (DSPC) was obtained from Lipoid, (Ludwigshafen am Rhein, Germany). PEG2000-Dimyristoyl glycerol (PEG-DMG), PEG2000-Dipalmitoyl glycerol (PEG-DPG), and PEG2000-Distearoyl glycerol (PEG-DSG) were obtained from NOF Corporation (Tokyo, JP). All oligonucleotides were ordered at Integrated DNA Technologies (Iowa, USA). An overview of the used siRNA, DNA barcode sequences and (index) primers can be found in **Supplementary Tables 1-4.**

Production of Lipid Nanoparticles encapsulating siRNA/DNA barcode

LNPs were prepared by microfluidic mixing using the NanoAssemblr® Benchtop (Precision Nanosystems, Vancouver, Canada). An ethanolic phase containing lipids was mixed with an acidic aqueous phase (25 mM sodium acetate, pH 4.0) containing nucleic acids leading to the formation of LNPs. Lipids were dissolved in 100% ethanol at a total lipid concentration ranging from 5-20 mM. LNPs were composed of DLin-MC3-DMA, cholesterol, DSPC and a PEG-lipid at a molar percentage of 50/38.5/10/1.5 mol%, respectively. 3 different PEG-lipids were used: PEG-DMG (PEG-C14), PEG-DPG (PEG-C16) and PEG-DSG (PEG-C18). The siRNA/barcode DNA mixture (9:1; siRNA:DNA; mol:mol) was encapsulated at a nitrogen-to-phosphate ratio (N/P) of 6. For cellular uptake experiments, Alexa647-labelled siRNA was used. For gene silencing experiments, unlabeled oligonucleotides were used. For both uptake and gene silencing experiments, no barcode was added to the oligonucleotide mixture. Lipid nanoparticles were produced at a total flow rate (TFR) of 4 ml/min and a flow rate ratio (aquous phase;organic phase) of 3 to 1. The first ± 0.2 mL of each LNP production was discarded. Immediately after production, LNPs were dialyzed against an excess of phosphate buffered saline (PBS) using Slide-a-Lyzer™ dialysis cassettes G2 with a molecular weight cutoff (MWCO) of 10.000 Da (Thermo Scientific, Waltham, MA, USA). After dialysis, if deemed necessary, LNPs were concentrated to an appropriate volume using Amicon® Ultra-15 centrifugational filter units with a MWCO of 10.000 Da (Merck, Darmstadt, Germany).

Nanoparticle Characterization

Size using Dynamic Light Scattering (DLS)

The hydrodynamic diameter of LNPs was measured by Dynamic Light Scattering (DLS) using a Zetasizer Nano S (Malvern Panalytical, Malvern, UK) equipped with a 4 mW HeNe laser of 633 nm. Samples were diluted appropriately in dulbecco's phosphate buffered saline (PBS) and scattering was measured at an angle of 173º at room temperature for 10 seconds and repeated at least 10 times. This procedure was repeated three times for each sample.

RNA determination and determination of encapsulation efficiency

The total RNA concentration was determined using the Quant-It™ Ribogreen RNA Assay kit (Thermo Scientific, Waltham, MA, USA) after lysis in 1.0 % (v/v) Triton X-100 and measured at

a final concentration of 0.5% (v/v) Triton X-100 (RNA_{tx-100}) whereas free/unencapsulated siRNA concentrations ($RNA_{TE/PBS}$) were determined in TE or PBS. The total and free RNA concentrations (µg/mL) and) were calculated using a reference calibration curve in 0.5% (v/v) Triton-X100 or TE/PBS buffer, respectively. The encapsulation efficiency was then calculated using the following formula ((RNA_{tx-100}- $RNA_{TE/PBS}$)/RNA_{tx-100})*100.

Cell Culture

Cell lines stably expressing a dual luciferase (dluc) cassette containing both *Firefly* and *Renilla* luciferases were generated by lentiviral transduction as described in a previous publication. [22] SKOV3-dluc and HEK293T-dluc were cultured in Dulbecco's modified Eagle Medium supplemented with 10% fetal bovine serum (FBS),1 mg/mL G418, 100 U/mL penicillin and 100 U/mL streptomycin. All cells were cultured at 37 °C and 5% CO_2.

Cellular uptake using fluorescent lipid nanoparticles

LNP uptake was analyzed by flow cytometry. SKOV3-dluc and HEK293T-dluc were seeded at a density of 30.000 cells per well in a 96-well plate, 24 hours prior to the assay**.** Then, cells were incubated with different nanoparticles at a total siRNA concentration of 50 nM. As a control, cells were incubated with PBS. Cells were incubated for 4 hours and cellular uptake was analyzed by flow cytometry. Cells were trypsinized, washed with PBS, resuspended in 0.2% (w/v) bovine serum albumin (BSA) in PBS and transferred to a 96 U-bottom well plate (Greiner) and analyzed on a FACS Canto II flow cytometer (BD, Franklin Lakes, NJ, US)

Cellular uptake of DNA barcoded lipid nanoparticles

Barcoded LNPs were produced by addition of a DNA barcode to the siRNA mixture (1:9 mol:mol barcode DNA:siRNA). Cellular uptake was analyzed in SKOV3-dluc cells. SKOV3-dluc cells were seeded 72 hours prior to the experiment at a concentration of 5.000 cells per well. Cells were incubated for 4 hours with LNPs at a concentration of 50 nM total barcode DNA/siRNA. Cells were washed with PBS, acid wash (0.5M NaCl, 0.2M acetic acid) and PBS, trypsinized , resuspended in 2% (w/v) BSA in PBS, centrifuged for 5 minutes at 500 x g, and resuspended in PBS containing a normalization barcode 1 (50nM barcode DNA). This barcode acted as internal standard to correct for possible differences in extraction efficiency and to normalize Ct values during quantitative PCR (qPCR) analysis. The barcode was extracted from the cells via a modified Bligh and Dyer extraction described by Yaari et al.[23] A mixture of chloroform and methanol was added yielding a solution of sample:choloform:methanol (1:1:1 v:v:v). This sample was centrifuged at 300 x for 5 min at 4 °C resulting in phase separation. The upper aqueous phase was transferred to a new tube and concentrated using vacuum concentration and further analyzed by qPCR.

Analysis of cell toxicity and gene silencing efficacy

The gene-silencing efficacy of LNPs was assessed in two different cell-lines: SKOV3-dluc HEK293T-dluc. SKOV3-dluc and HEK293T-dluc cells were seeded in a 96-well plate at a density of 5.000 cells/well 48 hours prior to transfection. LNPs were added at concentrations ranging

from 0 to 100 nM siRNA. As control, cells were transfected using Lipofectamine RNAiMAX according to the manufacturer's instructions. Luciferase activity was assessed after another 48 hours of culture. Luciferase activity was measured using the Stop & Glo System (Promega, Leiden, NL) according to the manufacturer's instructions. In short, medium was aspirated and replaced by 50 µL of fresh medium. 50 µL of Dual-Glo® reagent was added and cells were incubated for 10 minutes. After 10 minutes, 100 µL of lysate was transferred to a white 96 well plate and Firefly luciferase activity was measured. Then, 50 µL of Dual-Glo® Stop & Glo® reagent was added and after an incubation of 10 minutes *Renilla* luciferase activity was measured. Both Firefly luciferase and *Renilla* luciferase activities were measured on a Spectramax ID3 (Molecular Devices, San Jose, CA, USA) at an integration time of 1000 ms. For data analysis, firefly luciferase activity was normalized to *Renilla* luciferase activity and expressed as percentage of the blank – 0 nM siRNA – sample.

Cell Viability was measured using CellTiter 96® Aqueous MTS assay according to the manufacturer's instructions. Absorbance was measured at 490 nm using a Spectramax ID3.

Animal Experiments

Ethical statement on animal experiments

All animal experiments were performed with the Animal Welfare Body Utrecht's permission and complied with the Dutch Experiments on Animals Act (WOD) under license AVD115002015257. The research was carried out in accordance with the Guide for the Care and Use of Laboratory Animals.

LNP-barcode tissue distribution

Tissue distribution of a mixture of 3 different LNPs was analyzed in female C57Bl/6 mice (N=2, weight between 22-25gram, ± 12 week old, Charles River, Leiden, the Netherlands). LNPs of different composition were mixed at equal proportions of nucleic acid and injected intravenously via the tail vein at a total dose of 0.02 mg/kg RNA/DNA (estimated dose of barcode DNA = 0.007 mg/kg/LNP). Blood samples were taken 2 and 4 hours after administration via tail vein or cardiac puncture, respectively. Blood was collected in EDTA anti-coagulated tubes. Animals were sacrificed 4 hours after injection by cervical dislocation and perfused with PBS via the left ventricle cavity. Tissues were collected and snap frozen in liquid nitrogen until further analysis.

Fluorescent LNP tissue distribution

Tissue distribution of 3 different LNPs containing Alexa647-labelled siRNA was analyzed in female C57Bl/6 mice (N=1/formulation, weight between 20-22 gram, ± 15 week old, Charles River, Leiden, the Netherlands). LNPs of different composition were administered individually to C57Bl/6 mice (n = 1 / formulation) at a total dose of 0.3 mg siRNA / kg. Blood was collected directly after injection and after 2 and 4 hours in lithium-heparin blood collection tubes. Blood was centrifuged for 10 minutes at 2000 x *g* and 4 °C to obtain platelet-free plasma. After 4 hours, animals were terminated by i.p. administration of 60 mg/kg pentobarbital and perfused with PBS via the left ventricle cavity. Organs were collected and tissue distribution of the LNPs was immediately analyzed by measurement of Alexa647 fluorescence signal using a Pearl Impulse

Imager (Li-cor Biosciences, Lincoln, NE, USA). After imaging, organs were snap-frozen in liquid nitrogen and stored at -80 C until further analysis. Plasma samples were first diluted 5 x in PBS; then 25 µL of diluted platelet free plasma was transferred to a black 384 well plate. 25 µL of 1X RIPA buffer was added to each well and sample fluorescence was measured. Data was expressed as % of the value obtained at T = 1 min. Tissue lysates were prepared from pieces of liver, spleen, lungs, a single kidney, and the whole heart. Organs were weighed, transferred to a 2 mL tube containing ceramic beads (1.4mm) and 5 µL of RIPA-buffer was added for every milligram of tissue. Tissues were homogenized using a Mini bead-beater 8 (Biospec, Bartlesville, OK, USA) for 60 seconds. Samples were centrifuged for 10 minutes at 10.000 x g and 4°C. 25 µL of supernatant was transferred to a black 384 well plate and fluorescence was measured. . In tissue lysates, the results were expressed as fluorescence per mg tissue normalized for the injected dose. The blood plasma concentration of LNPs was expressed as percentage of the fluorescence measured directly after injection. Fluorescence in plasma and tissue lysates was analyzed by fluorescent spectroscopy on a Spectramax ID3 (Molecular Devices, San Jose, California, USA) at excitation/emission wavelengths of 620/660 nm, respectively.

Isolation of Barcodes from Cells/Tissue

The isolation of barcodes from animal tissue was adapted from a previously published protocol. [14] Barcodes were extracted from liquid and tissue samples using Clarity OTX columns according to the manufacturer's instructions. (Phenomenex, Torrance, CA, USA) Liquid samples (blood and LNP mixtures) were lysed using loading-lysis buffer provided by the manufacturerand loaded on a Clarity OTX column, washed and subsequently eluted. Organs were weighed, transferred to a 2 mL tube containing ceramic beads (1.4 mm) and 900 µL of lysis buffer was added. Tissues were homogenized using a mini bead-beater 8 for 60 seconds and centrifuged for 10 minutes at 10.000 x g and 4°C. The supernatant was loaded on a Clarity OTX column and barcodes were isolated according to the manufacturer's instruction. Crude oligo in elution buffer was subsequently concentrated using a vacuum concentrator and further purified by Zymo Oligo clean and concentrator columns (Zymo Research, Irvine, CA, USA). Purified barcodes were taken up in Aqua ad Injectabilia and stored at -80 °C until further analysis by qPCR or next-generation sequencing.

Analysis of barcode occurrence by quantitative PCR

2 µL of each sample was amplified by PCR using the Phusion® HF kit (Thermo Scientific, Waltham, MA, USA) and the following recipe: 5 µL of 5x HF Phusion buffer, 0.5µL dNTPs, 0.25 µL forward primer, 0.25 µL reverse primer, 0.25 µL Phusion DNA Polymerase, 3.1 µL 1X SybrGreen I (Thermo Scientific, Waltham, MA, USA), and 13.65 µL nuclease-free water. Cycling conditions were 98 °C for 15 s, 60 °C for 15 s, and 72°C for 30 s, repeated 40 cycles on a Bio-Rad CFX96 Touch real-time PCR detection machine (Bio-Rad, Hercules, CA,USA). For cellular uptake studies, samples were normalized based on amplification of a control barcode and uptake was expressed as fold change compared to the C14 sample. For the cell uptake experiment this was calculated as follows: for each sample a ∆Ct value was calculated: $\Delta CT = Ct_x - Ct_{reference}$ where x represents a specific barcode and reference refers to the normalization barcode which

was spiked in during sample workup. Then, a ΔΔCT value was calculated: $\Delta\Delta CT = \Delta C_x - \Delta CT_{14}$. Finally, the fold change was calculated via the following formula: fold change = $2^{-\Delta\Delta CT}$. The obtained results were normalized for the relative barcode occurrence in the used LNP mixture. For *in vivo* biodistribution experiments, a ΔCT value was calculated: $\Delta CT = \Delta CT_x - \Delta CT_{14}$. Then, the fold change was calculated via the following formula: fold change = $2^{\wedge - \Delta\Delta CT}$ and results were normalized for the relative barcode occurrence in the LNP mixture.

Analysis of barcode occurrence by next generation sequencing

For Next-Generation Sequencing (NGS)**,** 2 µL of each sample was amplified using 5 µL HF Phusion Buffer, 0.5 µL dNTPs, 0.5 µL 5 µM universal forward primer, 0.5 µL 5 µM index primer, 0.25 µL 5 µM Phusion DNA polymerase, 2 µL DMSO and 14 µL nuclease free water. Cycling conditions were 98°C for 15 s, 60°C for 15 s, and 72°C for 30 s, repeated 15-35 cycles, depending on the sample. Samples were loaded on a 4% (w/v) agarose gel and separated by gel electrophoresis, the product band was excised and purified by a gel extraction column (Qiagen, Venlo, Netherlands). Sample concentration was determined on a Qubit using a Qubit dsDNA HS Assay Kit (Thermo Scientific, Waltham, MA, USA) according to the manufacturer's instructions. Samples were pooled at a DNA amount of 5 ng DNA per sample and sequenced on a NextSeq500 machine with a read length of 1 x 75 bp (Illumina, San Diego, CA, USA). Sample analysis was performed according to a previously published protocol.[18] Barcode occurrence was expressed as fold change to the value obtained for particles containing PEG-C14

RESULTS AND DISCUSSION

Physicochemical characteristics of LNPs are not affected by the type of PEG-lipid or nucleic acid cargo

LNPs were produced via microfluidic mixing using a NanoAssmeblr® Benchtop. We produced 3 different formulations in which only the type of PEG lipid was varied. Three PEG-lipids with various alkyl chain lengths were selected, namely PEG-DMG (PEG-C14), PEG-DPG (PEG-C16) and PEG-DSG (PEG-C18). The alkyl chain length of PEG-lipids is known to influence LNP pharmacokinetics and dynamics in a very distinct manner.[19–21] Generally, an increased alkyl length results in lower desorption rates. For DLin-MC3-DMA containing particles, desorption of the PEG-C14 lipid results in opsonization by ApoE and subsequent rapid uptake of the particles by cells.[24] This opsonization is decelerated for longer alkyl chains, resulting in prolonged circulation time.

Physiochemical characterization of the three formulations revealed that the type of PEG-lipid did not affect particle size, polydispersity index or siRNA encapsulation efficiency.**(Figure 2A-C)** Moreover, the type of oligonucleotide (unlabeled siRNA, fluorescently labelled siRNA or an siRNA/barcode mixture) also did not affect any of the aforementioned parameters as shown in Figure 2A-C.
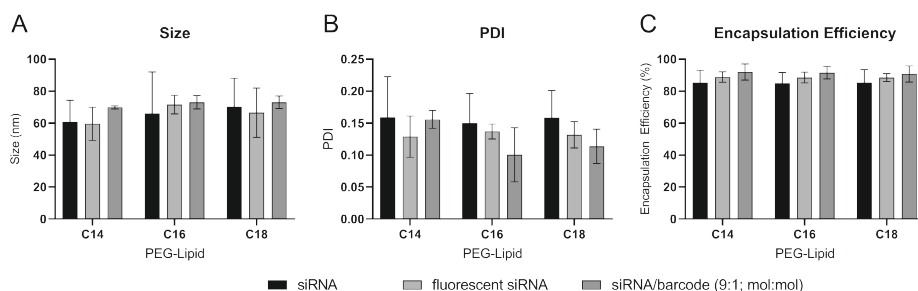
Figure 2: Particle characteristics are not influenced by the type of PEG-lipid (PEG-C14, PEG-C16, or PEG-C18) or oligonucleotide payload (siRNA, fluorescently labelled siRNA or siRNA/barcode DNA mixture) A) Size of LNPs as determined by Dynamic light scattering (DLS). **B)** Polydispersity Index (PDI) of LNPs as determined by DLS. **C)** RNA encapsulation efficiency (%) of different LNPs as determined by Quant-IT™ Ribogreen RNA assay (n = 2-5).

LNP gene-silencing and cellular uptake efficiency are affected by the type of PEG-lipid

First, we evaluated the effect of different PEG-lipids on functional parameters of LNPs such as gene-silencing and cellular uptake *in vitro*. It is important to confirm the effect of different PEG-lipids on functional characteristics of LNPs, such as cellular uptake and gene-silencing, in order to use these particles for validation of DNA barcoding technology.

The gene-silencing efficacy of different LNPs encapsulating siRNA targeting Firefly luciferase was analyzed in SKOV3 and HEK293T cells stably expressing a dual-luciferase construct containing both Firefly luciferase and *Renilla* luciferase. For LNP formulations containing PEG-C14 and PEG-C16, a clear, dose-dependent decrease in firefly luciferase expression was observed 48 hours after addition of LNPs.**(Figure 3A, Supplementary Figure 1A)** This effect was reduced for LNP-C18. At concentrations of 10 and 100 nM siRNA, differences in PEG-desorption rates were clearly reflected in the gene-silencing efficacy of LNPs: PEG-C14 > PEG-C16 > PEG-C18. Cell viability was not influenced by any of the tested LNP formulations at concentrations of 1 and 10 nM siRNA. A slight cell viability decrease could be observed for all formulations at a concentration of 100 nM in SKOV3, but not in HEK293T.**(Figure 3B, Supplementary Figure 1B)**
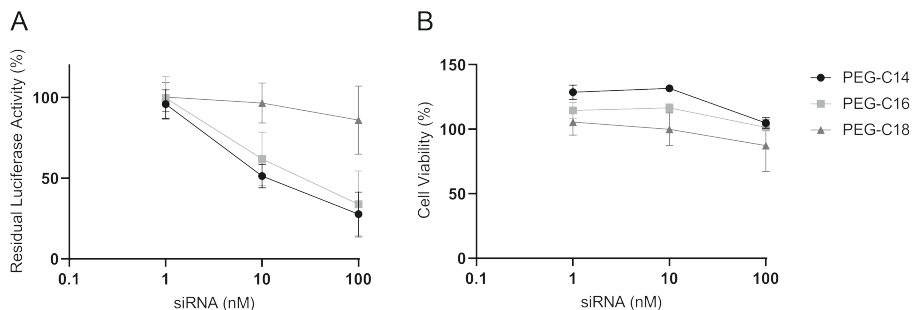
Figure 3: Alkyl chain length of PEG-lipid affects LNP-mediated functional siRNA delivery in SKOV3 cells. **A)** Gene-silencing and **B)** cell viability was evaluated in SKOV3-dluc. Cells were incubated with LNPs at concentrations ranging from 1 nM to 100 nM siRNA and gene silencing and cell viability were analyzed after 48 hours. Gene-silencing data are expressed as mean ± SD (n=2, biological replicates), cell viability data are expressed as mean ± SD (n=3, technical replicates).

Barcoding allows accurate assessment of uptake of pooled LNP formulations.

Next, we evaluated the use of DNA barcoding technology for analysis of cellular uptake efficiency and compared the results of DNA barcoding technology to the results obtained by detection of a fluorescently labelled siRNA. In addition, we measured the cellular uptake of LNPs added as single LNP formulation or as a mixture of LNP formulations, via barcode quantification using qPCR.**(Figure 4A)**

We incubated cells with different LNP formulations encapsulating either fluorescently labelled siRNA or DNA barcodes. For barcoded LNPs, three different LNP formulations were produced, each containing a unique barcode. The design of the barcodes was adapted from previous publications.[18] Barcodes contained universal primer sites for binding of next generation sequencing (NGS) adapters, a unique molecular identifier (UMI) and a predefined 8-nucleotide barcode.**(Figure 4B)** We designed barcode-specific PCR primers which could be used to specifically amplify each barcode**(Supplemental Figure 2)** so we could analyze barcode abundance via qPCR.**(Figure 4C**)

First, we verified that LNPs did not aggregate after mixing. DLS analysis showed that LNPs were uniform in size at a PDI <0.2. Upon mixing, no increase in size or PDI was observed indicating absence of aggregation.**(Figure 4DE)** Next, cells were incubated with LNPs for 4 hours, after which they were analyzed by flow cytometry or lysed after which DNA barcodes were extracted from cells and analyzed by qPCR. As hypothesized, uptake of LNPs decreased with increasing alkyl lengths of the PEG-lipid.**(Figure 4F)** Encouragingly, the relative cellular uptake of LNPs as determined by fluorescence measurements was comparable to that of barcoded LNPs as determined by qPCR, albeit that the absolute fold-changes differed. **(Figure 4G)** Moreover, the relative cellular uptake of different LNPs measured individually was comparable to that of mixed LNPs indicating that similar results can be obtained by multiplexed analysis of 3 different formulations at the same time via barcoding technology. **(Figure 4G)**
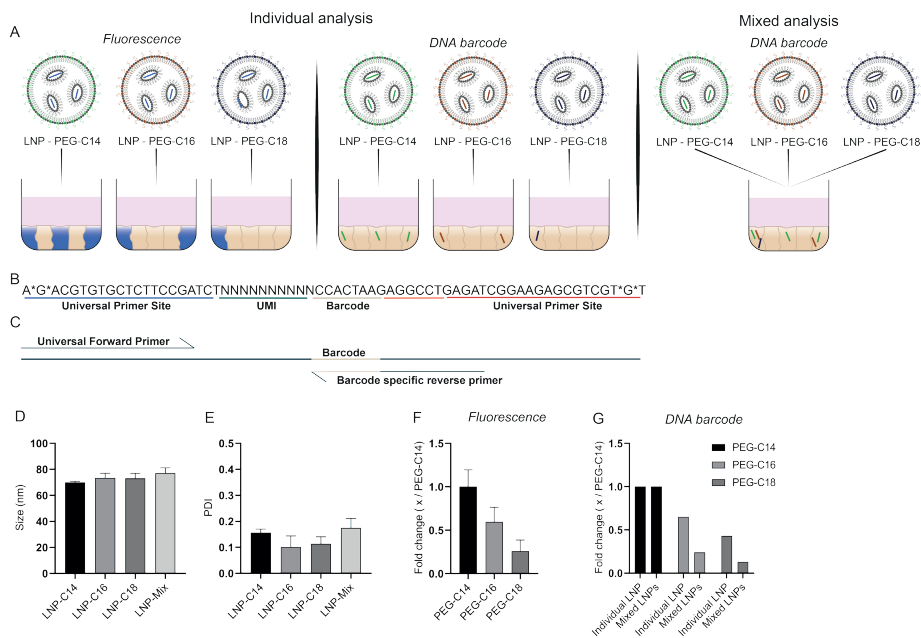
Figure 4: Analysis of LNP cellular uptake, via fluorescently labeled siRNA or barcode DNA shows comparable results. A) Graphic illustration of three different cellular uptake measurement methods: Left) Individual analysis of cellular uptake of LNPs by measurement of fluorescence via flow cytometry. Middle) Individual analysis of barcoded LNPs via qPCR Right) Mixed analysis of barcoded LNPs via qPCR. Three different LNP formulations were prepared encapsulating fluorescently labelled siRNA or siRNA with an LNP-specific DNA barcode at a ratio of 9:1 (siRNA/barcode DNA; mol/mol). **B)** DNA Barcodes were adapted from Dahlman et al.[14] and contained two universal primer binding sites, a 10 nt unique molecular identifier and a 8 nt barcode sequence. **C)** DNA barcodes can be amplified by (q)PCR using a universal forward primer and a barcode-specific reverse primer. **D)** Size of the three LNP formulations individually and after mixing as measured by DLS. **E)** PDI of the three different LNP formulations individually and after mixing as measured by DLS. **F)** Uptake of LNPs by SKOV3-dluc cells, as measured by flow cytometry. Cells were incubated at a concentration of 50 nM siRNA for 4 hours and uptake was measured by flow cytometry. The measured MFI was corrected by subtracting the MFI obtained for untreated cells and normalized to LNP – PEG-C14. Bars indicate mean ± SD (n=3, technical replicates). **G)** Alternatively, cells were incubated with individual LNP formulations or a mixture thereof at a concentration of 50 nM siRNA (individual LNPs) or 150 nM siRNA (mixed LNPs) for 4 hours after which the barcodes were extracted from cells. Barcode abundance was measured by qPCR and data is expressed as fold change to the value obtained for LNPs containing PEG-C14 (mean, n=3, biological replicates)

LNP circulation time and liver accumulation determined via DNA barcode quantification deviates from fluorescence-based methods

Finally, we aimed to validate the use of barcoding technology for analysis of LNP tissue distribution and compare it with fluorescence-based approach via detection of a fluorescently labelled siRNA molecule. First, we analyzed the pharmacokinetic profile and tissue distribution of LNP containing PEG-C14, PEG-C16 or PEG-C18 via measurement of fluorescent siRNA in blood and tissues. LNPs encapsulating fluorescently labelled siRNA were intravenously injected to

C57Bl/6 at a concentration of 0.3 mg siRNA/ kg. Tissue distribution was analyzed after 4 hours by whole organ fluorescence spectroscopy and measurement of fluorescence in tissue lysates.

For all formulations, the majority of LNP-encapsulated siRNA accumulated in liver and spleen. At increasing PEG-lipid alkyl length, an increased accumulation in the kidney was observed.**(Figure 5AB)** The use of different PEG-lipids resulted *in vivo* in clear differences in pharmacokinetic behavior between LNPs. LNP clearance from circulation was dependent on the alkyl length of the PEG-lipid, with shorter lipids the circulation half-life was reduced as compared to longer lipids.**(Figure 5C)**
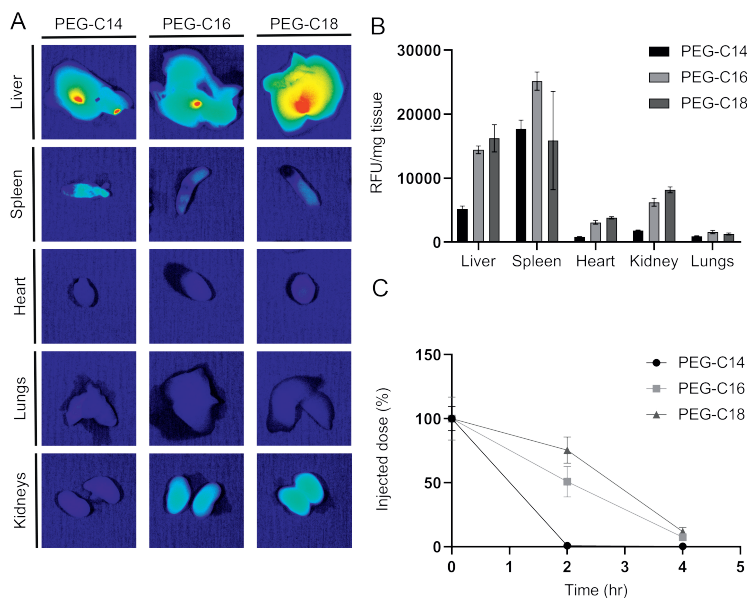
Figure 5: **LNPs mainly accumulate in liver and spleen irrespective of PEG-lipid alkyl chain length and LNP circulation time is increased with increasing PEG-lipid alkyl chain length. A)** Tissue distribution of fluorescently labeled LNPs was measured by whole-organ fluorescence spectroscopy. Fluorescence/ brightfield overlay images of murine organs harvested 4 hours after injection with 0.3 mg/kg siRNA. **B)** Distribution of fluorescent siRNA determined by ex vivo fluorescence of tissue lysates normalized for the plasma concentration measured directly after injection. Data is expressed as mean ± SD (n=2-3, technical replicates) **C)** Plasma concentration of LNPs over time. Plasma concentration is expressed as a percentage of the plasma fluorescence measured directly after injection. Data is expressed as mean ± SD (n=2, technical replicates).

Second, we aimed to compare the tissue distribution of LNPs measured via fluorescent siRNA to the tissue distribution of LNPs containing a DNA barcode measured by quantification of barcode DNA via qPCR and NGS. To this end, LNPs were pooled and injected in C57Bl/6 mice, barcodes were isolated from tissues and barcode abundance was analyzed either via qPCR or via NGS.**(Figure 6A)** In general, barcode levels in blood and liver tissues measured

via qPCR and NGS correlated well (R^2 >0.9).**(Supplementary Figure 3)** Measurement of LNP blood plasma concentration by barcode occurrence, either via qPCR or NGS, showed that LNPs containing PEG-C16 and PEG-C18 were better retained in blood plasma at 2 and 4 hours after injection compared to particles containing PEG-C14. These data confirm that LNPs containing PEG-C14 are rapidly eliminated from the circulation.**(Figure 6 BC)**

The circulation kinetics of PEG-C16 and -C18, as measured by qPCR and NGS, did not concur with the data from fluorescence measurements of labelled siRNA molecule. Using fluorescence measurements, we clearly observed a difference in the circulation kinetics of PEG-C16 and PEG-C18, which we did not observe in the analysis of barcoded LNPs via qPCR or NGS.**(Figure 6A-C)** The distribution of LNPs to the liver was also evaluated via qPCR and NGS. Here, the results were also only in partial agreement with the data obtained for fluorescent siRNA tissue distribution. The distribution of barcoded LNPs containing PEG-C18 to the liver was found to be lower as compared to barcoded LNPs containing PEG-C16 whereas analysis of fluorescent siRNA levels showed the opposite trend.**(Figure 6D-F)**

Taken together, these results do not yet validate the use of DNA barcodes as siRNA surrogate in *in vivo* tissue distribution studies and requires further study. There was a discrepancy between the results observed in the fluorescence distribution experiment as compared to the measurement of tissue distribution via DNA barcodes. We observed differences in both fold change between methods and differences between the samples.

The discrepancy between the fluorescence- and barcode-based study could be explained in several ways. First, it could be that the fluorescent probe attached to the siRNA might not reflect the actual distribution of intact RNA/DNA and therefore may be a weak surrogate marker for siRNA distribution. The fluorescent probe could be degraded via different metabolic pathways as compared to the DNA/RNA and therefore might not accurately reflect tissue distribution of the nucleotide component.[25] Differences in degradation kinetics of the fluorophore and the DNA and the fact that one quantification method is based on measurement of the fluorescent probe and another method is based on quantification of the intact oligonucleotide might account for the differences observed between fluorescence based methods and the qPCR/NGS based method. This problem could have been avoided by the detection of the siRNA molecule via PCR-based methods such as the use of stem-loop primers to quantitively measure siRNA molecules in samples.[26]

Secondly, cellular processing and endo-lysosomal processing of LNPs is highly dynamic and it previously has been shown that RNA can be recycled and exocytosed. Differences in pharmacokinetics but also differences in endo-lysosomal processing make interpretation of results at a single time-point difficult.[16]

Thirdly, the observed discrepancy in fold-change between quantification methods can be the result of differences between the detection methods such as sensitivity of the detector and linear range of detection.

Another interesting observation is that the results are not entirely in agreement with existing literature on the tissue distribution of LNPs containing PEG-C14, PEG-C16 or PEG-C18.

Based on literature, we expected that the relative concentration in blood plasma at 2 and 4 hour would clearly resemble the order PEG-C14<PEG-C16<PEG-C18 and in liver PEG-C14>PEG-

C16>PEG-C18. In blood plasma, we did observe such a relationship, however we could not discriminate between PEG-C16 and PEG-C18 for barcoded LNPs. In the liver, we did not observe the hypothesized relationship for any of the three detection methods.

We can think of several potential explanations for these phenomena. First, the rationale for increased hepatic siRNA delivery by shorter alkyl PEG-lipids is based on the fact that the LNP dictates the pharmacokinetic properties of the encapsulated oligonucleotide.[27] However, previously it has also been shown for C12-200 containing LNPs that the particles disintegrates within 1 hour after cellular uptake. From that point onwards, lipid and RNA occurrence might no longer overlap.[28] Moreover, for the DNA barcode method, measurement of DNA barcodes via qPCR/NGS requires the DNA barcode to be intact which is not needed for e.g. fluorescently labelled siRNA.

Future research should be aimed at further validation of the use of barcoded DNA as siRNA surrogate marker in biodistribution studies. Quantitative detection of intact siRNA molecules via PCR could be of help as it prevents the use of other surrogates such as fluorescently or radiolabeled siRNA. Moreover, this approach can be combined with a reporter system, such as Cre-LoxP reporter mice where cells successfully transfected by LNPs carrying Cre mRNA express tdTomato. The relative barcode occurrence in cells expressing tdTomato can be used as metric to analyze LNP-mRNA delivery efficiency.[29]

5

CONCLUSION

Here, we have evaluated the use of multiplexed analysis of different LNPs encapsulating specific DNA barcodes as an alternative to single particle screening based on fluorescence measurements. We observed no differences in cellular uptake levels of LNPs as measured by fluorescence-based methods or the barcode-based detection method *in vitro. In vivo*, we were able to detect and analyze pooled LNPs. Circulation kinetics results were comparable between barcoded DNA and fluorescence-based methods although barcoding did not reveal expected differences in circulation kinetics of PEG-C16 and C18. Quantification of hepatic siRNA delivery of LNPs yielded different results amongst measurement methods. Therefore the use of DNA barcodes as surrogate marker for siRNA biodistribution requires further validation. A possible approach is to quantify tissue distribution of siRNA molecules via PCR-based methods and compare those results to tissue distribution of barcoded DNA.
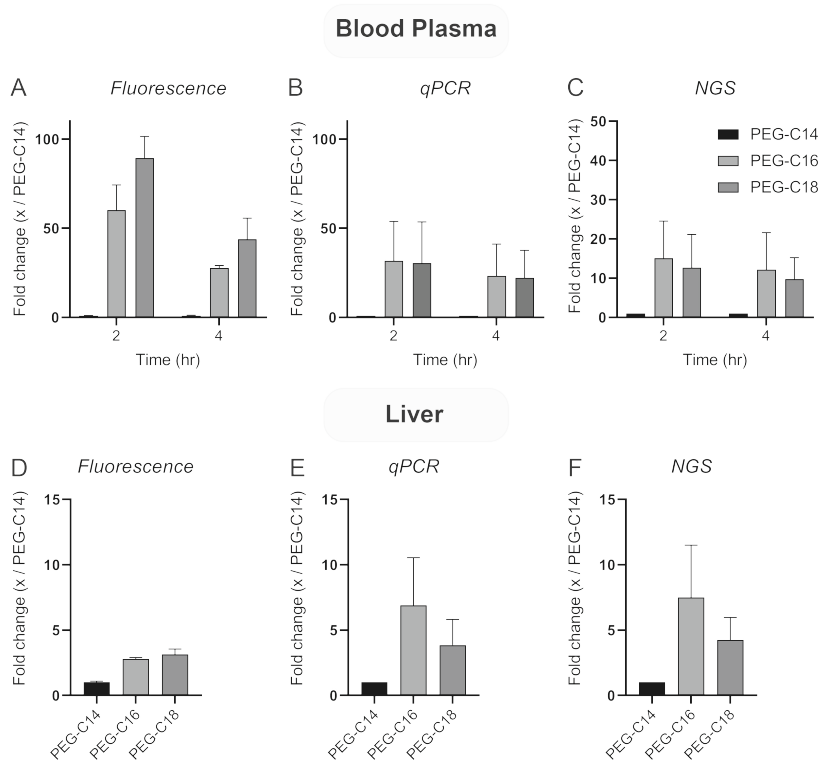
Figure 6: LNP tissue distribution differs depending on the LNPs detection method A) relative blood plasma concentration of LNPs composed of different PEG-lipids at 2 and 4 hours after i.v. injection (Figure 4C) expressed as fold change to formulation containing PEG-C14. Data expressed as mean ± SD (n=2, technical replicates) **B)** relative blood plasma concentration of pooled LNPs as measured by detection of specific barcodes via qPCR. Data is expressed as mean fold change to PEG-C14 ± SD (n=2, biological replicates) and normalized to spiked-in normalization barcode DNA. **C)** Relative blood plasma concentration of pooled LNPs as measured by next-generation sequencing. Data is expressed as fold change to PEG-C14 (Mean ± SD, N=2, biological replicates) and normalized for the input LNP mixture. **D)** Relative liver concentrations of different LNP formulations as measured by fluorescence in tissue lysates expressed as fold change to PEG-C14 (mean ± SD, N=3, technical replicates). **E)** Relative liver concentration of barcoded LNPs as measured by qPCR expressed as fold change to LNP-C14 (mean ± SD, N=2, biological replicates). **F)** Relative liver concentration of barcoded LNPs as measured by next generation sequencing expressed as fold change to LNP-C14 normalized for input DNA (mean ± SD, N=2, biological replicates)

REFERENCES

1. Alnylam Pharmaceuticals I. Alnylam Receives Approval of ONPATTRO™ (patisiran) in Europe [Internet]. 2019 [cited 2019 Jun 13]. Available from: http://investors.alnylam.com/news-releases/news-release-details/alnylam-receives-approval-onpattrotm-patisiran-europe

2. Urits I, Swanson D, Swett MC, Patel A, Berardino K, Amgalan A, et al. A Review of Patisiran (ONPATTRO®) for the Treatment of Polyneuropathy in People with Hereditary Transthyretin Amyloidosis. Neurol Ther. 2020;9(2):301–15.

3. Miao L, Zhang Y, Huang L. mRNA vaccine for cancer immunotherapy. Mol Cancer. Molecular Cancer; 2021;20(1):1–23.

4. Bahl K, Senn JJ, Yuzhakov O, Bulychev A, Brito LA, Hassett KJ, et al. Preclinical and Clinical Demonstration of Immunogenicity by mRNA Vaccines against H10N8 and H7N9 Influenza Viruses. Mol Ther. 2017;25(6):1316–27.

5. Pardi N, Hogan MJ, Pelc RS, Muramatsu H, Andersen H, DeMaso CR, et al. Zika virus protection by a single low-dose nucleoside-modified mRNA vaccination. Nature. 2017;543(7644):248–51.

6. Sabnis S, Kumarasinghe ES, Salerno T, Mihai C, Ketova T, Senn JJ, et al. A Novel Amino Lipid Series for mRNA Delivery : Improved Endosomal Escape and Sustained Pharmacology and Safety in Non-human Primates. Mol Ther. 2018;26(6):1509–19.

7. Cafri G, Gartner JJ, Zaks T, Hopson K, Levin N, Paria BC, et al. mRNA vaccine–induced neoantigen-specific T cell immunity in patients with gastrointestinal cancer. J Clin Invest. 2020;130(11):5976–88.

8. Evers MJW, Kulkarni JA, van der Meel R, Cullis PR, Vader P, Schiffelers RM. State-of-the-Art Design and Rapid-Mixing Production Techniques of Lipid Nanoparticles for Nucleic Acid Delivery. Small Methods. 2018;2(9):1700375.

9. Semple SC, Akinc A, Chen J, Sandhu AP, Mui BL, Cho CK, et al. Rational design of cationic lipids for siRNA delivery. Nat Biotechnol. 2010;28(2):172–6.

10. Jayaraman M, Ansell SM, Mui BL, Tam YK, Chen J, Du X, et al. Maximizing the potency of siRNA lipid nanoparticles for hepatic gene silencing in vivo. Angew Chem, Int Ed. 2012;51(34):8529–33.

11. Akinc A, Zumbuehl A, Goldberg M, Leshchiner ES, Busini V, Hossain N, et al. A combinatorial library of lipid-like materials for delivery of RNAi therapeutics. Nat Biotechnol. 2008;26(5):561–9.

12. Dong Y, Love KT, Dorkin JR, Sirirungruang S, Zhang Y, Chen D, et al. Lipopeptide nanoparticles for potent and selective siRNA delivery in rodents and nonhuman primates. Proc Natl Acad Sci U S A. 2014;111:3955–60.

13. Paunovska K, Da Silva Sanchez AJ, Sago CD, Gan Z, Lokugamage MP, Islam FZ, et al. Nanoparticles Containing Oxidized Cholesterol Deliver mRNA to the Liver Microenvironment at Clinically Relevant Doses. Adv Mater. 2019 Apr;31(14):e1807748.

14. Dahlman JE, Kauffman KJ, Xing Y, Shaw TE, Mir FF, Dlott CC, et al. Barcoded nanoparticles for high throughput in vivo discovery of targeted therapeutics. Proc Natl Acad Sci U S A. 2017;114(8):2060–5.

15. Kim J, Jozic A, Sahay G. Naturally Derived Membrane Lipids Impact Nanoparticle-Based Messenger RNA Delivery. Cell Mol Bioeng. 2020;13(5):463–74.

16. Paunovska K, Sago CD, Monaco CM, Hudson WH, Castro MG, Rudoltz TG, et al. A Direct Comparison of in Vitro and in Vivo Nucleic Acid Delivery Mediated by Hundreds of Nanoparticles Reveals a Weak Correlation. Nano Lett. 2018;18(3):2148–57.

17. Whitehead KA, Matthews J, Chang PH, Niroui F, Dorkin JR, Severgnini M, et al. In vitro - In vivo translation of lipid nanoparticles for hepatocellular siRNA delivery. ACS Nano. 2012;6(8):6922–9.

18. Dahlman JE, Kauffman KJ, Xing Y, Shaw TE, Mir FF, Dlott CC, et al. Barcoded nanoparticles for high throughput in vivo discovery of targeted therapeutics. Proc Natl Acad Sci U S A. 2017;114(8):2060–5.

19. Oude Blenke E. Chapter 2: Lipid nanoparticles and structural requirements for efficient transfections. In: Intracellular delivery of RNA therapeutics with lipid nanoparticles. 2017. p. 21–32.

5

20. Mui BL, Tam YK, Jayaraman M, Ansell SM, Du X, Tam YYC, et al. Influence of Polyethylene Glycol Lipid Desorption Rates on Pharmacokinetics and Pharmacodynamics of siRNA Lipid Nanoparticles. Mol Ther - Nucleic Acids. 2013;2(12):e139.

21. Chen S, Tam YYC, Lin PJC, Sung MMH, Tam YK, Cullis PR. Influence of particle size on the in vivo potency of lipid nanoparticle formulations of siRNA. J Control Release. 2016;235:236–44.

22. Evers MJW, van de Wakker SI, de Groot EM, de Jong OG, Gitz-François JJJ, Seinen CS, et al. Functional siRNA Delivery by Extracellular Vesicle–Liposome Hybrid Nanoparticles. Adv Healthc Mater. 2022 Mar 11;11(5):2101202.

23. Yaari Z, Da Silva D, Zinger A, Goldman E, Kajal A, Tshuva R, et al. Theranostic barcoded nanoparticles for personalized cancer medicine. Nat Commun. 2016;7:1–10.

24. Akinc A, Querbes W, De S, Qin J, Frank-Kamenetsky M, Jayaprakash KN, et al. Targeted delivery of RNAi therapeutics with endogenous and exogenous ligand-based mechanisms. Mol Ther. 2010;18(7):1357–64.

25. Sago CD, Lokugamage MP, Lando GN, Djeddar N, Shah NN, Syed C, et al. Modifying a Commonly Expressed Endocytic Receptor Retargets Nanoparticles in Vivo. Nano Lett. 2018;18(12):7590–600.

26. Czimmerer Z, Hulvely J, Simandi Z, Varallyay E, Havelda Z, Szabo E, et al. A Versatile Method to Design Stem-Loop Primer-Based Quantitative PCR Assays for Detecting Small Regulatory RNA Molecules. PLoS One. 2013;8(1).

27. Christensen J, Litherland K, Faller T, van de Kerkhof E, Natt F, Hunziker J, et al. Biodistribution and Metabolism Studies of Lipid Nanoparticle–Formulated Internally [3 H]-Labeled siRNA in Mice. Drug Metab Dispos. 2014 Mar;42(3):431–40.

28. Sahay G, Querbes W, Alabi C, Eltoukhy A, Sarkar S, Zurenko C, et al. Efficiency of siRNA delivery by lipid nanoparticles is limited by endocytic recycling. Nat Biotechnol. 2013;31(7):653–8.

29. Sago CD, Lokugamage MP, Paunovska K, Vanover DA, Monaco CM, Shah NN, et al. High-throughput in vivo screen of functional mRNA delivery identifies nanoparticles for endothelial cell gene editing. Proc Natl Acad Sci U S A. 2018 Oct 16;115(42):E9944–52.

SUPPLEMENTARY INFORMATION

Supplementary Table 1: siRNA sequences. ribonucleotide sequence of used short interfering RNA molecules. dT, dC, & dG indicate a deoxyribonucleic acid base

siRNA firefly luciferase	Sense: '5-GGA CGA GGU GCC UAA AGG AdCdG-3'
	Antisense: '5-UCC UUU AGG CAC CUC GUC CdCdG-3'
siRNA non specific	Sense: 5'-UGC GCU ACG AUC GAC GAU GdTdT-3'
	Antisense: 5'-CAU CGU CGA UCG UAG CGC AdTdT-3'

Supplementary Table 2: DNA Barcode sequences. * mark phosphorothioate bonds

Barcode (#)	Sequence ('5-'3)
1	A*G*ACGTGTGCTCTTCCGATCTNNNNNNNNNNNCCACTAAGAGGCCTGAGATCGGAAGAG-CGTCGT*G*T
2	A*G*ACGTGTGCTCTTCCGATCTNNNNNNNNNNNTGTTCCGTAGGCCTGAGATCGGAAGAG-CGTCGT*G*T
3	A*G*ACGTGTGCTCTTCCGATCTNNNNNNNNNNNGATACCTGAGGCCTGAGATCGGAAGAG-CGTCGT*G*T
4	A*G*ACGTGTGCTCTTCCGATCTNNNNNNNNNNNAGCCGTAAAGGCCTGAGATCGGAAGAG-CGTCGT*G*T
5	A*G*ACGTGTGCTCTTCCGATCTNNNNNNNNNNNCTCCTGAAAGGCCTGAGATCGGAAGAG-CGTCGT*G*T

Supplementary Table 3: Primer sequences used for quantitative PCR

Primer	Sequence ('5-'3)
Universal Forward	AGACGTGTGCTCTTCCGA
Reverse qPCR 1	ATCTCAGGCCTCTTAGTGG
Reverse qPCR 2	ATCTCAGGCCTACGGAACA
Reverse qPCR 3	ATCTCAGGCCTCAGGTATC
Reverse qPCR 4	ATCTCAGGCCTTTACGGCT
Reverse qPCR 5	ATCTCAGGCCTTTCAGGAG

5

Supplementary Table 4: Index Primers used for next generation sequencing (NGS)

Reverse Index Primer (#)	Sequence ('5-'3)
1	CAAGCAGAAGACGGCATACGAGATACATCGGTGACTGGAGTTCAGACGTGTGCTCTTCCGATC
2	CAAGCAGAAGACGGCATACGAGATTGGTCAGTGACTGGAGTTCAGACGTGTGCTCTTCCGATC
3	CAAGCAGAAGACGGCATACGAGATCACTGTGTGACTGGAGTTCAGACGTGTGCTCTTCCGATC
4	CAAGCAGAAGACGGCATACGAGATATTGGCGTGACTGGAGTTCAGACGTGTGCTCTTCCGATC
5	CAAGCAGAAGACGGCATACGAGATGATCTGGTGACTGGAGTTCAGACGTGTGCTCTTCCGATC
6	CAAGCAGAAGACGGCATACGAGATTACAAGGTGACTGGAGTTCAGACGTGTGCTCTTCCGATC
7	CAAGCAGAAGACGGCATACGAGATCGTGATGTGACTGGAGTTCAGACGTGTGCTCTTCCGATC
8	CAAGCAGAAGACGGCATACGAGATGCCTAAGTGACTGGAGTTCAGACGTGTGCTCTTCCGATC
9	CAAGCAGAAGACGGCATACGAGATTCAAGTGTGACTGGAGTTCAGACGTGTGCTCTTCCGATC
10	CAAGCAGAAGACGGCATACGAGATCTGATCGTGACTGGAGTTCAGACGTGTGCTCTTCCGATC
11	CAAGCAGAAGACGGCATACGAGATAAGCTAGTGACTGGAGTTCAGACGTGTGCTCTTCCGATC
12	CAAGCAGAAGACGGCATACGAGATGTAGCCGTGACTGGAGTTCAGACGTGTGCTCTTCCGATC
13	CAAGCAGAAGACGGCATACGAGATTGTTGACTGTGACTGGAGTTCAGACGTGTGCTCTTCCGAT
14	CAAGCAGAAGACGGCATACGAGATACGGAACTGTGACTGGAGTTCAGACGTGTGCTCTTCCGAT
15	CAAGCAGAAGACGGCATACGAGATTCTGACATGTGACTGGAGTTCAGACGTGTGCTCTTCCGAT
16	CAAGCAGAAGACGGCATACGAGATCGGGACGGGTGACTGGAGTTCAGACGTGTGCTCTTCCGAT
17	CAAGCAGAAGACGGCATACGAGATGTGCGGACGTGACTGGAGTTCAGACGTGTGCTCTTCCGAT
18	CAAGCAGAAGACGGCATACGAGATCGTTTCACGTGACTGGAGTTCAGACGTGTGCTCTTCCGAT
19	CAAGCAGAAGACGGCATACGAGATAAGGCCACGTGACTGGAGTTCAGACGTGTGCTCTTCCGAT
20	CAAGCAGAAGACGGCATACGAGATTCCGAAACGTGACTGGAGTTCAGACGTGTGCTCTTCCGAT
21	CAAGCAGAAGACGGCATACGAGATTACGTACGGTGACTGGAGTTCAGACGTGTGCTCTTCCGAT
22	CAAGCAGAAGACGGCATACGAGATATCCACTCGTGACTGGAGTTCAGACGTGTGCTCTTCCGAT
23	CAAGCAGAAGACGGCATACGAGATATATCAGTGTGACTGGAGTTCAGACGTGTGCTCTTCCGAT
24	CAAGCAGAAGACGGCATACGAGATAAAGGAATGTGACTGGAGTTCAGACGTGTGCTCTTCCGAT
Universal Forward Primer	AATGATACGGCGACCACCGAGATCTACACTCTTTCCCTACACGACGCTCTTCCGATCT
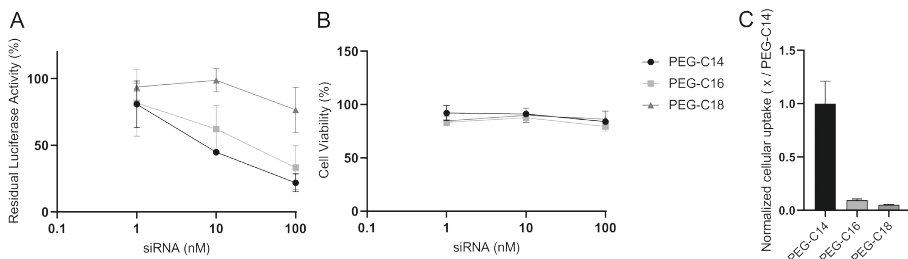
Supplementary Figure 1: Alkyl chain length of PEG-lipid affects functional siRNA delivery and cellular uptake in HEK293T-dluc. A) Gene-silencing and **B)** cell viability were evaluated in HEK293T-dluc. Cells were incubated with LNPs concentrations ranging from 1 nM to 100 nM siRNA and gene-silencing and cell-viability was analyzed after 48 hours. **C)** Cellular uptake of different PEGylated LNPs normalized to LNPs containing PEG-C14. Cells were incubated for 4 hours at 37 °C at a concentration of 50 nM siRNA and cellular uptake was measured by flow cytometry. Gene-silencing data are expressed as mean ± SD (n=2, biological replicates), cell viability and cellular uptake are expressed as mean ± SD (n=3, technical replicates).
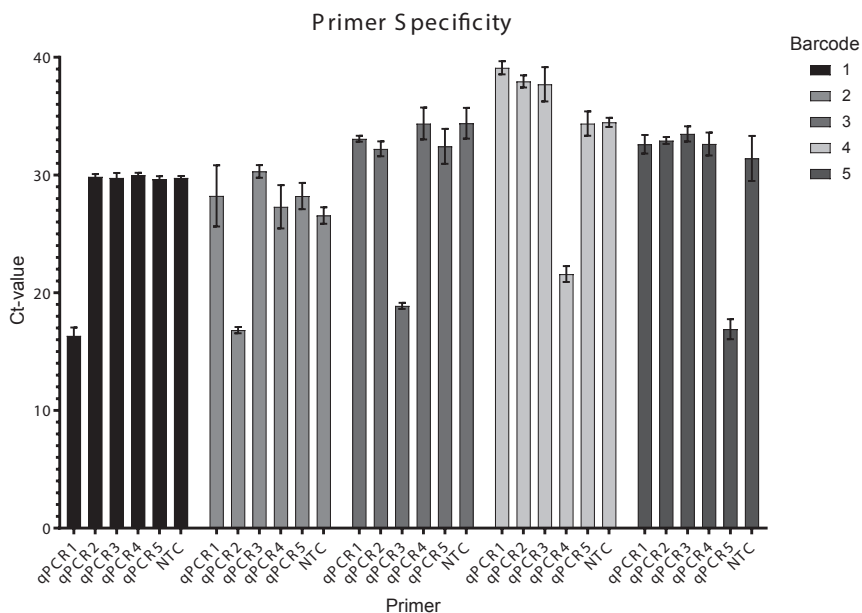
Supplementary Figure 2: qPCR primer specificity for barcodes used in in vitro experiments and in the in vivo validation study. 2 attomol barcode (1 – 5) was amplified using specific and non-specific primers (qPCR 1-5). Data is expressed as mean CT value ± SD (n=3, technical replicates). NTC: no template control
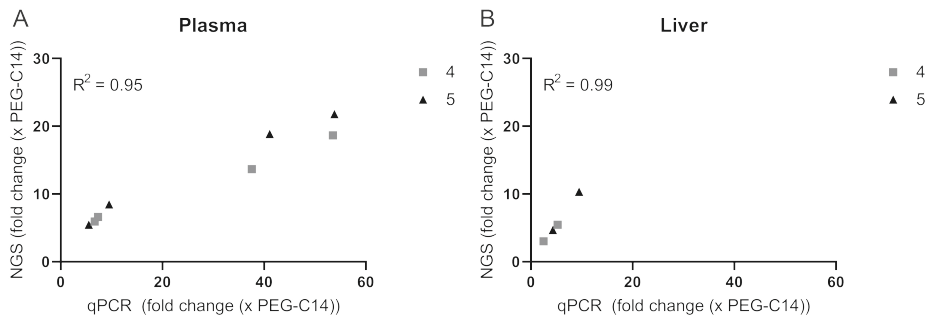
Supplementary Figure 3:Barcode occurrence measured via NGS and qPCR have a correlation coefficient > 0.9 indicating that both methods yield similar results. Relative barcode occurrence measured by NGS is plotted against relative barcode occurrence measured by qPCR for both blood plasma (A) and liver samples (B). Correlation is analyzed by linear regression using GraphPad Prism v9.

5

Functional siRNA Delivery by Extracellular Vesicle-Liposome Hybrid Nanoparticles

Martijn J.W. Evers[1], Simonides I. van de Wakker[2], Ellis M. de Groot[1], Olivier G. de Jong[1,3], Jerney J.J. Gitz-François[1], Cor S. Seinen[1], Joost P.G. Sluijter[2,4], Raymond M. Schiffelers[1], Pieter Vader[1,2]*

1: CDL Research, University Medical Center Utrecht, Utrecht, the Netherlands
2: Experimental Cardiology Laboratory, Department of Cardiology, University Medical Center Utrecht, Utrecht, the Netherlands
3: Department of Pharmaceutics, Utrecht Institute for Pharmaceutical Sciences (UIPS), Faculty of Science, Utrecht University, Utrecht, The Netherlands
4: Regenerative Medicine Centre, UMC Utrecht, University Utrecht, Utrecht, The Netherlands

6

ABSTRACT

The therapeutic use of RNA interference is limited by the inability of siRNA molecules to reach their site of action, the cytosol of target cells. Lipid nanoparticles, including liposomes, are commonly employed as siRNA carrier systems to overcome this hurdle, although their widespread use remains limited due to a lack of delivery efficiency. More recently, nature's own carriers of RNA, extracellular vesicles (EVs), are increasingly being considered as alternative siRNA delivery vehicles due to their intrinsic properties. However, they are difficult to load with exogenous cargo. Here, we prepared and evaluated EV – liposome hybrid nanoparticles (hybrids) as an alternative delivery system combining properties of both liposomes and EVs. We show that hybrids are spherical particles encapsulating siRNA, contain EV-surface makers and functionally deliver siRNA to different cell types. The functional behavior of hybrids, in terms of cellular uptake, toxicity and gene-silencing efficacy, is altered as compared to liposomes and varies among recipient cell types. Moreover, hybrids produced with cardiac progenitor cell (CPC) derived-EVs retain functional properties attributed to CPC-EVs such as activation of endothelial signaling and migration. To conclude, hybrids combine benefits of both synthetic and biological drug delivery systems and might serve as future therapeutic carriers of siRNA.

INTRODUCTION

RNA interference (RNAi) is a naturally occurring process through which messenger RNA (mRNA) translation is inhibited in a sequence-specific manner. This process is mediated by short interfering RNA (siRNA) molecules.[1,2] The ability of RNAi to specifically inhibit translation of (pathological) proteins makes it a powerful therapeutic agent applicable in various areas of disease.[3] However, effective delivery of siRNA molecules is limited as unmodified siRNA molecules are instable, immunogenic and cannot reach their site of action, i.e. the cytosol of target cells.[4–7] In order to protect and deliver siRNA into target cells, several RNA delivery systems have been developed, including metabolically stable GalNAc-conjugates and lipid-based delivery systems.[3] However, these systems have limitations since their tissue distribution and cellular uptake is mainly limited to specific subsets of cells in the spleen and liver while only 1-2% of the delivered siRNA reaches the cytosol. In addition, the lipids used in the formulation of lipid-based delivery systems can also show hepatotoxicity.[8–12]

The delivery of RNA molecules by naturally occurring RNA carriers, called extracellular vesicles (EVs), is an alternative to current delivery methods. EVs are small, lipid membrane vesicles secreted by a wide variety of cells, and contain biologically active complex molecules such as RNA, proteins, lipids and sugars.[13,14] EVs comprise a heterogeneous group of vesicles of different intracellular origins. At least two different subtypes can be classified based on their cellular biogenesis: exosomes and ectosomes, the latter also being referred to as microvesicles.

Exosomes (30-100 nm) originate in the endosomal pathway where inward budding of the endosomal membrane results in the formation of intraluminal vesicles which upon release are referred to as exosomes. Ectosomes (50-1000 nm) are released by the cell via direct pinching of the plasma membrane at the cell surface. EVs carry different RNA molecules such as mRNA and miRNA which can be functionally transferred to recipient cells and have been suggested to play important roles in (patho)physiological processes.[15–17] It is also possible to load non-naturally occurring RNA molecules, such as siRNA and sgRNA, in EVs to be functionally transferred to a recipient cell. [18–20]

As nature's own carriers of RNA, EVs might be an attractive alternative carrier system for therapeutic RNA as they have multiple potential benefits over current delivery vehicles in terms of delivery efficacy, intrinsic specific cell targeting properties, and toxicity/immunogenicity.[19–26] Interestingly, apart from the possible benefits for RNA delivery directly, EVs may, as intrinsically biologically active entities, induce additional regenerative or therapeutic effects such as induction of cell proliferation, neovascularization, immunomodulation and prevention of cell death.[27] Opposite to the beneficial effects of EVs, some risks might be associated with the use of EVs which originate from tumor cells as they have been implicated in cancer metastasis.[21]

Although EVs bear great potential as RNA delivery vehicles, their clinical development is hampered by a low loading efficiency of exogenous RNA molecules.[19,28,29] Multiple methods have been developed to achieve RNA loading into EVs either via loading during vesicle formation or after vesicle isolation.[30,31] However, for most methods, reported loading capacities are still several orders of magnitude lower compared to that of synthetic delivery systems.[31] Therefore,

6

an alternative approach for active loading of RNA therapeutics in EVs is required to capitalize on the beneficial properties of EVs as drug delivery vehicle.

Here, we propose a biomimetic approach to generate semi-synthetic hybrid nanoparticles based on EVs and liposomes termed EV-liposome hybrid nanoparticles (**hybrids**), thereby combining the beneficial properties of both liposomes and EVs in a single carrier of siRNA. To this end, we combined SKOV3 EVs and liposomes to produce hybrids by lipid-film hydration followed by extrusion. We physico-chemically characterized the particles and analyzed the incorporation of EV-associated membrane proteins in the hybrids via an antibody-based bead capture assay. Then, uptake, gene-silencing efficacy and toxicity of the hybrids was evaluated and compared to that of liposomes in multiple cell-lines. Finally, we used EVs derived from cardiac progenitor cells (CPCs) to generate hybrid nanoparticles and assessed whether the functional regenerative properties of CPC EVs were retained. The data show that we successfully produced hybrid nanoparticles which functionally deliver RNA and retain functional properties attributed to EVs.

RESULTS

Hybrids carry physicochemical features of both liposomes and EVs

First, SKOV3 EVs were isolated from conditioned medium of SKOV3 cells via an established size-exclusion chromatography protocol.[32] The protein composition of the isolated EVs was then analyzed by western blot to verify the enrichment of specific EV-marker proteins as compared to cell lysate. To this end, we analyzed expression of the transmembrane proteins CD81, CD63 and CD9 and luminal proteins Alix and TSG101. As a negative control, expression of endoplasmic reticulum protein Calnexin was analyzed. CD63, CD81, CD9 and Alix were enriched in EVs as compared to cell lysate **(Figure 1A)**. Expression of TSG101 and Actin in EVs was comparable to that in cell lysate while Calnexin was clearly negatively enriched. EV purity, as determined by the number of particles per µg protein was found to be consistent among isolations **(Supplementary Figure S1)**.[33] Mean and mode EV size was determined by nanoparticle tracking analysis (NTA) and found to be 100 nm and 75 nm, respectively. EV size, as determined by dynamic light scattering (DLS), was slightly higher at 150 nm with a polydispersity index of approximately 0.2 **(Figure 1B, C, D)**. The surface charge (zeta potential) of EVs was negative, -18 mV, as measured by laser Doppler electrophoresis **(Figure 1E)**. Cryo-electron microscopy revealed the typical spherical, unilamellar morphology of EVs **(Figure 1F)**. All together, these analyses confirmed successful isolation of EVs from conditioned medium of SKOV3 cells.[14]
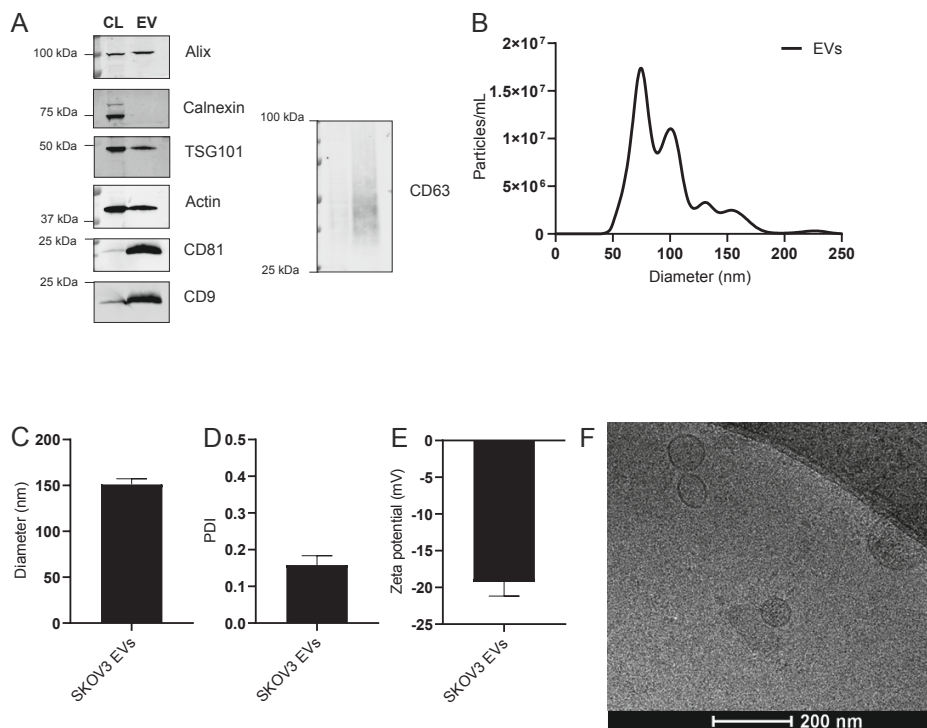
Figure 1: Physicochemical characterization of SKOV3 EVs. A) Western blot analysis of EV protein markers (Alix, TSG101, CD81, CD9 and CD63) and EV-negative markers (Calnexin) in SKOV3 cell lysate (CL) and SKOV3 EVs (EV). **B**) Size distribution of EVs as determined by NTA. **C)** Average diameter of EVs as determined by dynamic light scattering. **D)** Polydispersity index of EVs as measured by dynamic light scattering. **E)** Surface charge (zeta potential) of EVs as measured by laser Doppler electrophoresis. **F)** Cryo electron microscopy image of EVs isolated from SKOV3 cells. Data are shown as mean ± SD (n=3, technical replicates).

These EVs were then used for the production of hybrids encapsulating siRNA via lipid film hydration and subsequent extrusion. Liposomes and hybrids were prepared with DLin-MC3-DMA;1,2-dipalmitoyl-sn-glycero-3-phosphocholine (DPPC);cholesterol;18:1 Biotinyl PE;DMG-PEG in a molar ratio of 0.3;0.3;0.355;0.015;0.03 and processed to generate a lipid film. This lipid film was hydrated with siRNA to form siRNA loaded liposomes **(Figure 2A,B)**. For preparation of hybrids, SKOV3 EVs were added at the hydration step at two different ratios of EV-protein to total synthetic lipid (w/w), 1:100 and 1:50, and subsequently extruded to produce hybrids (**Figure 2C,D)**.
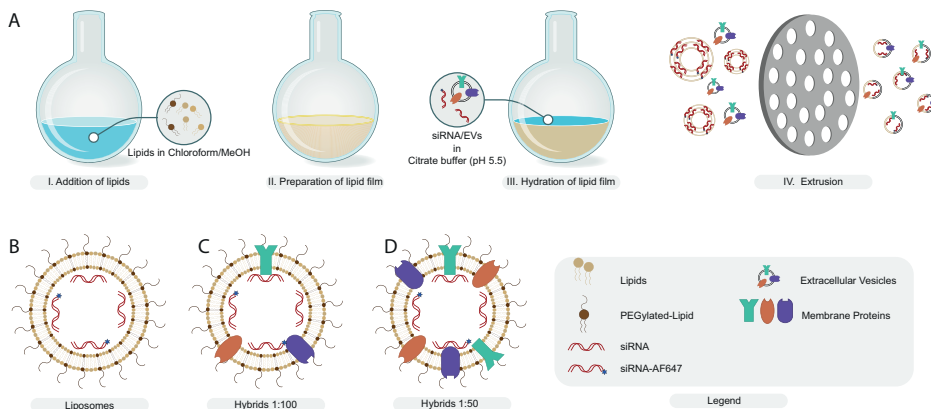
Figure 2: Production of liposomes and hybrids. A) Schematic illustration of hybrid production via thin-film hydration and extrusion. **B, C, D)** Schematic illustration of liposomes and hybrids encapsulating a mixture of fluorescent and non-fluorescent siRNA. Hybrids are produced at different protein-to-lipid ratios (w/w): 1:100 **(C)** and 1:50 **(D)**.

The particles were then analyzed for their physicochemical properties to evaluate the influence of increasing numbers of EVs in the formulation on size, polydispersity index (PDI), zeta potential, siRNA encapsulation efficiency and particle morphology **(Figure 3)**. The size and PDI of liposomes and hybrids were analyzed by DLS and NTA. The average size was close to 150 nm for all formulations as measured by DLS and approximately 100 nm as measured by NTA **(Figure 3A, E)**. PDI seemed to increase slightly as the amount of EV material in the formulation was increased. However, this increase was not statistically significant **(Figure 3B)**. We did observe that the zeta potential slightly decreased for hybrids as compared to liposomes but no difference was found between hybrids incorporating EVs at a ratio of 1:100 or 1:50 **(Figure 3C)**. The decreased surface charge of hybrids could be explained by the incorporation of the negatively charged EV membrane into the newly formed hybrid nanoparticle leading to a decrease in zeta potential. The encapsulation efficiency of siRNA reduced with increasing amounts of EVs in the formulation and decreased from approximately 80% for liposomes to only 50% for hybrids (1:50) **(Figure 3D)**. Furthermore, we quantified the overall yield of each production process in terms of siRNA and cholesterol and found that while the yield for liposomes was approximately 50% of both siRNA and cholesterol, the yield was slightly decreased for both hybrid formulations. Here, the influence of EV cholesterol content on the overall amount of cholesterol in the formulation was limited (0.6% and 1.2% in the 1:100 and 1:50 hybrid formulations, respectively) as EVs contained only ±0.13 μg cholesterol per μg protein (**Supplementary Figure S2**). Cryo-electron microscopy revealed that the morphology of the nanoparticles was spherical and that all formulations consisted of unilamellar nanoparticles **(Figure 3F-H)**.
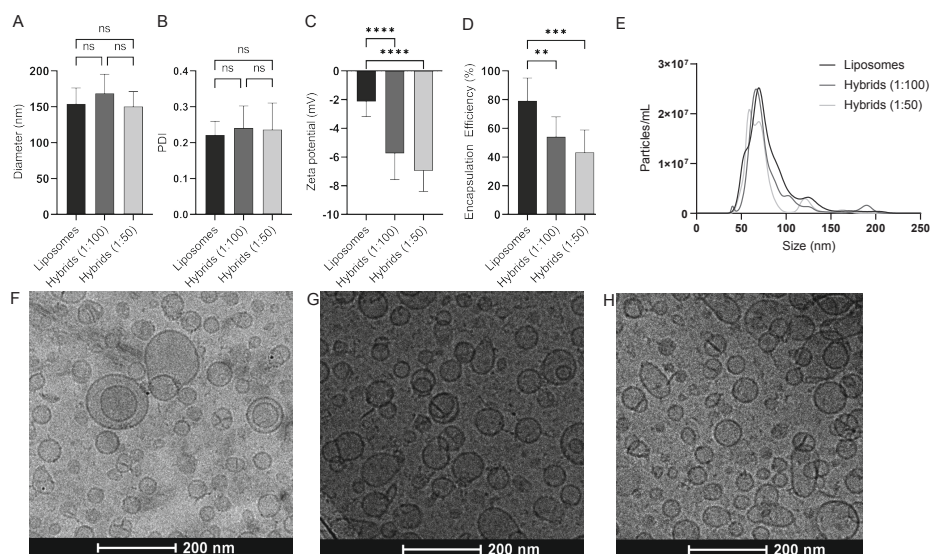
Figure 3: Physicochemical characterization of liposomes and hybrids. A) Nanoparticle size as determined by DLS. **B)** Polydispersity index of nanoparticles as determined by DLS. **C)** Zeta potential of nanoparticles as determined by laser doppler electrophoresis. **D)** RNA encapsulation efficiency of liposomes and hybrids. **E)** Nanoparticle size as determine by NTA. **F, G, H)** Nanoparticle morphology as determined by cryogenic electron microscopy of liposomes **(F)**, hybrids (1:100) **(G)**, and hybrids (1:50) **(H)**. Mean + SD are displayed. n=8-10 (biological replicates), one-way ANOVA with Tukey's post-test, ns= not significant, ** = p<0.01, *** = p<0.001, **** P<0.0001.

In order to verify successful hybrid formation, we next evaluated the presence of siRNA and synthetic lipids in liposomes and hybrids captured using magnetic beads coated with EV-enriched targets, including CD9, CD81 or CD63. We hypothesized that only after formation of EV-liposome hybrids, synthetic lipids and siRNA (AF647 labelled) could be detected on the beads **(Figure 4A)**. For all beads, a clear increase in siRNA-AF647 signal was observed for hybrid samples as compared to liposomes, which shows that only hybrids, but not liposomes, contain tetraspanins that can be captured the beads **(Figure 4B)**. We also observed that an increase in the number of EVs used in the formulation resulted in a higher siRNA-AF647 signal.

Next, we investigated whether the incorporation of synthetic lipids in hybrids could also be detected. We prepared liposomes and hybrids containing 0.2 mol% 18:1 Biotinyl Cap PE and performed a bead-pulldown with additional staining using streptavidin-PE. We found that 18:1 Biotinyl Cap PE was also successfully incorporated in the hybrids given the clear increase in PE-signal for hybrids. Moreover, this experiment confirmed that non-specific binding of liposomes to the beads is very limited given the low PE-signal for the liposome sample **(Figure 4C)**. In addition, the observed trend in PE signal corresponds to that of AF647-siRNA where the signal on CD9 beads is slightly higher compared to CD63 and CD81. All together, these results indicate that we successfully produced EV-liposome hybrid nanoparticles carrying EV surface proteins and synthetic lipids while simultaneously complexing siRNA.
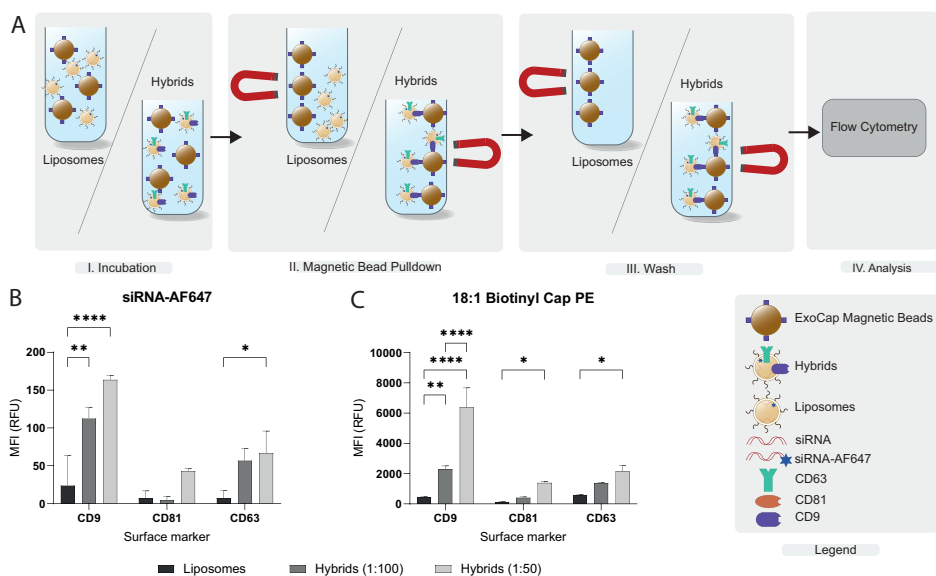
Figure 4: Bead capture analysis of siRNA-AF647 and 18:1 Biotinyl Cap PE in liposomes and hybrids on beads targeting CD9, CD63 or CD81. A) Schematic illustration of bead-capture assay. **B)** Flow cytometric analysis of siRNA-AF647 on ExoCap™ beads. Nanoparticles were incubated with beads targeting a single epitope, CD9, CD63 or CD81, washed and analyzed. **C)** Flow cytometric analysis of 18:1 Biotinyl Cap PE on ExoCap™ beads. Data are representative of three independent experiments and expressed as mean ± SD (n=3, technical replicates), one-way ANOVA with Tukey's post-hoc test, * = p<0.05, ** = p<0.01, **** P<0.0001.

Cellular uptake of hybrids is dependent on the EV-to-liposome ratio and differs per cell type

Next, we evaluated the cellular internalization efficiency of liposomes and hybrids as this is an important first step in the cytosolic delivery of siRNA. We incubated 3 different cell types – SKOV3, HEK293T, and U87-MG– for 4 hours with liposomes and hybrids (1:100 and 1:50) and analyzed siRNA-AF647 uptake by flow cytometry **(Figure 5)**. Uptake of hybrid (1:100) nanoparticles in all three cell types was decreased as compared to liposomes. This effect was found to be statistically significant in HEK293T and U87-MG cells. Interestingly, when more EV components were incorporated in hybrids (1:50), cellular uptake increased again, but only at statistically significant levels in HEK293T and U87 cells. Almost no nanoparticle uptake was seen at 4 °C which confirmed the effects seen are a result of active uptake processes **(Supplementary Figure S3)**. The differences in cellular uptake implicate that the cellular internalization of hybrids varies per cell type and that the uptake is affected by the amount of SKOV3 EVs incorporated in the hybrid formulation.
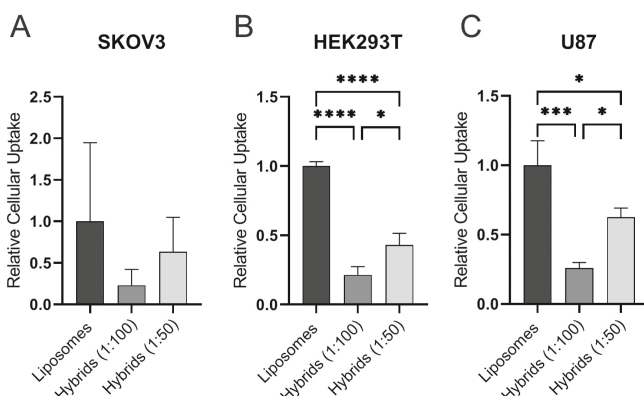
Figure 5: Cellular uptake of liposomes, hybrids (1:100) and hybrids (1:50) in A) SKOV3-dluc, **B)** HEK293T-dluc, **C)** U87-MG-dluc. Cells were incubated for 4 hours at 37 °C at a concentration of 25nM siRNA and cellular uptake was measured by flow cytometry. Data are representative of three independent experiments and expressed as mean ± SD (n=3, technical replicates), one-way ANOVA with Tukey's post-hoc test, * = $p < 0.05$, ***=$p < 0.001$, **** $P < 0.0001$.

Hybrids show limited toxicity and functionally deliver siRNA to multiple cell types

For successful application of liposomes and hybrids in RNA delivery, particles must be biocompatible and non-toxic. Therefore, we analyzed the toxicity of the nanoparticles using a cell viability assay. In SKOV3 cells, liposomes showed a dose-dependent decrease in cell viability whereas this effect was not observed for hybrids (1:100 & 1:50) indicating increased biocompatibility of hybrids as compared to liposomes. A difference in the effect on cell viability between liposomes and hybrids was not observed in HEK293T and U87-MG cells. In HEK293T cells, a small dose-dependent decrease in cell viability was seen for all nanoparticles with no differences between liposomes and hybrids. In U87-MG, administration of liposomes and hybrids did not affect the cell viability **(Figure 6)**.

Another possible advantageous functional characteristic of EVs as compared to liposomes could be an improved siRNA delivery efficiency.[19,20] Therefore, we evaluated the gene-silencing efficacy of hybrids as compared to liposomes using a luciferase reporter assay. Liposomes or hybrids encapsulating siRNA targeting firefly luciferase or a non-specific control siRNA were administered to SKOV3, HEK293T, and U87-MG **(Figure 7, Supplementary Figure S4)**. A clear dose-dependent decrease in firefly luciferase was observed in all cell lines. In SKOV3 and HEK293T cells, the gene-silencing effect of hybrids (1:100 and 1:50) was lower as compared to liposomes. In contrast, in U87-MG cells, gene silencing efficacy of hybrids (1:100 and 1:50) was similar to that of liposomes despite a lower uptake efficiency, which may point towards more efficient cytosolic siRNA delivery. There was no difference in gene-silencing efficacy between different EV-liposome hybrids (1:100 and 1:50). This indicates that under these conditions, gene-silencing efficacy was not critically dependent on the EV-protein to lipid ratio. All together, these data show that hybrids are able to functionally deliver siRNA to different cell types, although in these experiments the potency is reduced in SKOV3 and HEK293T cells as compared to liposomes.
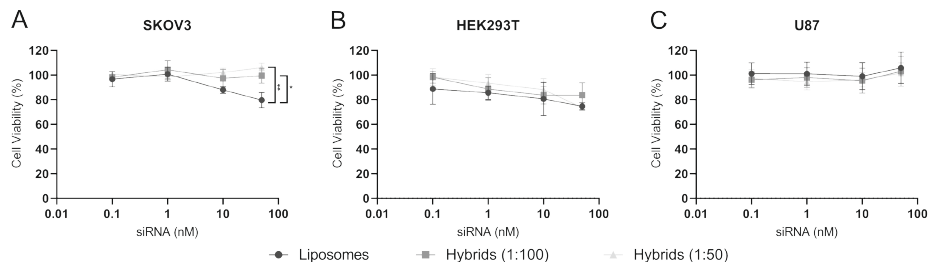
Figure 6: Cell viability of different cell types incubated with liposomes and hybrids as determined by an MTS assay. Cells were incubated with liposomes and hybrids at concentrations ranging from 0.1 nм to 50 nм siRNA and cell-viability was analyzed after 48 hours. **A)** SKOV3-dluc. **B)** HEK293T-dluc**. C)** U87-MG-dluc. Data are representative of three independent experiments and expressed as mean ± SD (n=2-3, technical replicates), one-way ANOVA with Tukey's post-hoc test, *=p<0.05, **=p<0.01.
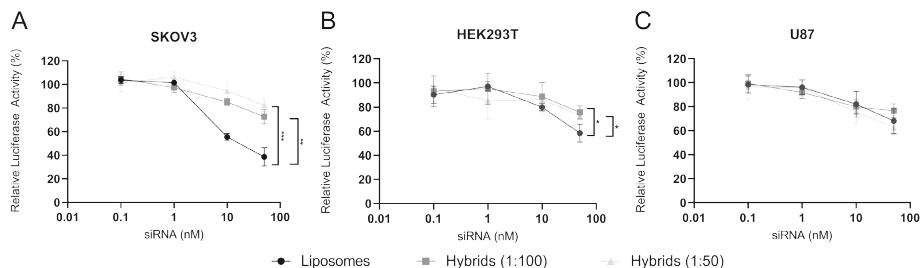
Figure 7: Gene silencing activity in different cell types treated with liposomes and hybrids nanoparticles encapsulating siRNA. Different cell types were incubated with liposomes and hybrids at concentrations ranging from 0.1 nм to 50 nм siRNA and gene-silencing was analyzed after 48 hours by measurement of luciferase expression. Data is plotted as the normalized ratio of firefly to renilla luciferase expression**. A)** SKOV3-dluc. **B)** HEK293T-dluc. **C)** U87-MG-dluc. Data are representative of three independent experiments and expressed as mean ± SD (n=3, technical replicates), one-way ANOVA with Tukey's post-hoc test, *=p<0.05, **=p<0.01, ***p<0.001.

Hybrids based on cardiac progenitor cell EVs retain functional regenerative properties

Finally, we investigated whether hybrids preserved the biological activity of EVs. To this end we generated hybrids with CPC EVs. CPC EVs have been shown to activate endothelial signaling pathways and migration, and activate *in vivo* angiogenesis.[34–36] The physicochemical properties were analyzed in a similar manner as for SKOV3 EV derived hybrids **(Supplementary Figure S5)**. Liposomes and hybrids had a size of approximately 150 nm at a PDI of ~ 0,2. Again, the surface charge of hybrids was lower compared to that of liposomes.

We then evaluated the functional capabilities of liposomes and CPC derived hybrids in two functional assays: an Akt phosphorylation assay and a scratch wound healing assay.

Akt is an important factor in signaling pathways involved in proliferation, angiogenesis, differentiation, adhesion, migration and cell survival and its phosphorylation is an indicator of functional CPC EV delivery.[37,38] HMEC-1 cells were serum-starved and subsequently incubated

for 30 minutes with hybrids (1:100 and 1:50) and EVs as well as PBS and liposomes as negative controls. After treatment, cells were lysed and the ratio of phosphorylated Akt/Akt was analyzed by western blot analysis. PBS and liposomes did not induce phosphorylation of Akt, whereas this was observed for hybrids (1:100 and 1:50) and EVs in a dose-dependent matter **(Figure 8A).** When analyzed using densitometry, hybrids (1:100 and 1:50) and EVs induced significantly more phosphorylation of Akt as compared to liposomes **(Figure 8B)**.

Secondly, we performed a scratch wound healing assay using a confluent monolayer of HMEC-1 cells. Samples were normalized based on particle counts as measured by NTA and a total dose of $2 \cdot 10^{12}$ particles for liposomes and hybrids was added as well as $3 \cdot 10^{10}$ particles for EVs which served as positive control. The closing of the scratch was then analyzed after 6 hours. Hybrids stimulated closure of the scratch to a larger extent than liposomes, and hybrids (1:50) further increased closure of the wound as compared to hybrids (1:100) **(Figure 8C-D)**. This indicates a dose-dependent effect of the amount of CPC EVs used in the formulation on wound closure.

These results are in good agreement with the endothelial signaling assays and indicate that hybrids produced using CPC EVs stimulate wound closure and induce phosphorylation of Akt.

6
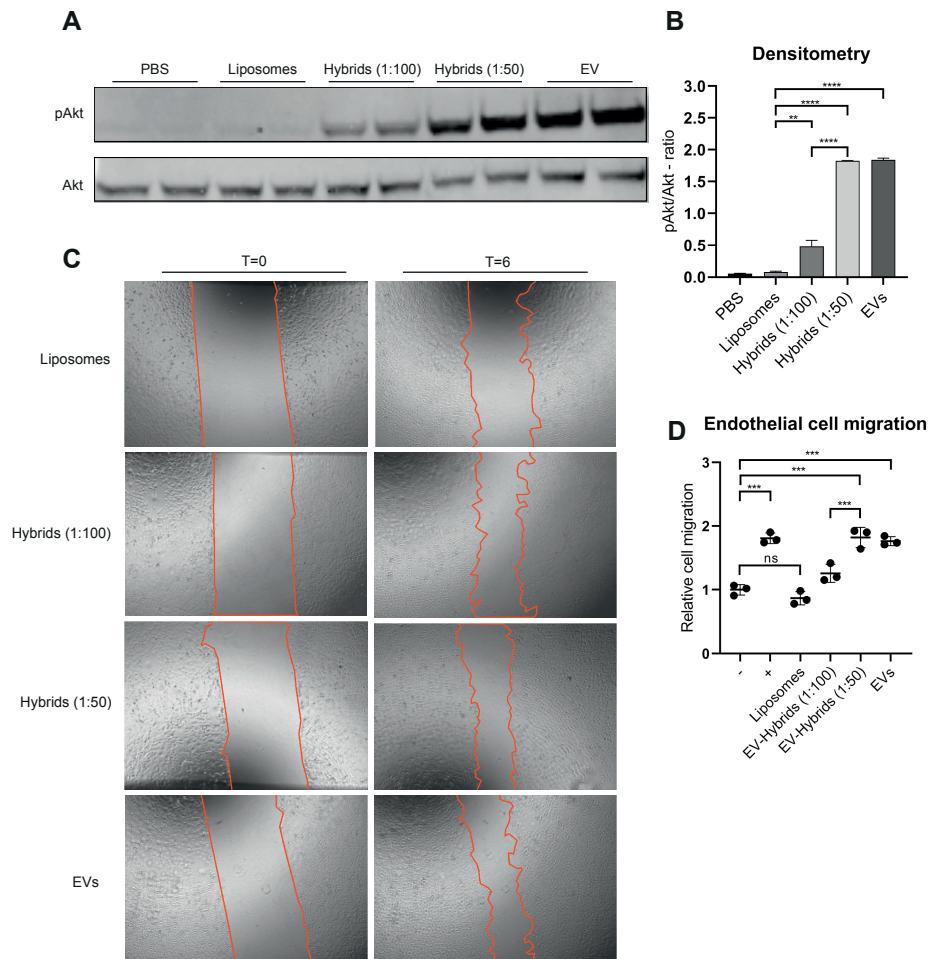
Figure 8: Endothelial signaling assay and scratch wound closing assay of HMEC-1 cells treated with liposomes and hybrids. A) Representative western blot analysis of phosphorylated Akt and Akt expression levels in HMEC-1 cells treated with liposomes, hybrids and EVs. Liposomes and hybrids were administered at a total particle dose of 2×10^{12} and EVs at a total particle dose of 3×10^{10}. **B)** Quantification of Akt and pAkt expression levels obtained via western blot analysis using densitometry expressed as pAkt/Akt-ratio. **C)** Representative images of scratch wound healing assay before (t=0) and after (t=6 hours) incubation with liposomes, hybrids (1:100), hybrids (1:50) and EVs. Liposomes and hybrids were administered at a total particle dose of $2\cdot10^{12}$ and EVs at a total particle dose of $3\cdot10^{10}$. **D)** Cell migration of HMEC-1 expressed relative to the negative control. Incubation of HMEC-1 cells with hybrids (1:50 and 1:100) and EVs increases wound closure as compared to liposomes. Data is expressed as mean + SD, one-way ANOVA with post-hoc test, ns= not significant, **=$p<0.01$, ***=$p<0.001$, ****=$p<0.0001$.

DISCUSSION

The delivery of RNAi therapeutics is challenging given the unfavorable characteristics of siRNA as a drug molecule. siRNA molecules are unstable in circulation, immunogenic and are unable due to their molecular properties, to cross cellular membranes to reach their cytosolic target site.

Here, we produced EV-liposome hybrid nanoparticles, which are nano-sized siRNA carriers formed through the merging of EVs and liposomes, via thin-film hydration and extrusion. The anticipated benefits originate from the combination of liposome related properties such as high RNA loading capacity and EV related properties such as increased delivery efficacy, cell targeting properties, and possible tissue regenerative properties.

The thin-film hydration and extrusion method has already been previously described to generate different hybrids based on the combination of EVs and liposomes.[39,40] For instance, Jhan et al. hydrated a lipid film in PBS and subsequently added 3T3- or A549-EVs followed by sonication and sequential extrusion through 400 nm, 200 nm and 100 nm membrane pores.[39] Raymajhi et al. hydrated the lipid film in the presence of J774A.1-EVs, sonicated and subsequently extruded the lipid mixture through membrane filters with 400 nm followed by 200 nm pores.[40] The use of mechanical extrusion to generate hybrids is not limited to EVs and lipid based-particles as it has also been used to incorporate cellular membranes, such as leukocyte membranes, in liposomes.[41–43] More recently, extrusion has also been used to surface coat gold nanoparticles with the membrane of EVs.[44]

An important variable in the generation of hybrids is the amount of EVs incorporated in the formulation. A useful metric to describe the amount of EVs incorporated in the formulation is the (EV) protein-to-(liposomal) lipid ratio. In literature, ratios can be found ranging from 1:5 to 1:1000 (protein/lipid (w/w)).[39–43] For instance, to incorporate the membrane of leukocytes into phosphatidylcholine liposomes ratios varying from 1:100 to 1:300 (protein/lipid; w/w) were used, whereas for the generation of 'macrophage derived hybrid exosomes' Rayamajhi et al. used a ratio of 1:5 (protein/lipid (w/w)).[40,41] A potential drawback of this metric is that proteins can also be contaminants of EV isolations which can vary from batch-to-batch and therefore potentially has implications for reproducibility. To account for this, we carefully monitored the number of particles per µg protein which was found to be highly consistent among different EV isolations. Here, we generated hybrids by hydration of a lipid film with EVs at protein-to-lipid ratios of 1:100-1:50 (w/w) and subsequent extrusion through membranes with pores of 1000 nm followed by 100 nm and then 50 nm. As the majority of EVs has a size below 100 nm, based on our observation in NTA analysis where we observed a size mode value of 75 nm, a 50 nm membrane was chosen as smallest membrane. A possible limitation of the aforementioned studies regarding EV based hybrid nanoparticles is that samples were extruded through pores around or above the median size of EVs which not necessarily results in deformation of the EV and subsequent reformation in a hybrid nanoparticle. In this study, we did take this into account and extruded EVs together with synthetic liposomes through a membrane with pore sizes of 50 nm.

We analyzed the yield of the production process of this formulation in terms of siRNA and synthetic lipid yield which was found to be maximally 50% of the input siRNA and cholesterol.

This could potentially be explained by the formation of siRNA/ionizable lipid aggregates which are lost during the extrusion process. Although this effect has been shown to be overcome by the addition of 40% ethanol (v/v) combined with a rise in temperature to 65 °C, we decided not to change the production process since higher temperatures and ethanol content could potentially detrimentally affect the EV membrane proteins.[45] When we looked at the influence of EV incorporation in the formulation on several particle characteristics such as size, PDI and zeta-potential we observed that increasing the amount of SKOV3 EVs incorporated in the formulation resulted in an increase in PDI, although this effect was not significant. For hybrids generated with CPC EVs, an increase in PDI was not observed. The surface charge, i.e. zeta potential, was decreased in hybrids which can most likely be attributed to incorporation of negatively charged EV membrane components. We did observe that RNA encapsulation efficiency in hybrids was decreased. This may be the results of competition for the electrostatic interaction with the ionizable lipid by negatively charged EV components such as RNA or negatively charged lipids or proteins. We also evaluated the morphology of the liposomes and hybrids. The extrusion process had no apparent detrimental effects on the morphology of hybrids as they appeared to be spherical, unilamellar membrane enclosed particles which are comparable to liposomes and EVs. We also confirmed that hybrid particles (containing both siRNA and synthetic lipid) were captured by beads coated with antibodies against several distinctive EV marker proteins such as CD9, CD63 and CD81 indicating that surface topology of EVs is at least partly transferred to the hybrids. Nevertheless, it remains challenging to assess the efficiency of this hybridization process and fully exclude the possibility of intact EVs being present in the formulation.

Next, we quantitatively compared multiple functional characteristics, including cellular uptake, gene-silencing efficacy and cell viability, of liposomes and extracellular vesicle -liposome hybrids. The cellular uptake of nanoparticles via endocytosis is influenced by many variables such as size, charge and the biomolecular corona.[46–49] It is known that uptake rate and route can vary between different lipid systems and EVs.[47,50–52] As the surface charge and membrane surface of hybrids differs from that of liposomes, we investigated the uptake efficiency of liposomes and hybrids. In HEK293T and U87-MG, we observed a decrease in uptake for hybrids (1:100) as compared to liposomes. At higher concentrations of EVs in the formulation (1:50), cellular uptake increased again. The latter observation suggests that the uptake mechanism is different for hybrids as compared to liposomes, changing from predominantly liposome-dictated to mainly EV-dictated. This may be relevant for cell-targeting purposes, as EVs may have intrinsic capacity to target specific cells or tissues.[21,24,53] Furthermore, this may affect endocytic routing and intracellular nanoparticle trafficking, which in turn may influence delivery efficiency.

An important drawback of the usage of liposomes or other lipid nanoparticles for RNA delivery is the dose/dose-regimen related hepatotoxicity which might be related to innate immune system activation.[8,54] In contrast to synthetic systems, EVs are generally considered to have low immunogenicity and are less toxic as observed in several preclinical studies.[55,56] Here, we observed a decrease in *in vitro* toxicity of hybrids as compared to liposomes in SKOV3 cells which could be the results of EV component incorporation in hybrids. The effect was only observed in SKOV3 cells suggesting cell-specific effects. These data should be interpreted with care as *in vitro* to *in vivo* translation of cell viability data for lipid-based drug delivery systems

is unclear. Moreover, the MTS-assay as performed in this manuscript lacked an assay positive control making it more difficult to assess the value of the absolute toxicity values. However, based on the results we could still assess relative differences between the three different nanoparticle types within the same experiments, which have shown to be reproducible.

Liposomes and hybrids both functionally delivered siRNA in a dose-dependent manner in three different cell types although the potency of hybrids was reduced in SKOV3 and HEK293T, but not in U87. Again, this is an intriguing observation as it implies that effects are cell type dependent. A possible explanation for the decrease in gene-silencing in HEK293T might be the decreased uptake. In contrast, the combination of decreased cellular uptake and comparable gene-silencing efficacy of liposomes and hybrids in U87-MG might suggest different intracellular trafficking resulting in more efficient escape of siRNA from the endo-lysosomal pathway for hybrids and is an interesting area to further explore.

Our observation that hybrids generated with SKOV3 EVs did not have a positive effect on gene-silencing efficiency differs from others. Coating of polyethyleneimine based siRNA particles with SKOV3 EVs resulted in increased potency in terms of gene-silencing efficacy of the EV-modified particle compared to the uncoated particle.[57] This apparent discrepancy may be a result of multiple different causes, including the production method and the resulting hybrid composition.

Several groups have applied the concept of extracellular vesicle – liposome hybrids to create nanoparticles for tumor-targeted drug delivery.[39,40,58] Here, we have shown that a similar approach can be used to convey tissue regenerative properties of CPC EVs to synthetic nanoparticles via the creation of extracellular vesicle -liposome hybrids. CPC EVs possess the ability to activate endothelial signaling and cell migration in HMEC-1.[34–36] We observed that hybrids also activated endothelial signaling and cell migration whereas liposomes did not. This demonstrates that hybrids produced via thin-film hydration and extrusion can be loaded with siRNA and retain functional properties of EVs. This implicates that hybrids potentially can be used as an efficient RNA drug delivery system while bearing intrinsic EV functionality at the same time. For instance, this can be of relevance in the salvage of myocardial tissue upon infarction where CPC EVs have shown to reduce scar size and improve ventricular function after permanent coronary occlusion.[59] Similarly, intracardiac delivery of a synthetic miRNA mimic of hsa-miR-590-3p via a lipid-based system resulted in reduced infarct size and improved cardiac output.[60] Given the results presented in this paper, hybrids might have the potential to combine both treatments in a single particle.

CONCLUSION

Currently, much is still unknown about how EV composition affects functionality and confers EVs with a potent RNA delivery capability. As long as such pivotal data is missing, the production of EV-liposome hybrids which fully reflect the functional capabilities of EVs remains challenging. The results presented here show that the production of hybrids via thin film hydration and subsequent extrusion results in hybrid particles with EV-like surface topology encapsulating

siRNA which can be functionally delivered. The incorporation of EV membrane components leads to functional differences. Depending on the cell type, uptake is altered, toxicity of hybrids as compared to liposomes is reduced and gene-silencing effects are retained. Moreover, we also show that intrinsic functionalities of CPC EVs such as the ability to activate endothelial signaling pathways and stimulate migration of HMEC are retained in hybrids. Thus, hybrid nanoparticles could combine the functional characteristics of both liposomes and EVs and serve as a 'best of both worlds' particle for therapeutic delivery of siRNA.

MATERIALS & METHODS

Materials

Cholesterol was obtained from Sigma-Aldrich (Saint-Louis, USA), DPPC from Lipoid GmbH (Ludwigshafen, Germany), DMG-PEG from NOF Corporation (Tokyo, Japan) and 18:1 Biotinyl Cap PE from Avanti Polar Lipids (Alabama, USA). DLin-MC3-DMA was synthesized in-house according to a published protocol.[61] All oligonucleotides were ordered at Integrated DNA Technologies (Iowa, USA). siRNA molecules were ordered as individual strands and annealed for 5 min at 97°C. The sequences used can be found in Supporting Table 1.

Cell Culture

Generation of cells stably expressing firefly and renilla luciferase

For the generation of stable dual luciferase cell lines, the PGK-FFluc-SV40-Rluc-NeoR_fusion cassette from the pmirGLO Dual-Luciferase miRNA Target Expression Vector (Promega, Leiden, NL) was isolated and transferred to a pHAGE2 lentiviral vector. First, pHAGE2-EF1a-IRES-NeoR-WPRE was restricted with SpeI and XbaI restriction enzymes (New England Biolabs, Ipswich, MA, USA) and religated to remove the EF1a promoter. Then, the PGK-FFluc-SV40-Rluc-NeoR_fusion cassette was isolated from the pmirGLO plasmid using BglII and BstBI restriction enzymes (New England Biolabs, Ipswich, MA, USA) and ligated into the newly formed pHAGE2-IRES-NeoR-WPRE vector digested with BamHI and ClaI restriction enzymes (New England Biolabs, Ipswich, MA, USA), generating a pHAGE2-PGK-FFluc-SV40-Rluc-NeoR_fusion-WPRE plasmid. All ligations were performed using a Quick Ligation Kit (all New England Biolabs, Ipswich, MA, USA) and ligation products were subsequently transformed into One Shot Stbl3 chemically competent E coli (ThermoFisher Scientific, Waltham, MA, USA). For lentiviral production, HEK293T cells were transfected overnight with psPAX2, pMD2.G, and pHAGE2-PGK-FFluc-SV40-Rluc-NeoR_fusion-WPRE plasmids at a 1:1:2 ratio using Lipofectamine 2000 (ThermoFisher Scientific, Waltham, MA, USA) according to the manufacturers' protocol. After 18 hours the culture medium was replaced, and lentiviral supernatant was collected after 48 hours. Lentiviral supernatant was cleared from any remaining cells by a 5 minutes 1000 x g centrifugation step and subsequent 0.45 µm syringe filter filtration, and stored at -80 °C until further use. Cells were transduced with lentiviral supernatants overnight in the presence of 8 µg/mL polybrene (ThermoFisher Scientific, Waltham, MA, USA). Starting 24 hours after lentiviral transduction, cells were cultured with 1000

µg/mL G418 for 5 days, after which they were cultured at a 500-1000 µg/mL G418, depending on the cell line, until further use. Transduced cells are referred to by the affix –dluc.

General Cell Culture

SKOV3, SKOV3-dluc, HEK293T-dluc and U87-MG-dluc were cultured in Dulbecco's modified Eagle Medium (Gibco) supplemented with 10% fetal bovine serum (FBS)(Gibco, Corning). SKOV3-dluc and HEK293T-dluc were cultured in the presence of 1000 µg/mL G418 (BioIVT) whereas U87-MG-dluc was cultured in the presence of 500 µg/mL G418. HMEC-1 were cultured in MCDB-131 medium supplemented with 10% FBS (Gibco), 2mM L-glutamine (Gibco), 10 ng/ml rhEGF (Peprotech), 50 nM Hydrocortisone (Sigma) in flasks / plates coated with 0.1% gelatin (Sigma). Cardiac progenitor cells (CPCs) were cultured in MEM 199 + Earle's Salts and L-glutamine (Gibco) which was supplemented with 22% EGM-2 medium (Lonza), 10% FBS and 1% MEM NEAA Nucleic acids (Gibco). All cells were cultured at 37 °C and 5% CO_2 in the presence of 100 U/mL penicillin and 100 U/mL streptomycin (Gibco).

Cell Culture and Isolation of SKOV3-EVs and CPC-EVs

For SKOV3-EV production, SKOV3 cells were seeded at an appropriate density and cultured for 48-72 hours to a confluence of 80-90 % after which the medium was replaced and cells were cultured for another 24 hours in Opti-Mem supplemented with Glutamax, 100 U/mL penicillin and 100 U/mL streptomycin. Conditioned medium is harvested after 24 hours and spun down for 5 minutes at 300 x *g* and for 15 minutes at 2000 x *g* to remove cells and cell debris, respectively. The supernatant is filtered through a 0.45 µM PES bottle top filter and concentrated to a volume of 15 mL by Tangential Flow Filtration (TFF) using Vivaflow 50R hydrosart casettes, with a membrane cutoff of 100 kDa. This concentrate is then further reduced to a volume of approximately 5 mL using 100 kDa Amicon Ultra-15 Centrifugal filter (Merck) and loaded on a HiPrep™ 16/60 Sephacryl® S-400 HR column (GE Healthcare, Uppsala, Sweden) connected to an ÄKTA Start system (GE Healtcare) containing an UV280 flow cell. For CPC-EVs, the procedure was slightly different. CPCs were seeded at an appropriate density and when a confluency of 80-100% was reached, cells were washed with PBS and medium was replaced for basal MEM199. The supernatant was collected after 24 hours and centrifuged for 15 minutes at 2000 x *g* to remove cells and cell debris and the supernatant was filtered through a 0.45 µM PES bottle top filter. Subsequently, the filtrate was concentrated by TFF using a minimate TFF capsule with a membrane cutoff of 100 kDa. Then EVs were isolated by size exclusion chromatography following the same procedure as described for SKOV3-EVs. After SEC, the fractions containing EVs were pooled, filtered through a 0.45µM syringe filter and concentrated using 100 kDa Amicon Ultra-15 Centrifugal filter (Merck). Then, the buffer was exchanged to 250 mM citrate buffer (pH 5.5) and the sample was again concentrated using Amicon Spin Filters with a membrane cutoff of 100 kDa. The protein concentration was determined via micro BCA protein determination kit (Thermo Scientific). EVs were stored at 4°C until further use. EVs were used to prepare hybrids within 72 hours after isolation.

Preparation and Analysis of Liposomes and EV-Liposome Hybrids (Hybrids)

Lipid were dissolved in a mixture of chloroform/methanol (9/1; v/v) and added to a round bottom flask at a molar ratio of 30:30:35.5:1.5:3 (DLin-MC3-DMA:DPPC:cholesterol:18:1 Biotinyl Cap PE:DMG-PEG). The organic solvent was evaporated using a RotoVap (Büchi Labortechnik, Flawil, Switzerland) at 60 °C and the resulting lipid film was dried under a flow of nitrogen for approximately 20 minutes. For the liposomes, the lipid film was hydrated using a mixture of siRNA targeting firefly luciferase and fluorescently labelled siRNA targeting firefly luciferase in a ratio of 1:1 (siRNA Luc: siRNA Luc-AF488 or AF647) dissolved in 250 m**M** citrate buffer (pH 5.5) for 1 hour at 45 °C. After hydration, the suspension was kept at 45 °C and extruded 5 times through a polycarbonate filter of 1.0 μm, then 5 times through 0.1 μm and finally 5 times through a polycarbonate filter of 0.05 μm using an Avanti Hand Extruder (Avanti Polar Lipids). Subsequently, the liposomes were dialyzed overnight at 4 °C against an excess of PBS using Slide-A-Lyzer™ G2 Dialysis Casette with a membrane cutoff of 100 kDa to change the pH to 7.4 and to remove unencapsulated siRNA. Hybrids were produced in a similar fashion, but in this case the lipid film was hydrated using a mixture of siRNA and extracellular vesicles. Extracellular vesicles were added at different ratios of vesicle protein to total lipid: 1:100 and 1:50 (protein/ total lipid; w/w).

Characterization of EVs, liposomes and hybrids

Particle size of liposomes and hybrids was measured via dynamic light scattering (DLS) on a Zetasizer Nano S (Malvern Panalytical, Malvern, UK). Samples were diluted with Dulbecco's PBS (DPBS) to an appropriate concentration and measured in triplicate. Liposomes, hybrid and EV size was also measured using Nanoparticle Tracking Analysis (NTA) on a NanoSight NS500 (Malvern, Panalytical, Malvern, UK). For NTA, samples were diluted in DPBS to an appropriate particle concentration and loaded in the sample chamber. Camera level, 16 was selected and sample was measured 3 times for 30 seconds and subsequently analyzed using Nanosight NTA 3.4 software at a sensitivity level of 5.

Particle surface potential was measured by laser Doppler electrophoresis on a Zetasizer Nano Z (Malvern Panalytical, Malvern, UK). Samples were diluted in 0.1x DPBS and sample was measured for 20 runs in triplicate.

The RNA concentration was determined based on the fluorescence emitted by the fluorescently labelled siRNA. Samples were diluted 1:1 in 2% TX-100 in PBS. A calibration curve of fluorescent siRNA was prepared in the same medium. Sample fluorescence was measured on a Spectramax ID3 (Molecular Devices, San Jose, California, US) at an excitation/emission wavelength of 490/530 nm or 620/665 nm for siRNA-AF488 or siRNA-AF647, respectively. Concentrations were determined based on a reference calibration curve.

The cholesterol concentration was determined using the LabAssay Cholesterol kit (DAKO, JP) in PBS or in the presence of 50% (v/v) isopropanol. Sample concentration was determined using a reference calibration curve. Absorbance was measured at 600 nm on a Spectramax ID3 (Molecular Devices, San Jose, California, US).

The encapsulation efficiency of siRNA was calculated by the following formula:

$$Encapsulation\ Efficiency\ (\%) = \frac{\frac{[siRNA]}{[cholesterol]}\ after\ dialysis\ (100kDa)}{\frac{[siRNA]}{[cholesterol]}\ before\ dialysis\ (100kDa)} * 100$$

Cryogenic Transmission Electron Microscopy

7 µl of liposomes or hybrid suspension were added to freshly glow-discharged Quantifoils and incubated for at least 10 minutes in a humidified environment and then vitrified using a FEI Mark IV Vitrobot (FEI, Hillsboro OR, USA). After vitrification, samples were stored in liquid nitrogen until imaging. Samples were imaged on a FEI Tecnai G^2 20 TWIN 200kV transmission electron microscope. Vitrified quantifoils were loaded in a Gatan 70° tilt cryo-transfer system which was pre-cooled using liquid nitrogen and inserted in the microscope. Samples were imaged at a magnification of 29.000x and samples images were acquired by the bottom mounted FEI High-Sensitive 4k x 4k Eagle camera.

Western Blotting

Protein concentration was determined via a micro BCA assay and approximately 10 µg protein was used per sample. Samples were mixed with 4x sample buffer (40% v/v glycerol, 8% w/v SDS, 8% v/v bromophenol blue, in 0.25 **M** Tris-HCL) with or without dithiothreitol (DTT) for reduced or non-reduced conditions, respectively. Samples were heated to 95 °C for 5 minutes and separated on a 4-12 Bis-Tris polyacrylamide gel (Thermo Scientific). Proteins were then electro transferred to Immobilon-FLR polyvinylidene difluoride (PVDF) membranes and blocked with 50% v/v Odyssey Blocking Buffer (LI-COR Biosciences) in Tris buffered saline (TBS). All immune-labeling was performed with 50% v/v Odyssey Blocking Buffer in TBS containing 0.1% Tween 20 (TBS-T). **Primary antibodies** were used overnight at 4 °C and included mouse anti-CD63 (Abcam, MEM-259; 1:1000), Mouse Anti-CD81 (Santa Cruz, SC-166029; 1:500), rabbit anti-TSG101 (Abcam, ab30871, 1:1000), mouse anti-Alix (Thermo Scientific, 3A9, 1:1000), mouse-anti-β-actin (Cell Signaling Technology, clone 8H10D10, 1:1000), rat anti-Calnexin (Tebu-Bio, N3C2, 1:1000), rabbit anti-AKT (Cell Signaling Technology, 9272S, 1:1000), rabbit anti pAKT (Cell Signaling Technology, 4060S,1:1000), and mouse anti-β-actin (Sigma, A5441,1:1000).

Secondary antibodies included Alexa Fluor 680-conjugated anti-rabbit antibodies (LI-COR Biosciences, A-21076, 1:7500 – 1:10.000), Alexa Fluor 680-conjugated anti-mouse antibodies (LI-COR Biosciences, A-21057; 1:7500-1:10.000), IRDye 800CW anti-mouse antibodies (LI-COR Biosciences, 926-32212, 1:7500-1:10.000) and IRDye 800CW anti-rabbit antibodies (LI-COR Biosciences, 926-32211, 1:7500-1:10.000). Imaging was performed on an Odyssey Infrared Imager (LI-COR Biosciences, Leusden, The Netherlands) at 700 nm and 800 nm.

Proof of hybridization: analysis using ExoCap CD9/CD81/CD63 beads

Samples were incubated overnight at 4 °C with 0.75 µL ExoCap beads (JSR Life Sciences, Tokyo, Japan) in a total volume of 50 µL 2% BSA in PBS (PBSA). Samples were normalized based on siRNA concentration. Samples were incubated separately with 3 different beads: CD9, CD81 and CD63. After incubation, beads were captured on a magnetic plate and washed three times with PBSA. Successful bead pulldown was analyzed by measurement of siRNA-AF647 using flow cytometry.

We also analyzed incorporation of a synthetic lipid. To this end, 1.5% 18:1 Biotinyl Cap PE (Avanti Polar Lipids, Alblaster, Alabama, USA) was incorporated in the lipid film of both the liposomes and the hybrids. The samples were incubated with ExoCap™ beads as described above. After the three initial washing steps, samples were incubated with PE-Streptavidin for 20 minutes and then washed three times. Samples were then suspended in 200 µL PBSA and measured by flow cytometry on a BD LSRFortessa (BD, Franklin Lakes, NJ, US). Flow Cytometry Data Analysis was performed using FlowJo v10 software.

Analysis of Cellular Uptake by Flow Cytometry

For the measurement of liposomal and hybrid cellular uptake flow cytometry was used. Cells were seeded at an appropriate density in a 48 well plate. SKOV3-dluc was seeded at 40.000 cells/well 24 hours prior to the assay, HEK293T-dluc was seeded at 20.000 cells/well 72 hours prior to the assay, U87-MG-dluc cells were seeded at 40.000 cells/well 24 hours prior to the assay. Then, cells were incubated with different nanoparticles at a total siRNA concentration of 25 nM/well. As a vehicle control, an equal volume of PBS was used. Cells were incubated for 4 hours and then cellular uptake was analyzed by flow cytometry. Cells were washed with PBS, trypsinized, taken up in full medium and transferred to a 96 U-Bottom well plate (Greiner). Cells were then washed with an acid wash (0.5 M NaCL, 0.2 M Acetic Acid), PBS and taken up in 2% PBSA for analysis on a LSRFortessa (BD, Franklin Lakes, NJ, US). For each experiment, cellular uptake was expressed as ratio of the uptake of the liposome sample. As a control, we measured uptake at 4 °C. To this end, cells were cooled 30 minutes prior to incubation in a fridge at 4 °C, samples added and incubated for 4 hours at 4 °C. After incubation, cells were kept on ice and washed with ice-cold PBS before trypsinization and further work-up as described earlier.

Gene-Silencing and Cell Viability

The gene-silencing efficacy of liposomes and hybrids was assessed in multiple cell-lines: SKOV3-dluc, U87-MG-dluc and HEK293T-dluc. All cells expressed a dual luciferase construct containing both *firefly* and *renilla* luciferase under G418 selection. SKOV3-dluc and HEK293T-dluc cells were seeded in a 96 well plate at a density of 5.000 cells/well 48 hours prior to transfection or 10.000 cell/well 24 hours prior to transfection. U87-MG-dluc were seeded at a density of 5.000 cells/well 24 hours prior to transfection. Samples were added at concentrations ranging from 0 to 50 nM siRNA. As a positive control, cells were transfected using Lipofectamine RNAiMAX according to the manufacturer's instructions. Luciferase activity was assessed after another 48 hours of culture. Luciferase activity was measured using the Stop & Glo System (Promega, Leiden, NL) according to the manufacturer's instructions. In short, medium was aspirated and replaced by 50 µL of fresh medium. 50 µL of Glo substrate is added and cells are incubated for 10 minutes. After 10 minutes, 100 µL of lysate is transferred to a white 96 well plate and firefly luciferase activity is measured. Then, 50 µL of Stop & Glo buffer is added and after an incubation of 10 minutes renilla luciferase activity is measured. Both firefly luciferase and renilla luciferase activity are measured on a Spectramax ID3 (Molecular Devices, San Jose, CA, USA) at an integration time of 1000 ms. For data analysis, firefly luciferase activity is normalized based on renilla luciferase activity and expressed as percentage of the blank – 0 nM siRNA – sample.

Cell viability was measured using CellTiter 96® AQueous MTS Reagent Powder according to the manufacturer's instructions. As a negative control, MTS medium was added to wells which did not contain any cells and this background value was subtracted from sample values. Samples were normalized to untreated, blank cells which value was set at 100 %. Absorbance was measured at 490 nm using a Spectramax ID3 (Molecular Devices).

Scratch migration assay

For the migration assay, HMEC-1 cells were seeded in a 48 well plate at a density of 90.000 cells/well 48 hours prior to the assay. A scratch was made by hand using a pipet tip and detached cells were washed away with MCDB-131 medium without any supplementation. Subsequently, the cells were incubated in the basal MCDB-131 medium with different samples in triplicate for 6 hours. PBS was used as a negative control. At t=0 hours and t=6 hours two pictures per well were made with the EVOS microscope (Life Technologies). The closing of the scratch was measured by image analysis using Image J software. The mean width of each scratch of t=0 hours was subtracted by the mean width at t=6 hours to determine the migrated area. The relative wound closure was calculated as compared to the negative control.

Endothelial Signaling Activation Assay

For the endothelial signaling activation assay, HMEC-1 cells were used to measure phosphorylation of AKT after incubation with liposomes, hybrids and EVs. HMEC-1 cells were seeded in a 48 well plate at a concentration of 90.000 cells/well and incubated for 48 hours. Then, the medium was replaced with basal medium (MCDB-131 medium without any supplementation), and the cells were starved for 3 hours in the basal medium. After 3 hours, samples were added to the wells and PBS was used as vehicle control. After 30 minutes, the medium was aspirated and the wells were washed with PBS. To lyse the cells, 100 µl complete lysis-M buffer (Roche, Basel, Switzerland) including protease inhibitors (Roche) and phosphatase inhibitors (Roche) was added and incubated for 5 minutes on ice. Every well was scraped and the lysate was transferred to an Eppendorf tube. Samples were vortexed and centrifuged for 15 minutes at 12.000 x g at 4 °C. Expression of AKT and phosphorylated AKT (pAKT) was analyzed by western blotting as described in section 5.8. Protein concentration of samples was measured by Pierce™ BCA Protein Assay Kit and samples were normalized based on protein concentration.

Statistical analysis

Data is presented as mean ± SD, unless otherwise stated. Differences in terms of particle characteristics and functionality between liposomes, hybrids (1:100) and hybrids (1:50) were analyzed by one-way ANOVA with Tukey's post-hoc test. An outcome was considered statistically significant if a P-value of ≤ 0.05 was obtained. Statistical analysis was performed using GraphPad Prism v8.3 software (GraphPad Software, San Diego, CA, USA).

6

ACKNOWLEDGEMENTS

Conflict of interest
R.M.S. is CSO and shareholder of EXCYTEX B.V., a company devoted to development of extracellular vesicle research tools. P.V. serves on the scientific advisory board of Evox Therapeutics.

REFERENCES

1. Elbashir SM, Harborth J, Lendeckel W, Yalcin A, Weber K, Tuschl T. Duplexes of 21-nucleotide RNAs mediate RNA interference in cultured mammalian cells. Nature. 2001;411(6836):494–8.

2. Fire A, Xu S, Montgomery MK, Kostas SA, Driver SE, Mello CC. Potent and specific genetic interference by double-stranded RNA in Caenorhabditis elegans. Nature. 1998;391(6669):806–11.

3. Setten RL, Rossi JJ, Han S. The current state and future directions of RNAi-based therapeutics. Nat Rev Drug Discov. 2019;18:421–46.

4. Morrissey D V, Blanchard K, Shaw L, Jensen K, Lockridge JA, Dickinson B, et al. Activity of stabilized short interfering RNA in a mouse model of hepatitis B virus replication. Hepatology. 2005;41(6):1349–56.

5. Kleinschmidt WJ, Ellis LF, Van Fbank RM, Murphy EB. Interferon stimulation by a double stranded RNA of a mycophage in statolon preparations. Nature. 1968;220(5163):167–8.

6. Whitehead KA, Dahlman JE, Langer RS, Anderson DG. Silencing or stimulation? siRNA delivery and the immune system. Annu Rev Chem Biomol Eng. 2011;2:77–96.

7. Dowdy SF. Overcoming cellular barriers for RNA Therapeutics. Nat Biotechnol. 2017;35(3):222–9.

8. Sabnis S, Kumarasinghe ES, Salerno T, Mihai C, Ketova T, Senn JJ, et al. A Novel Amino Lipid Series for mRNA Delivery: Improved Endosomal Escape and Sustained Pharmacology and Safety in Non-human Primates. Mol Ther. 2018;26(6):1509–19.

9. Sago CD, Krupczak BR, Lokugamage MP, Gan Z, Dahlman JE. Cell Subtypes Within the Liver Microenvironment Differentially Interact with Lipid Nanoparticles. Cell Mol Bioeng. 2019;12(5):389–97.

10. Yamamoto N, Sato Y, Munakata T, Kakuni M, Tateno C, Sanada T, et al. Novel pH-sensitive multifunctional envelope-type nanodevice for siRNA-based treatments for chronic HBV infection. J Hepatol. 2016;64(3):547–55.

11. Sato Y, Hatakeyama H, Hyodo M, Harashima H. Relationship Between the Physicochemical Properties of Lipid Nanoparticles and the Quality of siRNA Delivery to Liver Cells. Mol Ther. 2016;24(4):788–95.

12. Mui BL, Tam YK, Jayaraman M, Ansell SM, Du X, Tam YYC, et al. Influence of Polyethylene Glycol Lipid Desorption Rates on Pharmacokinetics and Pharmacodynamics of siRNA Lipid Nanoparticles. Mol Ther - Nucleic Acids. 2013;2(12):e139.

13. Yáñez-Mó M, Siljander PRM, Andreu Z, Bedina Zavec A, Borràs FE, Buzas EI, et al. Biological properties of extracellular vesicles and their physiological functions. J Extracell Vesicles. 2015;4(1):27066.

14. Théry C, Witwer KW, Aikawa E, Alcaraz MJ, Anderson JD, Andriantsitohaina R, et al. Minimal information for studies of extracellular vesicles 2018 (MISEV2018): a position statement of the International Society for Extracellular Vesicles and update of the MISEV2014 guidelines. J Extracell Vesicles. 2018;7(1):1535750.

15. Skog J, Wurdinger T, Rijn S Van, Meijer D, Gainche L, Sena-esteves M, et al. Glioblastoma microvesicles transport RNA and protein that promote tumor growth and provide diagnostic biomarkers. Nat Cell Biol. 2008;10(12):1470–6.

16. Pegtel DM, Cosmopoulos K, Thorley-Lawson DA, van Eijndhoven MAJ, Hopmans ES, Lindenberg JL, et al. Functional delivery of viral miRNAs via exosomes. Proc Natl Acad Sci. 2010;107(14):6328–33.

17. Valadi H, Ekström K, Bossios A, Sjöstrand M, Lee JJ, Lötvall JO. Exosome-mediated transfer of mRNAs and microRNAs is a novel mechanism of genetic exchange between cells. Nat Cell Biol. 2007;9(6):654–9.

18. de Jong OG, Murphy DE, Mäger I, Willms E, Garcia-Guerra A, Gitz-Francois JJ, et al. A CRISPR-Cas9-based reporter system for single-cell detection of extracellular vesicle-mediated functional transfer of RNA. Nat Commun. 2020;11:1113.

19. Reshke R, Taylor JA, Savard A, Guo H, Rhym LH, Kowalski PS, et al. Reduction of the therapeutic dose of silencing RNA by packaging it in extracellular vesicles via a pre-microRNA backbone. Nat Biomed Eng. 2020;4:52–68.

6

20. Murphy DE, de Jong OG, Evers MJW, Nurazizah M, Schiffelers RM, Vader P. Natural or Synthetic RNA Delivery: A Stoichiometric Comparison of Extracellular Vesicles and Synthetic Nanoparticles. Nano Lett. 2021 Feb 24;21(4):1888–95.

21. Hoshino A, Costa-Silva B, Shen TL, Rodrigues G, Hashimoto A, Tesic Mark M, et al. Tumour exosome integrins determine organotropic metastasis. Nature. 2015;527(7578):329–35.

22. Rana S, Yue S, Stadel D, Zöller M. Toward tailored exosomes: The exosomal tetraspanin web contributes to target cell selection. Int J Biochem Cell Biol. 2012;44(9):1574–84.

23. Alvarez-Erviti L, Seow Y, Yin H, Betts C, Lakhal S, Wood MJA. Delivery of siRNA to the mouse brain by systemic injection of targeted exosomes. Nat Biotechnol. 2011;29(4):341–5.

24. Kamerkar S, LeBlue VS, Kalluri R. Exosomes Facilitate Therapeutic Targeting of Oncogenic Kras in Pancreatic Cancer. Nature. 2017;546(7659):498–503.

25. Grapp M, Wrede A, Schweizer M, Hüwel S, Galla HJ, Snaidero N, et al. Choroid plexus transcytosis and exosome shuttling deliver folate into brain parenchyma. Nat Commun. 2013;4(2123).

26. Elsharkasy OM, Vader. Extracellular vesicles as drug delivery systems: why and how? Adv Drug Deliv Rev. 2020;159:332–43.

27. Roefs MT, Sluijter JPG, Vader P. Extracellular Vesicle-Associated Proteins in Tissue Repair. Trends Cell Biol. 2020;30(12):990–1013.

28. Vader P, Mol EA, Pasterkamp G, Schiffelers RM. Extracellular vesicles for drug delivery. Adv Drug Deliv Rev. 2016;106:148–56.

29. Haraszti RA, Miller R, Stoppato M, Sere YY, Coles A, Didiot MC, et al. Exosomes Produced from 3D Cultures of MSCs by Tangential Flow Filtration Show Higher Yield and Improved Activity. Mol Ther. 2018;26(12):2838–47.

30. Vader P, Kooijmans SA, Stremersch S, Raemdonck K. New considerations in the preparation of nucleic acid-loaded extracellular vesicles. Ther Deliv. 2014;5(2):105–7.

31. de Jong OG, Kooijmans SAA, Murphy DE, Jiang L, Evers MJW, Sluijter JPG, et al. Drug Delivery with Extracellular Vesicles: From Imagination to Innovation. Acc Chem Res. 2019;52(7):1761–70.

32. Nordin JZ, Lee Y, Vader P, Mäger I, Johansson HJ, Heusermann W, et al. Ultrafiltration with size-exclusion liquid chromatography for high yield isolation of extracellular vesicles preserving intact biophysical and functional properties. Nanomedicine Nanotechnology, Biol Med. 2015;11(4):879–83.

33. Webber J, Clayton A. How pure are your vesicles? J Extracell Vesicles. 2013;2(1):19861.

34. Vrijsen KR, Maring JA, Chamuleau SAJ, Verhage V, Mol EA, Deddens JC, et al. Exosomes from Cardiomyocyte Progenitor Cells and Mesenchymal Stem Cells Stimulate Angiogenesis Via EMMPRIN. Adv Healthc Mater. Germany; 2016 Oct;5(19):2555–65.

35. Vrijsen KR, Sluijter JPG, Schuchardt MWL, van Balkom BWM, Noort WA, Chamuleau SAJ, et al. Cardiomyocyte progenitor cell-derived exosomes stimulate migration of endothelial cells. J Cell Mol Med. 2010;14(5):1064–70.

36. Mol EA, Goumans M-J, Doevendans PA, Sluijter JPG, Vader P. Higher functionality of extracellular vesicles isolated using size-exclusion chromatography compared to ultracentrifugation. Nanomedicine Nanotechnology, Biol Med. 2017;13(6):2061–5.

37. Karar J, Maity A. PI3K/AKT/mTOR Pathway in Angiogenesis. Front Mol Neurosci. 2011;4:51.

38. Zhang Y, You B, Liu X, Chen J, Peng Y, Yuan Z. High-Mobility Group Box 1 (HMGB1) Induces Migration of Endothelial Progenitor Cell via Receptor for Advanced Glycation End-Products (RAGE)-Dependent PI3K/Akt/eNOS Signaling Pathway. Med Sci Monit. 2019;25:6462–73.

39. Jhan Y, Prasca-Chamorro D, Palou Zuniga G, Moore DM, Arun Kumar S, Gaharwar AK, et al. Engineered extracellular vesicles with synthetic lipids via membrane fusion to establish efficient gene delivery. Int J Pharm. 2020 Jan;573(July):118802.

40. Rayamajhi S, Nguyen TDT, Marasini R, Aryal S. Macrophage-derived exosome-mimetic hybrid vesicles for tumor targeted drug delivery. Acta Biomater. 2019;94:482–94.

41. Molinaro R, Corbo C, Martinez JO, Taraballi F, Evangelopoulos M, Minardi S, et al. Biomimetic proteolipid vesicles for targeting inflamed tissues. Nat Mater. 2016;15(9):1037–46.

42. Goh WJ, Zou S, Lee CK, Ou Y-H, Wang J-W, Czarny B, et al. EXOPLEXs: Chimeric Drug Delivery Platform from the Fusion of Cell-Derived Nanovesicles and Liposomes. Biomacromolecules. 2018;19(1):22–30.

43. Pitchaimani A, Duong T, Nguyen T, Aryal S. Biomaterials Natural killer cell membrane infused biomimetic liposomes for targeted tumor therapy. Biomaterials. 2018;160:124–37.

44. Van Deun J, Roux Q, Deville S, Van Acker T, Rappu P, Miinalainen I, et al. Feasibility of Mechanical Extrusion to Coat Nanoparticles with Extracellular Vesicle Membranes. Cells. 2020;9(8):1797.

45. Semple SC, Klimuk SK, Harasym TO, Dos Santos N, Ansell SM, Wong KF, et al. Efficient encapsulation of antisense oligonucleotides in lipid vesicles using ionizable aminolipids: formation of novel small multilamellar vesicle structures. Biochim Biophys Acta. 2001;1510(1–2):152–66.

46. Miller CR, Bondurant B, McLean SD, McGovern KA, O'Brien DF. Liposome-cell interactions in vitro: Effect of liposome surface charge on the binding and endocytosis of conventional and sterically stabilized liposomes. Biochemistry. 1998;37(37):12875–83.

47. Miao L, Lin J, Huang Y, Li L, Delcassian D, Ge Y, et al. Synergistic lipid compositions for albumin receptor mediated delivery of mRNA to the liver. Nat Commun. 2020;11(1):2424.

48. Jiang W, Kim BYS, Rutka JT, Chan WCW. Nanoparticle-mediated cellular response is size-dependent. Nat Nanotechnol. 2008;3(3):145–50.

49. Francia V, Schiffelers RM, Cullis PR, Witzigmann D. The Biomolecular Corona of Lipid Nanoparticles for Gene Therapy. Bioconjug Chem. 2020;31(9):2046–59.

50. Gilleron J, Querbes W, Zeigerer A, Borodovsky A, Marsico G, Schubert U, et al. Image-based analysis of lipid nanoparticle-mediated siRNA delivery, intracellular trafficking and endosomal escape. Nat Biotechnol. 2013;31(7):638–46.

51. Sahay G, Querbes W, Alabi C, Eltoukhy A, Sarkar S, Zurenko C, et al. Efficiency of siRNA delivery by lipid nanoparticles is limited by endocytic recycling. Nat Biotechnol. 2013;31(7):653–8.

52. Mulcahy LA, Pink RC, Carter DRF. Routes and mechanisms of extracellular vesicle uptake. J Extracell Vesicles. 2014;3(1):24641.

53. Wiklander OPB, Nordin JZ, O'Loughlin A, Gustafsson Y, Corso G, Mäger I, et al. Extracellular vesicle in vivo biodistribution is determined by cell source, route of administration and targeting. J Extracell Vesicles. 2015;4:26316.

54. Sato Y, Matsui H, Yamamoto N, Sato R, Munakata T, Kohara M, et al. Highly specific delivery of siRNA to hepatocytes circumvents endothelial cell-mediated lipid nanoparticle-associated toxicity leading to the safe and efficacious decrease in the hepatitis B virus. J Control Release. 2017;266:216–25.

55. Saleh AF, Lázaro-Ibáñez E, Forsgard MA-M, Shatnyeva O, Osteikoetxea X, Karlsson F, et al. Extracellular vesicles induce minimal hepatotoxicity and immunogenicity. Nanoscale. 2019;11(14):6990–7001.

56. Zhu X, Badawi M, Pomeroy S, Sutaria DS, Xie Z, Baek A, et al. Comprehensive toxicity and immunogenicity studies reveal minimal effects in mice following sustained dosing of extracellular vesicles derived from HEK293T cells. J Extracell vesicles. 2017;6(1):1324730.

57. Zhupanyn P, Ewe A, Büch T, Malek A, Rademacher P, Müller C, et al. Extracellular vesicle (ECV)-modified polyethylenimine (PEI) complexes for enhanced siRNA delivery in vitro and in vivo. J Control Release. 2020;319:63–76.

58. Sato YT, Umezaki K, Sawada S, Mukai S, Sasaki Y, Harada N, et al. Engineering hybrid exosomes by membrane fusion with liposomes. Sci Rep. 2016;6(1):21933.

59. Barile L, Cervio E, Lionetti V, Milano G, Ciullo A, Biemmi V, et al. Cardioprotection by cardiac progenitor cell-secreted exosomes: role of pregnancy-associated plasma protein-A. Cardiovasc Res. 2018 Jun;114(7):992–1005.

60. Lesizza P, Prosdocimo G, Martinelli V, Sinagra G, Zacchigna S, Giacca M. Single-Dose Intracardiac Injection of Pro-Regenerative MicroRNAs Improves Cardiac Function After Myocardial Infarction. Circ Res. 2017;120(8):1298–304.

61. Jayaraman M, Ansell SM, Mui BL, Tam YK, Chen J, Du X, et al. Maximizing the potency of siRNA lipid nanoparticles for hepatic gene silencing in vivo. Angew Chem, Int Ed. 2012;51(34):8529–33.

6

FUNCTIONAL SIRNA DELIVERY BY EXTRACELLULAR VESI-CLE-LIPOSOME HYBRID NANOPARTICLES

Martijn J.W. Evers[1], Simonides I. van de Wakker[2], Ellis de Groot[1], Olivier G. de Jong[1,3], Jerney J.J. Gitz-François[1], Cor S. Seinen[1], Joost P.G. Sluijter[2,4], Raymond M. Schiffelers[1], Pieter Vader[1,2]*

Supporting Information

SUPPLEMENTARY TABLE

Table S1: Oligonucleotide sequences

siRNA firefly luciferase	Sense: '5-GGA CGA GGU GCC UAA AGG AdCdG-3'
	Antisense: '5-UCC UUU AGG CAC CUC GUC CdCdG-3'
siRNA non specific	Sense: 5'-UGC GCU ACG AUC GAC GAU GdTdT-3'
	Antisense: 5'-CAU CGU CGA UCG UAG CGC AdTdT-3'

dT, dC, & dG indicate a deoxyribonucleic acid base

SUPPLEMENTARY FIGURES
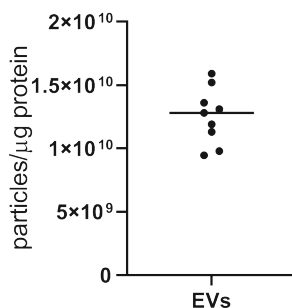
Figure S1: Batch to batch variability of EV purity.
EV purity is expressed as the number of particles per μg protein. Each datapoint represents an EV isolation. (n=9, biological replicates)
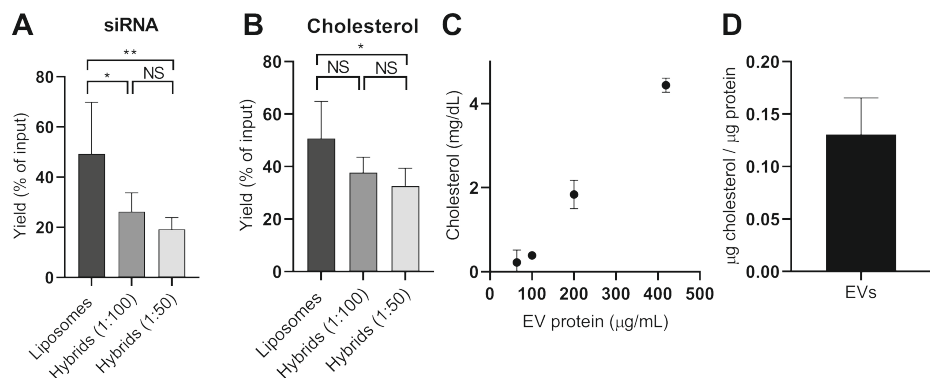
Figure S2: siRNA and cholesterol yield of production process.
The total amount of **A)** siRNA and **B)** cholesterol detected in liposomes and hybrids after dialysis expressed as percentage of the input amount. **C)** Cholesterol content of EVs at different EV-protein concentrations. **D)** Cholesterol content of EVs expressed per μg EV-protein. Data in A/B are shown as mean ± SD (n=6-7, biological replicates), One-way ANOVA with Tukey's post-hoc test, ns= not significant, * = p<0.05, ** = p<0.01. Data in C is shown as mean ± SD (n=3, technical triplicate). Data in D is shown as mean ± SD (n=2, biological replicate).
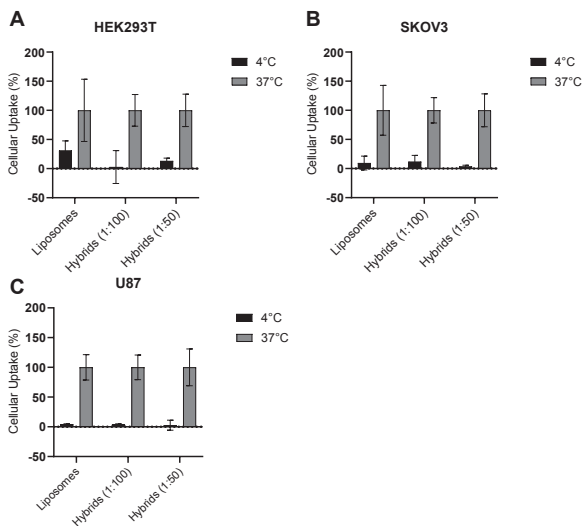
Figure S3: Cellular uptake analysis of liposomes and hybrids in different cell types Cellular uptake in **A)** HEK293T-dluc. **B)** SKOV3-dluc. **C)** U87-MG-dluc as determined by flow cytometry and plotted as a percentage relative to the uptake observed at 37 °C. Data are plotted as mean ± SD (n=3, technical replicates).
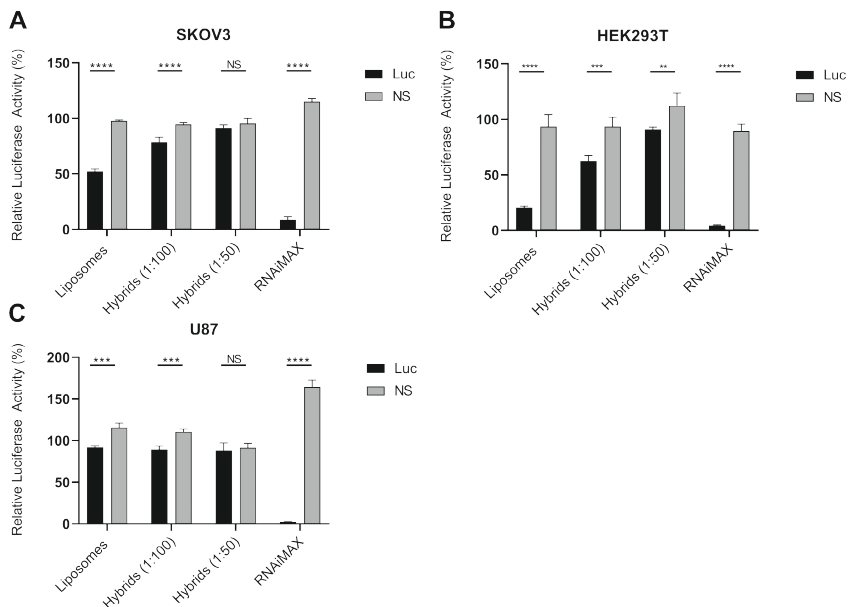
Figure S4: Gene silencing of firefly luciferase by liposome-, hybrid- or RNAiMAX mediated siRNA delivery in different cell types. siRNA targeting firefly luciferase (luc) or a non-specific siRNA (NS) was delivered via liposomes, hybrids or RNAiMAX and luciferase expression was measured after 48 hours incubation and normalized to renilla luciferase expression. Different cell types, **A)** SKOV3-dluc **B)** HEK293T-dluc **C)** U87-MG-dluc, were incubated with liposomes and hybrids at an siRNA concentration of 50 nM. For, RNAiMAX the concentration was 10 nM siRNA. Data are plotted as mean ± SD, n=3, technical replicates, two-way ANOVA with sidak's post-hoc test, ns = not significant, ** p = <0.01, *** = p <0.001, **** = p < 0.0001
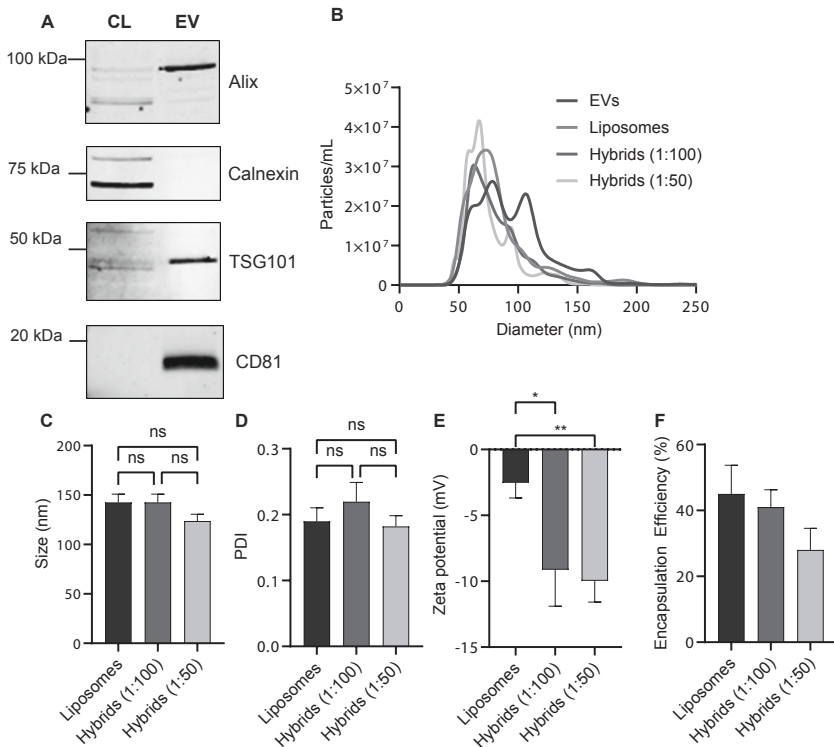
Figure S5: Characterization of CPC-derived EVs, liposomes and hybrids. A) Western Blot analysis of CPC cell lysate (CL) and CPC-derived EVs shows enrichment of typical EV markers Alix, TSG101 and CD81 and negative enrichment of a EV-negative marker, calnexin. **B)** NTA analysis of CPC-derived EVs, liposomes and hybrids. **C)** Nanoparticle size as determined by DLS. **D)** Polydispersity index of nanoparticles as measured by DLS. **E)** Zeta potential of nanoparticles as measured by laser doppler electrophoresis. **F)** RNA encapsulation efficiency of nanoparticles determined based on the cholesterol and siRNA concentrations before and after dialysis. Mean + SD is displayed for all samples (n=3, biological replicates), one-way ANOVA with tukey's post-hoc test, ns= not significant, * = p<0.05, ** = p<0.01.

Summary & Discussion

7

Drug delivery systems, such as LNPs and potentially in the future also EVs or EV-liposome hybrid nanoparticles, are the cornerstone of nucleic acid therapy development. Within the scientific community, it is widely recognized that adequate delivery of nucleic acids to their active site is one of the key challenges for the application of nucleic acid based therapies. In this thesis, the use of LNPs and EV-liposome hybrid nanoparticles for the delivery of siRNA and mRNA has been investigated.

The clinical breakthrough of LNPs during the COVID-19 pandemic

Over the course of this PhD trajectory from 2017 to 2021, lipid nanoparticles (LNPs) have matured as platform technology and went through major clinical developments. In 2018, Patirisan (Onpattro®) was approved by the FDA and EMA for the treatment of transthyretin amyloidosis.[1,2] Transthyretin amyloidosis is a rare disease affecting maximally ~40.000 patients in the world and therefore, the clinical use of LNPs initially remained limited.[3] However, the major breakthrough of LNPs as carrier of RNA therapeutics came in 2020 with the worldwide outbreak of SARS-CoV-2. In only 66 days after the sequence of SARS-CoV-2 was published, a phase I clinical trial assessing the safety of an LNP-mRNA (mRNA-1273) based vaccine was initiated. [4] At unprecedented speed, a vaccine carrying mRNA encoding prefusion stabilized SARS-COV-2 spike protein was developed. It was shown to prevent the SARS-CoV-2-related disease, COVID-19, with a groundbreaking efficiency of 94%.[5] Concomitantly, a similar LNP-based mRNA vaccine with equal efficacy as mRNA-1273 was developed elsewhere, illustrating the potency of LNP-platform technology for the rapid development of novel vaccines.[6] Currently, these two LNP-mRNA based vaccines play a very important role in combating the SARS-CoV-2 pandemic.

Over the course of this PhD trajectory, the LNP nucleic acid delivery platform has matured and has been applied successfully for hepatic siRNA delivery and mRNA delivery in various therapeutic areas. This thesis contributes to the continuing search to new applications of LNPs as delivery vehicle for RNA molecules and covers both siRNA and mRNA delivery to various organs.

Key aspects of the LNP platform

In **Chapter 2,** we described the exciting path of LNP development for siRNA delivery and the subsequent transition of LNPs for delivery of mRNA as well. We discussed several key 'design principles' for LNPs encapsulating siRNA including the role of ionizable lipids and PEG-lipids. Moreover, we summarized production methods for LNPs and explained the potential benefits of microfluidic mixing methods over conventional liposome/LNP production methods for the preparation of nucleic acid loaded LNPs. Finally, we discussed the applicability of LNPs for the delivery of other nucleic acids such as mRNA and pDNA and how different nucleic acids have different optimal compositions of LNPs. The key success factors of LNPs are 1) efficient encapsulation of nucleic acids, 2) potent ionizable lipids which enable cytosolic delivery, 3) a sheddable PEG coating increasing stability without reducing the efficacy, 4) scalable production methods.

Use of the LNP platform for hepatic siRNA delivery

In **Chapter 3** we used the clinical lipid formulation of Patisiran (Onpattro®) for the delivery of siRNA to silence the expression of two enzymes of the de novo ceramide synthesis pathway in the liver: CerS2 and DegS1. Increased concentrations of specific ceramides in plasma have been associated with negative outcomes in cardiovascular disease and are also involved in the pathophysiology of several metabolic diseases such as nonalcoholic steatohepatitis and type 2 diabetes in obese patients.[7–14] We hypothesized that gene-silencing of enzymes responsible for the synthesis of these lipids could potentially reduce their concentration in plasma. CerS2 is involved in the synthesis of ceramides with lipid chains ranging from 22 to 26 carbon atoms.[15] DegS1 is responsible for the final conversion of dihydroceramides to ceramides. Administration of LNP-siRNA targeting either CerS2 or DegS1 led to a reduction of hepatic mRNA transcript levels of CerS2 and DegS1, respectively. Decreased mRNA transcript levels were observed from 2 days after administration of LNP-siRNA and sustained until day 14, albeit the mRNA transcript levels gradually returned to initial levels over time. The effect of post-transcriptional silencing of CerS2 and DegS1 on plasma ceramide concentrations was variable. Gene-silencing of approximately 50% of CerS2 had no apparent effect on liver and plasma ceramide concentrations. Reduced expression of DegS1 did lead to a decreased conversion of dihydroceramides to ceramides as indicated by a decreased ceramide to dihydroceramide ratio in liver and plasma. In general, the reduction of CerS2 did not affect liver and plasma ceramide levels, which was in stark contrast with effects observed by others.[16] This effect might be a result of inadequate silencing of the CerS2 enzyme. Therefore, these data underline the potency of LNPs for nucleic acid delivery, but also show that it is important to optimize *in vivo* RNAi in terms of the potency of the siRNA molecule, the administered dose and dose regimen in order to yield sustained knockdown of mRNA transcript levels. Future research should reveal whether plasma ceramide reduction is truly an effective therapeutic strategy in cardiovascular disease and other metabolic diseases where ceramides play a role in the pathophysiology.

The transition of LNPs for siRNA delivery to mRNA delivery

LNPs were primarily developed for hepatic siRNA delivery. However, the most recently approved siRNA drugs targeting mRNAs in the liver are not based on LNPs. These heavily chemically modified RNA molecules do not need the LNP protection to stay intact and can be targeted to the liver by chemical coupling to a tri-antennary N-acetyl galactosamine.[17] These siRNA-conjugates seem to be less complex, have a more appealing dosing regime and patient pre-treatment with immunosuppressants, such as required for LNPs, is not necessary. However, for mRNA delivery the conjugate platform technology might not feasible due to chemical instability of the mRNA and inability to site-specifically modify the oligonucleotide to achieve the similar level of stability as is achieved for siRNA. Therefore, the LNP platform is likely critical for the successful clinical application of mRNA-based therapeutic strategies. Indeed, in the past years, the LNP platform has also been widely adopted for mRNA delivery.

In **Chapter 4** we showed that LNPs can functionally deliver mRNA to the ischemic area of the heart after myocardial infarction. For LNPs to functionally deliver the mRNA after intravenous administration, several barriers need to be overcome including extravasation from systemic

circulation. Under healthy conditions, this only occurs in tissue types such as liver and spleen containing fenestrated/sinusoidal capillaries through which the nanoparticles can extravasate. It is known that after myocardial infarction followed by ischemia-reperfusion injury (IRI), the vascular endothelium of the ischemic area becomes leaky. Therefore, we hypothesized that after ischemia-reperfusion injury, LNPs could extravasate and transfect cells in the heart. By analyzing the tissue distribution of fluorescently labelled LNPs, we showed that LNPs accumulate in the heart to a larger extent after IRI as compared to sham operated animals. The increased accumulation of LNPs also resulted in increased functional delivery of luciferase mRNA to the hearts as shown by increased reporter protein expression. We then used Ai9 Cre reporter mice to investigate which specific cell types were transfected. In this model, functional delivery of Cre mRNA results in Cre recombination leading to stable expression of tdTomato. Via this method we were able to identify cardiac fibroblasts as the major cell type being transfected in the heart at 7 days after injection. However, of note, the majority of LNP-mRNA still distributed to liver and spleen. The clinical translation of systemically administered LNPs for cardiac delivery might be hampered by potential side effects in liver and spleen related to the expression of the protein of interest. Therefore, local cardiac delivery might be the preferred route of administration. Alternatively, incorporation of miRNA target sites in the 3' untranslated region (UTR) of mRNA, for instance miR-122 for liver hepatocytes, might reduce off-target mRNA expression.[18]

Future research should be aimed at evaluating whether the achieved cardiac protein expression level is therapeutically relevant as the used models are very sensitive and are based on reporter proteins, designed for sensitive detection of expression. Potential applications of LNP-mRNA for cardiac delivery of mRNA are widespread. For example, the delivery of VEGF-A for cardiac regeneration, mutated FSTL1 for increased cardiomyocyte proliferation or IGF-1 for reduced cell apoptosis.[19–23] Given the dominant delivery of mRNA to cardiac fibroblasts we observed, an evident but challenging application could be reprogramming of cardiac fibroblast to cardiomyocytes via the delivery of Gata4, Mef2c and Tbx5.[24,25]

High throughput LNP tissue distribution screening for future LNP formulations
LNPs generally consist of 4 different types of lipids: an ionizable lipid, a helper lipid, cholesterol and a PEG-lipid at a specific empirically determined ratio. The lipid formulation can be optimized to meet certain criteria such as gene-silencing efficacy or protein expression for siRNA and mRNA/pDNA, respectively. Given the large amount of types of ionizable lipids, helper lipids, PEG lipids, and even types of cholesterol available, it is possible to generate tremendously large libraries of lipid formulations. Evaluating the efficacy and safety of such libraries typically requires an excessive amount of resources. In most literature, a two-step approach has been used: First, a large set of particles is pre-screened in vitro and evaluated based on a certain set of criteria. Second, the top performers from the in vitro screen are then evaluated in vivo. However, a substantial amount of evidence is emerging that the in vitro-in vivo correlation is poor for lipid based drug delivery systems, rejecting the core assumption of this approach that the effects observed in vitro predict the behavior in vivo. Moreover, large screening studies require lots of animals which are at odds with the 3R principle. In pursuit of an alternative strategy, the lab of James Dahlman developed a DNA barcoding approach to screen multiple formulations

in a single animal at the same time.[26] The system is based on encapsulation of a unique DNA barcode which can be detected and quantified, in vitro and in vivo, via next-generation sequencing (NGS). The system is highly versatile and in combination with other techniques can be used to assess relative biodistribution and relative mRNA delivery efficacy.[27] In combination with digital droplet quantitative PCR (qPCR) it is even feasible to measure absolute differences in tissue distribution.[28] However this technique is technically highly complex and requires expertise from multiple areas such as nanoparticle formulation design and production, next-generation sequencing and cell sorting, resulting in a high technological barrier before it can be applied.

In **Chapter 5** we aimed to set up and validate the DNA barcoding approach, based on the work of the Dahlman group, by measuring and comparing the in vivo biodistribution profiles of distinct LNP formulations in our lab. We compared the tissue distribution and blood plasma concentration profiles between LNPs containing three commonly applied PEG-lipids, namely PEG-C14, PEG-C16 or PEG-C18. These three formulations each have a well-defined and different tissue distribution and blood concentration profile. We analyzed the tissue distribution by quantification of a fluorescently labelled siRNA via fluorescence spectroscopy, quantification of DNA barcodes via qPCR and quantification of DNA barcodes via NGS. Analysis of the LNP plasma concentration – time curve for both fluorescent siRNA- and DNA barcode-based methods revealed that, in agreement with literature, LNPs containing PEG-C14 were rapidly cleared from the circulation. Based on qPCR and NGS analysis of DNA barcode occurrence, we were not able to distinguish differences in circulation kinetics between PEG-C16 and PEG-C18-based LNPs, in contrast to what was observed for the fluorescence-based siRNA detection method. In addition, based on literature, it was expected that shortly after injection, hepatic accumulation of LNPs decreased in the order PEG-C14>PEG-C16>PEG-C18.[29] However, the hepatic accumulation pattern obtained using the fluorescent-based detection of the siRNA molecule was not in line with literature, and showed only partial agreement with the data collected by analyzing barcode occurrence via qPCR/NGS. This observed discrepancy between detection methods may be explained by differences in the sensitivity and linear ranges of both detection methods. Previously, it has been shown that measurement of tissue distribution of LNPs via fluorescent based detection of an siRNA or detection of a DNA barcode using digital droplet PCR can result in different in vivo biodistribution profiles.[28]

Regardless of the observed discrepancies, DNA barcoding technology clearly offers exceptional potential to reduce the number of animals used, and to increase the efficiency of LNP formulation development. However, additional in-house validation is required.

Nature's carrier of RNA: extracellular vesicles. The future of nucleic acid drug delivery?

LNPs are still relatively inefficient at the delivery of their cargo leaving opportunities for improvement of this platform technology or implementation of other innovative technologies. Recently, it has been observed that extracellular vesicles (EVs), which are membrane-enclosed, naturally occurring carriers of RNA, might be several orders of magnitude more efficient in the delivery of RNA compared to current state-of-the-art drug delivery systems.[30,31] However, loading of exogenous nucleic acids, such as siRNA or mRNA, in EVs is challenging and yet inefficient.

Therefore, in **Chapter 6**, we assembled extracellular vesicle – liposome hybrid nanoparticles. We hypothesized that a hybrid nanoparticle would incorporate beneficial characteristics of both synthetic and biological particles for nucleic acid delivery. We showed that hybrid nanoparticles incorporated EV-surface makers. As compared to liposomes, the functional behavior of hybrids, such as cellular uptake and gene-silencing was found to be different. Most interestingly, the amount of SKOV3 EVs incorporated in the formulation seemed to have an influence on the cellular internalization of the particles indicating an effect of EV components on cellular uptake. Moreover, we showed that hybrid nanoparticles generated with CPC-EVs incorporated some of the functional characteristics attributed to CPC-EVs such as activation of endothelial cell migration and endothelial signaling. All together, these results show that EV-liposome hybrids might pose an attractive biomimetic strategy to incorporate EV characteristics into LNPs. However, such an approach would require several improvements regarding the production and characterization of EV-liposome hybrids. Currently, the yield and scale of the production process (i.e. extrusion) is limited. Potentially, microfluidic production of EV-liposome hybrids might provide an alternative hybridization strategy albeit that it requires the presence of organic solvents such as ethanol. Moreover, in our analyses, we could not fully exclude the presence and effects of intact EVs in our hybrid preparations. Currently, it is challenging to analyze the EV-liposome hybrids at a single particle level to, for instance, investigate the incorporation and orientation of EV-membrane proteins in the EV-liposome hybrid. The recent development of new methods such as EVQuant, which is a microscopy based method for single EV analysis, or techniques such single-molecule localization microscopy might provide tools to improve the analysis of EV-liposome hybrids.[32]

What's next? Future perspectives

During the SARS-CoV-2 pandemic, LNPs became the preferred vaccination platform in Europe for the prevention of COVID-19. In 2021, more than a billion doses of LNP-based vaccines have been administered in the EU alone. In essence, LNPs are a platform technology applicable to any mRNA of interest, and can therefore be used for vaccination against other infectious diseases such as Zika virus or Influenza. In fact, before the SARS-CoV2-pandemic, LNP-mRNA vaccine development was focused at infectious diseases such as Zika, Influenza and human immunodeficiency virus type 1.[33–35] Besides the use of LNP-mRNA in infectious disease, three trends can be distinguished in the use of LNPs for mRNA delivery: 1) LNP-mRNA in cancer immunotherapy 2) LNP-mRNA in CRISPR/Cas9 gene-editing and 3) hospital-based RNA therapeutics.

LNP-mRNA may be of great use in cancer immunotherapy. LNPs carrying mRNA encoding tumor associated antigen (TAA) or tumor specific antigens/neoantigens (TSA) can potentially be used to activate the patient's immune system and direct its activity towards tumor tissue with the ultimate aim to yield a clinical benefit.[36] The use of mRNA encoding tumor-specific antigens, or neoantigens, could provide a means to develop a highly personalized, cancer-specific and potent treatment for cancer. An initial trial in 2017 performed by Sahin et al. showed that all patients who received a mRNA vaccine containing multiple neo antigens developed a T-cell response against up to 60% of the predicted tumor specific neoantigens.[37] Unfortunately,

the concept of personalized cancer therapy remains challenging as indicated by a recent trial which showed the ability of LNPs to induce neoantigen-reactive T-cells but absence of a clinical response[36,38]. A more elaborate approach where neoantigen-recognition is combined with supporting activation signals may be an attractive approach.[39]

Currently, LNPs also have a profound role in the clinical translation of therapies based on CRISPR/Cas9. In 2021, Gillmore and colleagues reported that the administration of LNPs carrying Cas9 mRNA and sgRNA targeting the human transthyretin gene resulted in durable knockout of this gene as a result of guided Cas9 nuclease activity.[40] Knockout of the transthyretin gene resulted in reduced serum TTR protein concentration. In addition, the use of CRISPR/Cas9 for the insertion of a gene has been explored. NTLA-3001 is a CRISPR/Cas9-based therapy aiming to deliver and insert a functional copy of the alpha-1 antitrypsin gene (A1AT) in patients suffering from alpha-1 antitrypsin deficiency associated lung disease. Here, LNPs encapsulating Cas9 mRNA and an sgRNA sequence are co-delivered with an adeno-associated virus containing an insertion templating carrying A1AT resulting in stable expression of A1AT in non-human primates at physiologically relevant levels.[41]

RNA therapeutics hold the promise of truly personalized medicine which is already illustrated by the development of personalized mRNA cancer vaccines. A similar example is the development of a patient-customized antisense oligonucleotide: milasen. This antisense oligonucleotide therapeutic was specifically developed to modulate a patient-specific mutation which resulted in a rare neurological disorder.[42] Unfortunately, due to their small production scale, such therapies are generally no appealing business cases for big pharma.[43] Here, hospital-based RNA therapeutics might be an alternative. Basically, this concept entails the design, development and manufacturing of the drug substance and drug product within the environment of the hospital. The feasibility of such a concept has already been shown for the production of RNA in Houston where therapeutic RNAs are produced in a hospital based setting under cGMP.[43] Moreover, BionTech SE has developed the BioNTainer. This small-scale production facility for LNP-mRNA contains 2 modules of each 6 shipping containers. In one module, the mRNA is produced via In-vitro transcription and in the other module LNPs are formulated, both under cGMP conditions.[44] These examples show that it is feasible to produce RNA products, including LNP-mRNA, in a small confined space and potentially within the hospital environment. It can be envisioned that within years, patient specific LNP-mRNA therapies can be developed and manufactured within the hospital environment albeit there are several operational and regulatory challenges which need to be solved.

Whilst the LNP field has shown considerable successes, as outlined in the previous paragraphs, the application of LNP-mRNA for non-immunotherapy applications and extra-hepatic delivery of nucleic acids remains challenging.

Several non-immunotherapy LNP-mRNA programs are currently in clinical development as RNA protein replacement therapy for (rare) diseases such as cystic fibrosis, propionic acidemia or ornithine transcarbamylase deficiency.[45] Conceptually, achieving stable, continuous expression of the protein of interest is difficult due to the transient nature of mRNA expression. Moreover, the requirements that are most likely set on LNP-mRNA, in terms of safety and immunogenicity,

7

are potentially more stringent for non-immunotherapy purposes especially when it comes to immunotoxicity, limiting rapid development of such therapies[45].

At this moment, extra-hepatic delivery of nucleic acids by LNPs is considered a key challenge.[46] Minor successes have been obtained by applying targeting ligands to increase nucleic acid delivery outside the liver. Recent examples include CD4 targeted LNPs to increase uptake in CD4+ T-lymphocytes or PECAM-1 targeted LNPs to increase targeting to the lungs.[47,48] However, for both targeted approaches, residual hepatic expression of the encapsulated mRNA was still observed. Screening of large LNP libraries using a DNA barcoding approach as discussed in chapter 5, or a biomimetic approach using the EV-liposome hybrids as discussed in chapter 6 might of be value here. The use of DNA barcodes enables high throughput screening of LNP formulations and potentially aids in the discovery of new formulations that target extra-hepatic tissues. Research on EVs has shown that the lipid / protein composition of EVs can to some degree determine tissue tropism.[49,50] Such findings might provide future directions for development of extra-hepatic delivery of nucleic acids via LNPs

In summary, the past years have been really exciting for the nucleic acid delivery field. The widespread use of LNP-mRNA vaccines during the SARS-CoV-2 pandemic clearly was and still is a landmark event for nanoparticulate therapy. The potential applicability of LNP-mRNA reaches beyond its use as vaccination strategy for infectious disease, to areas such as cancer immunotherapy and gene editing therapy. The coming years will hopefully show whether LNPs can actually deliver on these promises.

REFERENCES

1. Alnylam Pharmaceuticals I. Alnylam Receives Approval of ONPATTRO™ (patisiran) in Europe [Internet]. 2019 [cited 2019 Jun 13]. Available from: http://investors.alnylam.com/news-releases/news-release-details/alnylam-receives-approval-onpattrotm-patisiran-europe

2. Alnylam Pharmaceuticals I. Alnylam Announces First-Ever FDA Approval of an RNAi Therapeutic, ONPATTRO™ (patisiran) for the Treatment of the Polyneuropathy of Hereditary Transthyretin-Mediated Amyloidosis in Adults [Internet]. 2019 [cited 2019 Jun 13]. Available from: http://investors.alnylam.com/news-releases/news-release-details/alnylam-announces-first-ever-fda-approval-rnai-therapeutic

3. Schmidt HH, Waddington-Cruz M, Botteman MF, Carter JA, Chopra AS, Hopps M, et al. Estimating the global prevalence of transthyretin familial amyloid polyneuropathy. Muscle and Nerve. 2018;57(5):829–37.

4. Corbett KS, Edwards DK, Leist SR, Abiona OM, Boyoglu-Barnum S, Gillespie RA, et al. SARS-CoV-2 mRNA vaccine design enabled by prototype pathogen preparedness. Nature. 2020;586(7830):567–71.

5. Baden LR, El Sahly HM, Essink B, Kotloff K, Frey S, Novak R, et al. Efficacy and Safety of the mRNA-1273 SARS-CoV-2 Vaccine. N Engl J Med. 2021;384(5):403–16.

6. Polack FP, Thomas SJ, Kitchin N, Absalon J, Gurtman A, Lockhart S, et al. Safety and Efficacy of the BNT162b2 mRNA Covid-19 Vaccine. N Engl J Med. 2020;383(27):2603–15.

7. Laaksonen R, Ekroos K, Sysi-aho m, Hilvo M, Vihervaara T, Kauhanen D, et al. Plasma ceramides predict cardiovascular death in patients with stable coronary artery disease and acute coronary syndromes beyond. Eur Heart J. 2016;37:1967–76.

8. Zelnik ID, Kim JL, Futerman AH. The Complex Tail of Circulating Sphingolipids in Atherosclerosis and Cardiovascular Disease. J Lipid Atheroscler. 2021;10(3):268.

9. Hilvo M, Wallentin L, Lakic TG, Held C, Kauhanen D, Jylhä A, et al. Prediction of residual risk by ceramide-phospholipid score in patients with stable coronary heart disease on optimal medical therapy. J Am Heart Assoc. 2020;9(10).

10. Hilvo M, Meikle PJ, Pedersen ER, Tell GS, Dhar I, Brenner H, et al. Development and validation of a ceramide- And phospholipid-based cardiovascular risk estimation score for coronary artery disease patients. Eur Heart J. 2020;41(3):371–80.

11. Nicholls M. Plasma ceramides and cardiac risk. Eur Heart J. 2017;38(18):1359–60.

12. Boon J, Hoy AJ, Stark R, Brown RD, Meex RC, Henstridge DC, et al. Ceramides contained in LDL are elevated in type 2 diabetes and promote inflammation and skeletal muscle insulin resistance. Diabetes. 2013;62(2):401–10.

13. Haus JM, Kashyap SR, Kasumov T, Zhang R, Kelly KR, Defronzo RA, et al. Plasma ceramides are elevated in obese subjects with type 2 diabetes and correlate with the severity of insulin resistance. Diabetes. 2009;58(2):337–43.

14. Adams JM, Pratipanawatr T, Berria R, Wang E, DeFronzo RA, Sullards MC, et al. Ceramide Content Is Increased in Skeletal Muscle from Obese Insulin-Resistant Humans. Diabetes. 2004;53(1):25–31.

15. Mullen TD, Hannun YA, Obeid LM. Ceramide synthases at the centre of sphingolipid metabolism and biology. Biochem J. 2012;441(3):789–802.

16. Law BA, Liao X, Moore KS, Southard A, Roddy P, Ji R, et al. Lipotoxic very-long-chain ceramides cause mitochondrial dysfunction, oxidative stress, and cell death in cardiomyocytes. FASEB J. 2018;32(3):1403–16.

17. Kulkarni JA, Witzigmann D, Thomson SB, Chen S, Leavitt BR, Cullis PR, et al. The current landscape of nucleic acid therapeutics. Nat Nanotechnol. 2021;16(6):630–43.

18. Jain R, Frederick JP, Huang EY, Burke KE, Mauger DM, Andrianova EA, et al. MicroRNAs Enable mRNA Therapeutics to Selectively Program Cancer Cells to Self-Destruct. Nucleic Acid Ther. 2018;28(5):285–96.

19. Zangi L, Lui KO, von Gise A, Ma Q, Ebina W, Ptaszek LM, et al. Modified mRNA directs the fate of heart progenitor cells and induces vascular regeneration after myocardial infarction. Nat Biotechnol. 2013;31(10):898–907.

7

20. Kaur K, Zangi L. Modified mRNA as a Therapeutic Tool for the Heart. Cardiovasc drugs Ther. 2020 Dec;34(6):871–80.

21. Magadum A, Singh N, Kurian AA, Sharkar MTK, Chepurko E, Zangi L. Ablation of a Single N-Glycosylation Site in Human FSTL 1 Induces Cardiomyocyte Proliferation and Cardiac Regeneration. Mol Ther - Nucleic Acids. 2018;13:133–43.

22. Carlsson L, Clarke JC, Yen C, Gregoire F, Albery T, Billger M, et al. Biocompatible, Purified VEGF-A mRNA Improves Cardiac Function after Intracardiac Injection 1 Week Post-myocardial Infarction in Swine. Mol Ther - Methods Clin Dev. 2018;9:330–46.

23. Huang C-L, Leblond A-L, Turner EC, Kumar AH, Martin K, Whelan D, et al. Synthetic Chemically Modified mRNA-Based Delivery of Cytoprotective Factor Promotes Early Cardiomyocyte Survival Post-Acute Myocardial Infarction. Mol Pharm. 2015;12(3):991–6.

24. Qian L, Huang Y, Spencer CI, Foley A, Vedantham V, Liu L, et al. In vivo reprogramming of murine cardiac fibroblasts into induced cardiomyocytes. Nature. 2012 May;485(7400):593–8.

25. Ma H, Wang L, Yin C, Liu J, Qian L. In vivo cardiac reprogramming using an optimal single polycistronic construct. Cardiovasc Res. 2015 Nov 1;108(2):217–9.

26. Dahlman JE, Kauffman KJ, Xing Y, Shaw TE, Mir FF, Dlott CC, et al. Barcoded nanoparticles for high throughput in vivo discovery of targeted therapeutics. Proc Natl Acad Sci. 2017;114(8):2060–5.

27. Sago CD, Lokugamage MP, Paunovska K, Vanover DA, Monaco CM, Shah NN, et al. High-throughput in vivo screen of functional mRNA delivery identifies nanoparticles for endothelial cell gene editing. Proc Natl Acad Sci. 2018 Oct 16;115(42):E9944–52.

28. Sago CD, Lokugamage MP, Lando GN, Djeddar N, Shah NN, Syed C, et al. Modifying a Commonly Expressed Endocytic Receptor Retargets Nanoparticles in Vivo. Nano Lett. 2018;18(12):7590–600.

29. Mui BL, Tam YK, Jayaraman M, Ansell SM, Du X, Tam YYC, et al. Influence of Polyethylene Glycol Lipid Desorption Rates on Pharmacokinetics and Pharmacodynamics of siRNA Lipid Nanoparticles. Mol Ther - Nucleic Acids. 2013;2(12):e139.

30. Murphy DE, de Jong OG, Evers MJW, Nurazizah M, Schiffelers RM, Vader P. Natural or Synthetic RNA Delivery: A Stoichiometric Comparison of Extracellular Vesicles and Synthetic Nanoparticles. Nano Lett. 2021 Feb 24;21(4):1888–95.

31. Reshke R, Taylor JA, Savard A, Guo H, Rhym LH, Kowalski PS, et al. Reduction of the therapeutic dose of silencing RNA by packaging it in extracellular vesicles via a pre-microRNA backbone. Nat Biomed Eng. 2020;4:52–68.

32. Hartjes TA, Slotman JA, Vredenbregt MS, Dits N, der Meel R, Duijvesz D, et al. EVQuant; high-throughput quantification and characterization of extracellular vesicle (sub)populations. bioRxiv [Internet]. 2020; Available from: https://www.biorxiv.org/content/early/2020/10/21/2020.10.21.348375

33. Pardi N, Hogan MJ, Pelc RS, Muramatsu H, Andersen H, DeMaso CR, et al. Zika virus protection by a single low-dose nucleoside-modified mRNA vaccination. Nature. 2017;543(7644):248–51.

34. Bahl K, Senn JJ, Yuzhakov O, Bulychev A, Brito LA, Hassett KJ, et al. Preclinical and Clinical Demonstration of Immunogenicity by mRNA Vaccines against H10N8 and H7N9 Influenza Viruses. Mol Ther. 2017;25(6):1316–27.

35. Pardi N, Secreto AJ, Shan X, Debonera F, Glover J, Yi Y, et al. Administration of nucleoside-modified mRNA encoding broadly neutralizing antibody protects humanized mice from HIV-1 challenge. Nat Commun. 2017;8:14630.

36. Beck JD, Reidenbach D, Salomon N, Sahin U, Türeci Ö, Vormehr M, et al. mRNA therapeutics in cancer immunotherapy. Mol Cancer. Molecular Cancer; 2021;20(1):1–24.

37. Sahin U, Derhovanessian E, Miller M, Kloke BP, Simon P, Löwer M, et al. Personalized RNA mutanome vaccines mobilize poly-specific therapeutic immunity against cancer. Nature. Nature Publishing Group; 2017;547(7662):222–6.

38. Cafri G, Gartner JJ, Zaks T, Hopson K, Levin N, Paria BC, et al. mRNA vaccine–induced neoantigen-specific T cell immunity in patients with gastrointestinal cancer. J Clin Invest. 2020;130(11):5976–88.

39.   EU Clinical Trials Register. Clinical Trials Register - 2021-004277-31 [Internet]. [cited 2022 Jun 8]. Available from: https://www.clinicaltrialsregister.eu/ctr-search/search?query=etherna

40.   Gillmore JD, Gane E, Taubel J, Kao J, Fontana M, Maitland ML, et al. CRISPR-Cas9 In Vivo Gene Editing for Transthyretin Amyloidosis. N Engl J Med. 2021;385(6):493–502.

41.   Burns S. Consecutive Genome Editing in Non-Human Primate achieves durable production of human Alpha-1 Antitrypsin and reduction of the native protein [Internet]. 2021 [cited 2022 Jun 24]. p. 1–20. Available from: https://3o5c4w3neipl16yvhj3nfqam-wpengine.netdna-ssl.com/wp-content/uploads/AATD-2021-ESGCT-Final.pdf

42.   Kim J, Hu C, Moufawad El Achkar C, Black LE, Douville J, Larson A, et al. Patient-Customized Oligonucleotide Therapy for a Rare Genetic Disease. N Engl J Med. 2019;381(17):1644–52.

43.   Damase TR, Sukhovershin R, Boada C, Taraballi F, Pettigrew RI, Cooke JP. The Limitless Future of RNA Therapeutics. Front Bioeng Biotechnol. 2021;9(628137).

44.   Biontech SE. Introducing a scalable manufacturing solution for Africa [Internet]. 2022. Available from: https://investors.biontech.de/news-releases/news-release-details/biontech-introduces-first-modular-mrna-manufacturing-facility/

45.   Vlatkovic I. Non-Immunotherapy Application of LNP-mRNA: Maximizing Efficacy and Safety. Biomedicines. 2021 May 10;9(5):530.

46.   Semple SC, Leone R, Barbosa CJ, Tam YK, Lin PJC. Lipid Nanoparticle Delivery Systems to Enable mRNA-Based Therapeutics. Pharmaceutics. 2022;14(2).

47.   Tombácz I, Laczkó D, Shahnawaz H, Muramatsu H, Natesan A, Yadegari A, et al. Highly efficient CD4+ T cell targeting and genetic recombination using engineered CD4+ cell-homing mRNA-LNPs. Mol Ther. 2021 Nov;29(11):3293–304.

48.   Parhiz H, Shuvaev V V, Pardi N, Khoshnejad M, Kiseleva RY, Brenner JS, et al. PECAM-1 directed re-targeting of exogenous mRNA providing two orders of magnitude enhancement of vascular delivery and expression in lungs independent of apolipoprotein E-mediated uptake. J Control Release. 2018 Dec;291:106–15.

49.   Murphy DE, de Jong OG, Brouwer M, Wood MJ, Lavieu G, Schiffelers RM, et al. Extracellular vesicle-based therapeutics: natural versus engineered targeting and trafficking. Exp Mol Med. 2019 Mar 15;51(3):32.

50.   Elsharkasy OM, Nordin JZ, Hagey DW, de Jong OG, Schiffelers RM, Andaloussi S EL, et al. Extracellular vesicles as drug delivery systems: Why and how? Adv Drug Deliv Rev. 2020;159:332–43.

7

Appendices

&

NEDERLANDSE SAMENVATTING

Inleiding

Zoals de titel beschrijft gaat dit proefschrift over natuurlijke en synthetische op lipiden gebaseerde nanodeeltjes (LNP) voor de therapeutische afgifte van RNA. Anders dan deze technische termen wellicht doen vermoeden, heeft dit onderwerp grote impact op de volksgezondheid. Deze nanodeeltjes vormen bijvoorbeeld de basis van de (effectief gebleken) vaccins voor de bestrijding van de SARS-CoV-2 epidemie. Met dit proefschrift wordt een bijdrage geleverd aan het onderzoek naar de ontwikkeling en toepassing van natuurlijke en synthetische, op lipide gebaseerde nanodeeltjes voor de afgifte van RNA.

RNA-therapieën

RNA-therapieën kunnen de expressie van genen en daarmee de productie van eiwitten beïnvloeden. RNA-therapieën zijn geneesmiddelen gebaseerd op een RNA-molecuul. Dit proefschrift is gericht op twee typen RNA-moleculen:
- een klein interfererend RNA-molecuul (short-interfering RNA; siRNA), en;
- een boodschapper RNA-molecuul (messenger RNA; mRNA).

In het lichaam werkt de aanmaak van eiwitten kort weergegeven als volgt. Een gen, bestaande uit het nucleïnezuur DNA, wordt via transcriptie eerst overgeschreven naar een mRNA-molecuul. Dit mRNA-molecuul wordt vervolgens gebruikt om een eiwit aan te maken. Als dit eiwit bijvoorbeeld verkeerd is aangemaakt, kan RNA-therapie dit proces beïnvloeden. Er zijn twee vormen van RNA-therapie voor dit proefschrift relevant:

1. een mechanisme genaamd RNA-interferentie, waardoor de aanmaak van een eiwit geremd wordt. Dit gebeurt heel specifiek door de afbraak van een mRNA-molecuul, die de codering van het betreffende eiwit bevat. Dit gebeurt door het toedienen van een siRNA-molecuul met gelijkenis in de nucleïnezuursequentie van het af te breken mRNA-molecuul. Het siRNA-molecuul zorgt er met die gelijkenis voor dat alleen het beoogde mRNA-molecuul wordt afgebroken door een eiwitcomplex genaamd "RNA-induced silencing complex". Dit kan in verschillende ziektebeelden mogelijk een therapeutisch effect hebben.

2. het gebruik van mRNA-moleculen als geneesmiddel. Het toedienen van een mRNA molecuul dat codeert voor de juiste variant van het eiwit, waardoor het lichaam de correcte variant van het eiwit aanmaakt, kan mogelijk een therapeutisch effect hebben. Men kan ook mRNA toedienen van een lichaamsvreemd eiwit waardoor het lichaam zelf antistoffen aanmaakt tegen dit eiwit. In het coronavaccin wordt bijvoorbeeld gebruik gemaakt van mRNA-moleculen welke coderen voor een eiwit dat grote gelijkenis vertoont met het eiwit van betreffende virusdeeltje. Door intramusculaire toediening wordt het eiwit tot expressie gebracht. Dit heeft een immunologisch respons als resultaat, wat inhoudt dat antistoffen tegen het virus worden aangemaakt welke bescherming bieden tegen een infectie met het betreffende virusdeeltje.

Uitdagingen en innovaties

De klinische toepassing van RNA-therapieën werd langere tijd bemoeilijkt door meerdere problemen. Een RNA-molecuul is niet stabiel, kan ongewenst het immuunsysteem activeren

en is erg lastig af te leveren op de plek in de cel waar het actief moet zijn. Dit laatste wordt gezien als één van de grootste uitdagingen voor RNA-therapieën.

Grofweg liggen twee technologische innovaties ten grondslag aan het succes van enkele RNA-therapieën in de afgelopen paar jaar.

De eerste technologische innovatie is het gebruik van chemisch gemodificeerde ribonucleïnezuren voor de productie van RNA-therapieën. Hierdoor zijn de RNA-moleculen stabieler en immunologisch relatief inert.

De tweede technologische innovatie is het gebruik van geneesmiddelafgiftesystemen zoals natuurlijke en synthetische nanodeeltjes. Door het RNA-molecuul bijvoorbeeld te verpakken in een klein synthetisch vetbolletje is het stabieler en is het mogelijk om het RNA-molecuul af te leveren aan het cytosol van de cel. Het gebruik van LNPs voor het afleveren van RNA-therapieën was initieel gericht op het afleveren van siRNA-moleculen aan de lever. Uit onderzoekresultaten bleek dat LNPs van een specifieke compositie na intraveneuze toediening voornamelijk in staat waren om het RNA-molecuul af te leveren aan levercellen. De focus van het onderzoek naar LNPs voor de afgifte van RNA-moleculen verlegde zich gedurende dit promotietraject naar de therapeutische afgifte van mRNA-moleculen. Op dit moment is het nog steeds een grote uitdaging om RNA-moleculen af te leveren aan andere organen dan de lever.

Naast synthetische LNPs bestaan er ook biologische nanodeeltjes, die ook wel extracellulaire membraanblaasjes (EVs) worden genoemd. Uit recent onderzoek blijkt dat deze EVs waarschijnlijk betrokken zijn bij de uitwisseling van RNA tussen cellen. Hierdoor wordt verondersteld dat EVs erg efficiënt zijn in het afleveren van RNA-moleculen, mogelijk zelfs beter dan de huidige synthetische afgiftesystemen. EVs zijn daarom interessant als mogelijke drager van therapeutisch RNA. Op dit moment zijn er alleen nog veel uitdagingen voor gebruik van EVs. Zo is het lastig om EVs op grote schaal te produceren en te beladen met therapeutische RNA-moleculen.

Samenvatting

Hoofdstuk 2 gaat over de ontwikkeling van LNPs voor de afgifte van siRNA-moleculen. Een LNP bestaat doorgaans uit vier verschillende soorten lipiden. Een ioniseerbaar kationisch lipide, een lipide dat structuur biedt, een PEG-lipide en cholesterol. We bespreken de structuur en functionaliteit van een LNP en leggen een relatie met de farmacokinetische en -dynamische eigenschappen van een LNP. We zetten daarnaast de verschillende productiemethoden en hun voor- en nadelen uiteen. Ten slotte kijken we naar de mogelijkheid om ook mRNA of DNA af te leveren met LNPs.

Hoofdstuk 3 is gericht op CerS2 en DegS1, twee eiwitten die betrokken zijn bij de productie van ceramiden. Het onderzoek betreft de vraag of we de expressie van deze eiwitten kunnen remmen met behulp van siRNA-moleculen verpakt in een LNP. Ceramiden worden voornamelijk geproduceerd in de lever en verhoogde concentraties van ceramiden in het bloedplasma worden in verband gebracht met verschillende cardiovasculaire en metabole ziekten zoals artherosclerose en niet-alcoholische leververvetting. We veronderstelden dat het verminderen van de eiwitexpressie in de lever van CeRS2 en DegS1 mogelijk een reductie van plasmaceramiden teweeg kon brengen. Om dit te onderzoeken hebben we een mengsel van

verschillende siRNA-moleculen (siPool) gericht tegen CerS2 of tegen DegS1 verpakt in een LNP en toegediend aan proefdieren. Voor zowel CerS2 als DegS1 resulteerde dit in een reductie van mRNA-moleculen in de lever. Het effect hiervan op de concentratie van plasmaceramide was wisselend. Voor zowel CerS2 als DegS1 observeerden we geen effect van mRNA-reductie in de lever op de concentratie van ceramiden in de lever. De totale ceramideconcentratie in bloedplasma, voor CerS2 en DegS1, was verlaagd ten opzichte van een controlegroep. Samenvattend laat dit, maar ook ander onderzoek, zien dat het waarschijnlijk mogelijk is om de bloedplasmaconcentratie van ceramiden te beïnvloeden door de eiwitten betrokken bij de productie hiervan te verminderen. De toekomst moet uitwijzen of dit een inderdaad een effectieve strategie is voor de behandeling van verschillende cardiovasculaire en metabole ziekten.

Het onderzoek in **Hoofdstuk 4** gaat over de mogelijkheid een mRNA-molecuul in een LNP af te leveren aan het hart na een myocardinfarct. Voor de succesvolle afgifte van een mRNA-molecuul moeten vele barrières overwonnen worden, zoals het verlaten van de systemische bloedcirculatie. In een gezond mens komt dit veelal voor in weefseltypen zoals de lever of milt. Deze organen hebben karakteristieke bloedvaten waardoor kleine deeltjes uit de circulatie kunnen ontsnappen. In een gezond hart is dit niet mogelijk. Het is echter bekend dat na een hartinfarct het endotheel van de bloedvaten in het hart mogelijk aangetast zijn, waardoor nanodeeltjes naar het weefsel kunnen ontsnappen. Om dit te onderzoeken hebben we fluorescente LNPs geïnjecteerd in proefdieren met ischemie/reperfusie schade in het hart. Hieruit bleek dat een deel van de LNPs inderdaad na ischemie/reperfusie schade de systemische circulatie verlaat en ophoopt in het hart. Dit fenomeen zagen we niet in een gezond dier. Hierbij moet wel vermeld worden dat het merendeel van het mRNA nog steeds wordt afgeleverd in de milt en lever en de afgifte niet specifiek naar het hart is. Het effect beperkte zich niet tot het afleveren van LNPs met mRNA in het hartweefsel. Het afgeleverde mRNA bleek ook functioneel met eiwitexpressie tot gevolg. Functionele afgifte van het mRNA namen we voornamelijk waar in cardiale fibroblasten en in mindere mate ook in cardiomyocyten.

Zoals eerder beschreven bestaat een LNP vaak uit 4 verschillende categorieën vetten. Iedere categorie bestaat weer uit een veelvoud aan unieke vetmoleculen die in verschillende onderlinge verhoudingen te mengen zijn voor het vormen van een LNP. Het resultaat van deze grote verscheidenheid aan moleculen en veelvoud aan verhoudingen is dat men bijna oneindig veel verschillende LNPs kan maken. Maar welk deeltje is dan het beste? Het antwoord op deze vraag verschilt natuurlijk per ziektebeeld en per RNA-molecuul, maar kan gevonden worden door een veelvoud aan LNPs te testen. Historisch gezien testte men LNPs veelal eerst in vitro waarna vervolgens LNPs met goede karakteristieken in vivo getest werden. Eén van de voorkomende problemen van deze aanpak is onder meer de lage voorspellende waarde van in vitromodellen. Ook het testen van iedere mogelijke formulering in vivo is geen goede oplossing om meerdere redenen: dit is kostbaar en in strijd met het principe om dieronderzoek te vervangen, verminderen dan wel verfijnen. In de afgelopen jaren is er, door James Dahlman en medewerkers, een methode ontwikkeld om vele LNPs gelijktijdig in één dier te testen. Deze methode is gebaseerd op het laden van een DNA-streepjescode in een LNP, waardoor het mogelijk is iedere unieke LNP-formulering van een unieke code te voorzien. Men kan de verschillende LNPs mengen en gelijktijdig injecteren in een muis. Door vervolgens in de verschillende weefseltypes de DNA-

streepjescodes te 'scannen', kan gelijktijdig iets worden gezegd over de weefselverdeling van meerdere LNPs. Deze methode is complex en niet eenvoudig op te zetten. In **Hoofdstuk 5** hebben we geprobeerd deze methode zowel in vitro als in vivo te valideren. Hiertoe hebben we drie LNP-formuleringen gebruikt die onderling verschillend zijn, maar waarvan de eigenschappen al goed bestudeerd zijn, zoals de opname door de cel, weefselverdeling en farmacokinetiek. We hebben deze eigenschappen op drie manieren gemeten en vergeleken met elkaar en de literatuur. De eerste manier is gebaseerd op een meetmethode op basis van fluorescentie. De tweede manier is gebaseerd op het meten van DNA-barcodes door kwantitatieve PCR. De derde manier is het meten van DNA-barcodes met 'next-generation sequencing'. De drie methoden vertoonden in vitro grote gelijkenis met elkaar en was in lijn met het verwachtingspatroon op basis van literatuur. Wel was sprake van discrepantie tussen de drie methoden en de literatuur bij het onderzoek in vivo, in het bijzonder op het gebied van weefselverdeling. Daardoor is extra validatie van deze methode nodig voor gebruik.

Op het moment is de afgifte van RNA-therapieën relatief inefficiënt. Geschat wordt dat ongeveer 1-2% van de lading op de juiste manier wordt afgeleverd. Recentelijk heeft men ontdekt dat extracellulaire membraanblaasjes mogelijk efficiënter zijn in de afgifte van RNA aan cellen dan het geval is bij afgifte met LNPs. Het gebruik van extracellulaire membraanblaasjes wordt tot op heden bemoeilijkt door o.a. de beperkte mogelijkheid om moleculen zoals siRNA of mRNA te laden in EVs.

In **Hoofdstuk 6** hebben we een hybride nanodeeltje gemaakt bestaande uit componenten van zowel EVs als van LNPs. We veronderstelden dat een hybride nanodeeltje de voordelen van natuurlijke en synthetische nanodeeltjes kan combineren. We laten in dit hoofdstuk zien dat hybride nanodeeltjes bepaalde eiwitten bevatten die voorkomen in het membraanoppervlak van EVs. Daarnaast laten we zien dat bepaalde eigenschappen van het hybride nanodeeltje worden beïnvloed door de hoeveelheid EVs die gebruikt worden in de formulering. Daarnaast hebben we hybride nanodeeltjes gemaakt met EVs afkomstig van cardiale voorlopercellen en aangetoond dat we enkele functionele eigenschappen van deze CPC-EVs kunnen incorporeren in het hybride nanodeeltje.

In **Hoofdstuk 7** geven we een Engelstalige samenvatting van dit proefschrift. Daarnaast werpen we een blik op de mogelijke toekomst van natuurlijke en synthetische en op lipide gebaseerde nanodeeltjes. De afgelopen jaren is duidelijk geworden dat LNPs met mRNA een belangrijke rol hebben gespeeld in de bestrijding van de uitbraak van SARS-CoV-2. In potentie kunnen LNPs gebruikt worden als vaccinatiestrategie voor andere infectieuze ziekten zoals Zikavirus of Influenza. Op dit moment zien we veelbelovende resultaten bij het gebruik van LNPs met mRNA bij immunotherapie voor de behandeling van kanker en voor de afgifte van componenten van CRISPR-Cas, een techniek om genen aan te passen. In de komende jaren zal duidelijk worden of LNPs daadwerkelijk deze belofte kunnen inlossen.

&

CURRICULUM VITAE

Martijn Evers was born on the 6th of February 1992 in 's-Hertogenbosch. In 2010, he completed his gymnasium at Maurick College, Vught after which he started a B.Sc. in Pharmacy at University of Utrecht. After completion of his B.Sc, he enrolled in the master's program Drug Innovation at Utrecht University. At that time, he developed an interest in drug delivery of nucleic acids. His major internship, under supervision of Erik Oude Blenke en Enrico Mastrobattista, was focused on the quantification of nucleic acids in lipid based RNA formulations and the coating of liposomes with endosomolytic peptides. In February 2017, he joined the group of Prof. Raymond M. Schiffelers at the University Medical Centre Utrecht as graduate student. For four years he worked on the delivery of RNA therapeutics using natural and synthetic lipid-based delivery systems under the daily supervision of Dr. P. Vader and Dr. S.A.A. Kooijmans, an effort that resulted in this PhD thesis. Currently, he is continuing his career as scientist at Nanocell Therapeutics.

LIST OF PUBLICATIONS

Publications from this thesis

M.J.W. Evers, J.A. Kulkarni, R. van der Meel, P.R. Cullis, P.Vader, R.M. Schiffelers. State-of-the-art design and rapid-mixing production techniques of lipid nanoparticles for nucleic acid delivery, Small Methods. 2018;2:1700375. doi: 10.1002/smtd.201700375

M.J.W. Evers, S.I. van de Wakker, E.M. de Groot, O.G. de Jong, J.J.J. Gitz-François, C. Seinen, J.P.G. Sluijter, R.M. Schiffelers, P Vader. Functional siRNA delivery by Extracellular Vesicle – Liposome Hybrid Nanoparticles. Adv. Healtc Mater. 2021 Aug 11;e2101202. doi: 10.1002/adhm.202101202

M.J.W.Evers, W.Du, Q. Yang, S.A.A. Kooijmans, A.Vink, M. van Steenbergen, P. Vader, S.C.A. de Jager, S.A. Fuchs, E. Mastrobattista, J.P.G. Sluijter, Z.Lei, R. Schiffelers. Delivery of modified mRNA to damaged myocardium by systemic administration of Lipid Nanoparticles. J Control. Release. 2022 Mar;343:207-216. doi: 10.1016/j.jconrel.2022.01.027

Other publications

S. Bevers, S.A.A. Koooijmans, E. van de Velde, **M.J.W.Evers**, S. Seghers, J.J.J.M. Gitz-François, N.C.H. van Kronenburg, M.H.A.M Fens, E. Mastrobattista, L.Hassler, H Sork, T. Lehto. K Ezzat Ahmed, S. El Andaloussi, K Breckpot, M Maes, D van Hoorick, T Bastogne, R.M Schiffelers. S. de Koker. mRNA-LNP vaccines tuned for systemic immunization induce strong antitumor immunity by engaging splenic immune cells. Mol Therapy, 2022 Sep 7;30(9):3078-3094. doi: 10.1016/j.ymthe.2022.07.007

D.E. Murphy, O.G. de Jong, **M.J.W. Evers,** M. Nurazizah, R.M. Schiffelers, P. Vader. Natural or Synthetic RNA delivery: A Stoichiometric Comparison of Extracellular Vesicles and Synthetic Nanoparticles. Nano Letters 2021 Feb 24;21(4):1888-1895. doi: 10.1021/acs.nanolett.1c00094

M.H Aldosari, M. den Hartog, H. Ganazida, **M.J.W. Evers,** E. Mastrobattista, H. Schellekens. Feasibility study for bedside production of recombinant human acid a-Glucosidase: technical and financial considerations. Curr. Pharm. Biotechnol. 2020;21(6):467-479. doi: 10.2174/1389 201021666200217113049

O.G. de Jong, S.A.A. Kooijmans, D.E. Murphy, L. Jiang, **M.J.W. Evers**, J.P.G. Sluijter, P Vader, R.M. Schiffelers. Drug Delivery with Extracellular Vesicles: from Imagination to Innovation Acc. Chem.Res. 2019;52(7):1761-1770. doi: 10.1021/acs.accounts.9b00109

E. Oude Blenke, **M.J.W.Evers,** V.Baumann, J Winkler, G.Storm, E.Mastrobattista, Critical evaluation of quantification techniques for siRNA formulated in lipid nanoparticles, Int.J.Pharm. 2018;528(2):793-802. doi: 10.1016/j.ijpharm.2017.12.035

E. Oude Blenke, M. Sleszynska, **M.J.W. Evers**, G.Storm, N.I. Martin, E.Mastrobattista, Strategies for the activation and release of the membranolytic peptide melittin from liposomes using endosomal pH as trigger, Bioconjugate Chem. 28(2) (2017) 574-582. doi: 10.1021/acs.bioconjchem.6b00677

E. Oude Blenke, **M.J.W. Evers**, E. Mastrobattista, J. van der Oost, CRISPR-Cas9 gene editing: Delivery Aspects and therapeutic potential, J.Control.Release. 244 (2016) 139-148. doi: 10.1016/j.jconrel.2016.08.002

ACKNOWLEGDEMENTS

Zo. Wat ben ik blij dat ik eindelijk iets luchtigs kan schrijven. Promoveren voelde voor mij vaak aan als meer dan alleen werken. Het was voor mij een commitment welke niet alleen op professioneel vlak maar ook op persoonlijk vlak veel van mij vroeg. Het heeft me niet alleen gevormd als wetenschapper maar ook als mens. Een ervaring waarvan ik nu (pas) kan zeggen dat ik hem niet had willen missen. De keerzijde van de medaille is dat ik zou liegen als ik ontken dat ik vaker dan één keer de handdoek in de ring heb willen gooien. Mijn punt: dit promotietraject had ik niet 4 jaar lang met plezier gedaan zonder een geweldige werkomgeving, een fijne groep vrienden en een lieve en zorgzame familie. Mijn dank aan jullie <u>allen</u> is overweldigend groot.

Prof. Dr. Raymond M. Schiffelers, beste Ray. Bedankt voor het vertrouwen. In mijn vooralsnog korte carrière heb jij een hele belangrijke rol gespeeld: je hebt me aangenomen als promovendus, bent van onschatbare waarde geweest tijdens het promotietraject, hebt me vervolgens in contact gebracht met mijn huidige werkgever, NanocellTX, en bent daarnaast ook deels meeverhuisd naar NanocellTX. Je eeuwige optimisme, aanstekelijke lach en bovendien prettige aanwezigheid zijn enkele van je geroemde eigenschappen. Ik denk dat mede hierdoor CDL Research een stimulerende en voor mij veilige omgeving was om mijzelf te kunnen ontplooien. Ik zou je enorm tekort doen door alleen dit te benoemen. Ik bewonder hoe jij je, naast je rol als wetenschapper (die witte labjas staat je nog steeds goed), laveert in het complexe krachtenveld van de wetenschap en het UMCU. Daarnaast denk je actief na over hoe je CDL research moet positioneren in een veranderende wereld zonder krampachtig vast te houden aan oude dogma's.

Prof. Dr. W.W. van Solinge, beste Wouter. Bedankt voor de begeleiding in de afgelopen 4 jaar. Ik kijk met veel plezier terug op onze maandelijkse meetings. Het heeft mij enorm geholpen om structuur te creëren in de (wetenschappelijke) chaos in mijn hoofd. Daarnaast was het leuk om te zien hoe jij de data interpreteerde en mogelijkheden zag om er meer mee te doen. Wat me in het bijzonder is bijgebleven is het vermogen om besproken ideeën binnen no time om te zetten in concrete acties, kleine experimenten en hulp waar nodig. Bedankt!

Dr. P. Vader, beste Pieter. Ik denk dat promoveren met jou als dagelijks begeleider en copromotor een van de beste leerscholen is die ik me had kunnen wensen. Wat heb ik veel geleerd van jou. Ik had vaak het idee dat je al mijn experimenten in je hoofd al had uitgevoerd. Ik hoefde maar met de puzzelstukjes aan data te komen en binnen een mum van tijd wist je de vervolgstappen in een juiste opzet met de correcte controles. Gaandeweg mijn PhD probeerde ik me hieraan op te trekken, wat soms toch wel frustrerend aanvoelde als het me niet lukte. Nu ben ik er alleen maar dankbaar voor. Eerlijkheid gebied me ook te zeggen dat ik op menig moment wenste dat je EVs niet zo interessant en fascinerend vond. Wat een gedoe zeg, dat kweken en isoleren. Helaas zijn lipiden en polymeren ook niet alles en zijn extracellulaire vesicles de toekomst, toch? Als iemand het uit kan vinden, dan ben jij het!

Dr. S.A.A. Kooijmans, beste Sander. Hard werken, zeiken, veel lachen en een biertje op zijn tijd. Boven alles, om grenzen te verleggen moet je vaak op je bek gaan toch? Ik kijk met veel plezier terug op de vele uren in het GDL en CKL. De gezamenlijke frustratie van muizenorganen die de FACS verstoppen waardoor belangrijke dierexperimenten weer in het honderd lopen. Door

&

Prof. Dr. Enrico Mastrobattista en **Dr. Erik Oude Blenke.** Mijn eerste stappen in de wetenschappelijke wereld zijn gezet onder jullie begeleiding. Mede door jullie kon ik beginnen in Ray's groep als promovendus, waarvoor dank. **Erik**, je kritische blik brengt me nog steeds veel. Ik waardeer het contact dat we nog steeds hebben. Je bent van alles op de hoogte en jouw inzichten werken vaak erg verhelderend. Ik hoop ergens dat we ooit nog eens samen kunnen werken maar geniet eerst maar van het nieuwe avontuur in Kopenhagen.

De (voormalig) technicians van UU Pharmaceutics en in het bijzonder **Joep, Roel, Mies en Louis**. **Joep/Roel**, de eerste handelingen in het lab zijn ooit verricht onder jullie supervisie. Bedankt voor het leren van de fijne kneepjes van de celweek en al het andere biochemische werk. **Mies**, dat ik ooit nog in het synthese lab zou komen: wie had dat gedacht. Het was leuk om samen met jou wat lipiden te synthetiseren en zo een andere kant van het veld te zien! **Louis,** de ongekroonde liposomenkoning van het Went en Wied. Geniet van je pensioen!

Alle collega's van CDL Research/Exp Cardio: wat zijn jullie toch een leuke groep mensen. Bijzonder om te zien hoe zo veel verschillende disciplines samen op een lab werken. Het CDL voelt aan als een warm bad en dat komt door eenieder van jullie.

Dr. Olivier de Jong. Wat een natuurkracht ben jij zeg. Het is geweldig om te zien hoe de motivatie er voor mijn gevoel vanaf spat. Voor mij ben jij een wetenschapper universalis: plezier in onderwijs en onderzoek. Daarnaast altijd bereid zijn te helpen, bergen werk te verzetten in algemeen belang, oog te hebben voor iedereen, veel kennis en kunde en naast dit alles weet je dan ook nog een eigen onderzoekslijn op te zetten. Ga er maar aanstaan! Bedankt voor je bijdrage aan hoofdstuk 6, het spik en span houden van het CDL (ik gok dat je gemist wordt) en een luisterend oor.

Arnold! Ik besef me steeds meer in wat voor een goed georganiseerde omgeving ik gewerkt heb. Ik heb zo een vermoeden dat jij, en natuurlijk ook alle andere technicians, daar een grote rol in spelen. Je staat voor velen altijd klaar om te helpen met de kleinste dingen naast alle andere organisatorische taken. Ik vraag me soms af hoe je het doet! P.S. Sorry dat ik mijn labjas nooit aanhad. Wellicht kan met die hoge gasprijs de thermostaat wat tandjes omlaag, dan beloof ik je dat ik hem draag. **Cor,** bedankt voor alle gewonnen weddenschappen. De voorspellende waarde van sterren blijkt vooralsnog even goed te zijn als die van cellen in een petrischaal. Zonder gekkigheid, bedankt voor alle uren die je in EM en CRYO-EM gestopt hebt. Het is nagenoeg een kunstvorm om zulke plaatjes te schieten! **Git**, de mater familias van het CDL R. Altijd in voor een leuk praatje, behulpzaam en oprecht geïnteresseerd. Hetzelfde geldt voor je rode bloedcelgroep partner in crime **Jennifer,** altijd goed gemutst op het lab! **Simone**, de nieuwe generatie. Altijd feest met jou op het lab. Gekke bekken trekken op een hoger niveau. **Annet,** van alles op de hoogte, weet hoe de hazen lopen op het CDL R, hart op de juiste plek. Bedankt! **Arjan.** Jammer dat ik nooit van die magische flow setups onder de microscoop gebruik heb kunnen maken. Het ziet er altijd gaaf uit. Bedankt voor het in leven houden van de FACS canto! **Martijn H & Leida**: stille krachten van het CDL R. Jullie verrichten fantastisch werk! **Joukje:** idem. Bedankt voor je hulp.

Dr. Michal Mokry & Noortje, thanks for the collaborative effort on chapter 5. I really enjoyed working together with you on next-generation sequencing.

&

132; Dave, Zaïr, Anne B, Anne E, Françoise. Wat een plezier. Met 4 mensen zonder broers/zussen in de groep denk ik soms wel dat jullie mijn "brothers and sisters from another mother" zijn.

Ik had me voorgenomen niet zoveel te schrijven. Helaas mislukt. Ik wil het dankwoord graag afsluiten met mijn (schoon)familie en aanstaande vrouw.

Marie-José & Walter: bedankt voor de warmte waarmee jullie mij in jullie gezin hebben opgenomen als schoonzoon. Daarnaast waardeer ik enorm hoe geïnteresseerd jullie zijn in het wel en wee van dit promotietraject (en al het andere). **Jurre:** bijzonder knap hoe jij je eigen business uit de grond stampt. Trots! Daarnaast waardeer ik je enorm en haal ik plezier uit de gezonde sportieve competitie; volgend jaar ga ik weer fietsen;).

Ik kan niet onder woorden brengen hoe gelukkig ik ben dat ik op de wereld ben gekomen bij jullie, papa & mama**. Lieve mama**, al meer dan 10 jaar ben je een soort 2 in 1 ouder, iets waarvoor ik veel bewondering heb. Je onvoorwaardelijke steun, liefde en support maar ook soms kritische noot helpen mij een beter mens te zijn. **Lieve papa (†),** ik hoop, en stiekem weet ik, dat je trots bent. Ik ben blij dat jij en een aantal van je wijze levenslessen er nog altijd in mijn gedachten bij zijn. Dankzij jou en mama ben ik nu in het leven waar ik altijd al heb willen zijn. Ik mis je.

Allerliefste Mirt, je bent simpelweg de beste. Er zijn geen woorden die kunnen beschrijven hoe dankbaar ik ben dat jij in mijn leven bent. Tijdens alle pieken en dalen van mijn PhD was je er voor me, vierden we kleine successen, kreeg ik een trap onder m'n reet of was je een luisterend oor. Liefde!